

Newcastle University

Faculty of Science, Agriculture and Engineering

School of Engineering



**Landslide monitoring using mobile device and
cloud-based photogrammetry**

Polpreecha Chidburee

Thesis submitted for the degree of

Doctor of Philosophy

February 2019

Abstract

Landslides are one of the most commonly occurring natural disasters that can cause a serious threat to human life and society, in addition to significant economic loss. Investigation and monitoring of landslides are important tasks in geotechnical engineering in order to mitigate the hazards created by such phenomena. However, current geomatics approaches used for precise landslide monitoring are largely inappropriate for initial assessment by an engineer over small areas due to the labour-intensive and costly methods often adopted. Therefore, the development of a cost-effective landslide monitoring system for real-time on-site investigation is essential to aid initial geotechnical interpretation and assessment.

In this research, close-range photogrammetric techniques using imagery from a mobile device camera (e.g. a modern smartphone) were investigated as a low-cost, non-contact monitoring approach to on-site landslide investigation. The developed system was implemented on a mobile platform with cloud computing technology to enable the potential for real-time processing. The system comprised the front-end service of a mobile application controlled by the operator and a back-end service employed for photogrammetric measurement and landslide monitoring analysis. In terms of the back-end service, Structure-from-Motion (SfM) photogrammetry was implemented to provide fully-automated processing to offer user-friendliness to non-experts. This was integrated with developed functions that were used to enhance the processing performance and deliver appropriate photogrammetric results for assessing landslide deformations. In order to implement this system with a real-time response, the cloud-based system required data transfer using Internet services via a modern 4G/5G network. Furthermore, the relationship between the number of images and image size was investigated to optimize data processing.

The potential of the developed system for monitoring landslides was investigated at two different real-world UK sites, comprising a natural earth-flow landslide and coastal cliff erosion. These investigations demonstrated that the cloud-based photogrammetric measurement system was capable of providing three-dimensional results to sub-decimeter-level accuracy. The results of the initial assessments for on-site investigation could be effectively presented on the mobile device through visualisation and/or statistical quantification of the landslide changes at a local-scale.

Acknowledgements

First of all, I would like to express my deepest gratitude to my primary supervisor, Prof Jon Mills, for his kindness, support, immense knowledge, motivation, guidance and useful advice throughout the research. I would like to thank my supervisory team, Dr Pauline Miller and Dr Karolina Fieber for their contribution, time, support and guidance in this the research. Furthermore, I would like to acknowledge the British Geological Survey (BGS) for allowing access to the Hollin Hill landslide site, and Martin Robertson, Maria Peppas, Magdalena Smigaj and Elias Berra for kindly supporting data collection activities. I would like to thank all staff and technicians at Newcastle University who helped and supported me throughout this research.

I would like to gratefully acknowledge the Royal Thai Government and Naresuan University for the scholarship and financial support that gave me a chance to study at Newcastle University.

I would also like to thank all my friends for their help, happiness and funny moments in Newcastle upon Tyne. I am very grateful to my family for their love, support, encouragement and faith in me. Finally, I am especially thankful to my dearest parents for all support in my life.

Tables of Contents

Abstract	i
Acknowledgements	iii
List of Figures	xi
List of Tables	xvii
List of Abbreviations	xxi
Chapter 1. Introduction	1
1.1 Overview	1
1.2 Research problem and background of landslide monitoring	3
1.2.1 Definition and potential problems.....	3
1.2.2 Motivation for study	4
1.3 Aim and objectives.....	4
1.4 Research scope.....	5
1.5 Thesis structure	6
Chapter 2. Techniques for landslide monitoring	7
2.1 Introduction.....	7
2.2 Landslide hazards and landslide monitoring	7
2.2.1 Geotechnical and geophysical techniques	10
2.2.1.1 Extensometers.....	10
2.2.1.2 Inclimeters	12
2.2.1.3 Piezometers and pore pressure sensors	14
2.2.1.4 Electrical resistivity tomography (ERT)	14
2.2.1.5 Additional instruments	15
2.2.2 Geomatics techniques	17
2.2.2.1 Total stations.....	21

2.2.2.2	Global Navigation Satellite System (GNSS).....	23
2.2.2.3	Terrestrial laser scanning (TLS)	25
2.2.2.4	Ground-based synthetic aperture radar (GBSAR)	28
2.2.2.5	Close-range photogrammetry.....	29
2.3	Summary.....	32
Chapter 3. A close-range photogrammetric methodology for landslide monitoring		35
.....		
3.1	Introduction.....	35
3.2	A photogrammetric solution for deformation measurement of landslides	36
3.2.1	Imaging devices and sensors.....	36
3.2.2	Camera calibration.....	38
3.2.3	Photogrammetric network configuration	44
3.2.4	Photogrammetric processing solution.....	46
3.2.4.1	Structure-from-motion based photogrammetric processing	47
3.2.4.2	SfM-Photogrammetric processing software	48
3.2.5	Landslide analysis methods	50
3.2.6	Summary of the photogrammetric solution for landslide monitoring	51
3.3	A mobile platform-based landslide monitoring system for on-site investigation.	52
3.3.1	Mobile device technology.....	52
3.3.2	Cloud computing technology	54
3.3.3	System design and integration.....	55
3.3.4	Summary of the mobile platform based landslide monitoring system	58
3.4	Improving photogrammetric processing for landslide monitoring analysis	58
3.4.1	Pre-image matching.....	59
3.4.2	Lens distortion correction	62
3.4.3	Geo-referencing.....	63
3.4.3.1	Geo-referencing with GNSS/TLS based target observation.....	64

3.4.3.2 Geo-referencing without GNSS/TLS based target observation	65
3.4.4 Automatic de-noising	66
3.4.5 Vegetation filtering.....	68
3.4.6 Change assessment	70
3.5 System development	72
3.5.1 System layout.....	72
3.5.2 Implementing system.....	74
3.5.3 Development of a mobile application.....	79
3.5.4 Summary of the developed system.....	81
3.6 Summary.....	81
Chapter 4. Performance evaluation	83
4.1 Introduction.....	83
4.2 Photogrammetric landslide monitoring using mobile devices.....	83
4.2.1 Experimental design	84
4.2.2 Test results	85
4.3 SfM-photogrammetric processing based on cloud computing	87
4.3.1 Experimental design	87
4.3.2 Test results	89
4.4 Optimisation of imaging network	93
4.4.1 Experimental design	93
4.4.2 Test results	97
4.5 Performance evaluation of developed functions for photogrammetric processing	104
4.5.1 Pre-image matching.....	104
4.5.2 Lens distortion correction	107
4.5.3 Geo-referencing.....	108
4.5.4 Automatic de-noising	110

4.5.5 Vegetation filtering.....	113
4.5.6 Change assessment.....	116
4.6 Summary.....	118
Chapter 5. System implementation	121
5.1 Introduction.....	121
5.2 Natural earth-flow landslide monitoring experiment.....	121
5.2.1 Study area.....	122
5.2.2 Experimental design	124
5.2.3 Test results	127
5.2.4 Assessment of photogrammetric accuracy.....	131
5.2.5 Inspection of landslide monitoring analysis.....	132
5.3 Coastal cliff monitoring experiment.....	139
5.3.1 Study area.....	139
5.3.2 Experimental design	140
5.3.3 Test results	143
5.3.4 Assessment of photogrammetric accuracy.....	146
5.3.5 Cliff erosion monitoring analysis	148
5.4 Summary.....	154
Chapter 6. Discussion of results.....	155
6.1 Introduction.....	155
6.2 System inspection.....	156
6.2.1 Mobile devices (smart phone case)	157
6.2.2 The cloud-based server	159
6.3 Performance assessment	160
6.4 Assessment of photogrammetric accuracy	163
6.5 Assessment of landslide monitoring analysis	166
6.6 Potential challenges of operation	168

6.7 Summary.....	169
Chapter 7. Conclusions and future work.....	171
7.1 Introduction.....	171
7.2 Summary of work.....	171
7.3 Research contributions	174
7.4 Suggestions for future work.....	176
7.4.1 Precision improvement of SfM-photogrammetric processing.....	176
7.4.2 Automated target detection for geo-referencing	177
7.5 Concluding remarks	179
Appendix A.....	181
Appendix B.....	185
Appendix C.....	187
Module 1: Photogrammetric measurement	187
1) Create a new project or select an existing project.....	187
2) Create a new epoch for photogrammetric measurement.....	188
3) Upload a new image dataset	190
4) Settings for data processing	191
4.1) Pre-processing.....	191
4.1.1) Lens distortion correction	192
4.1.2) Pre-image matching	192
4.2) Geo-referencing	192
4.2.1) None.....	192
4.2.1) With GNSS-based target observations	192
4.2.1) With real-time, GNSS-based target observations.....	193
4.2.2) With distances between points	195
4.3) Post-processing	196
4.3.1) Cropping.....	197
4.3.2) De-noising.....	197
4.3.3) Vegetation filtering.....	197
5) Process the photogrammetric measurement	197

6) Display the photogrammetric results.....	198
Module 2: Landslide monitoring analysis	199
1) Select the project.....	199
2) Select the epochs for a multi-epoch analysis.....	199
3) Setting of cloud comparison method using M3C2 technique.....	201
3.1) Main parameters.....	201
3.2) Core points.....	201
3.3) Normals.....	202
3.4) Registration error.....	202
4) Process the landslide monitoring analysis	202
5) Display the results of landslide monitoring analysis.....	203
References	205

List of Figures

Figure 2-1: Illustration of slope movement in the pre-failure stage (Sassa <i>et al.</i> , 2007)..	9
Figure 2-2: Illustration of opening wire extensometers (Zhang <i>et al.</i> , 2018).	10
Figure 2-3: Illustration of extensometer in a borehole: a) device components; and b) stages in the changed positions of a wire extensometer used for the investigation of landslide displacements (Corominas <i>et al.</i> , 2000).....	11
Figure 2-4: Illustration of a tape extensometer network for rock mass monitoring (Devoto <i>et al.</i> , 2013).....	11
Figure 2-5: Comparison of landslide displacement data from distance measurement devices and an extensometer (Kristensen and Blikra, 2013).	12
Figure 2-6: Measurement of horizontal displacements using an inclinometer (Segalini and Carini, 2013).....	13
Figure 2-7: Comparison of differences in cumulative displacements in two directions using an inclinometer (Milenkovic <i>et al.</i> , 2013).	13
Figure 2-8: Comparison of the relationship between rainfall and piezometric level (Wasowski <i>et al.</i> , 2013).	14
Figure 2-9: Illustrations of (a) the locations of installation for ERT landslide monitoring, and (b) 3D model of landslide obtained from ERT monitoring (Chambers <i>et al.</i> , 2013).	15
Figure 2-10: Illustration of tilt and water content sensors implemented in a wireless unit (Uchimura <i>et al.</i> , 2013).	16
Figure 2-11: Example of a weather station, including rainfall gauge and thermometer (Bednarczyk, 2013).....	16
Figure 2-12: Example of a historical landslide inventory obtained from multi-temporal remote sensing (Martha <i>et al.</i> , 2012).	18
Figure 2-13: Comparison of landslide monitoring for deformation velocities using SAR satellites from: (a) ALOS/PALSAR data; and (b) ENVISAT/ASAR ascending data (Zhang <i>et al.</i> , 2015).....	19
Figure 2-14: (a) A total station used for (b) rock mass monitoring at Cadireta; and (c) the installation of reflecting prisms on rock needles (Janeras <i>et al.</i> , 2017).....	22
Figure 2-15: (a) A total station and (b) the establishment of targets for landslide movement monitoring in slope areas (Sarkar <i>et al.</i> , 2013).	22

Figure 2-16: Time-series landslide movements of targets measured by total station: (a) horizontal movements; (b) vertical movements (Sarkar <i>et al.</i> , 2013).....	23
Figure 2-17: GNSS in the detection of landslide movements: (a) GNSS-base station; and (b) GNSS-moving station (Malet <i>et al.</i> , 2013).	24
Figure 2-18: Monitoring of the Villerville landslide in France using GNSS observations (Malet <i>et al.</i> , 2013).....	24
Figure 2-19: Illustrations of (1) point clouds from a TLS survey, (2) a DTM derived from the point cloud (Denora <i>et al.</i> , 2013).	26
Figure 2-20: Illustration of different DTMs used for monitoring the Montaguto landslide in Campania, Italy (Denora <i>et al.</i> , 2013).....	26
Figure 2-21: Illustration of point clouds from different TLS locations (Kuhn and Prüfer, 2014).	27
Figure 2-22: The use of GBSAR for measuring: (a) landslide movements; and (b) rock deformation (Caduff <i>et al.</i> , 2015).	28
Figure 2-23: Illustration of processes for visualization of terrestrial radar data from GBSAR (Caduff <i>et al.</i> , 2015).	29
Figure 2-24: The Tartano valley landslides (Italy): (a) overview of landslide; (b) configuration of photogrammetric imaging network used for landslide monitoring (Scaioni, 2015).....	30
Figure 2-25: Assessment of landslide changes at the Super-Sauze landslide in the southern French Alps using photogrammetry (Stumpf <i>et al.</i> , 2015).	31
Figure 3-1: Calibration template for (a) PhotoModeler, (b) Matlab and OpenCV.....	39
Figure 3-2: Photogrammetric configuration for camera calibration.	40
Figure 3-3: Radial lens distortion of the Nexus 6, as determined from the three different calibration routines.....	43
Figure 3-4: Imaging geometry (a) small B/D ratio (b) large B/D ratio (Alsadik, 2014).44	
Figure 3-5: Example of photogrammetric network design for Hollin Hill landslide monitoring.	46
Figure 3-6: Image acquisition for SfM (Westoby <i>et al.</i> , 2012).....	48
Figure 3-7: SfM-photogrammetric processing software used in Geoscience applications (Eltner <i>et al.</i> , 2016).	49
Figure 3-8: The methods of multi-epoch analysis for landslide monitoring.	50
Figure 3-9: Sensors integrated on a modern smart phone (Daponte <i>et al.</i> , 2013).	53

Figure 3-10: Example of a real-time satellite image processing for change detection analysis on an iPad (Lee and Kang, 2013).....	55
Figure 3-11: Example of a single-camera based photogrammetric system for long-term, in-situ landslide monitoring (Travelletti <i>et al.</i> , 2012).....	56
Figure 3-12: The model for the implementation of a photogrammetric solution for landslide monitoring on mobile cloud computing adopted in this research.	57
Figure 3-13: Photogrammetry-based landslide monitoring workflow.	59
Figure 3-14: Example of 3D reconstruction for (a) imaging configuration and the matrix comparisons of image matching between (b) an image sequence and (c) a non-image sequence.	60
Figure 3-15: The example of a pair-list of image matches from an image sequence.....	62
Figure 3-16: The workflow of the developed function for 3D reconstruction using lens distortion correction.....	63
Figure 3-17: Illustration of the developed function for GNSS/TLS target observation.	65
Figure 3-18: Illustrations of the developed function of scaling for geo-referencing using distances of known objects.....	66
Figure 3-19: Example of noise in a point cloud from the SfM- photogrammetric approach applied to a natural landslide: the red circles highlight noisy points.....	67
Figure 3-20: Example of automatic de-noising based on the SOR filter (PCL, 2017)...	68
Figure 3-21: A workflow for vegetation filtering of the photogrammetric results.	69
Figure 3-22: The outline of the key parameters used in the M3C2 algorithm (Lague <i>et al.</i> , 2013).	70
Figure 3-23: The outline of the workflow for landslide monitoring analysis.	71
Figure 3-24: A generic landslide monitoring workflow using a photogrammetric approach.	72
Figure 3-25: System architecture based on mobile cloud computing for photogrammetric measurement and landslide monitoring.	73
Figure 3-26: The workflow of data processing for photogrammetric measurement based on a multi-cloud server.	75
Figure 3-27: The workflow of the photogrammetric measurement module based on a multi-cloud server.....	77
Figure 3-28: The workflow of the landslide monitoring analysis module based on a multi-cloud server.	78

Figure 3-29: Example of the user interface for the developed mobile application of the landslide photogrammetric monitoring system.	80
Figure 4-1: Methodology in the camera comparison experiment.....	84
Figure 4-2: Illustration of camera positions for photogrammetric image capture.....	87
Figure 4-3: Methodology in the photogrammetric processing comparison experiment.	88
Figure 4-4: Photogrammetric point clouds obtained from the three adopted SfM approaches; (a) VisualSfM & PMVS, (b) Autodesk 123D Catch, (c) Agisoft PhotoScan, and the TLS validation data (d).	89
Figure 4-5: The distribution of distance differences between each SfM result and the TLS data; (a) PhotoScan, (b) 123D Catch and (c) VisualSfM & PMVS.....	91
Figure 4-6: Comparison between photogrammetric configuration of each approach. ...	95
Figure 4-7: Methodology in the optimisaion of imaging network experiment.	96
Figure 4-8: Comparison of image matching matrix for the relationship between each image in each approach.	97
Figure 4-9: Comparison of the relationship between the number of points and point density of photogrammetric results obtained from each SfM approach.	99
Figure 4-10: Comparison of photogrammetric point clouds obtained from different number of images and different image size.....	100
Figure 4-11: Comparison of the relationship between data processing time obtained from each SfM approach and the RMSE of differences between each SfM result and the TLS data in each approach.....	102
Figure 4-12: Data processing time obtained from each approach.	103
Figure 4-13: Comparison of data processing time at each stage obtained from the SfM-photogrammetric processing using VisualSfM and PMVS.....	105
Figure 4-14: Percentage comparisons of data processing time in each stage of the SfM-photogrammetric approach using VisualSfM and PMVS with three image datasets; (a) 36 images, (b) 48 images and (c) 60 images.	105
Figure 4-15: Comparison of processing time from different image matching methods and the number of images; (a) image matching time and (b) data processing time.....	106
Figure 4-16: Comparison between original image and image after applying lens distortion correction; (a) before and (b) after.....	107
Figure 4-17: Configuration for photo control targets.....	109

Figure 4-18: Comparison of the mean distances of K-nearest neighbours using different parameters for automatic de-noising; (a) $N = 500$, $n = 1$ and (b) $N = 1000$, $n = 2$. The green and red lines show the mean distance and the threshold of outlier classification, respectively..... 111

Figure 4-19: Comparison of photogrammetric results when using different parameters for automatic de-noising; a) original point cloud, b) point cloud after automatic de-noising using $N = 500$, $n = 1$ and (c) point cloud after automatic de-noising using $N = 1000$, $n = 2$. The red circles show the outliers in the point cloud. 112

Figure 4-20: The histograms of green vegetation index from two point clouds acquired on (a) 20 March 2015 and (b) 10 June 2015. 114

Figure 4-21: Comparison of point clouds before and after vegetation filtering acquired on (a) 20 March 2015 and (b) 10 June 2015. 114

Figure 4-22: Comparison of conceptual diagrams for cloud comparison method using between (a) C2M and (b) M3C2 (Barnhart and Crosby, 2013). 116

Figure 4-23: Comparison results of change assessment using cloud comparison method based on (a) M3C2 and (b) C2M. 117

Figure 5-1: Overview of test site location at Hollin Hill landslide observatory: the red box shows the area used for this experiment. 122

Figure 5-2: Photograph of the main scarp at the top of the Hollin Hill landslide used for the photogrammetric monitoring experiment. 123

Figure 5-3: Illustration of landslide characteristics at Hollin Hill landslide: the red box shows the area used for the landslide monitoring experiment (Merritt *et al.*, 2014). 123

Figure 5-4: Illustration of photogrammetric configuration for each epoch. 125

Figure 5-5: The methodology scheme for the accuracy assessment of photogrammetric results at different epochs. 126

Figure 5-6: Illustrations of the different types of targets used for geo-referencing. 127

Figure 5-7: Photogrammetric point clouds obtained after applying each post-processing step; a) cropping, b) de-noising, and c) vegetation filtering. 129

Figure 5-8: Comparison of each image dataset used in the SfM photogrammetric approach at different times: the red boxes distinctly show the different brightness of images. .. 130

Figure 5-9: Three point clouds of photogrammetric results at different epochs from PhotoScan software acquired on: (a) 10 June 2015, (b) 12 February 2016 and (c) 26 May 2016. 132

Figure 5-10: Elevation difference of photogrammetric results at different times from the developed system (SkyPMMS) used in the assessment of landslide changes. 133

Figure 5-11: Elevation difference of photogrammetric results at different times from PhotoScan software used in the assessment of landslide changes.....	134
Figure 5-12: Illustration of the location of BGS pegs used in landslide monitoring....	137
Figure 5-13: Illustrations of coastal cliff site at two epochs acquired on: (a) 27 November 2016 and (b) 13 April 2017.....	139
Figure 5-14: Camera positions and viewing directions between two epochs acquired on (a) 27 November 2016 and (b) 13 April 2017.....	140
Figure 5-15: The methodology scheme for the accuracy assessment of photogrammetric results at different epochs.....	141
Figure 5-16: Comparison of four point clouds obtained using (a) raw images (SkyPMMS), (b) images corrected for lens distortion with the fixed calibration mode (SkyPMMS), (c) PhotoScan (d) and TLS survey (27 November 2016).....	144
Figure 5-17: Comparison of four point clouds obtained using (a) raw images (SkyPMMS), (b) images corrected for lens distortion with the fixed calibration mode (SkyPMMS), (c) PhotoScan (d) and TLS survey (13 April 2017).....	145
Figure 5-18: Comparison of distance differences between two datasets acquired on 27 November 2016 and 13 April 2017 from (a) the TLS approach, (b) the photogrammetric results using VisualSfM & PMVS and (c) PhotoScan using M3C2.....	150
Figure 5-19: The comparison of statistically significant change between two datasets acquired on 27 November 2016 and 13 April 2017 from (a) the TLS approach, (b) the photogrammetric results using VisualSfM & PMVS and (c) PhotoScan using M3C2.	151
Figure 5-20: Histograms of the distance differences between two point clouds acquired on 27 November 2016 and 13 April 2017 using M3C2 from (a) TLS survey, (b) photogrammetric results using VisualSfM & PMVS and (c) PhotoScan.	152
Figure 6-1: Front-end service: (a) mobile application; (b) web browser.....	157
Figure 6-2: The implementation of a DSLR or consumer-grade camera for image acquisition applied in the developed system.	159
Figure 6-3: Workflow of data processing for SfM-photogrammetry based on mobile devices and cloud computing (Nocerino <i>et al.</i> , 2017).	161
Figure 6-4: Extraction of (a) landslide scarp using analysis of the surface roughness index, and (b) orthophoto derived from UAV approach (Al-Rawabdeh <i>et al.</i> , 2016).....	168
Figure 7-1: Example of imagery used for photogrammetric landslide monitoring between (a) before and, (b) after masking of vegetation (Zhan and Lai, 2015).....	177
Figure 7-2: Example of (a) automatic detection of (b) coded target used for geo-referencing: the coded target is automatically found in the red boxed area.....	178

List of Tables

Table 2-1: Types of landslide in different velocity classes (Cruden and Lan, 2015).....	8
Table 2-2: Types of landslide activity (Cruden and Lan, 2015).	8
Table 2-3: Comparison of ground-based geomatics approaches for landslide monitoring (adapted from: Wang, 2013).	32
Table 3-1: Comparison of technical specifications between the two adopted smart phones: iPhone 4 and Nexus 6.	37
Table 3-2: Technical specifications of the Nikon D300 DSLR camera used in the research.	38
Table 3-3: Camera calibration results for the Nexus 6 smart phone camera using three different calibration routines.	42
Table 3-4: The options of the SfM-MVS approach (Micheletti <i>et al.</i> , 2015a).	48
Table 4-1: Statistics of distance errors between SfM models and TLS data for direct registration and after applying the ICP algorithm.	86
Table 4-2: Statistics of differences between the different SfM-outputs and the TLS data.	90
Table 4-3: Estimated data transfer time from a smart phone to the cloud server for 36 images (260MB in total).	92
Table 4-4: Comparison of B/D ratio used in each image dataset.	94
Table 4-5: Comparison between image resolution and size used in each approach.....	96
Table 4-6: Comparison of mean value for the differences between each SfM approach and the reference TLS data.....	98
Table 4-7: Comparison of RMSE value for the differences between each SfM approach and the reference TLS data.....	98
Table 4-8: Comparison of processing time between the different camera station and image resolution using SkyPMMS on the cloud.	101
Table 4-9: Comparison of image resolution between estimated file size and estimated upload time used in each approach. The data in brackets are estimated upload time using a 4G and a Wi-Fi network, respectively.	101
Table 4-10: Data processing time of each stage in the SfM workflow obtained from different numbers of images.....	104

Table 4-11: Comparison of image matching time and data processing time using full- and pre-image matching method.	106
Table 4-12: Statistics of distance differences between the different SfM results and the TLS data.	108
Table 4-13: Statistics of measuring distances between each photo control target.	109
Table 4-14: Statistics of distance differences between the SfM results obtained from different geo-referencing with the dimensions of known objects and applying ICP and the TLS data.	110
Table 4-15: Comparison for statistics of differences between the TLS data and the SfM point clouds before and after automatic de-noising.	113
Table 4-16: Statistics of differences between the SfM point clouds and reference TLS data and the comparison between before and after vegetation filtering.	115
Table 4-17: The appropriate parameters based on a point cloud comparison method using M3C2 (Stumpf <i>et al.</i> , 2015).	116
Table 4-18: Statistics of differences between two photogrammetric results using M3C2 and C2M cloud comparison method.	118
Table 4-19: Summary of findings from Chapter 4 experimentation.	119
Table 5-1: Comparison of a B/D ratio used in each epoch.	125
Table 5-2: Results after target-based geo-referencing of each epoch.	126
Table 5-3: Comparison of processing time between the different SfM software and the different performance of GPU cloud server.	128
Table 5-4: Point cloud comparisons of photogrammetric results at different times and the TLS data.	128
Table 5-5: Statistics of the differences between TLS data and SfM-photogrammetric results for each epoch after post-processing stages using C2M.	131
Table 5-6: Comparison statistics of elevation changes from TLS data and different SfM-photogrammetric approach (SkyPMMS and PhotoScan).	135
Table 5-7: Comparison between cumulative displacement of GNSS survey and elevation changes of TLS data and SfM approach.	138
Table 5-8: Comparison of B/D ratio used at each epoch.	141
Table 5-9: Statistics of the results from geo-referencing using photo control targets and after applying ICP.	142

Table 5-10: Comparison between the SfM-photogrammetric results and TLS data acquired on 27th November 2016 and 13th April 2017.	143
Table 5-11: Statistics of distance differences between TLS data and SfM results from original and images corrected for lens distortion with fixed calibration mode.....	146
Table 5-12: Statistics of distance differences between TLS data and SfM results from images corrected for lens distortion with the fixed calibration mode after applying ICP.	147
Table 5-13: Statistics of distance differences between TLS data and SfM results from images corrected for lens distortion with the fixed calibration mode, different georeferencing.....	147
Table 5-14: Statistics of the distance differences between two epochs acquired on 27 November 2016 and 13 April 2017 from (a) TLS survey, (b) SfM-photogrammetric approach of VisualSFM & PMVS and (c) PhotoScan using M3C2.....	153

List of Abbreviations

ALS	Airborne laser scanning
BGS	British Geological Survey
C2C	Cloud-to-cloud comparison
C2M	Cloud-to-mesh distance
CCD	Charge coupled device
CLI	Command line interface
CMOS	Complementary metal oxide semiconductor
CPU	Central processing unit
DEM	Digital elevation model
DLT	Direct linear transformation
DoD	DEM of difference
DPW	Digital photogrammetric workstation
DSLR	Digital single-lens reflex
DTM	Digital terrain model
ERT	Electrical resistivity tomography
FOV	Field of view
GBSAR	Ground-based synthetic aperture radar
GI	Green vegetation index
GNSS	Global navigation satellite system
GPS	Global positioning systems
GPU	Graphical processing unit
HTTP	Hyper text transfer protocol
ICP	Iterative closest point
ICT	Information and communication technology
IDE	Integrated development environment
IMU	Inertial measurement unit
InSAR	SAR Interferometry
IoT	Internet of things
LIDAR	Light detection and ranging technology
M3C2	Multiscale model-to-model cloud comparison
MVS	Multiview-stereo
Radar	Radio detection and ranging
SAR	Synthetic aperture radar
SfM	Structure-from-Motion
SIFT	Scale-invariant feature transform
SOR	Statistical outlier removal

SURF	Speeded-up robust features
TLS	Terrestrial laser scanning
UAV	Unmanned aerial vehicle
VM	Virtual machine

Chapter 1. Introduction

1.1 Overview

Landslides are generally found to be one of the most common environmental disasters occurring in natural terrain and man-made slopes (Davies, 2015). Landslides can have a disastrous effect on infrastructure, buildings and facilities, causing a serious threat to human life, economic loss, and society (Lee and Jones, 2004; Regmi *et al.*, 2015). The assessment and monitoring of landslide hazards therefore plays an important role in the mitigation of damage to humans, society and the environment (Koizumi *et al.*, 2013). Furthermore, the development of landslide monitoring systems may also help to enhance understanding of landslide behaviour. Thus, the investigation of landslide hazards should be undertaken appropriately and regularly. In particular, the monitoring and inspection in early-stage ground movements are essential for reducing the risk of landslides (Sassa *et al.*, 2007). For example, the investigation of landslide movements by geologists and geotechnical engineers adopts different approaches ranging from simple, traditional methods to professional technologies, depending on the monitoring purposes and financial costs. However, current geomatics approaches used for precise landslide monitoring are somewhat inappropriate for initial assessment by an engineer over small areas due to the labour-intensive and costly methods often adopted (Niethammer *et al.*, 2012). Therefore, the development of a cost-effective landslide monitoring system for real-time on-site investigation is desirable in order to aid initial geotechnical interpretation and assessment of landslide phenomena.

With regard to using conventional geomatics approaches for ground-based landslide monitoring, the following problems are identified in their adoption for initial on-site assessment:

1. High financial-cost of equipment and maintenance for surveying (Travelletti *et al.*, 2012);
2. Non-friendliness in operations (Piermattei *et al.*, 2015);
3. Requirement for data processing and analysis by experts (Teza *et al.*, 2007);
4. Difficulties in managing and processing of data in the field (James and Robson, 2012);

Due to the increasing development of mobile device technology, high-resolution digital cameras can be employed to potentially offer a cost-effective photogrammetric solution (Wang, 2013). In particular, close-range photogrammetric techniques using images from a mobile device camera (e.g. a modern smartphone) is proposed for a low-cost, non-contact monitoring approach in terms of implementation, operation and equipment for landslide investigation. Furthermore, the development of the Internet of things (IoT), including Internet services and cloud computing technology, plays an increasingly important role in implementing and deploying near-real-time processing in geoinformatics applications on mobile platforms (Lee and Kang, 2013). Such developments could lead to a low-cost, real-time photogrammetric solution for in-situ landslide monitoring using a mobile device.

This research therefore focuses on exploiting modern smart phone technology to develop a photogrammetric measurement system for real-time monitoring of landslides. The development of the mobile platform-based photogrammetric services is implemented using cloud-based computing technology to offer the potential for the development of a real-time on-site measurement system. The study involves analytical processes in order to obtain temporal change information for landslides. The developed functionality of the system is utilised to facilitate the photogrammetric processing and landslide monitoring analysis through a mobile application for non-experts. Validation is performed at two existing test sites to prove the efficiency of the developed system.

1.2 Research problem and background of landslide monitoring

1.2.1 Definition and potential problems

Landslide monitoring involves the acquisition of information on an unstable slope and the utilization of the observations to assess its condition and the active processes that might result in failure of the slope. The development of landslide monitoring is essential to retrieve critical information underlying slope failure. However, landslides are usually associated with various natural phenomena and are complex. To minimise the impact of potential landslide hazards through monitoring, it is essential to study the behaviour and destructive intensity of a landslide, which is mainly related to kinetic parameters such as velocity and acceleration.

Landslide instrumentation and monitoring have been increasingly developed based on both geotechnical/geophysical and geomatics techniques (Kapeller *et al.*, 2013). However, each method of landslide monitoring has inherent advantages and disadvantages that should be considered to develop an appropriate landslide monitoring system for on-site investigation. In particular, both geotechnical and geophysical investigations are well-established and offer effective acquisition of sub-surface information (Uhlemann *et al.*, 2016). However, despite being suitable for landslide monitoring, limitations include the discrete character of observations and restricted spatial coverage. Furthermore, the establishment of geotechnical and geophysical monitoring systems can be labour-intensive, invasive and not always cost-effective (Miller *et al.*, 2012).

In landslide risk assessment, surface observations using geomatics techniques can play an important role in providing topographic information for landslide monitoring. However, the applicability of geomatics techniques in ground-based landslide monitoring has its own limitations, especially the high financial costs traditionally associated with instrumentation, operation and maintenance. Moreover, processing in the field is difficult to manage, and therefore these techniques are generally not suitable for real-time, on-site investigations of landslide monitoring. To reduce the risk of landslide hazards, the development of an appropriate monitoring system for real-time, on-site investigation is important to help initial geotechnical interpretation and assessment.

1.2.2 Motivation for study

In terms of landslide monitoring applications, most ground-based geomatics approaches are primarily targeted at highly precise measurement. Due to the often labour-intensive, time-consuming and costly methods adopted, these approaches are inappropriate for the initial assessment of on-site investigations, especially in the case of small landslides.

Considering the destructive impacts of landslide hazards, the monitoring of small areas should be undertaken appropriately and regularly. For the initial assessment of landslide processes, a close-range photogrammetric technique can be used for landslide monitoring as it is a lower cost approach in terms of implementation, operation and equipment (Travelletti *et al.*, 2012). The huge demand for spatial information on the kinematics of landslides in order to be used for the assessment of landslide processes in real-time is noticeably increasing. However, the adoption of a close-range photogrammetric system for on-site investigation is still difficult because it necessitates management of a large amount of data in real-time.

The development of advanced technologies in recent years have become more important for data acquisition in landslide monitoring applications. Mobile devices can now be employed to provide information from the field because they have many useful sensors for in-situ observations. Thus, this research attempts to develop a cost-effective photogrammetric measurement system for a real-time, in-situ landslide monitoring based on a mobile device platform.

1.3 Aim and objectives

This research aims to exploit mobile device and other modern information and communication technology (ICT) in order to develop a photogrammetric measurement and monitoring solution for real-time slope stability hazard analysis. To achieve this aim, the objectives of the research are:

1. To investigate the potential of commonly used approaches and technologies in landslide monitoring and to propose the basic requirements of a low-cost photogrammetric solution for initial landslide assessment during on-site investigations by non-photogrammetrists;

2. Building on objective 1, to develop the mobile platform-based photogrammetric services associated with cloud-based computing technology for the provision of real-time slope monitoring information;
3. To exploit the photogrammetric results by developing appropriate functionality to assess landslide temporal change directly using a mobile device;
4. To ensure the accuracy and reliability of the results and the capabilities of the low cost sensors found on common mobile devices for landslide monitoring applications by validating the developed system at real-world test sites;

1.4 Research scope

System development of an in-situ landslide monitoring was based on a low-cost solution in terms of implementation and operation. System implementation has therefore utilised only off-the-shelf software and tools. Firstly, close-range photogrammetry has offered a flexible, low-cost approach to monitoring. Secondly, affordable mobile devices (such as tablets, smart phones) with built-in digital cameras provided a cost-effective instrument for image acquisition. The user can also employ the operation of the system through this mobile device. Thirdly, the low-cost photogrammetric processing solution was based only on free-software. Furthermore, the development of the system has been implemented with other free or open source software packages, such as that for camera calibration and point cloud processing. Finally, the use of cloud-computing services, such as the cloud-based server, cloud storage, etc., were implemented to facilitate development.

1.5 Thesis structure

Chapter 1 has provided an overview of the thesis and presented the aim and objectives of this research.

Chapter 2 reviews the background of landslide hazards and reviews the capability of different approaches for landslide monitoring, which subsequently informs the design and development of a low-cost, real-time landslide monitoring system.

Chapter 3 presents the close-range photogrammetric methodologies adopted for on-site investigation of landslide hazard analysis. The details of the development and implementation of a mobile platform-based landslide monitoring system are reported in this chapter.

Chapter 4 reports the inspection of the system developed on the cloud and performance evaluation of functions employed for improved photogrammetric processing and landslide monitoring analysis.

Chapter 5 involves the real-world testing and assessment of the developed system by monitoring at existing sites comprising different types of landslide hazard.

Chapter 6 discusses the suitability of the system adopted for in-situ landslide monitoring based on the findings, which are reported in Chapters 4 and 5.

Chapter 7 summarises the studies undertaken and presents the contributions and potential future work in this research.

Chapter 2. Techniques for landslide monitoring

2.1 Introduction

Advanced technologies have been developed in various ways in recent years for application to the monitoring and inspection of landslide hazards. The capability of each technique for landslide monitoring is discussed in this chapter. Taking into consideration measurement methods in the investigation of landslide hazards, the results of a review of these approaches is utilised for the design and development of a low-cost, real-time landslide monitoring system in this research.

2.2 Landslide hazards and landslide monitoring

Climate change is a global issue and is one of the leading factors influencing natural disasters (Datar *et al.*, 2013). At present, natural disasters are also increasing in terms of frequency, complexity and destructive capacity (Sassa *et al.*, 2007). Climate change also leads to many types of severe natural disaster, such as floods, drought, heavy storms, earthquakes and landslides. Among the many forms of natural disaster, landslides are one of the most common, causing a serious threat to human life and economic losses to society. Therefore, reducing the risk of landslides is an important consideration in preparing capability for disaster mitigation.

A landslide is defined as “the movement of rock, debris or earth down a slope” (Lee and Jones, 2004). Occurrences of landslides usually result from both internal and external factors which can cause changes in their physical mechanisms. External factors influencing the stability of slopes are mainly triggered by rainfall or earthquakes, whereas sub-surface conditions of physical components and ground water levels are the primary internal factors (Scaioni, 2015). However, landslides are associated with various natural phenomena and are highly complex. To minimise the impact of landslide hazards through monitoring, it is essential to study the behaviour and destructive intensity of a landslide, which is mainly related to kinetic parameters such as velocity and acceleration.

Typically, landslide occurrences can cause a variety of behaviour. Landslides are usually classified in terms of both movement and materials. The type of material involved is described by the addition of an adjective in front of the landslide category, while landslide movement can be classified in terms of the displacement rate of material, as indicated in Table 2-1. Descriptions of each landslide type are shown in Table 2-2.

Table 2-1: Types of landslide in different velocity classes (Cruden and Lan, 2015).

Class	Movement rate	Velocity
7	Extremely rapid	>5 m/sec
6	Very rapid	3 m/min
5	Rapid	1.8 m/hr
4	Moderate	3 m/week
3	Slow	1.6 m/year
2	Very slow	16 mm/year
1	Extremely slow	<16 mm/year

Table 2-2: Types of landslide activity (Cruden and Lan, 2015).

State of activity	Style of activity	Rate of movement	Material	Type
Preparatory	Complex	Extremely rapid	Rock	Fall
Marginal	Composite	Very rapid	Soil:	Debris
Active	Multiple	Rapid		Earth
Reactivated	Successive	Moderate		Sand
Suspended	Single	Slow		Silt
Inactive		Very slow		Clay
				Topple
				Slide
				Spread
				Flow

The deformation monitoring of an active landslide can help to display a general failure and movement (Figure 2-1). Due to pre-failure movement in landslides, the monitoring of small displacements can help in reducing the risk of damage from a landslide occurring (Lee and Jones, 2004).

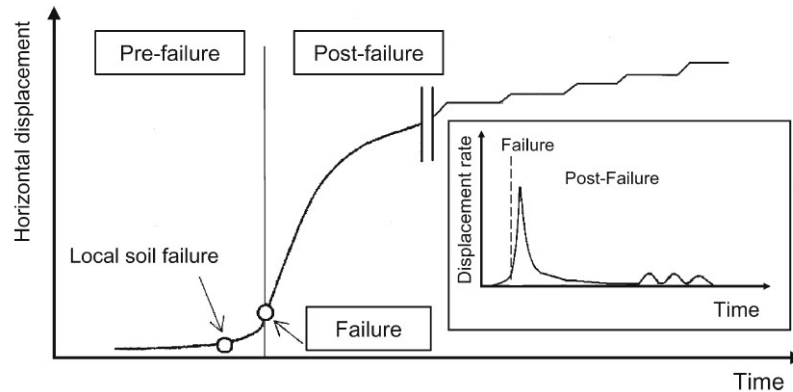


Figure 2-1: Illustration of slope movement in the pre-failure stage (Sassa *et al.*, 2007).

Both the behaviour and type of landslides are taken into consideration in the design of landslide monitoring systems and to represent the limitations of each monitoring approach. The design of an appropriate landslide monitoring system is related to four factors (Travelletti *et al.*, 2012) :

- Landslide type and size;
- The range of observed velocity;
- The required frequency of data acquisition;
- The desired accuracy and the financial constraints;

Landslide instrumentation and monitoring are generally developed based on both geotechnical/geophysical techniques and geomatics techniques (Kapeller *et al.*, 2013). However, each method of landslide monitoring has both advantages and disadvantages. In order to develop an appropriate landslide monitoring system for on-site investigation, a review of landslide monitoring techniques based on different approaches is presented.

2.2.1 Geotechnical and geophysical techniques

Fundamental knowledge of both geology and geotechnics is essential in being able to explain the first steps of landslide activity (Intrieri *et al.*, 2012). In-depth studies of landslide processes also benefit from such an understanding in order to identify the critical conditions of slope instability. The development of landslide monitoring is based on geotechnical and geophysical approaches to retrieve critical information underlying slope failure. At present, many geotechnical and geophysical techniques may be used, ranging from simple, traditional methods such as extensometers, inclinometers or tiltmeters, piezometers and pore pressure sensors to professional landslide monitoring sensors which utilise electrical resistivity tomography (ERT). The main techniques used in both geological and geotechnical engineering are reviewed in this section.

2.2.1.1 Extensometers

Extensometers are one of the classical instruments used for in-situ landslide investigation, and are commonly employed to measure the displacement of ground surface or vertical movement in the ground between fixed points along the sliding direction. Extensometers are installed according to the type of measurement point required: 1) an opening measured on the landslide surface; or 2) in a borehole to detect changes in shear surfaces at depth, as shown in Figure 2-2 and Figure 2-3.

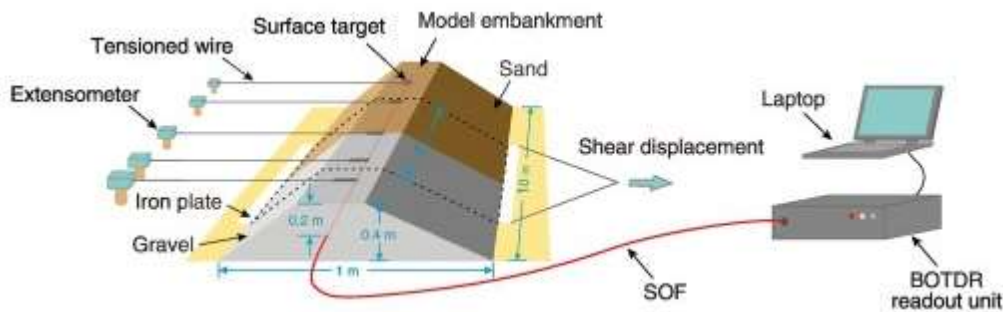


Figure 2-2: Illustration of opening wire extensometers (Zhang *et al.*, 2018).

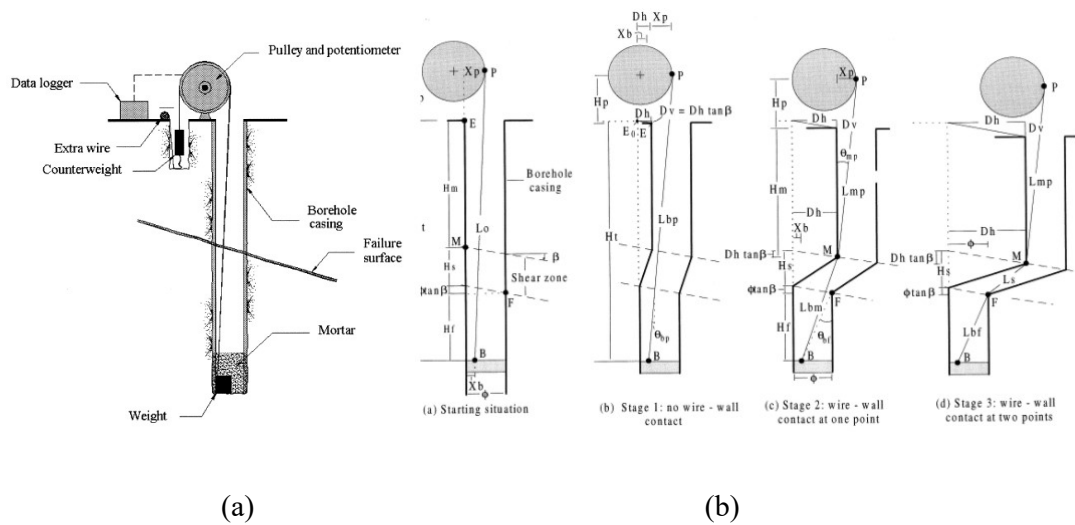


Figure 2-3: Illustration of extensometer in a borehole: a) device components; and b) stages in the changed positions of a wire extensometer used for the investigation of landslide displacements (Corominas *et al.*, 2000).

In addition, in monitoring change associated with landslides, measurements are taken with various types of extensometers, such as probe or magnet extensometers using vibrating wire electronics, or fibre optics and rod extensometers using sliding rods. For example, the assessment of large movements due to cracks over a landslide surface can be observed by connecting simple wire-to-wire extensometers (Bandara *et al.*, 2013). For rock mass monitoring, as shown in Figure 2-4, conventional tape extensometers are extensively used to detect large movements on the surface (Arosio *et al.*, 2013; Devoto *et al.*, 2013; Stefani *et al.*, 2013). However, before a slope failure, the installation of instruments can interfere with the measurement of movements due to drilling and the setting up of geotechnical tools (Tuan *et al.*, 2013).

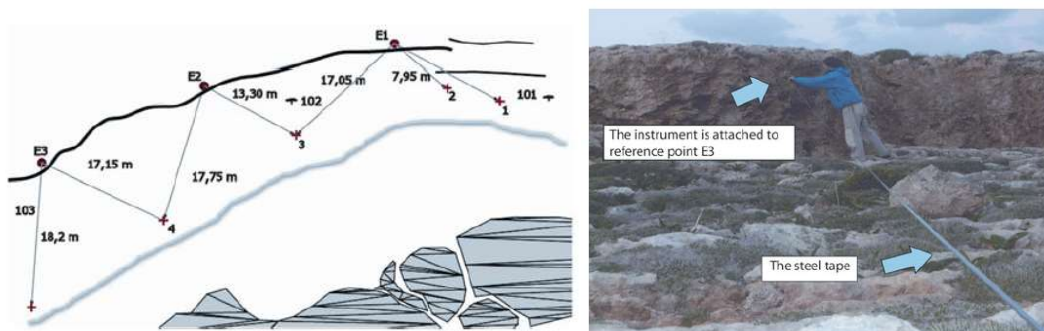


Figure 2-4: Illustration of a tape extensometer network for rock mass monitoring (Devoto *et al.*, 2013).

Deformation monitoring may be affected by different weather conditions, such as moisture and temperature level variations as a result of seasonal changes. However, extensometers can provide reliable data when compared to other survey methods; for example using laser distance measurement device. As shown in Figure 2-5, extensometers can provide displacement data with little noise during the winter.

The assessment of landslide displacement and slope stability using extensometers can deliver continuous monitoring. Moreover, extensometer sensors are usually employed in early warning systems (Bandara *et al.*, 2013). Although these conventional geotechnical tools give highly reliable measurements in landslide monitoring, some uncertainty may be caused by interaction between their electronic components including transducers and digital converters (Intrieri *et al.*, 2012).

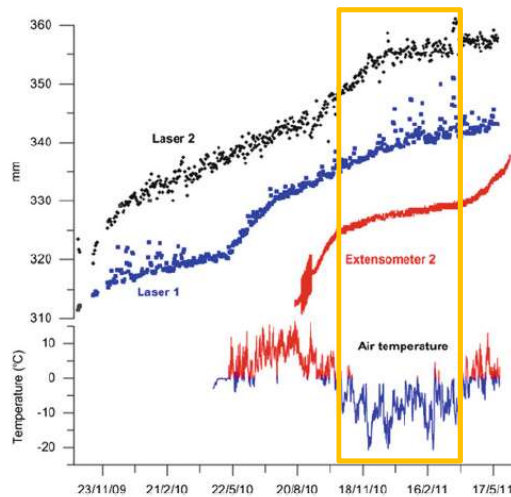


Figure 2-5: Comparison of landslide displacement data from distance measurement devices and an extensometer (Kristensen and Blikra, 2013).

2.2.1.2 Inclinerometers

Based on landslide monitoring sensors, conventional inclinometers are usually instruments designed to measure horizontal deflections in the ground. Moreover, these sensors reveal the precise depth of the slip plane or a multi-slip surface (Di Maio *et al.*, 2013). Figure 2-6 shows the installation of an inclinometer sensor in a borehole for ground measurements. For inclinometer-based landslide monitoring, movement results can reveal differences in cumulative displacement in two measuring planes (Figure 2-7).

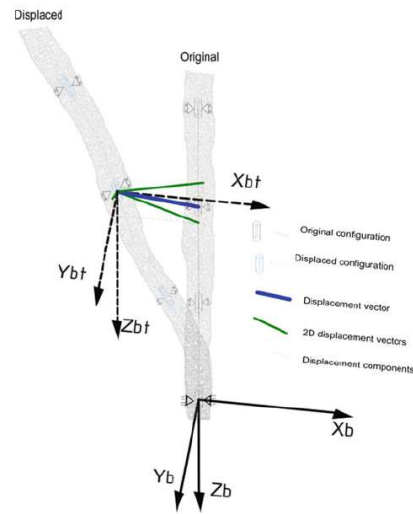


Figure 2-6: Measurement of horizontal displacements using an inclinometer (Segalini and Carini, 2013).

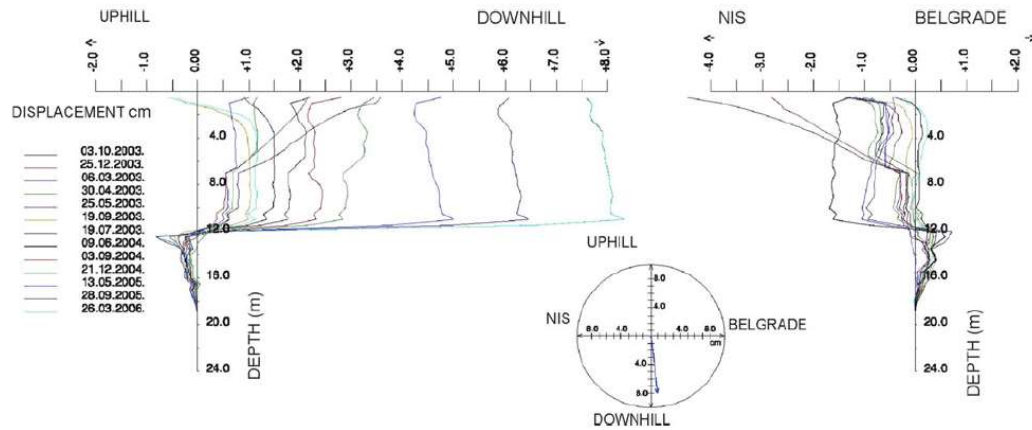


Figure 2-7: Comparison of differences in cumulative displacements in two directions using an inclinometer (Milenkovic *et al.*, 2013).

Typically, the displacement rates and the depth of shear surfaces are determined using time-series data from an inclinometer sensor. For automated monitoring of sub-surface deformations, the installation of inclinometers in a borehole is usually more complicated and expensive than with extensometers due to the high-cost of the inclinometer sensor. Moreover, unreliability of the mechanical system is often related to casing deformation (Segalini and Carini, 2013). Therefore, inclinometers can often provide only low spatial resolution information concerning sub-surface deformations surrounding a borehole (Uhlemann *et al.*, 2016).

2.2.1.3 Piezometers and pore pressure sensors

For ground water monitoring, piezometers and pore pressure sensors are generally used to measure water levels and pore-water pressure in a borehole. These sensors can also provide essential information in order to predict slope stability due to the relationship of soil water-saturation in landslide monitoring. To acquire hydrological data for landslide monitoring, the piezometer technique can help to reveal significant seasonal changes related to shorter-term variations in ground water levels, as shown in Figure 2-8. In a subsurface investigation using piezometers, Wasowski *et al.* (2013) identified that short-term rainfall events are found to be among the main factors associated with shallow landslide occurrences.

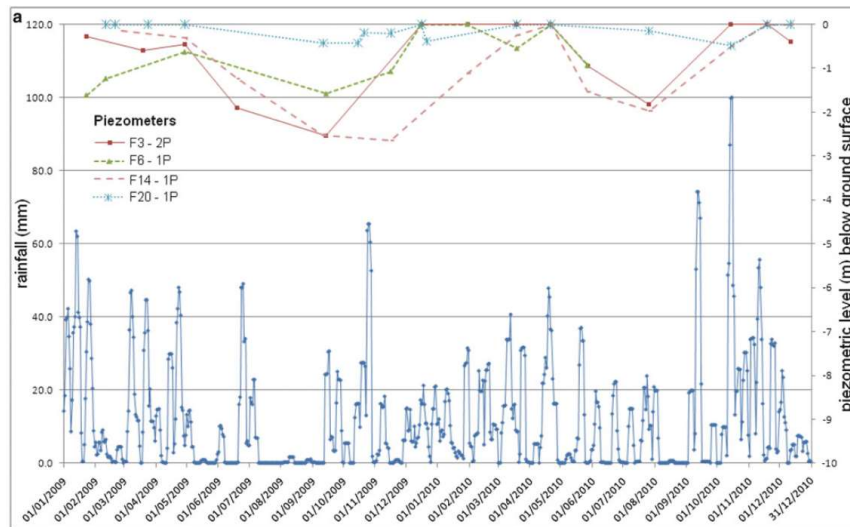


Figure 2-8: Comparison of the relationship between rainfall and piezometric level (Wasowski *et al.*, 2013).

2.2.1.4 Electrical resistivity tomography (ERT)

ERT is a geoelectrical ground imaging technique used in professional landslide monitoring sensors to study landslide structure and the process of slope failure (Chambers *et al.*, 2013). In particular, geophysical measurements based on the ERT method are used to study the depths of sliding surfaces and water zones in the ground through observation of resistivity data (Reci *et al.*, 2013). ERT monitoring can also provide highly precise data on the mechanisms of sub-surface deformations for 3D modelling investigations of landslides (Figure 2-9 (b)).

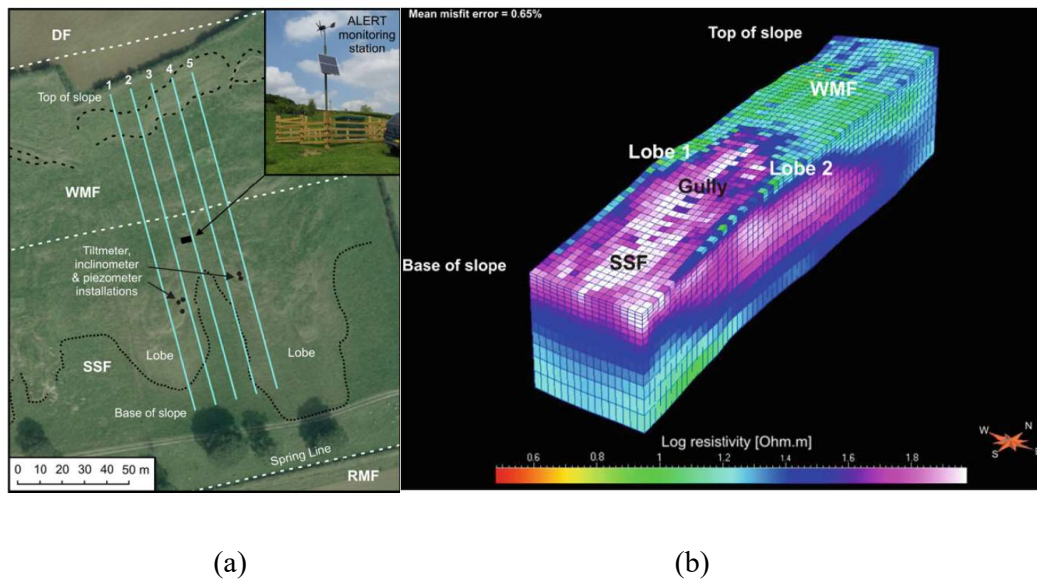


Figure 2-9: Illustrations of (a) the locations of installation for ERT landslide monitoring, and (b) 3D model of landslide obtained from ERT monitoring (Chambers *et al.*, 2013).

However, this approach sometimes requires the installation of ERT monitoring arrays on hard material, as per Figure 2-9 (a), with a layout of electric cables and electrodes (Furuya *et al.*, 2013). Although ERT monitoring is more suitable for studying the processes of landslides over time, in the case of active landslide monitoring the movement of electrodes can misrepresent the changes in resistivity in the subsurface. Consequently, 3D landslide models need to be calibrated with time-lapse resistivity data (Wilkinson *et al.*, 2010). In-situ observations using the ERT method can also be applied to provide motion data for near-real-time landslide monitoring (Chambers *et al.*, 2013). Therefore, electrical resistivity surveys are used to provide subsurface information in landslide monitoring.

2.2.1.5 Additional instruments

Tilt meters or sensors can be used to monitor the displacement of slopes, and are similar to geotechnical approaches using extensometers. However, the installation of a tilt sensor is simpler because no long wires are required. Moreover, the maintenance costs are also low (Uchimura *et al.*, 2013). Typically, tilt sensors can also be integrated with other sensors, such as volumetric water content sensors, as shown in Figure 2-10.

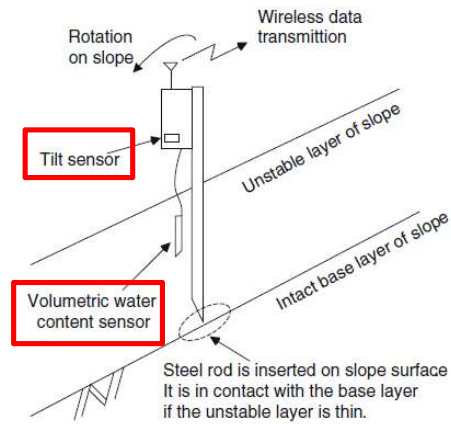


Figure 2-10: Illustration of tilt and water content sensors implemented in a wireless unit (Uchimura *et al.*, 2013).

Landslide movements are often triggered by rainfall. In particular, heavy rainfall events have a direct effect on increasing the volumetric water content in the ground. In simple rainfall-induced landslides, rainfall gauges are used for the direct measurement of rainfall in landslide monitoring. Also, thermometers are used to observe the weather conditions around landslide areas, as shown in Figure 2-11.



Figure 2-11: Example of a weather station, including rainfall gauge and thermometer (Bednarczyk, 2013).

In conclusion, geotechnical and geophysical landslide monitoring involving both conventional techniques such as extensometers, inclinometers and piezometers and recent developments including ERT monitoring can provide efficient, accurate and useful information for in-situ investigations of slope stability. In particular, both geotechnical and geophysical investigations are well-established and offer effective acquisition of sub-surface information (Uhlemann *et al.*, 2016). However, despite being suitable for landslide monitoring, limitations include the discrete character of observations and restricted spatial coverage. The establishment of geotechnical and geophysical monitoring systems can also be labour-intensive, invasive and not always cost-effective (Miller *et al.*, 2012). Consequently, the installation of such systems is often more suitable once a landslide is known to exist (Perrone *et al.*, 2014), and these monitoring systems are also recommended for at-risk hillsides (Kapeller *et al.*, 2013). Therefore, geotechnical and geophysical investigations with additional instruments such as rainfall gauges and thermometers are more suitable for the implementation of landslide early warning systems (Intrieri *et al.*, 2012).

2.2.2 Geomatics techniques

Geomatics technologies have been extensively used for the acquisition of geospatial data for various earth science applications in the last few decades. Geomatics techniques which can be used to measure surface movements in landslides include global navigation satellite systems (GNSS), satellite remote sensing, light detection and ranging (lidar) technology and photogrammetry. Geomatics techniques can be sub-divided in many ways, but can be generally split into two main groups for the purposes of landslide monitoring: airborne/space-borne and ground-based approaches. Both can be used to investigate the kinetics of landslides, consisting of ground movements and displacement rates. For the study of landslide processes, sub-surface changes often only reveal themselves through surface expressions of movement, where surface deformations will often reveal underlying patterns of slope failure (Miller *et al.*, 2008). Although geotechnical and geophysical techniques can provide highly accurate subsurface information in landslide monitoring, surface observations using geomatics techniques can play an important role in low-cost monitoring for landslide assessment. Thus, a brief overview of geomatics techniques based on airborne/space-borne and ground-based

approaches is presented to inform the appropriate solution for subsequent development of a landslide monitoring system.

In terms of space- and airborne-based landslide monitoring approaches, these remote sensing techniques are widely used for data acquisition from multiple altitudes and platforms. Geospatial data can be collected using remote sensing techniques such as satellite observations, synthetic aperture radar (SAR), lidar, aerial photogrammetry or unmanned aerial vehicle (UAV) platforms. Each approach may provide different details of spatial information, depending on the level of altitude for observation (Lillesand *et al.*, 2008). Thus, each remote sensing technique should be considered to investigate its potential in landslide monitoring.

Based on the observations from high altitudes, modern satellite remote sensing can be used to identify landslides over large areas (Behling *et al.*, 2014). In general, satellite approaches are based on two types of imaging system, which include optical sensors or passive sensing, and microwave or active sensing. Earth observation from satellites such as Landsat and SPOT can deliver multispectral image data that can be analysed and interpreted as geographical information for landslide monitoring. Then, a historical landslide inventory can be carried out using multi-temporal analysis of geographical information collected at different times, as shown in Figure 2-12. Historical landslide inventories also have many benefits in landslide risk assessment and disaster management (van Westen *et al.*, 2013).

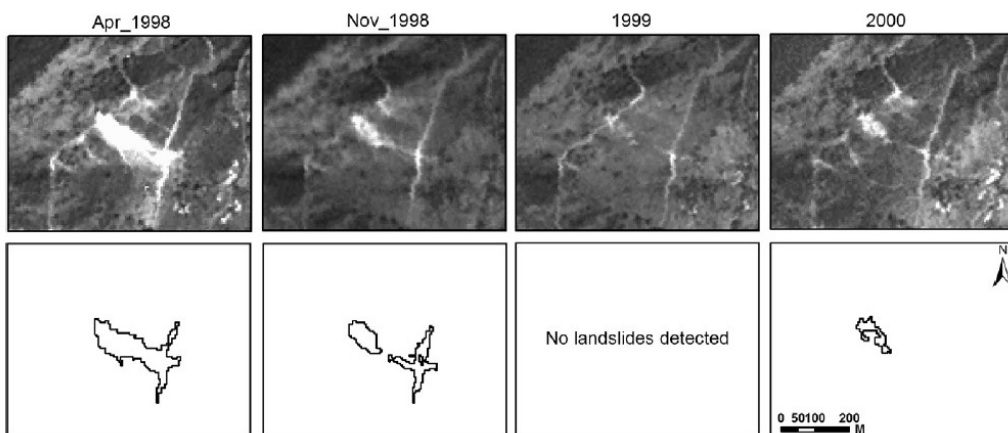


Figure 2-12: Example of a historical landslide inventory obtained from multi-temporal remote sensing (Martha *et al.*, 2012).

Remote sensing using spaceborne radar is an active, day-or-night imaging system which can penetrate the atmosphere and is not influenced by solar illumination for data acquisition. A popular Radar imaging technique for surface monitoring in geoscience applications is SAR interferometry (InSAR). However, data processing and analysis of phase difference information using the InSAR method for measuring precise landslide displacements is complex for non-experts (Lillesand *et al.*, 2008). Moreover, InSAR-based landslide monitoring is more suitable for the inspection of slow-moving landslides over large areas, as shown in Figure 2-13 (Zhang *et al.*, 2015).

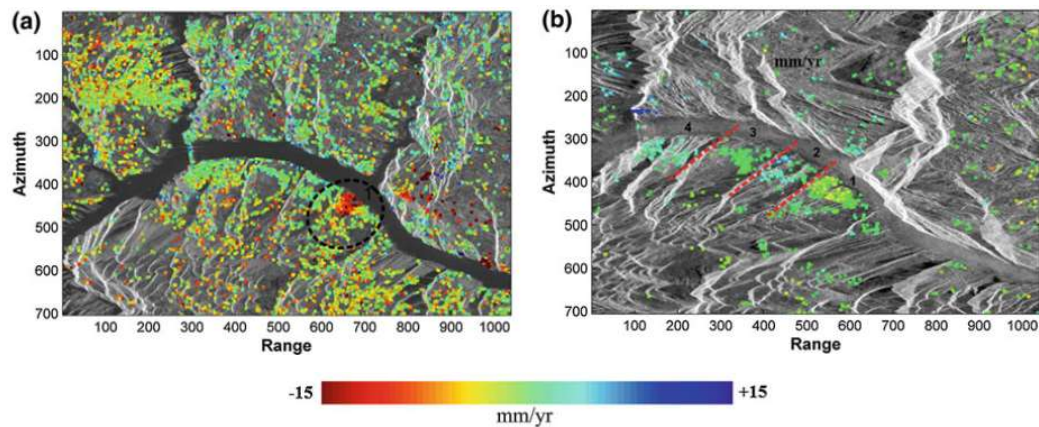


Figure 2-13: Comparison of landslide monitoring for deformation velocities using SAR satellites from: (a) ALOS/PALSAR data; and (b) ENVISAT/ASAR ascending data (Zhang *et al.*, 2015).

In terms of airborne-based landslide monitoring, aerial photogrammetry can deliver aerial imagery and derived digital elevation model (DEM) from analytical stereoplotters and digital photogrammetric workstations (DPWs). Orthophoto mapping can be produced by ortho-rectifying imagery using a DEM. Meanwhile airborne laser scanning (ALS) can directly measure the earth's surface using lidar and GNSS technology to provide high-accuracy and high-resolution 3D geospatial data in the form of a digital terrain model (DTM). This useful geospatial information is often used for landslide detection, and the historic deformation of landslides can be investigated using a multi-temporal approach. Although both methods can quickly produce mapping for landslide monitoring over large areas, the costs of surveying in this way are usually high. Moreover, the detection of deformation does not allow the inspection of small landslide features because of the inability to monitor landslides at lower spatial scales (Piermattei *et al.*, 2015).

In addition, topographic complexity creates occlusions in aerial photogrammetric approaches for assessing landslide deformations, especially over mountainous areas due to large elevation differences and rough surfaces (Kääb, 2002). As a result of this, the challenge of generating precise DEMs for small areas in order to quantify change created by landslides can be problematic (Micheletti *et al.*, 2015b). Due to uncertainties in DEM generation, topographic data over complex surfaces may be degraded by optical variations in photogrammetric approaches, especially when image quality is inadequate for processing (Lim *et al.*, 2005). In the case of the coastal cliff monitoring, there might be problems with the application of aerial photogrammetry and airborne laser scanning. For example, these approaches may be unsuitable for near-vertical slope monitoring because they cannot deliver sufficient surface information of a coastal cliff for change detection due to shadowing (Rosser *et al.*, 2005).

Compared to landslide monitoring with lower altitude data, small UAVs can be deployed to apply photogrammetric or lidar approaches, which have been increasingly utilised for data acquisition in recent years due to the cost-effectiveness of the method and the ability to provide highly accurate high-resolution geospatial data (Niethammer *et al.*, 2012). In general, data collection based on UAV platforms can prove more convenient and flexible than satellite and airborne platforms for observation when studying landslide processes (Lucieer *et al.*, 2014). A mini-UAV system typically comprises a multi-rotor or a fixed-wing UAV installed with an off-the-shelf or consumer-grade digital camera and on-board GNSS. However, a lightweight system is important in order to limit the power consumption of a mini-UAV platform. The main limitation of mini-UAV surveying is the fact that weather conditions such as strong (or even moderate) gusts of wind, fog or mist may affect the flight during observation. Consequently, it is difficult to control the quality of image data acquired (Peppas *et al.*, 2016). Also, the use of blurred images in photogrammetric measurement may lead to vertical deformations in 3D reconstructions (James and Robson, 2012).

Typically, remote-sensing datasets can be principally used to investigate surface displacements associated with landslides (Travelletti *et al.*, 2012). In particular, landslide inventory mapping and landslide susceptibility analysis can be conducted using geospatial information gathered using remote-sensing techniques. The main advantage of remote sensing for landslide monitoring is that it is less labour-intensive than

conventional geotechnical or geophysical techniques. However, traditional airborne- and satellite-based remote sensing approaches are generally more suitable for landslide detection over large areas (Niethammer *et al.*, 2012). If such approaches are used for small area monitoring, data need to be collected frequently, which results in high expense. Moreover, real-time data processing is difficult to manage, and therefore these techniques are generally not suitable for on-site investigations of landslide monitoring.

Although high-magnitude landslides may be catastrophic for human life and communities, small- and medium-magnitude landslides occur more frequently than high-magnitude landslides (Lee and Jones, 2004). Consequently, they result in severe impacts, especially in terms of economic loss. Considering these destructive impacts, landslide monitoring for small areas should be undertaken appropriately and regularly. There are many geomatics techniques which utilise ground-based platforms suitable for the investigation of small landslide displacements and features, such as total stations, GNSS, terrestrial laser scanning (TLS), ground-based synthetic aperture radar (GBSAR) and close-range photogrammetry. The following sections explain the most commonly used ground-based landslide monitoring techniques that may be used to find an appropriate solution for on-site investigation.

2.2.2.1 Total stations

Total stations are mostly used in surveying and civil engineering because they can provide direct measurements with high precision in terms of both angles and distances (Uren and Price, 2010). In a topographic survey for geoscience applications, landslide displacement and monitoring can be traditionally undertaken using total stations. The total station can be used for measuring three-dimensional coordinates derived from angle and distance measurements. At present, some models of total station, such as robotic total stations, can be automatically or remotely controlled in order to provide more convenient and automated measurement. Typically, electronic distance measurements using a total station requires reflectors or reflecting prisms that are permanently established at observation locations to detect landslide movements, as shown in Figure 2-14.

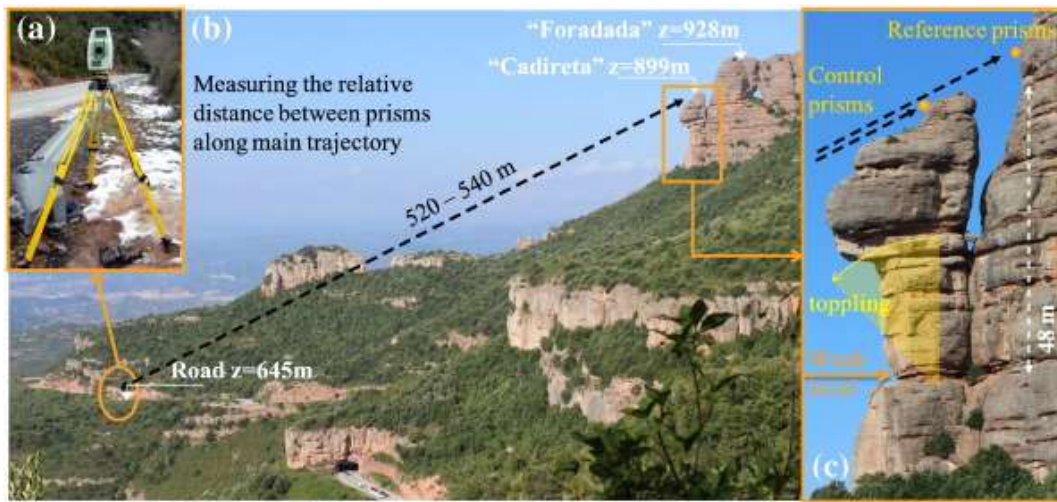


Figure 2-14: (a) A total station used for (b) rock mass monitoring at Cadireta; and (c) the installation of reflecting prisms on rock needles (Janeras *et al.*, 2017).

In reflectorless measurements, some models of total station can make distance measurements without using reflectors or prisms. The advantage of reflectorless mode is that it can be used for the measurement of points that are inaccessible or dangerous. However, although a reflector is not required for distance measurements when operating in reflectorless mode, it is inevitable that some form of target needs to be used for observing landslide displacement from point to point over time (Figure 2-15). For instance, the changes of the target locations mounted on the tops of houses can be measured by a total station to assess landslide movements for investigating slope stability (Figure 2-16).



Figure 2-15: (a) A total station and (b) the establishment of targets for landslide movement monitoring in slope areas (Sarkar *et al.*, 2013).

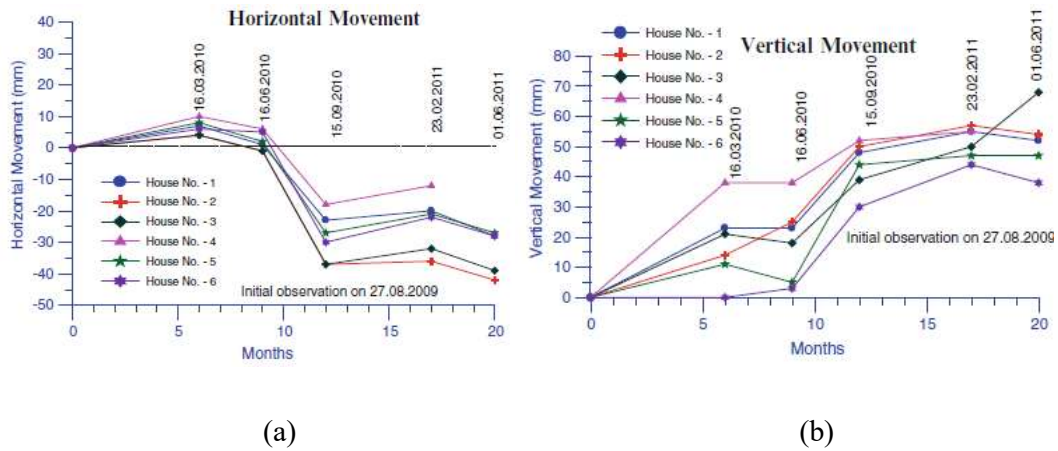


Figure 2-16: Time-series landslide movements of targets measured by total station: (a) horizontal movements; (b) vertical movements (Sarkar *et al.*, 2013).

Although the conventional geodetic method using total stations can provide highly accurate instantaneous measurements of landslide movements, the accuracy of measurement might be affected by the environmental conditions between the total station and the target. In particular, for long-range observations, the accuracy of measurement decreases significantly due to atmospheric problems and the capability of the instrument. Moreover, if a more precise total station is required for landslide monitoring, the costs of instrumentation increases and can become prohibitive (Uren and Price, 2010).

2.2.2.2 Global Navigation Satellite System (GNSS)

For acquisition of geospatial information used in landslide monitoring, GNSS or global positioning system (GPS) technology can be used to locate landslide features. In general, for any measurement point, a modern GNSS surveying receiver can calculate the three-dimensional coordinates equivalent in precision to those taken by a total station. However, the accuracy of location measurement based on GNSS depends on the survey methods adopted and GNSS equipment used (Uren and Price, 2010). Typically, the differential GNSS method is extensively used for highly precise location measurements, and the positions of a GNSS receiver can be used to measure landslide movements at different times (Figure 2-17). For example, the permanent monitoring of the Villerville landslide in Normandy, France, using GNSS measurements is illustrated in Figure 2-18.

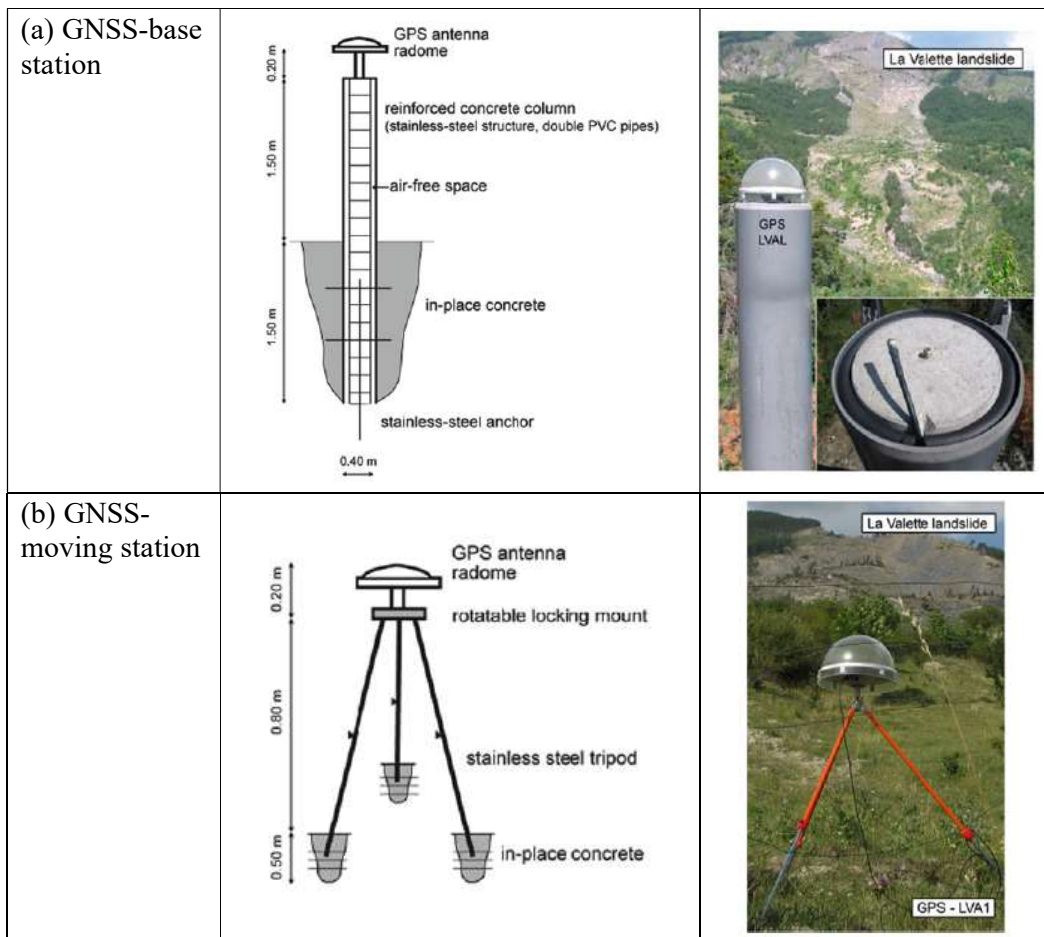


Figure 2-17: GNSS in the detection of landslide movements: (a) GNSS-base station; and (b) GNSS-moving station (Malet *et al.*, 2013).

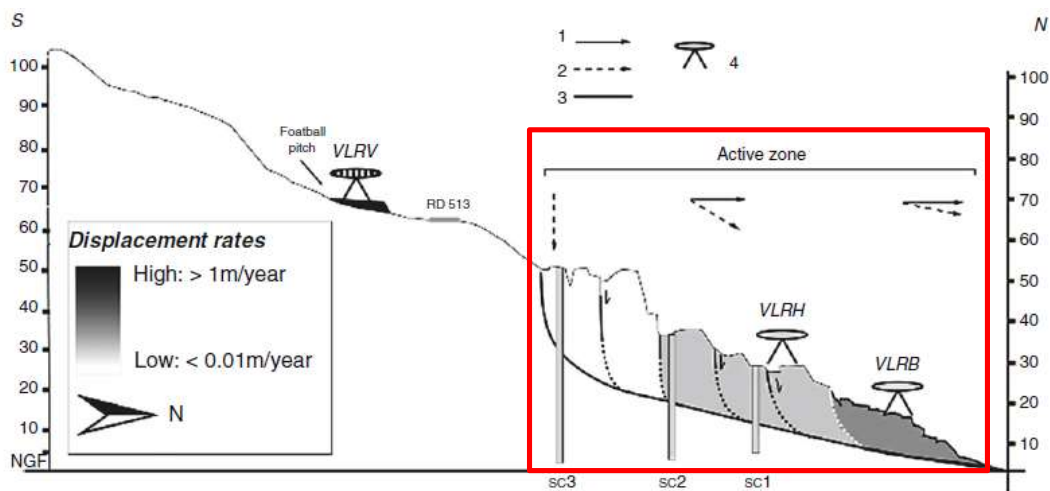


Figure 2-18: Monitoring of the Villerville landslide in France using GNSS observations (Malet *et al.*, 2013).

Compared with landslide monitoring using a total station, the observation data obtained from GNSS measurements can be collected immediately, and then transferred automatically. In an in-situ landslide investigation, a data logging system can be utilised in near real-time GNSS measurement for data collection and transfer without human interaction. This technique can also offer the potential for the detection of landslide movements in an early warning system (Intrieri *et al.*, 2012). However, the method of GNSS measurement is more complicated due to the need for the processing and analysis of GNSS signals, and therefore experts are required to process location measurements.

In conclusion, conventional geomatics methods for landslide monitoring using total stations and GNSS measurements can provide highly precise 3D absolute coordinates that are suitable for long-range surveying. However, the main drawback of these techniques is that they provide only discrete point measurements of landslide displacement. In addition, the targets and instruments often need to be installed in landslide areas. Therefore, total stations and GNSS are frequently based on contact monitoring techniques which only provide low spatial coverage for landslide detection (Piermattei *et al.*, 2015).

2.2.2.3 Terrestrial laser scanning (TLS)

The TLS technique utilises lidar technology to capture data from object surfaces via ground-based observation, which can generate 3D point clouds of continuous surfaces. The application of TLS survey is widely used in earth sciences, particularly in terms of monitoring changes in geomorphic surfaces in natural environments. In particular, TLS can deliver highly accurate, high-resolution point clouds which can be extremely valuable in detailed landslide assessment (Scaioni, 2015). For instance, TLS surveys have been used to provide point clouds at different times, as shown in Figure 2-19, and the monitoring of landslide deformations has been carried out using multi-temporal DTM analysis, as illustrated in Figure 2-20.

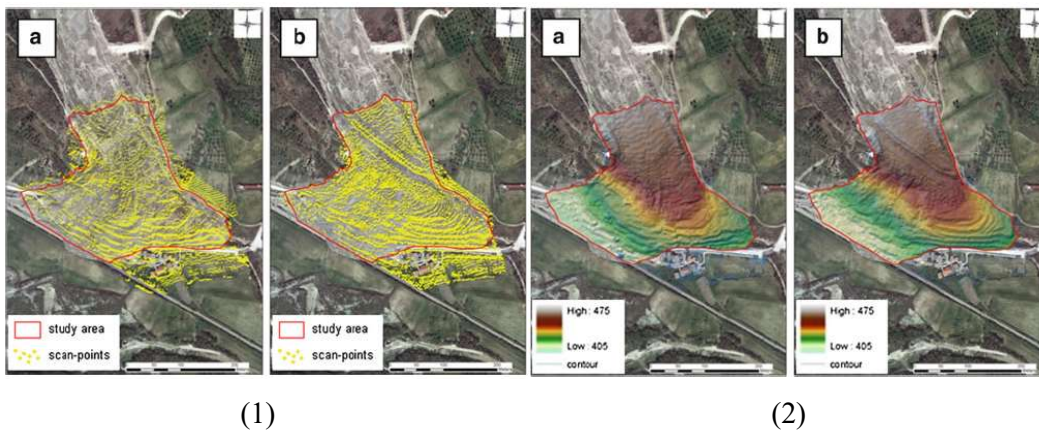


Figure 2-19: Illustrations of (1) point clouds from a TLS survey, (2) a DTM derived from the point cloud (Denora *et al.*, 2013).

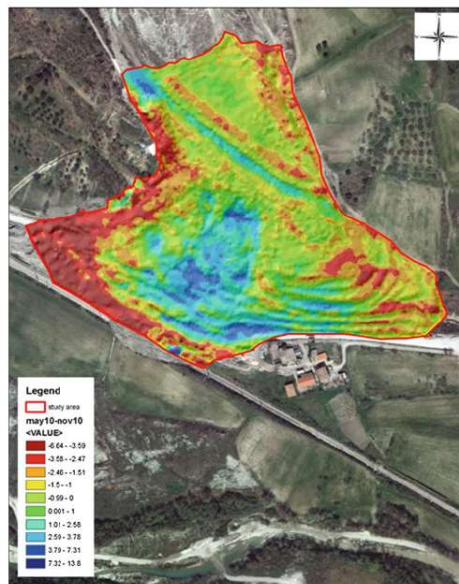


Figure 2-20: Illustration of different DTMs used for monitoring the Montaguto landslide in Campania, Italy (Denora *et al.*, 2013).

Compared to other optical methods, an advantage of using TLS is that it can be operated during the day or night without the need for illumination because laser light is used to measure distances, in an active remote sensing technique (Lillesand *et al.*, 2008). However, the main drawback of TLS equipment is that it is costly and generally requires expertise in operation. For field surveys, the TLS equipment might also be too heavy, which can result in transport or logistical difficulties (Piermattei *et al.*, 2015).

When monitoring landslides in complex terrain using TLS, collection times can be relatively slow, particularly if data must be collected from multiple locations to ensure full coverage of the area, as shown in Figure 2-21. Ground control points and reflector targets are often required for geo-referencing and registration to combine each point cloud. Consequently, data processing may be complicated for non-experts. Furthermore, gaps in the data can occur in landslide areas due to the oblique perspective from ground-based observation, and terrain occlusions in the line-of-sight (Teza *et al.*, 2007). In the case of the coastal cliff monitoring, the use of terrestrial laser scanning often generates gross errors at the edges of scans due to the relief displacement of terrain along the line-of-sight scanning (Lim *et al.*, 2005). Although TLS surveys are used to deliver high-resolution point clouds for the assessment of landslide movements, reductions in the number of points may be required to facilitate the capability of software and computer for data processing (Palenzuela *et al.*, 2013).

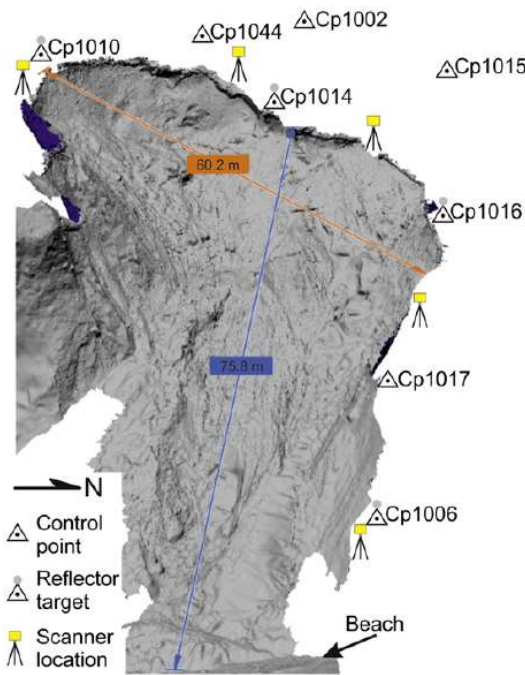


Figure 2-21: Illustration of point clouds from different TLS locations (Kuhn and Prüfer, 2014).

2.2.2.4 Ground-based synthetic aperture radar (GBSAR)

GBSAR utilises the radar interferometric technique to measure displacements in deformation monitoring, which plays an important role in the detection of surface changes for geoscience applications such as the study of landslides, glaciers and snow (Monserrat *et al.*, 2014). In particular, GBSAR has been increasingly applied in the last decade for landslide monitoring of, for example, earth-flows and rockslides (Agliardi *et al.*, 2013) and coastal cliff erosion (Mazzanti *et al.*, 2015). The application of this technique can deliver time-series data useful in the detection of landslide deformation. Furthermore, GBSAR can be installed for in-situ investigation to measure surfaces (Figure 2-22).

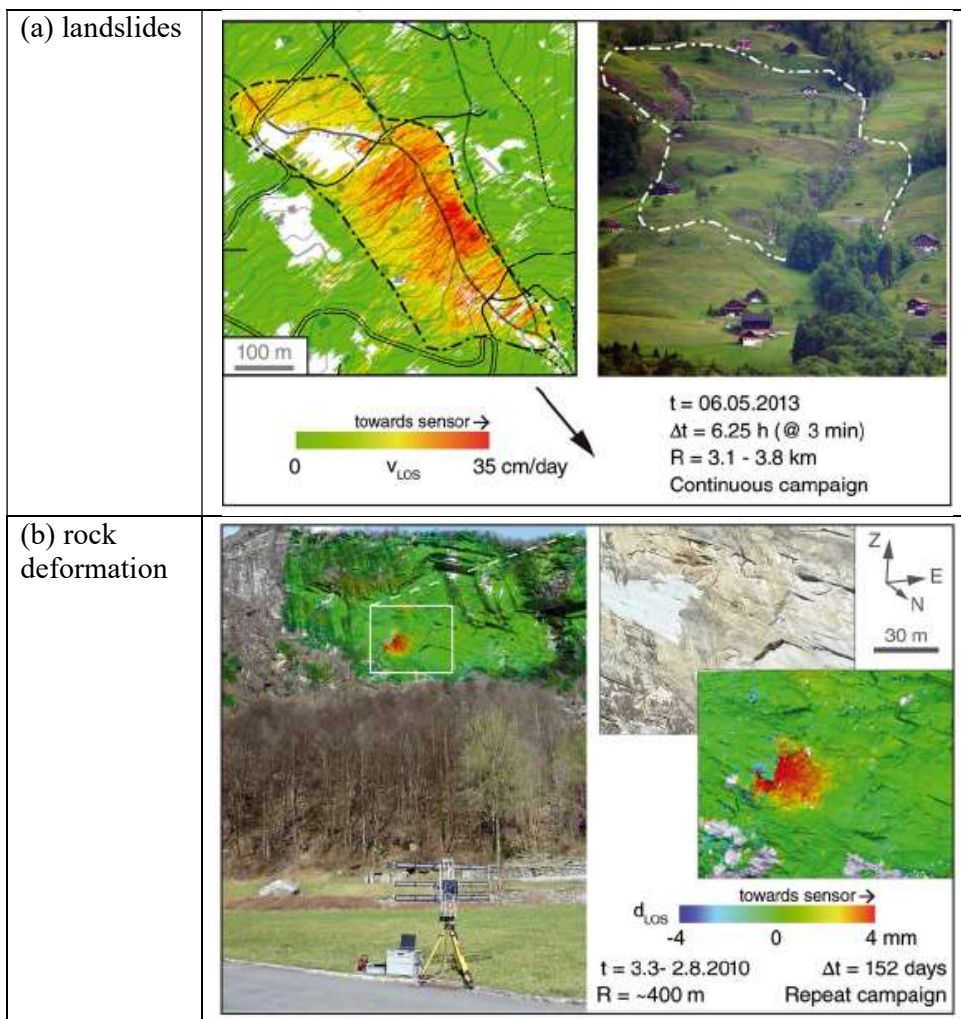


Figure 2-22: The use of GBSAR for measuring: (a) landslide movements; and (b) rock deformation (Caduff *et al.*, 2015).

Based on it being a technique using an active sensor for measurements, GBSAR is similar to TLS in that it can be operated during the day or night and in any weather conditions (Antolini *et al.*, 2013). GBSAR provides measurements of landslides displacements over large areas, but these observations must be corrected for topography, necessitating the collection of further reference data such as from TLS or photogrammetry (Bardi *et al.*, 2014; Caduff and Rieke-Zapp, 2014). Moreover, atmospheric effects can affect the quality of measurements (Bozzano *et al.*, 2011). Consequently, GBSAR is only suitable for application by expert users. It is also costly, and requires significant post-processing to derive meaningful deformation measurements, as shown in Figure 2-23.

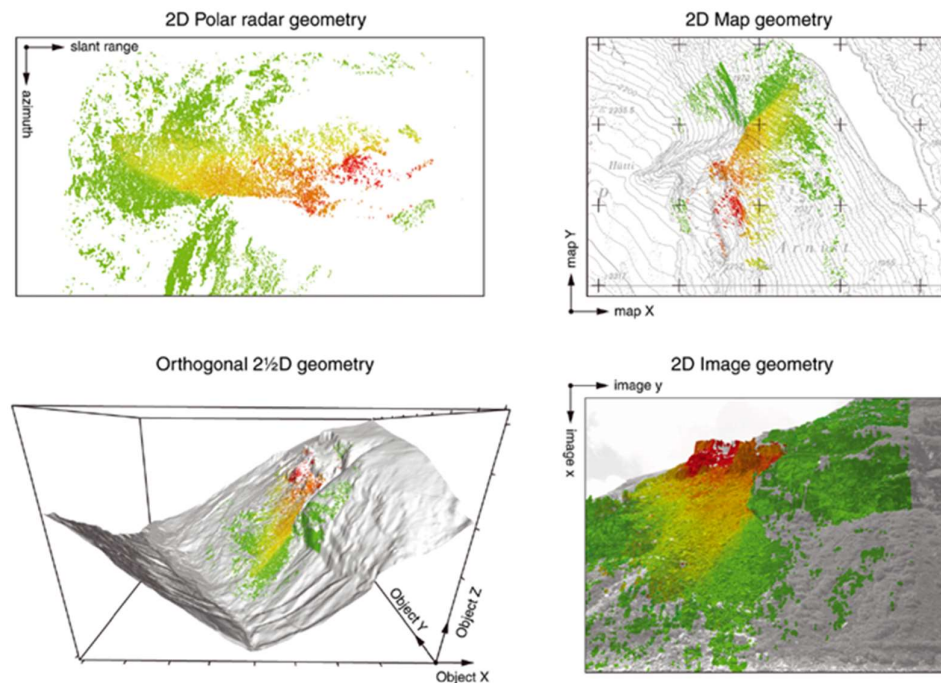


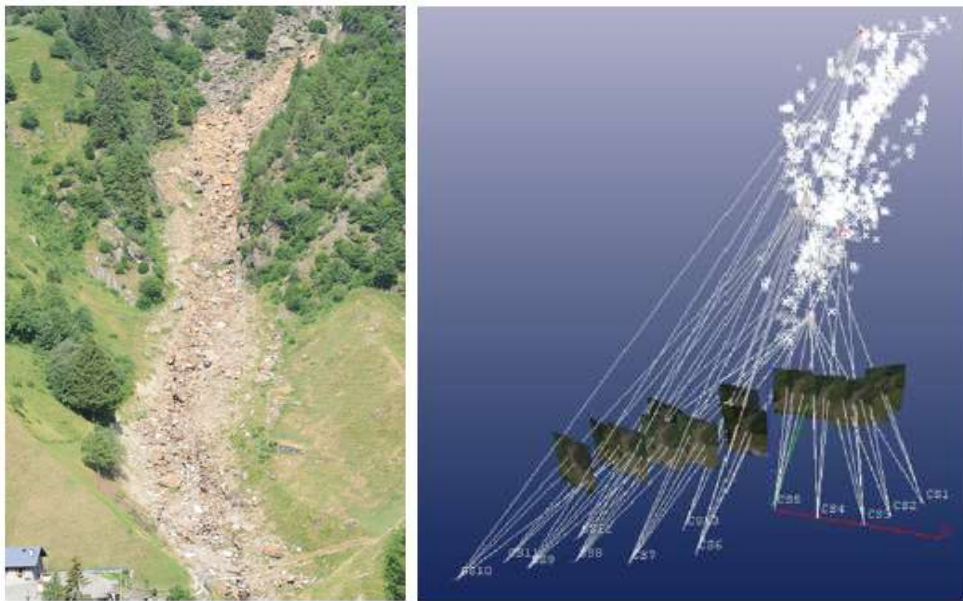
Figure 2-23: Illustration of processes for visualization of terrestrial radar data from GBSAR (Caduff *et al.*, 2015).

2.2.2.5 Close-range photogrammetry

Close-range photogrammetry is a non-contact measurement technique which encompasses various methods of image measurement in order to derive the position of an object from photographs, where the imaging distance is typically less than 300 meters (Luhmann *et al.*, 2006). Ground-based photogrammetric monitoring can be used in geoscience applications such as the study of earth-flows or landslides, gully erosion,

coastal erosion and glacial processes (Eltner *et al.*, 2016). In particular, photogrammetric approaches have been extensively used for landslide monitoring, as shown in Figure 2-24 (Akca, 2013; Stumpf *et al.*, 2015).

Close-range photogrammetric techniques can also be used to acquire geospatial information in landslide monitoring, and yield photogrammetric outputs which are useful for the quantitative interpretation and analysis of landslides (Figure 2-25). Classical photogrammetric outputs typically involve DTM and orthophotography. Petley *et al.* (2005) showed that the results from surface monitoring data might reveal patterns of movement in a landslide, which is the basis of a monitoring system in order to mitigate landslide hazards. Clearly, close-range photogrammetric techniques could provide a measurement solution for landslide hazards.



(a)

(b)

Figure 2-24: The Tartano valley landslides (Italy): (a) overview of landslide; (b) configuration of photogrammetric imaging network used for landslide monitoring (Scaioni, 2015).

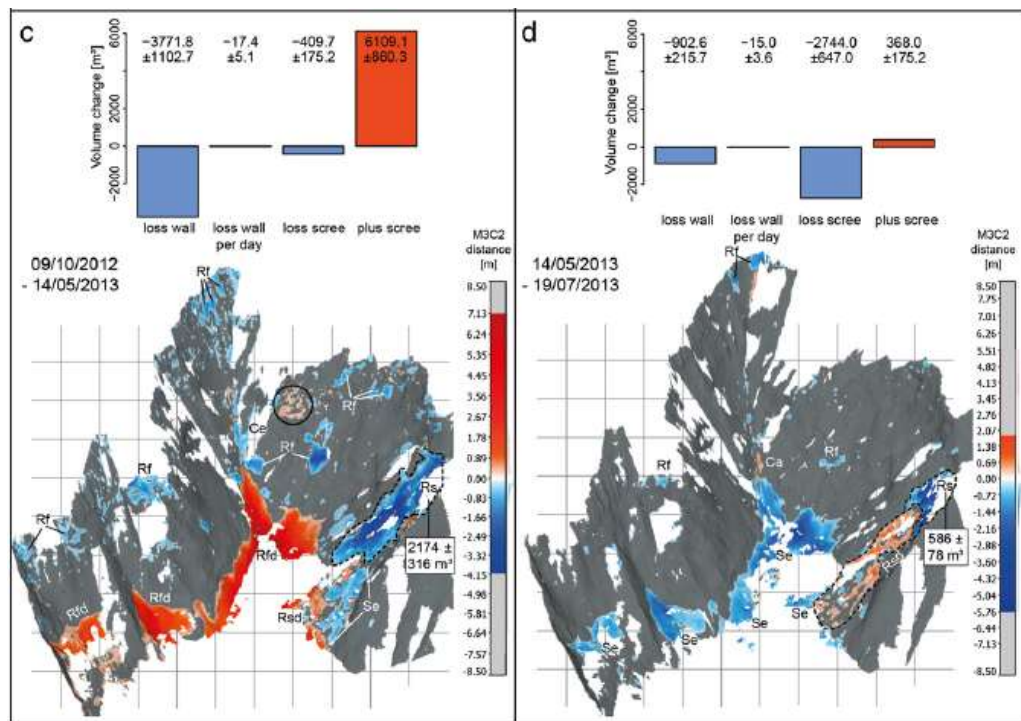


Figure 2-25: Assessment of landslide changes at the Super-Sauze landslide in the southern French Alps using photogrammetry (Stumpf *et al.*, 2015).

In comparison to other ground-based approaches, close-range photogrammetry can provide high measurement precision, potentially from mm to a few cm at 100 m range, and in this sense it is comparable to TLS and GBSAR. In addition, photogrammetry offers instantaneous data capture. Consequently, the benefits of photogrammetry are the speed of data acquisition and convenience in operation (Motta *et al.*, 2013). Furthermore, the costs associated with instrumentation and maintenance for the use of photogrammetric surveys are considerably lower than those for TLS and GBSAR (Travelletti *et al.*, 2012). Therefore, close-range photogrammetry can offer a cost-effective method for the acquisition of geospatial information for the assessment of landslide processes.

In consideration of the execution cost for landslide monitoring systems, a photogrammetric approach can offer a low-cost monitoring system by combining the use of an inexpensive imaging device (e.g. a smartphone or a consumer-grade digital camera) with an affordable personal computer and free-license software for data processing. Meanwhile, landslide monitoring based on laser scanning, GNSS and GBSAR approaches invariably use expensive and sophisticated instrument. For example, the price

of a laser scanner or is usually more than £20,000 and GBSAR greater than £100,000. Moreover, whilst continually falling in price, the instrumentation cost of highly precise GNSS equipment is £10,000. In the case of photogrammetry, the cost of a modern smartphone or consumer-grade digital camera is approximately £500 and an affordable processing system is below £1,000. Evidently, the financial cost of standard instrumentation for the conventional methods typically spend an order of magnitude greater than the photogrammetric approach.

2.3 Summary

Investigation and monitoring of landslides are important tasks in geotechnical engineering in order to mitigate hazards created by such phenomena. Many of the more common geomatics, geotechnical and geophysical engineering approaches which have been adopted for landslide investigation and monitoring have been discussed in this chapter. Each approach has its advantages and disadvantages in generating measurements of landslide movements that might be useful for the in-situ monitoring of landslides. However, ground-based approaches are efficiently used for on-site investigations in landslide monitoring systems. The characteristics of each geomatics approach, based on a ground platform, for landslide monitoring are summarised in Table 2-3.

Table 2-3: Comparison of ground-based geomatics approaches for landslide monitoring (adapted from: Wang, 2013).

Characteristics	Ground-based approaches				
	Total station	GNSS	TLS	GBSAR	Close-range photogrammetry
Monitoring method	Non-contact	Contact	Non-contact	Non-contact	Non-contact
Instrument cost	Medium	High	High	High	Low
Coverage areas in monitoring	Small	Small	Large	Large	Large
Spatial resolution	Point-based	Point-based	High	High	High

Although existing geomatics approaches are used for precise landslide monitoring, this initial assessment of small landslide areas is inappropriate for on-site investigation due to the often labour-intensive and costly methods used. Close-range photogrammetric techniques can offer a flexible, cost-effective, non-contact monitoring approach to on-site landslide investigation. In the next chapter, close-range photogrammetry, which is a clearly attractive approach for the assessment of landslide processes, is utilised to develop an appropriate monitoring system for real-time on-site investigation in order to aid initial geotechnical interpretation and assessment.

Chapter 3. A close-range photogrammetric methodology for landslide monitoring

3.1 Introduction

A close-range photogrammetric approach has enormous potential for the acquisition of geospatial information that is used for geoscience applications. In particular, the assessment of landslide deformation can use photogrammetric results acquired at different times. Important advantages of close-range photogrammetry, evident from several reviews in the previous chapter, are that it offers the use of a low-cost approach for efficient monitoring of landslide hazards. In this research, the development of a low-cost monitoring system based on a mobile platform such as a smart phone is proposed. Moreover, the basic photogrammetric processing based on the Structure-from-Motion (SfM) technique can provide user-friendliness for non-experts due to the potential for fully-automated data processing for 3D model reconstruction from images. Nevertheless, the limitation of SfM-based photogrammetric processing with the relatively low-performance processors adopted on mobile devices remains one of the main difficulties at present. A photogrammetric measurement and monitoring system based on mobile cloud computing technology can offer a potential solution to this, facilitating real-time processing of on-site investigation for landslide hazards analysis. With photogrammetric measurement and landslide monitoring on a mobile device, the development of a front-end service for the operator can be obtained straightforwardly from the photogrammetric results and landslide assessment. Moreover, improved functions for photogrammetric processing have shown enormous potential for back-end services to enhance photogrammetric results for landslide monitoring analysis. This chapter therefore reports the methodologies adopted for the development and implementation of a mobile platform based photogrammetric monitoring system for on-site investigation of landslide hazard analysis.

3.2 A photogrammetric solution for deformation measurement of landslides

Close-range photogrammetric techniques are believed to be suitable for adoption for monitoring purposes, as reviewed in the previous chapter, because the approach can offer a potentially low-cost solution in terms of implementation and operation. However, there are many difficulties in using such an approach for on-site investigation. To develop an effective close-range photogrammetric system for landslide monitoring there are therefore some important issues to be considered, as follows (Scaioni, 2015):

- Imaging devices or sensors used;
- Photogrammetric configuration adopted;
- Photogrammetric processing method and software utilised;
- Landslide analysis methods employed;

Moreover, when using photogrammetric processing workflows for on-site investigation of landslide monitoring, the developed system needs to manage and process a large amount of information if a real-time response is required.

With regard to the above-mentioned issues, several topics related to the methodologies of this research are explained in this chapter to achieve the objectives outlined in Chapter 1.

3.2.1 Imaging devices and sensors

A digital camera has an important role in image acquisition in any photogrammetric application since image quality depends largely on the imaging sensors adopted. Currently, there are many types of digital cameras being used for photogrammetric image collection, including DSLR cameras, consumer-grade or compact cameras, and mobile device cameras. For an optical sensor based on such digital cameras, a CCD (charge coupled device) or CMOS (complementary metal oxide semiconductor) sensor is used to record imagery instead of traditional film. The sensors are used to transform the natural light from the observed objects into electronic signals. The majority of digital cameras on mobile devices use a CMOS sensor with fixed focal length lens since this low-cost camera needs to be tiny enough to support the device assembly. In contrast, other digital cameras may use either CCD or CMOS as the adopted imaging sensor, usually with a higher

quality lens when compared to that found on mobile devices. As a result, it is often the case that mobile device camera provide lower quality imagery as a result of the adopted lens and imaging sensor. Nevertheless, the resolution of cameras on mobile devices has dramatically increased in recent years. One advantage of mobile devices with a high-resolution digital camera (> 5 megapixels) is the acquired images can be readily used for photogrammetric monitoring applications (Wang, 2013).

The smart phone camera tested for photogrammetric landslide monitoring in this research was primarily the Nexus 6, with 13-megapixel sensor; this was due to the fact that it was one of the state-of-the-art mobile device cameras at the outset of the research. To provide a comparison against other smart phone cameras, an iPhone 4's camera, with 5-megapixel sensor, was also tested. The selection of this typical device was based on the basic functionality of a regular smart phone at the time. A comparison of the technical specification for the two smart phones utilised is outlined in Table 3-1.

Table 3-1: Comparison of technical specifications between the two adopted smart phones: iPhone 4 and Nexus 6.

Characteristics	iPhone 4	Nexus 6
Processor	Apple A4, 800 MHz	Krait 450, 2.7 GHz quad-core
RAM	512 MB	3 GB
Image format	2592 x 1936; 5-megapixel	4160 x 3120; 13-megapixel
Sensor size	4.0 x 3.0 mm	4.7 x 3.5 mm
Pixel size	1.5 μm	1.12 μm
Lens maximum aperture	N/A	f/2.0
Shutter speed (sec)	1/15-1/1000	N/A
Output format	JPEG	JPEG

Comparing the developed methodology to conventional close-range photogrammetry using a higher quality camera, such as a DSLR, was necessary to ensure the potential of the photogrammetric approach for landslide monitoring. The DSLR camera tested was a Nikon D300 fitted with an AF Nikkor 28 mm f/2.8D lens. The technical specification of the DSLR camera and the 28 mm lens is outlined in Table 3-2.

Table 3-2: Technical specifications of the Nikon D300 DSLR camera used in the research.

Nikon D300 DSLR camera	
Image format	4288 x 2848; 12.3-megapixel
Sensor size	23.6 x 15.8 mm
Pixel size	5.6 μm
Shutter speed (sec)	1/8,000~30
Output format	JPEG, TIFF and Raw
AF Nikkor 28mm f/2.8D lens	
Focal length	28 mm
Aperture range prime	f2.8 – f22
Format	FX/35mm
Maximum Angle of View (DX-format)	53°
Maximum Angle of View (FX-format)	74°

All digital cameras mentioned above are non-metric cameras which were not primarily designed for the purpose of photogrammetric measurement, so investigation into their interior orientation is necessary. To achieve high-precision photogrammetric measurement for landslide monitoring, and investigate the potential of affordable image-based mobile technology, it was therefore necessary to examine the geometric characteristics of all adopted cameras through the process of camera calibration.

3.2.2 Camera calibration

The purpose of camera calibration is to determine the geometric camera model described by the parameters of interior orientation (e.g. focal length, image coordinates of principal point, lens distortion and other additional parameters). There are many camera calibration approaches, including laboratory, test field, plumb-line, on-the-job and self-calibration (Luhmann *et al.*, 2006). In particular, self-calibration is a basic method of camera calibration based on the bundle adjustment technique (Fraser, 2013). Moreover, automated self-calibration using a flat template or a grid is extensively used for camera calibration in digital photogrammetry as this method of camera calibration is based on a fully automatic procedure and offers user-friendliness for non-expert operators (Wang *et al.*, 2010). Calibration accuracy depends on the methods used in photogrammetric measurement, the number of images and the quality of the convergent image network

(Luhmann *et al.*, 2016). In this research, automated camera self-calibration was adopted based on three different available routines:

- 1) The close-range photogrammetric software PhotoModeler;
- 2) A camera calibration application for Matlab;
- 3) A camera calibration program developed using a Python script with OpenCV library;

For the automated camera self-calibration method, a planar target field or chess board template is used; PhotoModeler uses a calibration template with coded targets, as shown in Figure 3-1(a), while Matlab and OpenCV use a calibration template in the form of a chessboard, as shown in Figure 3-1(b). Both calibration templates were printed on A0 paper for the purposes of the reported exercises.

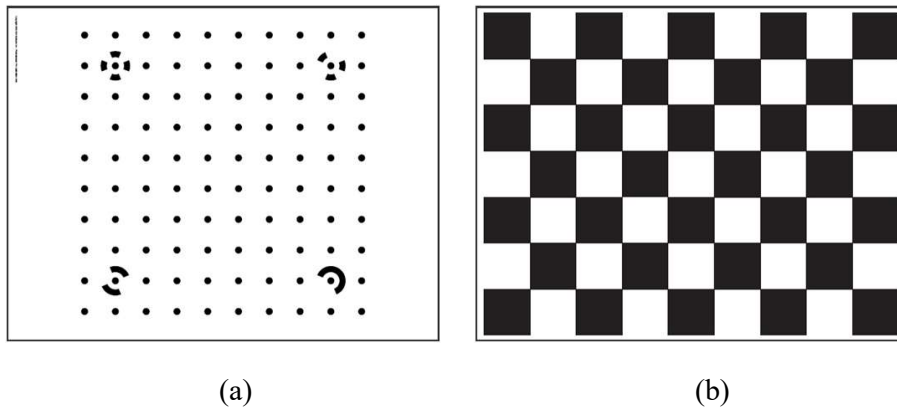


Figure 3-1: Calibration template for (a) PhotoModeler, (b) Matlab and OpenCV.

The self-calibration method requires acquisition of many images of the same calibration template from different viewing angles. Image capture covered all parts of the employed flat templates and the height of the camera was approximately 1 m above the template. Self-calibration was performed using twelve convergent images taken from three different orientations of camera from four sides of the template. This photogrammetric network configuration is illustrated in Figure 3-2.

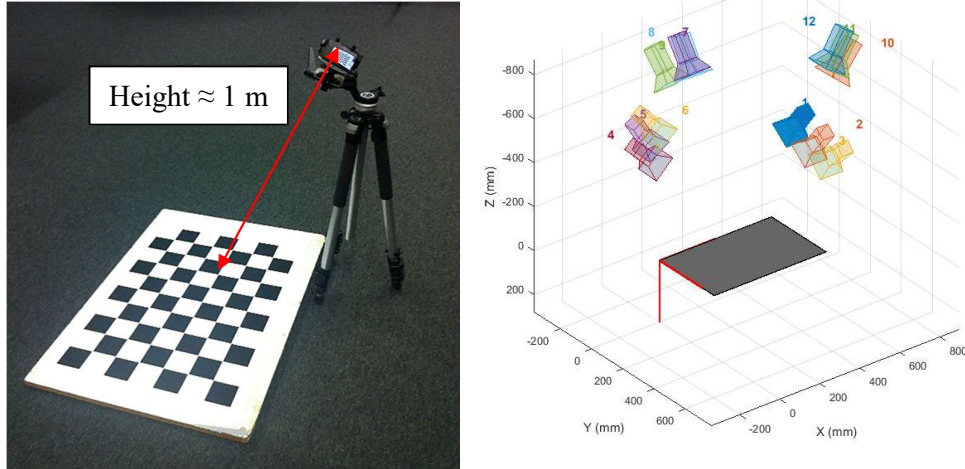


Figure 3-2: Photogrammetric configuration for camera calibration.

The parameters of interior orientation were calculated based on five repeated calibrations in order to provide the most appropriate camera model and improve the reliability of calibration results. However, the results from the three different approaches utilised different units. The calibration results from PhotoModeler are shown in the unit of millimetres (mm), whereas Matlab and OpenCV are shown in the unit of pixels. In order to compare the calibration results from those software packages, the results from Matlab and OpenCV were therefore required to be converted into mm. For the main parameters of the camera model (e.g. focal length, principal point in x and y), the calibration results in the unit of pixels can be converted into mm by simply multiplying by the pixel sensor size (mm). On the other hand, some parameters (especially lens distortion and other additional parameters from the different software) cannot be directly converted because they use different units for the additional parameters.

Lens distortion can be separated into radial distortions and tangential distortions. Radial distortions are caused by the shape of the lens that may not be perfect. Tangential distortions result from the assembly process of the camera lens as a whole. The radial lens distortions are modelled using Brown's distortion model (Brown, 1971), as shown in equation (3-1):

$$\Delta r'_{rad} = K_1 r'^3 + K_2 r'^5 + K_3 r'^7 + \dots \quad (3-1)$$

However, Carbonneau and Dietrich (2017) showed how these parameters can be converted using equations (3-2) to (3-4).

$$K_1(\text{focal units}) = K_1(\text{pixel units}) * f^2 \quad (3-2)$$

$$K_2(\text{focal units}) = K_2(\text{pixel units}) * f^4 \quad (3-3)$$

$$K_3(\text{focal units}) = K_3(\text{pixel units}) * f^6 \quad (3-4)$$

where f is the focal length in the unit of pixels. The resultant calibration results for each determined parameter of the Nexus 6 are shown in Table 3.3.

Table 3-3: Camera calibration results for the Nexus 6 smart phone camera using three different calibration routines.

Parameter	Nexus 6					
	PhotoModeler		MATLAB		OpenCV	
	Mean	σ	Mean	σ	Mean	σ
Focal Length (mm)	3.798	0.004	3.783	0.005	3.773	N/A
Xp - principal point x (mm)	2.320	0.004	2.326	0.005	2.333	N/A
Yp - principal point y (mm)	1.735	0.004	1.732	0.006	1.731	N/A
Fw - format width (mm)	4.639	0.002	Not calculated			
Fh - format height (mm)	3.481	N/A				
K1 - radial distortion 1	-1.25×10^{-02}	6.72×10^{-02}	-1.29×10^{-02}	8.49×10^{-02}	-1.32×10^{-02}	N/A
K2 - radial distortion 2	3.02×10^{-03}	2.23×10^{-02}	3.25×10^{-03}	3.20×10^{-02}	3.33×10^{-03}	N/A
K3 - radial distortion 3	$0.00 \times 10^{+00}$	$0.00 \times 10^{+00}$	$0.00 \times 10^{+00}$	$0.00 \times 10^{+00}$	$0.00 \times 10^{+00}$	N/A
P1 - tangential distortion 1	-8.73×10^{-04}	1.05×10^{-04}	-9.92×10^{-05}	6.27×10^{-04}	-2.77×10^{-05}	N/A
P2 - tangential distortion 2	5.82×10^{-05}	7.70×10^{-04}	-3.80×10^{-05}	6.33×10^{-04}	-2.26×10^{-05}	N/A
Image measurement precision: Overall RMS (pixels)	0.944		1.167		1.372	

According to the camera calibration results for each parameter, as shown in Table 3-3, PhotoModeler, MATLAB and OpenCV approaches were comparable. The standard deviation (σ) of MATLAB results was slightly higher than for PhotoModeler. Considering the reported RMS values, PhotoModeler demonstrated the highest measurement precision. It is likely that the different experimental results cause the methods adopted in the software, with these software packages using different approaches to photogrammetric processing and camera modelling. MATLAB and OpenCV use the direct linear transformation (DLT) method based on the pinhole camera model (Bradski and Kaehler, 2008), while PhotoModeler uses the method of space resection based on the bundle adjustment (Zhang *et al.*, 2010). Although the calibration parameters were not identical, the values for each of the main parameters from the three adopted routines were only slightly different, especially the parameters of focal length, principal point offset and radial distortion (K1, K2 and K3). However, the parameters of tangential distortion (P1 and P2) from MATLAB and OpenCV had dramatically different values to those from PhotoModeler (Table 3-3).

The radial lens distortion parameters of the Nexus 6, which were determined by equation (3-1) from the three routines, are shown in Figure 3-3. Based on these results, it may be concluded that MATLAB and OpenCV provided relatively similar camera calibration results for this type of smart phone camera when compared to PhotoModeler. The camera calibration results for the Nikon D300 DSLR camera and the iPhone4 smart phone camera are shown in Appendix A.

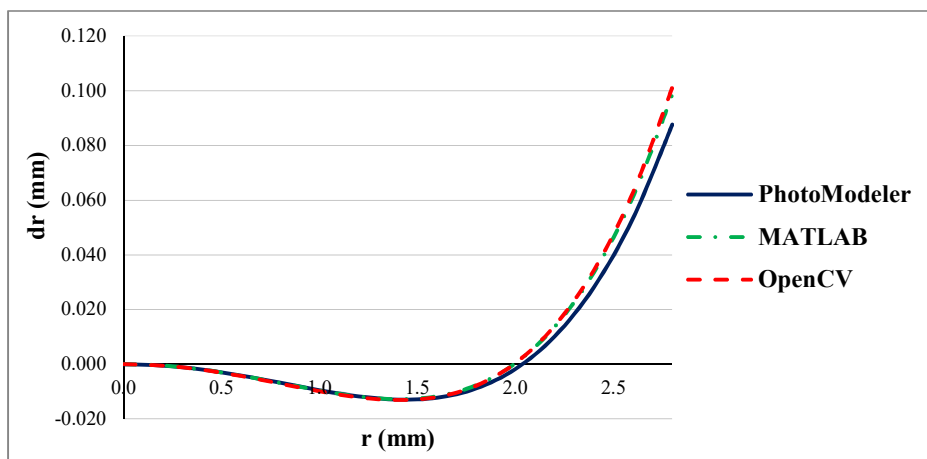


Figure 3-3: Radial lens distortion of the Nexus 6, as determined from the three different calibration routines.

3.2.3 Photogrammetric network configuration

Imaging network geometry is an important factor to achieve a high-accuracy in photogrammetric measurement. The adoption of multi-station networks are extensively used in photogrammetry for geospatial applications, including landslide monitoring (Scaioni, 2015). To provide a photogrammetric solution suitable for non-expert users and also ensure the requirement of high accurate photogrammetric results for landslide monitoring, photogrammetric network design was used to determine suitable camera locations and the number of necessary camera stations. Nonetheless, several important factors should be taken into consideration during image acquisition of the object, as follows (Luhmann *et al.*, 2006):

- Base to depth ratio (B/D);
- Maximum allowable camera-to-object distance;
- Field of view (FOV) of the camera;
- Convergent imaging networks;

Firstly, the base to depth ratio (B/D) of imaging geometry should ideally be in the range of 0.1-0.3. The geometry of the intersecting ray at each object point is used to find the location and the orientation of the imagery. The sufficiency of images when creating a 3D model is to have suitable baselines between those images. A small B/D ratio can lead to an inappropriate geometry, resulting in an increase in errors for determined depths, as illustrated in Figure 3-4. Based on the study of Hullo *et al.* (2009) and following the 3x3 CIPA rules (Waldhäusl and Ogleby, 1994), the optimal B/D ratio should be between 0.1-0.3 for an effective 3D reconstruction and a high accuracy of ray intersection.

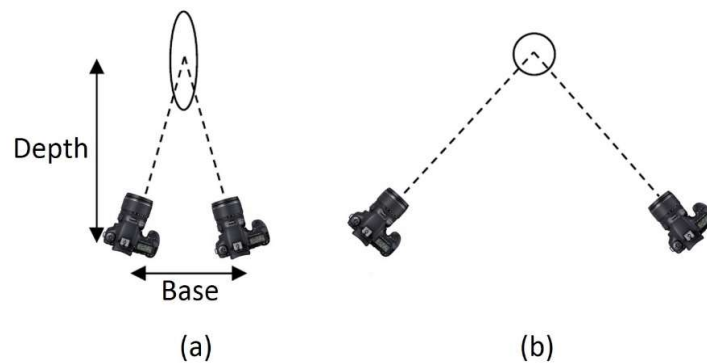


Figure 3-4: Imaging geometry (a) small B/D ratio (b) large B/D ratio (Alsadik, 2014).

Secondly, the distance between the camera and the object should be close-range since the image scale has a direct impact on the precision of photogrammetric measurement. Consequently, the precision of any optical triangulation system results from the measurement resolution and the mean camera-to-object distance (Fryer *et al.*, 2007). However, the algorithms used in digital image processing directly influences measurement resolution according to the pixel size of the imaging sensor. To control the photogrammetric precision, it is necessary to find the maximum allowable camera-to-object distance, d_{max} , which can be calculated using equation (3-5) (Luhmann *et al.*, 2006).

$$d_{max} = \frac{\bar{\sigma}_c c \sqrt{k}}{q \sigma} \quad (3-5)$$

where $\bar{\sigma}_c$ is the standard error in the XYZ object point coordinate, c is image scale, q is a design factor expressing the strength of the basic camera station configuration (0.4-1.1), σ is the standard error in the image coordinate and k is the number of images per camera station. Following equation (3-5), the distance between the camera and the object (depth) is also influenced by many factors such as a field of view of the camera, measurement resolution and positional accuracy.

Thirdly, FOV of the camera generally requires to be in the range 40-80° for close-range photogrammetric measurement in engineering applications (Fryer *et al.*, 2007). For this reason, the operator has to use a camera with a suitable FOV. The coverage from each camera station can be estimated using the FOV computational formula (Luhmann *et al.*, 2006) shown in equation (3-6):

$$FOV = 2 \times \tan^{-1} \left(\frac{s'}{2c} \right) \quad (3-6)$$

where s' is the maximum distance between two corners of the imaging sensor and c is the focal length of the lens.

The appropriate values for parameters of both d_{max} and FOV for a mobile phone digital camera used in this research following equation (3-5) and equation (3-6) are shown in Appendix B.

Finally, convergent imaging networks are required to provide effective 3D reconstruction from the imagery. Image acquisition should fully cover the study area (360° coverage), with necessary overlaps to enable appropriate photogrammetric reconstruction. As mentioned above, the imaging plan is performed following these concerns to help the operator taking a suitable image network. By way of example, an imaging plan of the Hollin Hill survey using a mobile device is illustrated in Figure 3-5. With regard to finding an optimum camera station location, the maximum allowable camera-to-object distance was < 15 m, following equation (3-5), and the minimum distance between each camera station was approximately 2-3 m using a B/D ratio of 0.1-0.3.

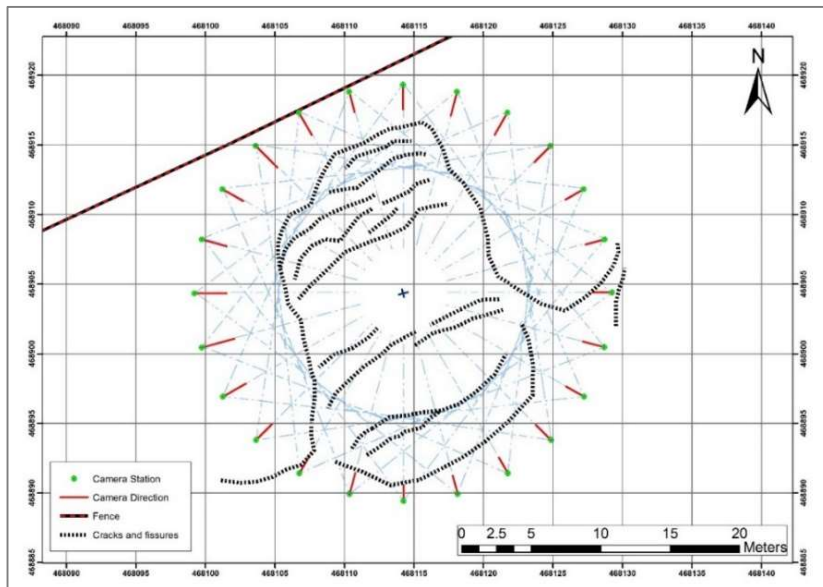


Figure 3-5: Example of photogrammetric network design for Hollin Hill landslide monitoring.

3.2.4 Photogrammetric processing solution

Although close-range photogrammetric techniques can be adopted for monitoring purposes, conventional photogrammetric processing still has some drawbacks for users. For example, the requirements involving network design, ground control points, photogrammetric software and a proficient photogrammetrist are essential for conventional photogrammetry (Fryer *et al.*, 2007). The SfM pipeline can potentially overcome the many traditional constraints of digital photogrammetry, especially user-

friendliness to non-experts and lower costs. This gives opportunity for the development of a photogrammetric processing system suitable for landslide monitoring.

3.2.4.1 Structure-from-motion based photogrammetric processing

In the last decade there has been a revolution in topographic measurements using photogrammetric computer vision for a number of geoscience and geomorphological applications, including land deformation of alluvial fans (Micheletti *et al.*, 2015a), coastal erosion (James and Robson, 2012), gully headcut erosion (Gómez-Gutiérrez *et al.*, 2014) and landslide monitoring (Stumpf *et al.*, 2015). In particular, the development of SfM and multiview-stereo (MVS) techniques has improved the accessibility of photogrammetric workflows for non-expert users, and increased automation (Westoby *et al.*, 2012; Javernick *et al.*, 2014). At the same time, it has also been shown that the quality of results can conform to expected levels of accuracy for conventional photogrammetric processing (Micheletti *et al.*, 2015a).

The workflow of the SfM-MVS based photogrammetric approach consists of two main stages for 3D model reconstruction from imagery. Firstly, the SfM technique requires a set of images taken from different positions in front of the object of interest (as shown in Figure 3-6). The SfM workflow is mainly comprised of three processes: 1) feature detection in each image, with features extracted by Scale-invariant feature transform (SIFT) (Lowe, 2004) or Speeded-up robust features (SURF) (Bay *et al.*, 2008); 2) matching within the image dataset; and 3) a bundle adjustment used to estimate camera positions and orientations and extract a sparse point cloud. Secondly, the MVS process can be defined as performing the dense image matching from the SfM output. This construction is used to efficiently filter out noisy data and generate the so-called 'dense point cloud'.

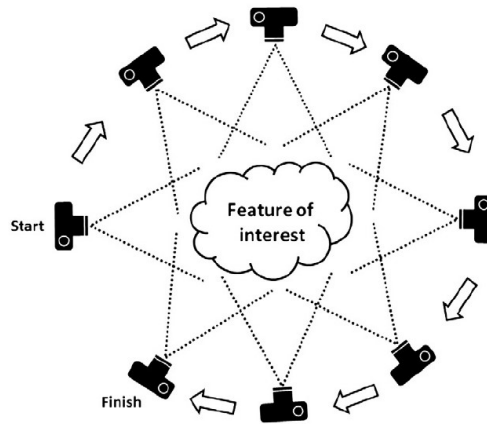


Figure 3-6: Image acquisition for SfM (Westoby *et al.*, 2012).

3.2.4.2 SfM-Photogrammetric processing software

With processing software based on SfM-photogrammetry for 3D model reconstruction, there are recently several commercial SfM-MVS software packages (e.g. AgiSoft PhotoScan, PhotoModeler) and open source or free software packages (e.g. Bundler Photogrammetry Package, VisualSFM & PMVS/CMVS). Moreover, web services such as Photosynth and Autodesk 123D Catch can provide free SfM-MVS based photogrammetric processing on the Internet. However, each SfM-MVS approach has both advantages and disadvantages, with a study by Micheletti *et al.* (2015a) reporting the effectiveness of each approach depending on the specific applications, as highlighted in Table 3-4.

Table 3-4: The options of the SfM-MVS approach (Micheletti *et al.*, 2015a).

Availability of photogrammetry	Main Characteristics
Traditional photogrammetry	Higher reliability and quality, high cost, expert knowledge
SfM-MVS photogrammetry (commercial software packages)	High quality but also greater automation, and low cost
Local SfM-MVS software (open source software packages)	Mostly free and semi-automated processing, low quality
Internet-based SfM-MVS system	No cost, near real-time, fully automated processing, lowest quality

In an investigation into the adoption of processing software for SfM-photogrammetry, Eltner *et al.* (2016) reported that PhotoScan is the most popular SfM software used in

geoscience applications over the previous five years (2012-2016), as presented in Figure 3-7. Photoscan may be the most favoured SfM-photogrammetric software due to its friendliness for non-expert users. However, the employability of this commercial software to implement on landslide monitoring system still has limitations since this commercial software is relatively high-cost and also refuses to allow accessibility via the Internet (Agisoft, 2016).

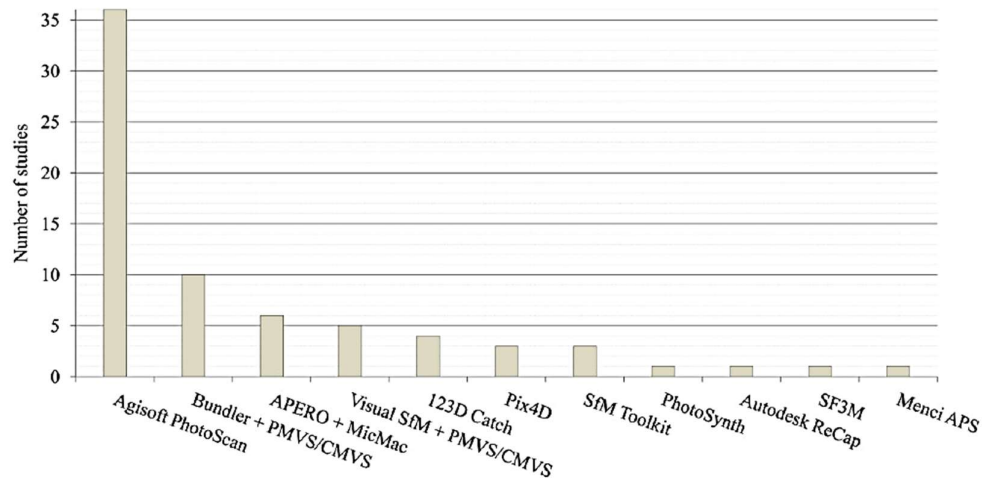


Figure 3-7: SfM-photogrammetric processing software used in Geoscience applications (Eltner *et al.*, 2016).

For the development of an effective photogrammetric measurement solution related to a low-cost approach in this research, the photogrammetric processing for on-site investigation uses only non-commercial and freely available software. As regards the comparison of processing software for SfM photogrammetry (Figure 3-7), the free and/or open source software packages 1) Bundler and PMVS/CMVS; 2) APERO and MicMac; and 3) VisualSfM and PMVS/CMVS were the most utilised for monitoring applications (after PhotoScan). To compare and highlight the optimal potential processing software for system implementation, it was therefore necessary to investigate these software packages. In a useful study of freely available SfM software for landslide monitoring, Stumpf *et al.* (2015) revealed that APERO and MicMac provided more accurate results than VisualSfM and PMVS. However, the difference of photogrammetric accuracy between the two results was insignificant (at the millimetre level) for the purposes of assessing landslide deformations. Although VisualSfM and PMVS showed slightly lower accuracy results, this software offers a higher degree in automated processing

compared to APERO and MicMac and was therefore adopted in this research. Moreover, in terms of the processing performance for SfM photogrammetry, VisualSFM and PMVS can efficiently use both CPU and GPU processors for photogrammetric processing (Sawyer *et al.*, 2012), whereas, APERO and MicMac or Bundler and PMVS still has the drawback that they can use only a CPU processor. As a result of the use of high-performance GPU processing power, VisualSFM and PMVS were therefore believed to require less processing time. Therefore, VisualSFM and PMVS were identified as an effective SfM-photogrammetric processing solution for development of the proposed landslide monitoring system.

3.2.5 Landslide analysis methods

In considering landslide monitoring, the technique of multi-epoch analysis is used to assess landslide processes from photogrammetric results at different times. In particular, the methods based on 3D model comparison are generally used for analysis of landslide deformation which can be divided into area- and point-based approaches, as shown in Figure 3-8 (Lague *et al.*, 2013; Scaioni, 2015).

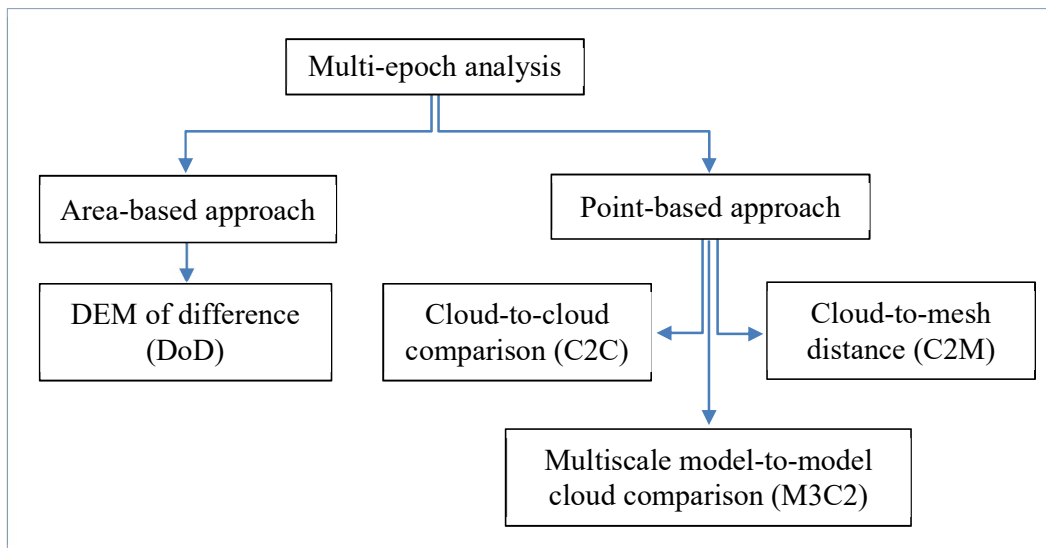


Figure 3-8: The methods of multi-epoch analysis for landslide monitoring.

For the area-based comparison method, DEM of Difference (DoD) is a general technique of comparison between two surface models in the form of DEMs to evaluate the changes of landslide surfaces. However, in the case of point clouds obtained from

photogrammetric results, it is necessary to generate DEMs from two point cloud datasets prior to comparison. Moreover, it is difficult to find a suitable DEM resolution for analysis in order to maintain the details of the original data, especially the point cloud roughness. Thus, the comparison methods for multi-epoch analysis in this research only used point-based approaches in order to avoid the processing of surfaces interpolated from the measured point cloud.

Regarding point-based approaches of 3D model comparison, the methods can be directly carried out using comparison of two point clouds. Although cloud-to-cloud comparison (C2C) and cloud-to-mesh distance (C2M) are normally used to find the differences between two point clouds, it is possible that gross errors result from an insufficient overlapping area between both two point clouds, such as void areas. Meanwhile, multiscale model-to-model cloud comparison (M3C2) was recently proposed as a method of point cloud comparison to consider the source of uncertainties over surfaces (such as roughness of surface, registration error and surface changes). In particular, the different varieties of natural surfaces, such as bare-earth areas or vegetated terrain, have a direct effect on comparison results (Lague *et al.*, 2013). The photogrammetric results from landslide areas may often be saddled with these concerns. To minimise these effects for point cloud comparison, landslide monitoring in this research is therefore based on multi-epoch analysis using the point cloud comparison M3C2 technique. The M3C2 point cloud comparison method was implemented in the stage of change assessment. Details of this approach are presented in the later sections on change assessment.

3.2.6 Summary of the photogrammetric solution for landslide monitoring

The detail of close-range photogrammetric approaches for landslide monitoring can be divided into several stages, as follows: (1) Camera calibration is an important procedure to examine the interior orientation of the camera. The use of open-source tools and automatic camera calibration routines, evaluated for mobile device cameras, showed similarly-accurate results as calibration tools available in commercial software. (2) The adopted photogrammetric network configuration should be based on multi-station networks and convergent imagery. The guideline for image capture determines the basic requirements comprising the maximum allowable camera-to-object distance and the distance between each camera station. (3) Modern SfM workflows offer the potential for

implementing a photogrammetric approach in terms of providing a high degree of automated processing. The investigation of the non-commercial, open-source SfM software packages VisualSfM and PMVS offer the promise of a low-cost photogrammetric processing solution for landslide monitoring.

3.3 A mobile platform-based landslide monitoring system for on-site investigation

Photogrammetric processing for landslide monitoring is usually performed in the office after image collection since the operator needs to transfer and process imagery on a workstation. This constraint may lead to one of the biggest obstacles in a real-time photogrammetric on-site investigation. Although, at present, a high-performance processor in a personal or a laptop computer might be able to deal with a requisite photogrammetric processing in the field, this research is based on the development of a stand-alone application for landslide monitoring. That probably makes the operator inconvenient for in-situ investigations. To overcome these difficulties, on-line photogrammetric processing and monitoring of landslide hazards is proposed.

For the development of a photogrammetric system for on-site investigation, it is likely that a mobile device camera can be adopted as a low cost sensor for dynamic monitoring applications. Mobile devices are also potentially useful instruments for on-site investigation in geotechnical engineering and geophysics. A serious weakness with photogrammetric monitoring system using mobile devices for on-site investigation, however, is the requirement for real-time processing of observations. In order to achieve the requirements for a real-time landslide monitoring application, processing captured data using mobile cloud computing technology can potentially offer the possibility for a real-time measurement system.

3.3.1 Mobile device technology

Mobile devices have recently become powerful instruments with low-cost imaging sensors that are suited for close-range photogrammetry monitoring applications (Yun *et al.*, 2012; Wang, 2013; Micheletti *et al.*, 2015a). Mobile devices are usually classified according to their purpose of usage into either tablet or smart phone. The mobile device adopted in this research is a simple smart phone (aka mobile phone) because it is generally

more comfortable, convenient and portable for on-site investigation. Moreover, the majority of modern smart phones currently contain many sensor technologies, such as GNSS, digital compass, accelerometers, gyroscopes and/or magnetometers (Figure 3-9). These sensors might also provide useful information for photogrammetric measurement solution now and in the future. Nevertheless, tablet devices could also be adopted for such research.

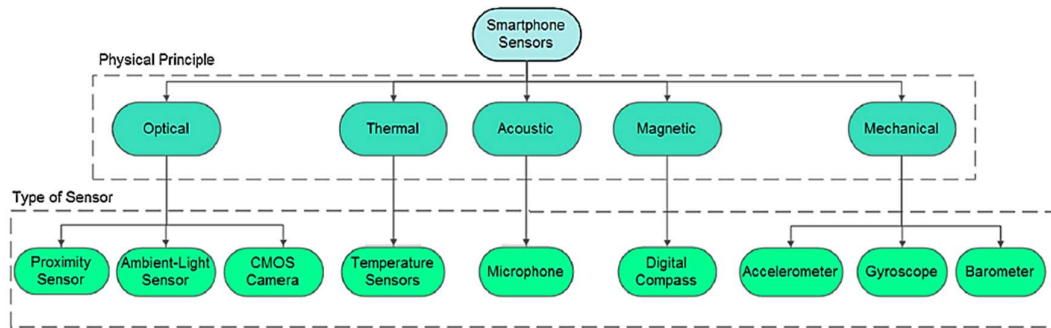


Figure 3-9: Sensors integrated on a modern smart phone (Daponte *et al.*, 2013).

GNSS microchip technology for use on mobile devices has been continuously developing, including smaller size and lower cost, and consequently has become an essential sensor for the majority of mobile devices. Most recent GNSS sensors on mobile devices are multi-constellation which can observe several navigation satellite systems (e.g. GPS, Galileo, GLONASS or BeiDou) in order to achieve a higher accuracy of positioning for navigation purposes. The horizontal location accuracy obtained from GNSS-based mobile devices is > 4 m (Yoon *et al.*, 2016). Nevertheless, the GNSS observation from such a sensor on a smart phone still provides a low-accurate location of the camera station and does not provide sufficient precision of observations for photogrammetric processing (Kehl *et al.*, 2016).

In addition, there are a variety of mobile platform operating systems, including Android, Windows and iOS, that lead to different standards, programming languages and development tools (Corral *et al.*, 2012). For research purposes, the development of an application on the Google Android OS is generally more favourable than iOS and Windows mobile because Android supports open source (Wang, 2013). However, the primary purpose of mobile devices is not for photogrammetric processing. Moreover, one current drawback of smart phones or mobile devices is the relatively low-performance

processing power compared to both personal computers and laptop computers. Photogrammetric processing on a mobile device is therefore one of the greatest challenges, and very difficult to achieve in real-time for 3D reconstruction from the imagery. To overcome these difficulties and find a solution to managing and processing large amounts of image data for photogrammetric measurement in (near) real-time, it was decided to transfer the task of photogrammetric processing from the mobile device onto cloud computing services (Chidburee *et al.*, 2016). The proposed landslide monitoring system was therefore developed and implemented based on the cloud.

3.3.2 Cloud computing technology

The rapid development of ICT plays an important role. Cloud computing is now being effectively used to access computing resources and data storage on the Internet (Liao *et al.*, 2017). A huge demand for a real-time geospatial processing based on the cloud has resulted. For example, the study of Karimi and Roongpiboonsopit (2012) shows that there are many challenges associated with computationally-intensive geospatial applications when a real-time response is needed. Using cloud computing for data-intensive, time-sensitive geospatial applications is advantageous because it provides an efficient resource for storing and manipulating very large amounts of geospatial information. Thus, cloud computing can offer real-time processing potential for geospatial applications.

In addition, Internet technology has rapidly developed in terms of both speed and device connection. The IoT, a modern IT technology, offers the opportunity to connect many types of device to the Internet other than the ordinary computer. With the development of mobile networks, telecommunication technology via 3G networks has changed into 4G networks, making it is possible to achieve data rates of 2-20 Mbps (Ohmori *et al.*, 2001). Meanwhile, in the near future, a new 5G technology in the UK is developing that will cover 90% of the population by 2027 (Oughton and Frias, 2017). In the aspect of engineering, a 5G network will provide data rates of approximately 1-10 Gbps (Chih-Lin *et al.*, 2016). This has opened up the potential for harnessing additional processing power for mobile devices from the cloud. Mobile cloud computing, which solves the resource problem of mobile devices in terms of the available computing power, can provide computing resources based on cloud computing technology (Fernando *et al.*, 2013; Ayad *et al.*, 2015).

In terms of mobile cloud computing in geospatial applications, Lee and Kang (2013) defined a mobile cloud service as a mobile application service based on cloud computing which can maintain a steadily high performance. This results in the advantage of flexible scalability of cloud computing resources. Lee and Kang developed a remote-sensing application on a mobile platform to analyse change detection of satellite images, as shown in Figure 3.10. Moreover, their study also reported a test on an iPad with geo-based image processing functions on the Amazon web service in a cloud environment that fulfills users' requirements for real-time geospatial processing on a mobile device. Therefore, cloud-based technology has sufficient potential to solve real-time geospatial problems in the context of landslide monitoring.

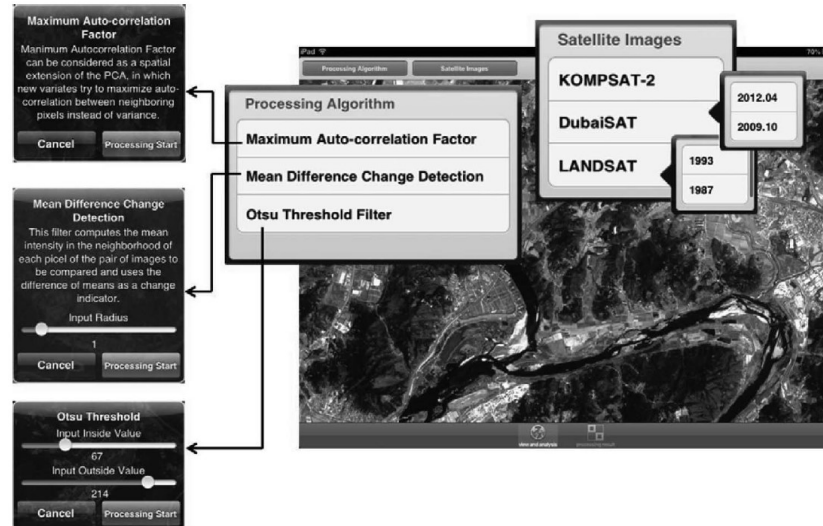


Figure 3-10: Example of a real-time satellite image processing for change detection analysis on an iPad (Lee and Kang, 2013).

3.3.3 System design and integration

Regarding a conventional in-situ photogrammetric approach for landslide monitoring, a single-camera system is generally used to collect the requisite dataset of sequential images. Such a system contains one camera mounted on a fixed pillar, a control system with a data logger and the power unit supplied by a solar panel (Figure 3-11). Normally, analysis of landslide deformation from such a system was carried out using image correlation for 2D displacement on the imagery (Scaioni, 2015). Moreover, additional information, such as a DSM from lidar, is used to re-project from 2D displacement into

3D movement in local units (Travelletti *et al.*, 2012). Although such single-camera, real-time photogrammetric systems are currently used in early warning systems for landslide monitoring, such an approach still has some serious drawbacks. For example, the level of investment in instruments for such an approach is usually high-cost, both in setup and maintenance. Such an approach is therefore most suitable for areas at high-risk to landslide hazards. As a result, it might not support in-situ initial assessment of the need for continuous landslide monitoring. For geotechnical engineering or geophysics, a system that can detect the preliminary stages of a landslide is an important requirement.

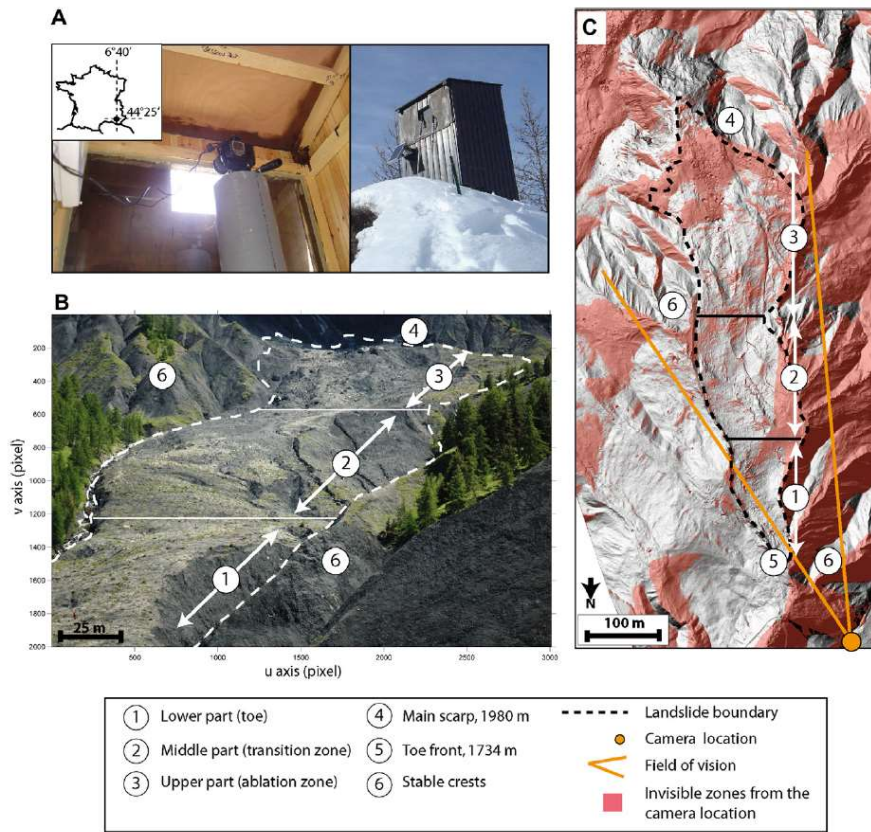


Figure 3-11: Example of a single-camera based photogrammetric system for long-term, in-situ landslide monitoring (Travelletti *et al.*, 2012).

In the case of a generic ground-based photogrammetric approach for landslide monitoring, data collection using photogrammetry can offer time-savings compared to a comparable TLS survey (James and Robson, 2012). With regard to on-site initial assessment, data processing in the field is necessary to achieve a real-time response. Although Castillo *et al.* (2015) developed efficient and free software packages for a

photogrammetric workflow, data processing with this software package for in-situ investigation remains a significant challenge due to time-consuming processes. As discussed above, mobile devices and cloud computing technology are therefore used to overcome serious issues of system development for on-site investigation.

Based on the requirements of developing a photogrammetric measurement and monitoring system for on-site investigation, a mobile platform can offer a portable device for the initial assessment of landslide processes. Mobile cloud computing technology can support real-time processing. A smart phone was used to capture images from all around a landslide area, transfer data for processing on the cloud and display the results of landslide deformation, while the cloud was used for photogrammetric processing and landslide monitoring analysis. The outline of system operation is illustrated in Figure 3-12.

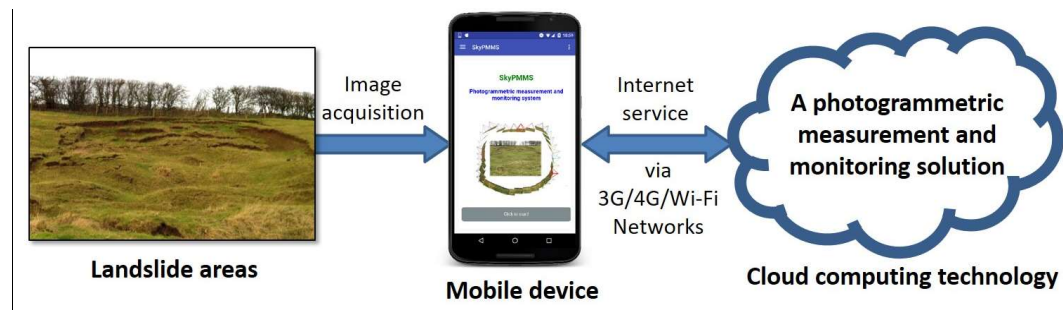


Figure 3-12: The model for the implementation of a photogrammetric solution for landslide monitoring on mobile cloud computing adopted in this research.

Regarding Figure 3-12, the operator can manage the cloud-based photogrammetric measurement and monitoring system on a smart phone through Internet services via a 3G/4G or a Wi-Fi network. The main functionality of developed system may be classified on the basis of tasks for on-site investigation, as follows:

1. High-precision photogrammetric measurement;
2. Automated photogrammetric processing;
3. High-precision geo-referencing;
4. Minimising generic outliers;
5. Automated landslide monitoring analysis;
6. Real-time system and full service operation.

3.3.4 Summary of the mobile platform based landslide monitoring system

With the difficulties of data processing for real-time landslide monitoring on a mobile device, it is necessary to find a solution to manage and process large amounts of information. The difficulties of data processing for real-time response of a system can be solved by mobile cloud computing technology. Mobile cloud computing can manage those problems through the development of mobile application software to utilise external resources from cloud computing technology. The cloud can provide high-performance computing power in order to compensate for the low-performance processor found in the majority of most mobile devices (Fernando *et al.*, 2013). It is a combination of cloud computing and mobile networks that brings benefits for mobile users, network operators, as well as cloud computing providers. Finally, mobile device and cloud computing technology is used in the development of a photogrammetric measurement and monitoring solution.

3.4 Improving photogrammetric processing for landslide monitoring analysis

Although SfM-based photogrammetry can generate 3D model information for monitoring applications via automated processing, the workflows involving image reconstruction and analysis for photogrammetric monitoring in scientific geoscience applications are still complicated (Kaiser *et al.*, 2014). Most commercial SfM software packages offer full photogrammetric processing workflows, but some advanced functions lack details and are treated as a black box for processing. Therefore, the development of a system in this research is only based on open-source software in order to provide a low-cost solution. When performing photogrammetric processing of open SfM-software, the requirement of additional functions in terms of pre-processing, geo-referencing and post-processing is necessary to achieve the appropriate photogrammetric results for monitoring purposes (Castillo *et al.*, 2015). The development of an appropriate analysis workflow is also used to assess the change of landslide processes that is observed using the monitoring system, as illustrated in Figure 3-13. In order to develop an efficient system in terms of real-time response, it is also necessary to develop advanced functions for reducing time-consuming processes.

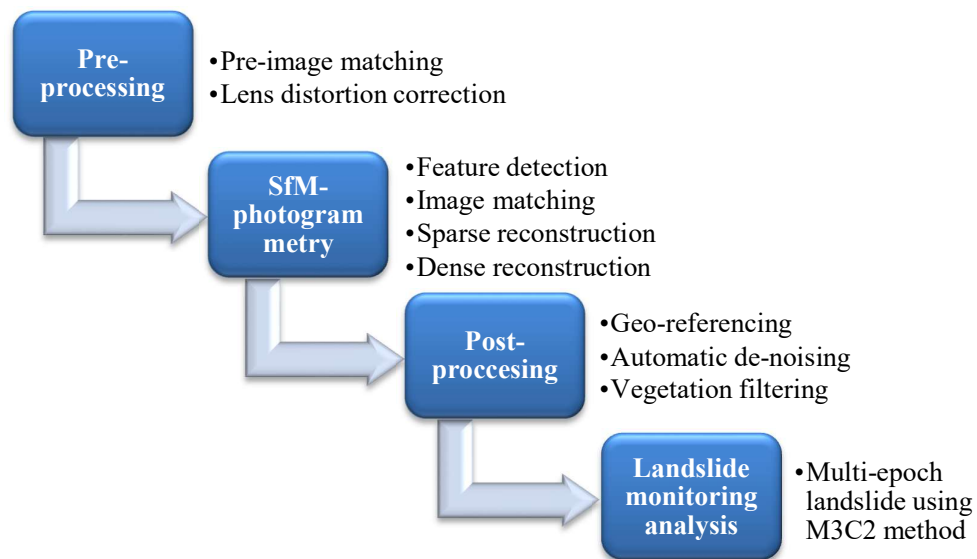


Figure 3-13: Photogrammetry-based landslide monitoring workflow.

3.4.1 Pre-image matching

A fully automated processing workflow based on the SfM-photogrammetric approach primarily uses the basic algorithms of 3D model reconstruction from imagery. Although this advantage can offer the convenience of photogrammetric processing for non-expert operators, it might lead to time-consuming processes in cases of datasets with a large number of images. Such an issue could create difficulties for real-time photogrammetric processing. The workflows of a photogrammetric measurement solution should incorporate an additional algorithm to reduce processing time in the stages of 3D reconstruction. To deal with time constraints of such a problem, a pre-image matching stage is proposed for reducing the time-consuming process of identifying image correspondence in SfM.

Image matching, one of the workflows for the SfM-based photogrammetry, is generally used to find correspondence between each image in the photoset using key features on the imagery. Basically, image matching supposes no-correspondence between each image. Consequently, the image matching algorithm is carried out by a full-pairwise matching of all images. In the case of image acquisition, observation with a systematic, methodical approach can generate useful information in terms of the sequence in which images were captured. Normally, the image sequence is carried out by a frame-to-frame

coherence. From the benefits of sequential images, the relationship between each image may be shown in chronological sequence. The algorithm of pre-image matching, one of the pre-processing workflows before SfM-based photogrammetry is performed, is developed to make a pair-list of image correspondences from image sequences.

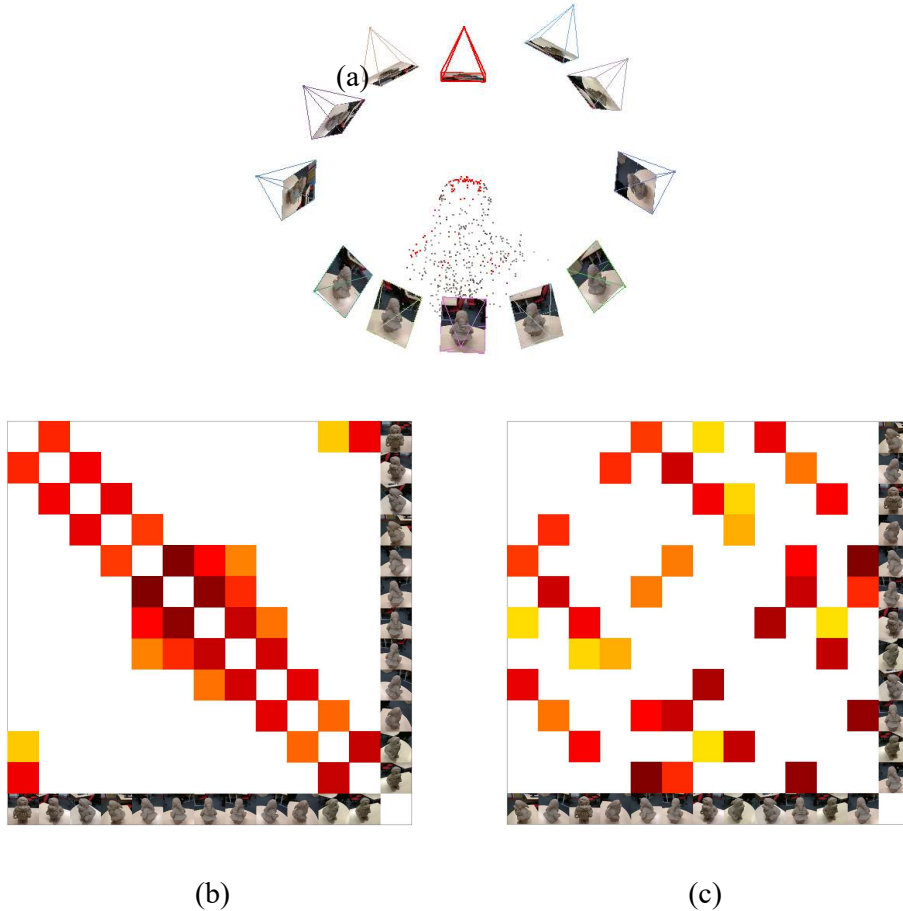


Figure 3-14: Example of 3D reconstruction for (a) imaging configuration and the matrix comparisons of image matching between (b) an image sequence and (c) a non-image sequence.

Following the illustration of Figure 3-14, the matrix of image matching for an image sequence can highlight the relationship between each image and an adjacent image (Figure 3-14(b)). In contrast, for a non-image sequence the image matching matrix was confused (Figure 3-14(c)), meaning there is no correspondence between adjacent images. For images captured from fully covered objects and chronological image capture, image sequences usually result from data acquisition. One advantage of sequent images is a reduced time in matching when using sequential matching. To find the image pairs for

matching, a pre-image matching algorithm was carried out using the pseudocode, as follows:

- Open the directory of image dataset;
- READ all image files into the list of image dataset;
- READ the input of the number of overlapping images;
- For each image in the list of image dataset:
 - SET the central image;
 - Search for the left-hand side image following number of overlaps:
 - READ the image file into the list of left-hand side image dataset;
 - If all of the following left-hand side image dataset, then:
 - WRITE a pair of each left-hand side image name with the central image name into txt file;
 - Search for the right-hand side image following number of overlaps:
 - READ the image file into the list of right-hand side image dataset;
 - If all of the following right-hand side image dataset, then:
 - WRITE a pair of each right-hand side image name with the central image name into txt file;
- Then close the directory.

To explain the workflow of the algorithm developed for pre-image matching as shown in pseudocode above, the previous and the subsequent images are chosen for each image by following the number of overlaps. However, after pre-image matching, the process of image matching is still required, and is performed later at the SfM-based photogrammetry stage. In cases of later additional images or an infill of the circular configuration (Figure 3-14(a)), this algorithm has limitations in immediately identifying new pairs. The recommendation for such situations is therefore not to run pre-image matching and instead perform only image matching.

The function of this algorithm was developed using the Python programming language to derive a pair-list of image matches in the form of a text file. However, the image pairs for subsequent matching depend on the number of overlapping images. The operator can

select the appropriate number of overlaps for at least three images. The example of a pair-list for image matching was computed from an image sequence, as illustrated in Figure 3-15.

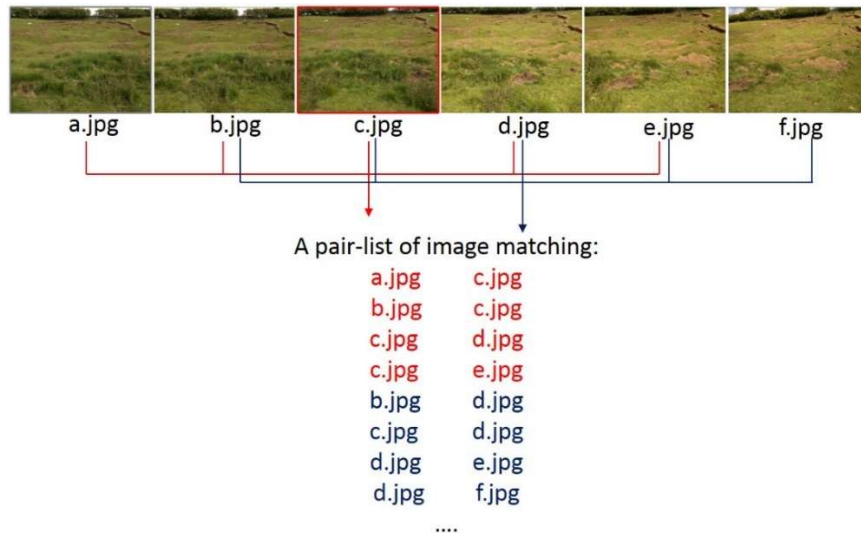


Figure 3-15: The example of a pair-list of image matches from an image sequence.

3.4.2 Lens distortion correction

Lens distortion, especially radial, is one of the systematic errors that directly affect measurements from the imagery. To achieve a high-accuracy photogrammetric measurement, these errors should be minimized prior to photogrammetric processing. Most commercial SfM-based photogrammetric software packages can provide full photogrammetric workflows, whereas open-source SfM-software such as VisualSFM requires the addition of some functions to enhance the photogrammetric workflow. The function of lens distortion correction, for example, is not available to create undistorted images. Thus, a function for undistorted image creation in the pre-processing stage of the SfM photogrammetry pipeline is proposed.

The development of the function for lens distortion correction was carried out using a Python script with OpenCV library (Bradski and Kaehler, 2008). This function allows the operator to set the parameters of the camera model (focal length, principal point and lens distortion). As already detailed, these parameters were examined for the smart phone camera using automated self-camera calibration using the camera calibration tool in

Matlab software (Bouguet, 2000). The undistorted images were then used with the fixed calibration mode in VisualSfM for photogrammetric processing to reconstruct 3D models. The workflow of the function for lens distortion correction is illustrated in Figure 3.16.

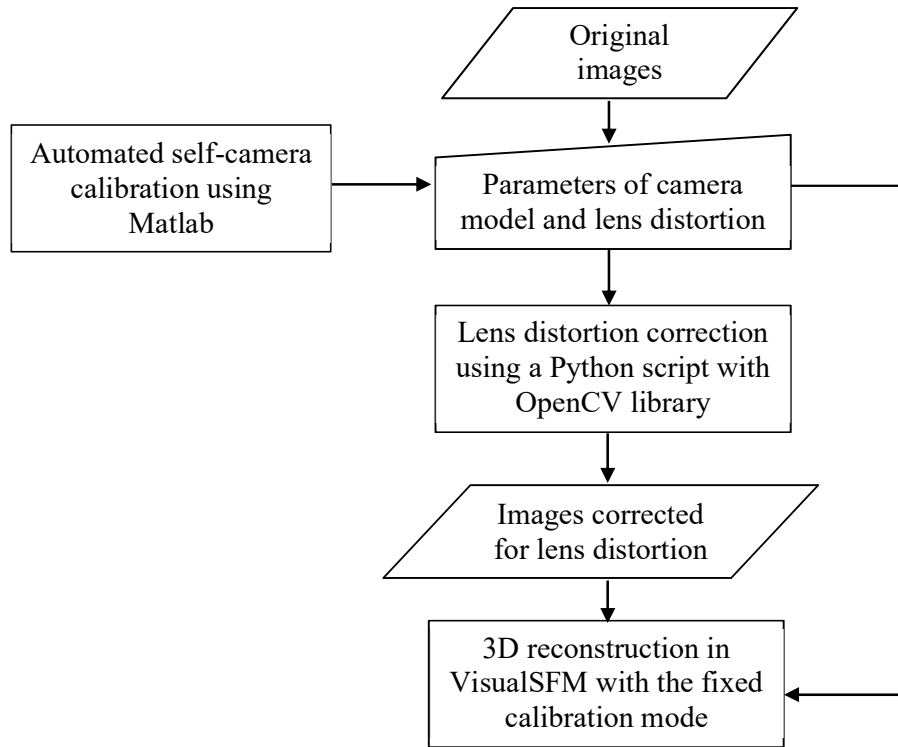


Figure 3-16: The workflow of the developed function for 3D reconstruction using lens distortion correction.

3.4.3 Geo-referencing

After 3D reconstruction from the imagery using the SfM workflow, photogrammetric results usually do not have any spatial information because its approach does not require ground control to calculate camera parameters and orientations. To assess landslide processes using multi-epoch analysis, photogrammetric results at different epochs have to be geo-referenced into the same coordinate system before comparison (Scaioni, 2015). Although the SfM-based photogrammetric processing does not require ground control points or targets, the use of targets is essential to achieve a high-level of precision for geo-referencing of photogrammetric results. In the case of geo-referencing with photo control targets, observations should take place directly on the imagery rather than in the derived

point cloud. In this research, the use of some form of photo control targets is a requirement for geo-referencing.

The methods of geo-referencing based on the system development may be classified by techniques of observing the locations of targets. Although the locations of the photo control targets may be observed using GNSS or TLS survey, because of the requirement for high-accuracy, this approach would be costly in terms of equipment and labour. Moreover, the requirement of post-processing for GNSS/TLS data would be prohibitive. Based on the practicalities of survey for landslide monitoring, geo-referencing without GNSS or TLS observation is therefore offered as an option for in-situ investigation. As a result of this, the functional development of geo-referencing is implemented into two methods of target observation with & without GNSS/TLS directly from the imagery on the smart phone.

3.4.3.1 Geo-referencing with GNSS/TLS based target observation

GNSS or TLS observations are required to provide the locations of targets for this method of geo-referencing. After post-processing of the GNSS or TLS data, the 3D coordinates of target locations are imported into the smart phone. The development of a function for manual geo-referencing on the smart phone is used to make a pair-list of target positions between image coordinates and the corresponding real world coordinates obtained from either the GNSS or TLS observation. The observation of targets can be made directly in the imagery through the function developed for geo-referencing. After target observation, a pair-list of target positions is exported into a text file format suitable for use in geo-referencing the photogrammetric results in VisualSFM. This approach to geo-referencing is illustrated in Figure 3.17.

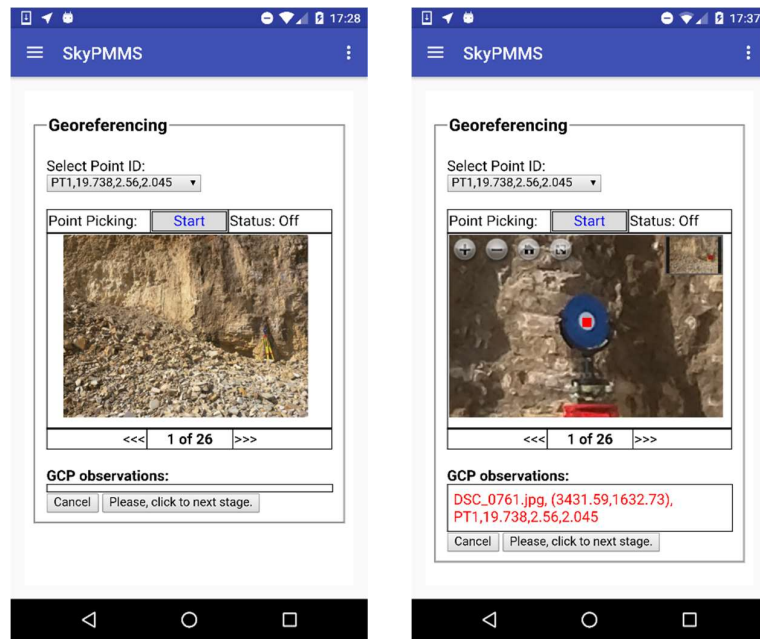
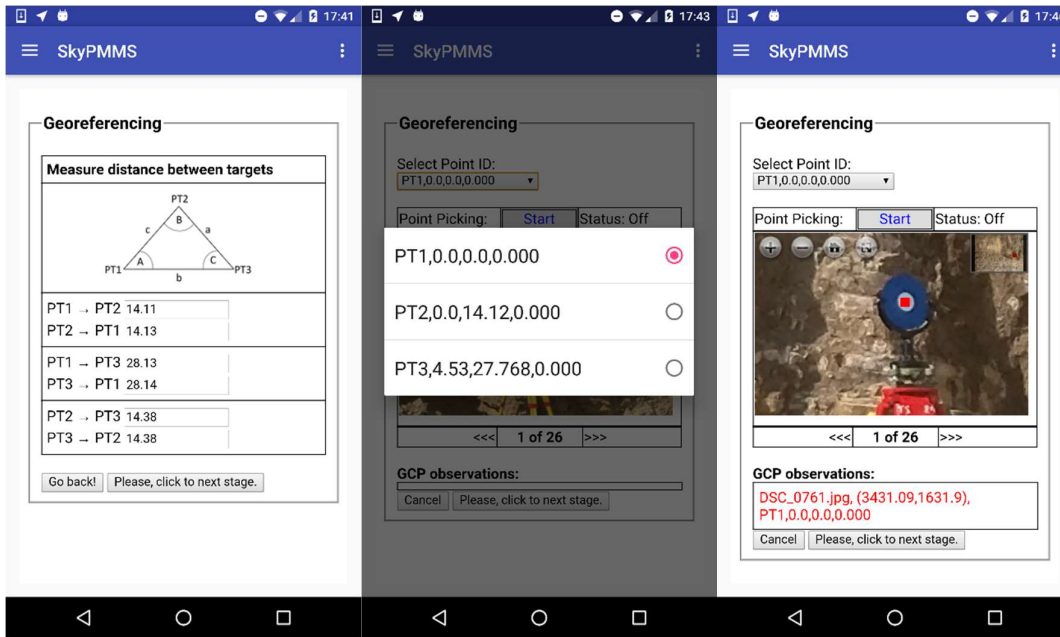


Figure 3-17: Illustration of the developed function for GNSS/TLS target observation.

3.4.3.2 Geo-referencing without GNSS/TLS based target observation

To avoid using GNSS or TLS survey for target locations, an alternative solution to geo-referencing was developed. This approach is divided into three stages. Firstly, the scaling of the photogrammetric results using distances between targets is performed. The observation of distances between targets can be carried out using a tape measure or laser distance measurement device to provide a precise distance measurement. Measuring six distances between a pair of three targets is the minimum requirement for scaling the photogrammetric results (Figure 3-18(a)). To generate pseudo-position of targets from these distances, the locations in 3D coordinates of three targets are calculated using a Python script with NumPy and SciPy libraries (Figure 3-18(b)). Then, the location of the targets is directly observed in image data through the developed function (Figure 3-18(c)).

Secondly, the alignment of photogrammetric results at different epochs is carried out manually using the point pairs picking tool in CloudCompare. The point pairs for alignment are selected from the key features in the point cloud. Thirdly, to enhance alignment of two point clouds, automatic geo-referencing is carried out using the iterative closest point (ICP) algorithm without scaling in CloudCompare.



(a)

(b)

(c)

Figure 3-18: Illustrations of the developed function of scaling for geo-referencing using distances of known objects.

This application of scaling with the distances of known objects on a smart phone was developed to provide accurate dimensions for photogrammetric results. However, this approach is not yet fully implemented on the system because web-based point cloud processing is necessary for the stage of manual alignment between epochs. At present, the web-based technology for point cloud is limited only to a 3D viewer for visualization. The practical application therefore still requires future development of a web-based service for point cloud processing. Thus GNSS/TLS is necessary for geo-referencing.

3.4.4 Automatic de-noising

Routine image capture using a mobile device camera in a natural environment cannot fully control the intensity of light at time of image capture. Image acquisition may therefore result in different image quality in terms of contrast and brightness. Moreover, the different kinds of surface type over landslide areas, such as grasses or trees, will be recorded. These concerns lead to an uncontrollable factor in photogrammetry. As a result, the SfM-photogrammetric results are often prone to matching errors in the multi-view stereo dense surface reconstruction process. Noise can be generated in the point cloud

due to repetitive texture patterns or poor image contrast in the imagery (Scaioni, 2015). This is particularly so over vegetated surfaces such as those found in a natural landslide, as presented in Figure 3.19, and these can have a direct impact on the quality of results.

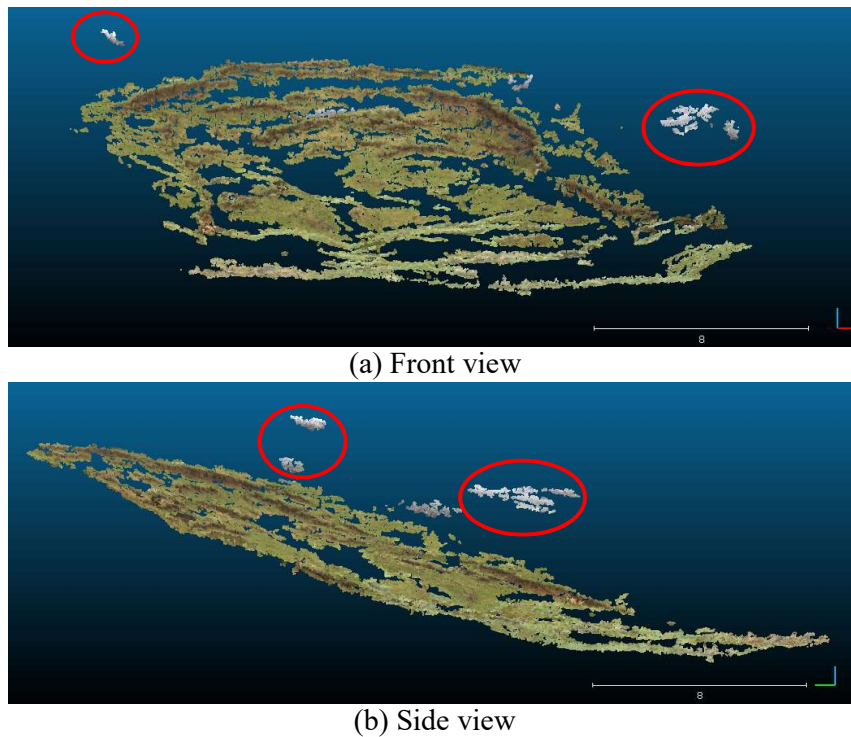


Figure 3-19: Example of noise in a point cloud from the SfM- photogrammetric approach applied to a natural landslide: the red circles highlight noisy points.

To reduce the negative effect of gross errors, a de-noising stage is used to remove noise from the point cloud and improve the quality before the assessment of landslide processes. The de-noising is based on the application of a statistical outlier removal (SOR) filter. In this method, a computation at each point is performed to determine the average distance between itself and the neighbouring point dataset. The removal of points is determined by a criterion of statistical analysis based on the neighbour's distances. The distribution of their resulting distances is supposedly normal. A mean and a standard deviation of this statistical analysis are considered as the criterion of de-noising. If the mean distance of each point is further from the criterion then these point are defined as outliers and noisy points are removed from the point cloud. An example of automatic de-noising is shown in Figure 3.20.

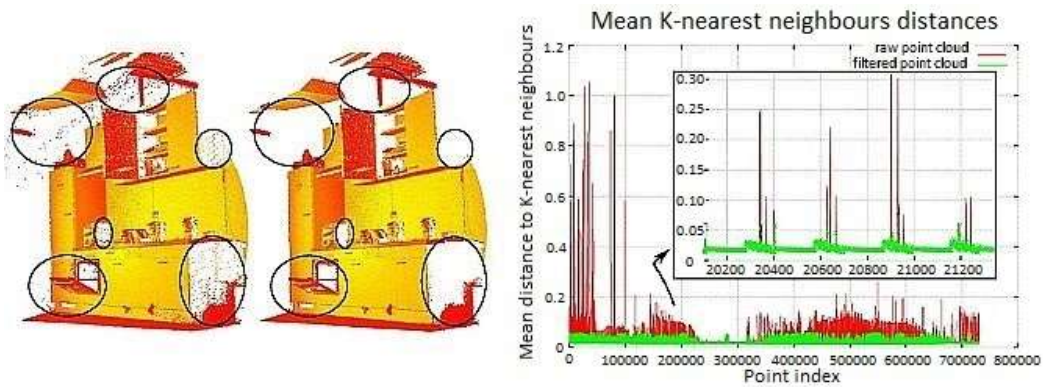


Figure 3-20: Example of automatic de-noising based on the SOR filter (PCL, 2017).

The automatic de-noising filter was carried out using functions based on the system through command line syntax of the SOR filter in CloudCompare software. The selection of the optimum parameters for automatic de-noising is necessary to remove outliers from photogrammetric results. These parameters include the number of points to use and the statistic of standard deviation. However, the developed function can offer the setting of both parameters directly by the operator.

3.4.5 Vegetation filtering

Although a photogrammetric approach can provide the high-accuracy results required for landslide monitoring applications, photogrammetric approaches still have a significant drawback in that they cannot penetrate the surfaces of vegetated areas. In particular, vegetated surfaces (such as grass) are usually found in a natural landslide that directly affects photogrammetric results for surface deformation monitoring. Moreover, seasonal changes also result in different heights of vegetated surfaces over landslides. Consequently, the uncertainty of surfaces obtained from vegetation effects can cause unreliable assessment of landslide processes. The results obtained from the SfM-photogrammetric approach over vegetated surfaces require elimination of this effect before landslide monitoring analysis. Vegetation filtering is proposed to extract only bare-earth points of photogrammetric results and thereby ensure an appropriate assessment, especially in the case of a natural landslide. Thus, Figure 3-21 shows the workflow of a filter to remove points over vegetated surfaces.

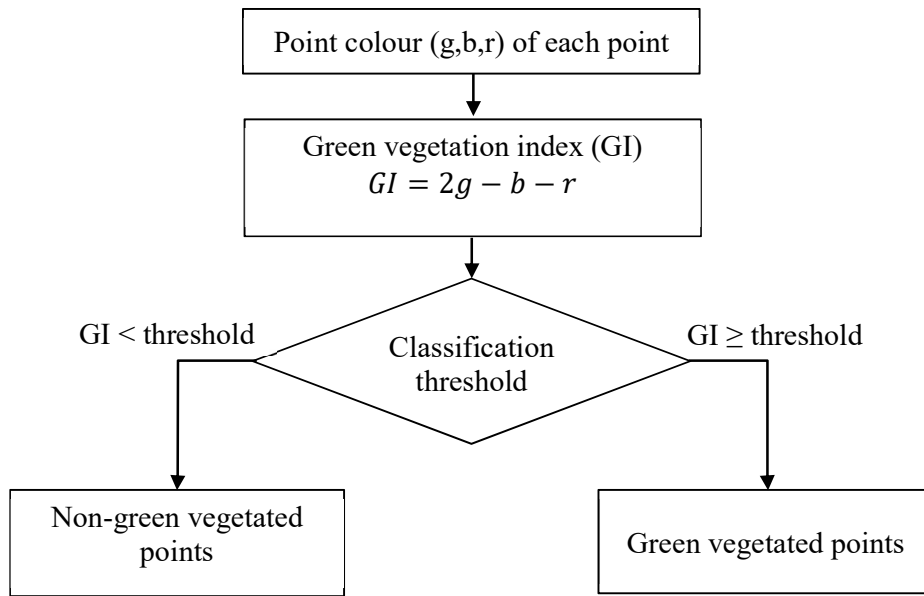


Figure 3-21: A workflow for vegetation filtering of the photogrammetric results.

Vegetation filtering was carried out using the green vegetation index obtained from point colours (RGB). The green vegetation index is calculated as shown in equation (3-7) (Meyer and Neto, 2008).

$$GI = 2g - b - r \quad (3-7)$$

where GI is the green vegetation index; r , b and g are the RGB values of each point. Focusing on the classification of the point cloud by the value of green vegetation index for each point, the setting for the threshold value of green vegetation index is carried out by the operator. All points that are less than the threshold value are non-green vegetated points and are assumed as bare-earth points. In contrast, points that are greater than the threshold value are assumed as points over vegetated surfaces, and are removed from the point cloud. The developed function on the system was carried out using a Python script with a function to export the point cloud file format through CloudCompare software.

3.4.6 Change assessment

After the post-processing stages for photogrammetric results, including geo-referencing, automatic de-noising and vegetation filtering, the quality of photogrammetric results are improved for landslide monitoring analysis. The enhanced results at different epochs are used for multi-epoch analysis to assess landslide processes. Following the landslide analysis methods in section 3.2.5, the M3C2 technique of point cloud comparison method was used for assessment of the landslide changes to deliver the preliminary results of landslide monitoring in this research.

The key parameters (Figure 3-22) of the M3C2 method for multi-epoch analysis are used for the change detection of landslides, including:

- D - the scale factor or normal scale;
- d - the project scale;
- p_{max} - the height of the projection cylinder or the maximum distance;

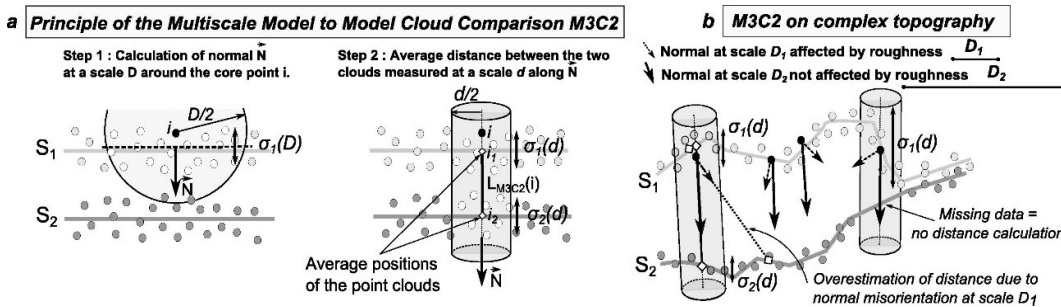


Figure 3-22: The outline of the key parameters used in the M3C2 algorithm (Lague *et al.*, 2013).

To explain the M3C2 algorithm as shown in the figure above, there are three main stages in a comparison to find the differences between two point clouds. Firstly, the normal vector is determined using the scale factor, D , to find a direction of the different distance in the comparison. Next, the distance is calculated along a normal vector within a cylinder of diameter d to determine the difference. Finally, if the difference is more than the maximum distance, p_{max} , it is assumed it cannot be calculated due to missing data. It is acknowledged that the M3C2 parameters might be complicated for non-experts to

understand. Thus, details of the appropriate values for those parameters are reviewed and described in the next chapter.

Although the M3C2 algorithm in CloudCompare is generally used for point cloud comparison to calculate the differences between two point clouds, this approach is difficult to implement on the landslide monitoring system due to its advanced plug-in software. To employ the M3C2 method in the system development, an open-source M3C2 tool was therefore implemented into the workflow for landslide monitoring analysis, as illustrated in Figure 3-23.

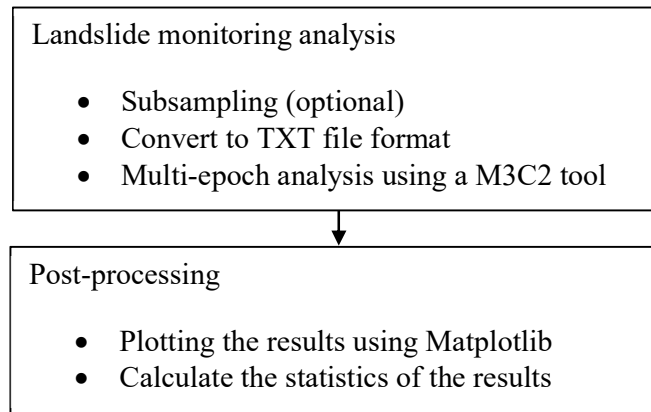


Figure 3-23: The outline of the workflow for landslide monitoring analysis.

There are several procedures required for landslide monitoring using multi-epoch analysis based on the M3C2 technique. Firstly, the input datasets of two point clouds might need to be subsampled using CloudCompare through command line syntax if it is required to decrease the number of points for timesaving analysis. Secondly, the two point clouds are converted to TXT file format using CloudCompare in order for analysis using the M3C2 tool. Thirdly, the differences between the two point clouds are determined using M3C2 tool, and the results of different distances generated in TXT file format. Next, to represent the differences between both point clouds, a graph showing the results is generated using a Python script with Matplotlib library. Finally, the statistics of the differences comprising the value of mean, the standard deviation, minimum and maximum are calculated and represented using a Python script.

3.5 System development

The workflow of photogrammetric measurement and monitoring process can be divided into two main modules: 1) photogrammetric measurement for providing 3d reconstruction results of the different epochs; 2) landslide monitoring analysis to assess the changes of landslide processes between two epochs. The main workflows of landslide monitoring in this research are shown in Figure 3-24.

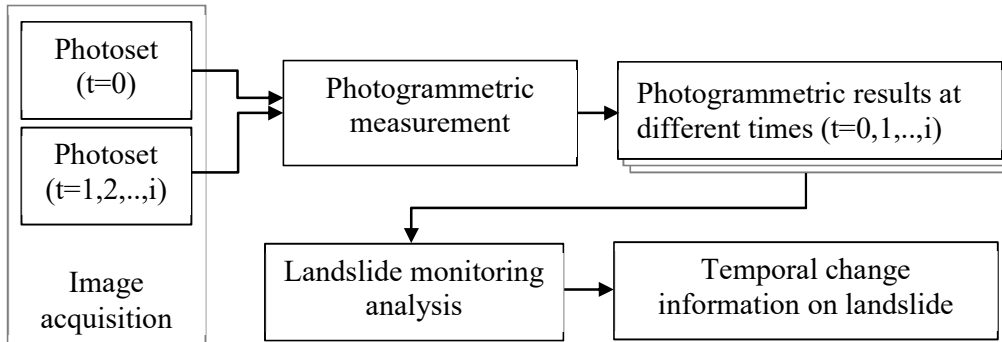


Figure 3-24: A generic landslide monitoring workflow using a photogrammetric approach.

The development of each afore-mentioned function for enhanced photogrammetric processing, including pre-processing, geo-referencing and post-processing is applied in the workflows of the SfM-based photogrammetric approach. The developed workflow of change assessment is used for landslide monitoring analysis. The details of implementation and development of these two modules using mobile cloud computing technology are described in this section.

3.5.1 System layout

From the design of a photogrammetric measurement and landslide monitoring system for on-site investigation in this research, the solution was based on simplicity and flexibility for the operator. The architecture of system development was designed based on mobile cloud computing services. The components of the system are divided into two main aspects:

1) a remote, cloud-based server that is used to temporarily store and process image data in order to generate the photogrammetric results and analyse the landslide from those results;

2) a local client, running on the mobile device, is used to upload images to the cloud, set processing options and then subsequently display the photogrammetric results (such as 3D point clouds of the landslide area). Moreover, it is used to control analysis of landslide monitoring and then display the results after landslide monitoring analysis.

This developed system, which is named Sky Photogrammetric Measurement and Monitoring System or SkyPMMS, was based on client-server communication via the Hyper Text Transfer Protocol (HTTP) using the Internet service, as shown in Figure 3-25.

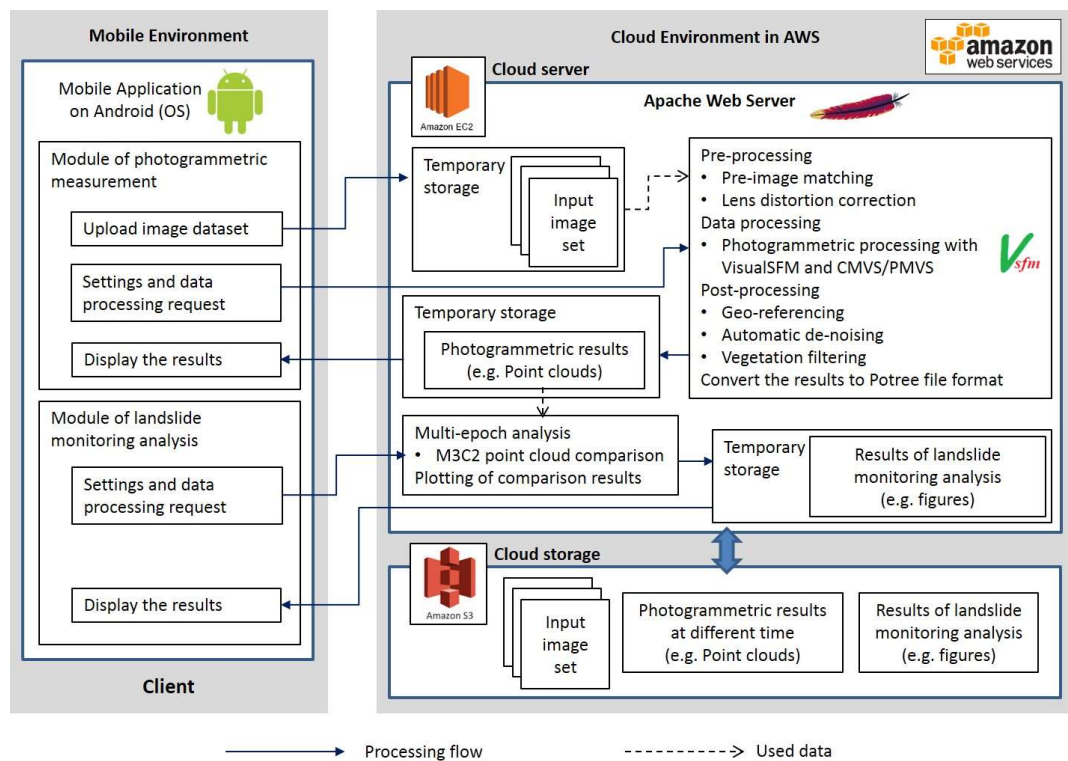


Figure 3-25: System architecture based on mobile cloud computing for photogrammetric measurement and landslide monitoring.

SkyPMMS uses a public cloud server that adopts the Amazon Elastic Compute Cloud (Amazon EC2) instance (Amazon Web Services, 2016) as a cost-effective service with flexible handling. For example, the price of AWS cloud computing services depends on

pay-per-use. Moreover, the elasticity of cloud computing can help to automatically manage the processing workload on a system such as data processing based on a multi-cloud server. The Amazon Simple Storage Service (Amazon S3), a cloud storage service, is used to back up the image data and the results from both the photogrammetric measurement and landslide monitoring analysis in order to avoid losing data. The SkyPMMS client uses the thin client approach, which is able to access the system through the standard web browser on a smart phone. However, the development of a mobile application can make accessibility to the system more convenient for the user. Thus, a front-end and back-end are developed in the system of SkyPMMS according to the requirements of the user.

3.5.2 Implementing system

Data processing for 3D reconstruction based on the SfM-photogrammetric approach required high-performance computing through the use of a GPU processor. GPU computing uses highly parallel processing based on many-core technology to deal with the computationally-intensive modules of the SfM workflow. Processing based on this solution can achieve a near real-time response. The system was implemented on a GPU cloud server in the g2.2xlarge Amazon EC2 instance type in order to handle the high processing demands of the SfM software modules. In addition, another type of Amazon EC2 instance for a GPU cloud server, which uses a higher-memory of GPU, can offer sufficiently faster processing times to meet the demands of a real-time monitoring system.

However, the price of cloud computing services depends on the performance of components on a cloud server such as CPU, memory and storage. In particular, the price of data processing on a GPU cloud server is usually higher than a basic cloud server. In order to develop a system that minimises cost for data processing, the options of data processing on multi-cloud servers were developed to be chosen by the user. The operator needs to optimise the use of the cloud server from the expense of data processing and processing time on the cloud. In this research, the back-end of the system for data processing is divided into two basic cloud servers, comprising a GPU cloud server and a cloud server without GPU (Figure 3-26).

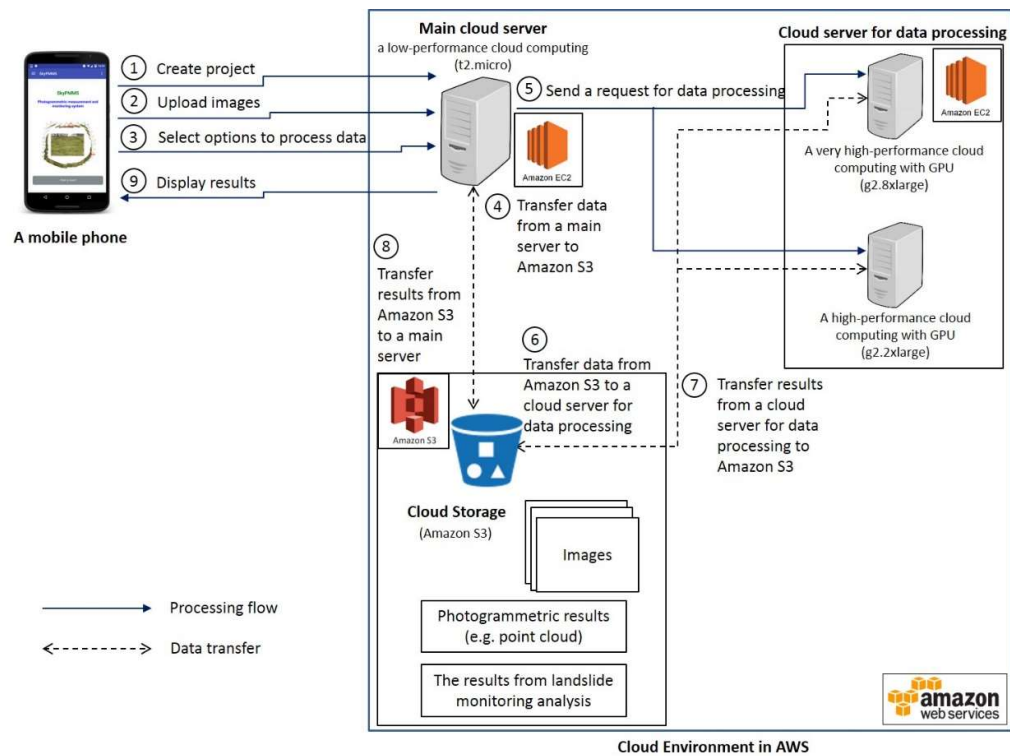


Figure 3-26: The workflow of data processing for photogrammetric measurement based on a multi-cloud server.

For data processing based on multi-cloud servers, the components of this system have many functions. Firstly, a main cloud server of the t2.micro Amazon EC2 instance type, the lowest-cost of AWS cloud server, is used to control data transfer between mobile platform-to-cloud server and cloud-to-cloud servers, receive and send a request for data processing, and then respond to display the results on a smart phone. Secondly, a GPU cloud server in the g2.2xlarge or g2.8xlarge Amazon EC2 instance type is used to process the photogrammetric measurement of the SfM software and provide landslide change analysis. Finally, the Amazon S3, a cloud storage service, is used for central storage to transfer data between two cloud servers. Although this method may lead to delayed processing due to having many stages for data transfer between each cloud server, a reduced time delay between stages is insignificant for data processing. During the temporary disuse of data processing for photogrammetric measurement and landslide monitoring analysis, the user can stop the GPU cloud server working. This minimises expense of the pay-as-use cloud based system. The solution of data processing on a multi-cloud server therefore performs a balance of the workload on cloud computing to provide a low-cost approach to system development. For the execution of this system developed

for landslide monitoring, the monthly costs of both photogrammetric processing and monitoring analysis using the Amazon cloud server and cloud storage are approximately £20 (2018 prices).

To implement the system on a multi-cloud server, the development of the back-end service is divided into two key modules in SkyPMMS, following the illustration presented in Figure 3.25. With the module of photogrammetric measurement to generate the photogrammetric results (Figure 3.27), the cloud servers implement several procedures and software routines, as follows:

- 1) jQuery File Upload is used to upload image files from the mobile device to the main cloud server.
- 2) Image data are transferred from the main cloud server and stored in the Amazon S3 cloud storage using the AWS Command Line Interface (CLI).
- 3) The settings of data processing are sent to the GPU cloud server with a request for processing and then the image data is retrieved from the Amazon S3 cloud storage.
- 4) The developed functions of pre-processing for the SfM technique, such as pre-image matching and lens distortion correction are used to prepare the image data before photogrammetric processing.
- 5) VisualSfM is used for 3D reconstruction of the imagery from landslide monitoring areas and then MVS techniques using CMVS/PMVS (Furukawa *et al.*, 2010; Furukawa and Ponce, 2010) generates point clouds.
- 6) The advanced functions of post-processing such as geo-referencing, automatic denoising and vegetation filtering are used to prepare the results prior to landslide deformation assessment.
- 7) The PotreeConverter open source code (Schütz, 2015) is used to convert the results to Potree format to utilise rendering of the point clouds, and then the results are transferred from the GPU cloud server and stored on the Amazon S3 cloud.

In addition, the main cloud server is used to retrieve the results from the cloud storage and update the view of the point cloud through a web-based 3D viewer. This implementation of the back-end service uses the HTML rendering code with a PHP script in order to control the workflow of the photogrammetric measurement system on both the cloud servers and display the output.

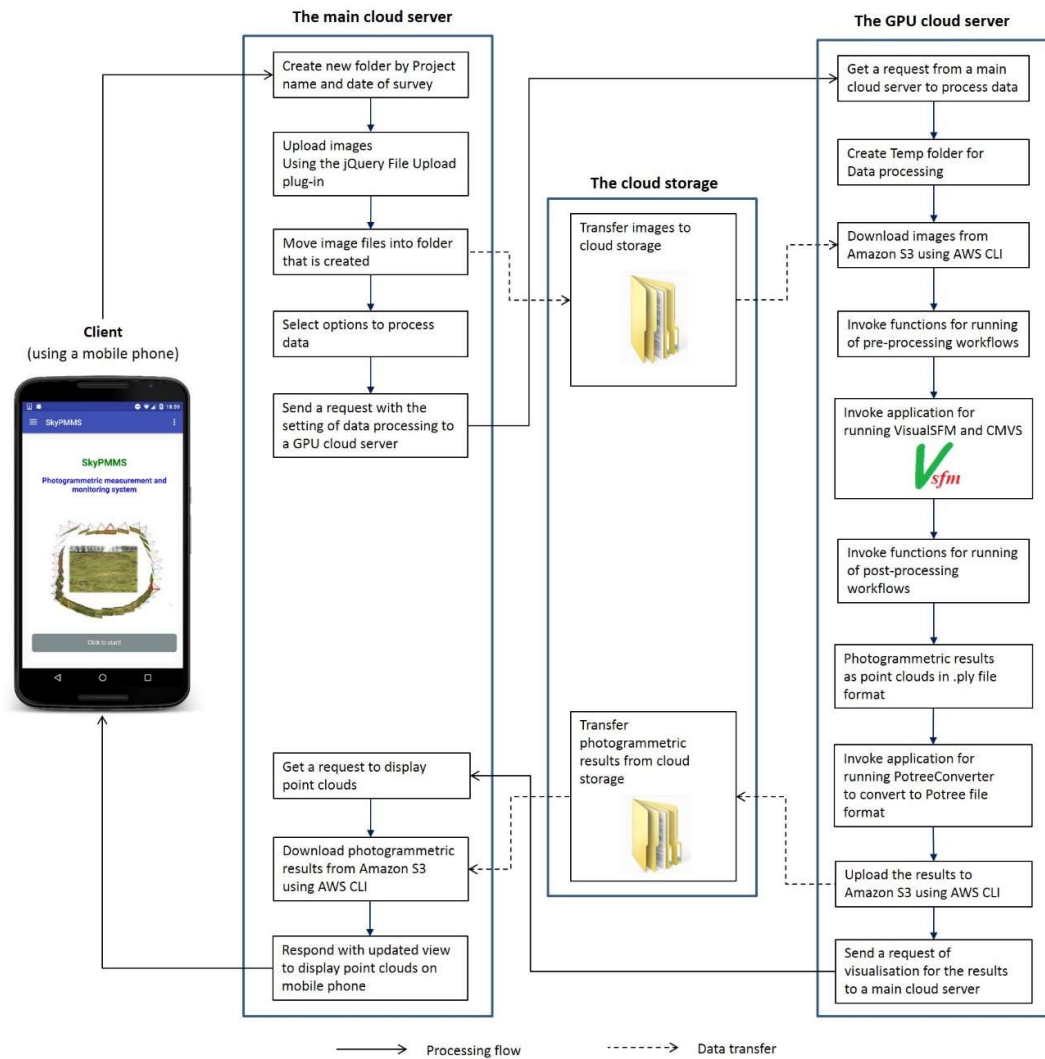


Figure 3-27: The workflow of the photogrammetric measurement module based on a multi-cloud server.

With regards to the second main module of the back-end service (Figure 3.28), there are several tasks implemented on the cloud servers to analyse multi-epoch datasets in order to assess landslide processes over time, as follows:

- 1) The main cloud server is used to retrieve the settings of multi-epoch analysis from a smart phone and send a request for analysis to a cloud server for data processing.
- 2) The cloud server for data processing retrieves the photogrammetric results from the Amazon S3 cloud storage according to the settings of multi-epoch analysis, and then performs the change assessment of landslides (following the workflow in section 3.4.6).

- 3) The results from landslide monitoring analysis are transferred from this cloud server and stored on the Amazon S3 cloud server and stored on the Amazon S3 cloud.

Furthermore, the main cloud server is used to retrieve the results from the cloud storage and update representation of the output to the mobile platform. SkyPMMS also employs the thin client approach through HTML5 technology such that it can operate using a standard web browser on multiple platform types (e.g. smart phone, tablet, desktop computer).

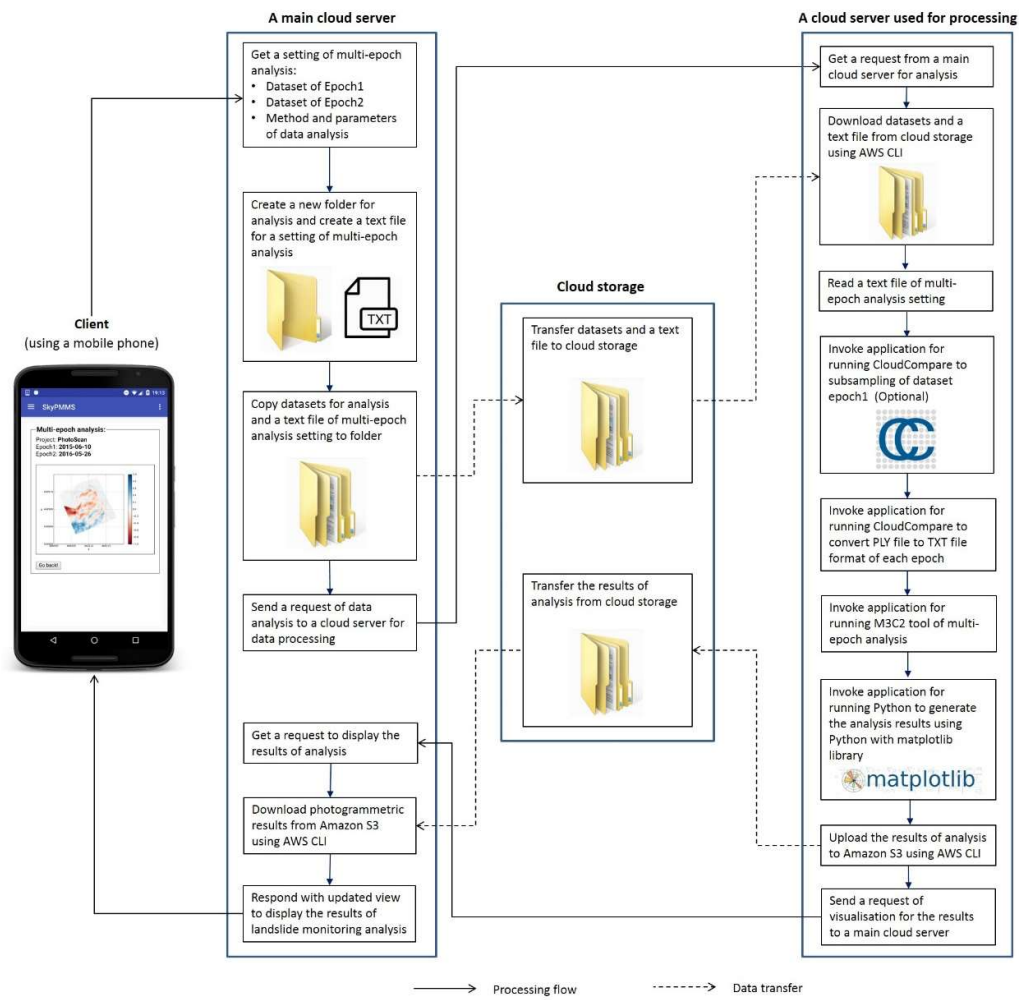


Figure 3-28: The workflow of the landslide monitoring analysis module based on a multi-cloud server.

3.5.3 Development of a mobile application

The mobile application is used as the front-end viewing platform for SkyPMMS in order to connect to the landslide monitoring system on the cloud environment. This application also helps the operator to control the system on a smart phone for on-site investigation of landslide monitoring. The development of this mobile application is based on an Android OS using the Java programming language in the Android Studio integrated development environment (IDE). The development of the front-end utilizes WebView to display web pages for Android mobile application that is similar to a standard web browser on a smart phone. The front-end client using a mobile application has an advantage over using a standard web browser in that it does not request the URL of the main cloud server.

The main features of this front-end side of SkyPMMS can be classified according to the two main modules of the system, as shown in Figure 3-25. First, the photogrammetric measurement module is used to upload images, select options for processing, send data processing requests and illustrate point cloud results in a 3D viewer on a smart phone. Second, the landslide monitoring analysis module is used to select photogrammetric results, set the parameters of the M3C2 method and display the output of analysis in a 2D viewer. Figure 3-29 shows the user interface for the mobile application of both modules. The manual of this mobile application is provided in Appendix C.

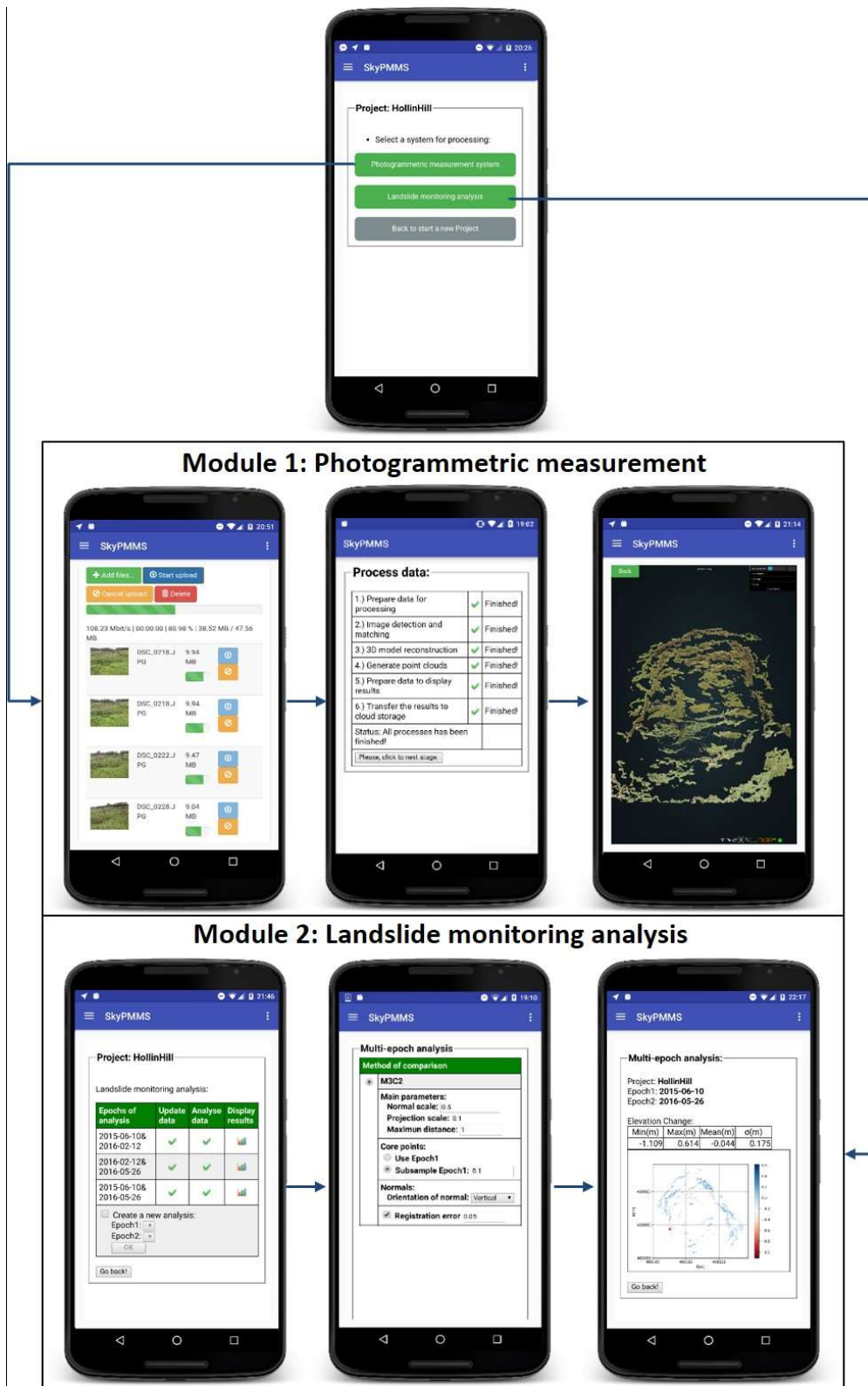


Figure 3-29: Example of the user interface for the developed mobile application of the landslide photogrammetric monitoring system.

3.5.4 Summary of the developed system

The SkyPMMS system was developed in the form of a Web-based service for photogrammetric measurement and landslide monitoring. The cloud server and cloud storage service were implemented for the back-end of the system. The multi-cloud server was applied to manage data processing for a real-time response. Photogrammetric processing on the GPU cloud server worked efficiently to resolve the problem of computationally-intensive workflows of the SfM software. The connection of the system uses Internet via a 3G/4G or a Wi-Fi network on mobile devices. The operator can utilize the developed system through a mobile application to process landslide monitoring in-situ.

3.6 Summary

A photogrammetric monitoring solution using mobile devices has been proposed for on-site investigation of landslide monitoring to deliver a low-cost approach for geology, geophysics or geotechnical engineering. The system implementation and development for on-site investigation of landslide monitoring is designed based on a mobile platform with cloud computing technology to enable real-time processing. SfM-based photogrammetry is used for photogrammetric processing that is fully-automated processing. Although the use of non-commercial SfM software for 3D reconstruction from the image data is required for the development of a low-cost landslide monitoring system, the development of advanced functions was necessary to deliver appropriate photogrammetric results before assessing landslide processes. Focusing on the stages related to pre- and post-processing of SfM photogrammetry, the developed functions are used to improve the quality of results and enhance the performance of data processing. The development of workflows for landslide monitoring analysis are used to deliver the preliminary results for assessing the changes in landslide deformation. The landslide photogrammetric monitoring system utilises automated workflows to offer friendliness for the operator. Evaluation of the developed functions ensured satisfactory system performance before assessing and testing the solution at the landslide test areas. Experimental studies of the system are described in the next chapter.

Chapter 4. Performance evaluation

4.1 Introduction

The development of a monitoring system in this research aims to offer a low-cost, real-time photogrammetric solution for the initial assessment of landslide hazards using a smart phone. The primary evaluation of the photogrammetric potential of a smart phone camera and the allied processing software was essential to ensure the quality of results for landslide monitoring purposes. In the case of on-site investigation, the developed system was expected to deliver a real-time photogrammetric measurement and monitoring solution directly on the employed mobile device. The performance of developed functions for the improved photogrammetric processing and landslide monitoring on the cloud is evaluated in this chapter.

4.2 Photogrammetric landslide monitoring using mobile devices

Before developing a solution for photogrammetric measurement and implementing landslide monitoring on a smart phone, it was necessary to evaluate the photogrammetric results from a smart phone camera to investigate the potential of affordable image-based mobile technology for landslide monitoring. A smart phone camera with a 5-megapixel sensor was evaluated as a typical off-the-shelf camera. Moreover, in this experiment imagery was collected using a DSLR camera with a high-quality sensor in order to compare against the photogrammetric results from a low-cost smart phone camera. The evaluation of the photogrammetric results from different processing softwares for both cameras was used to examine the capability for measuring landslide movement.

4.2.1 Experimental design

In a comparison of using different digital cameras for landslide monitoring, a smart phone (iPhone 4) and a DSLR (Nikon D300) camera were tested. The details of both digital cameras were described in the previous chapter. Two image datasets were captured on 20 March 2015 around a natural landslide slope at the British geological survey (BGS)'s Hollin Hill landslide observatory using both cameras at the same positions. Each image dataset comprised 48 images. Targets were established and used for photo control points in geo-referencing to provide photogrammetric results in the same coordinate system. The location of targets was determined using a TLS survey. Moreover, a higher-resolution, higher-accuracy dataset was collected on the same day using TLS observation to enable an accuracy assessment of photogrammetric results. In this experiment, the methodology was carried out as illustrated in Figure 4-1.

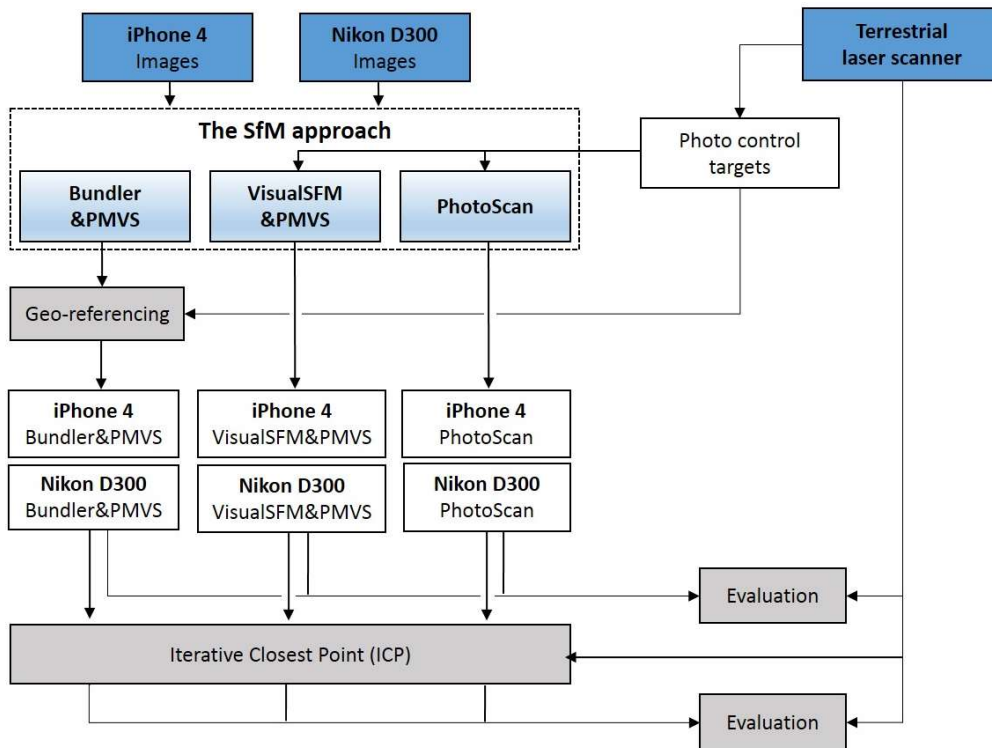


Figure 4-1: Methodology in the camera comparison experiment.

With regard to the SfM-photogrammetric processing, 3D reconstruction of both image datasets was performed using three software packages, including: 1) AgiSoft PhotoScan; 2) VisualSfM & PMVS; 3) Bundler & PMVS. For geo-referencing in PhotoScan and

VisualSfM & PMVS, the observation of targets was directly carried out in the imagery. These photogrammetric results were in the form of 3D point clouds with geospatial information. On the other hand, photogrammetric results obtained from Bundler & PMVS had to be georeferenced using the resultant point clouds and the point pairs picking tool in CloudCompare. For assessment of photogrammetric accuracy, the comparison between photogrammetric results and higher quality data from the TLS survey was performed using the C2M distance in CloudCompare. This comparison method was computed by associating each point in the evaluation dataset (the SfM models) with its closest point in the reference dataset (the TLS data). As a result of this, the differences between the SfM models and the TLS data were calculated as three-dimensional distance errors. However, geo-referencing might cause additional errors in the transformation processes. To reduce this negative effect, the ICP algorithm (without adjustment of scaling) was applied to the photogrammetric results before comparison (James and Robson, 2012; Micheletti *et al.*, 2015a)

4.2.2 Test results

Unfortunately, the Bundler photogrammetry package, comprising Bundler and PMVS, could not deliver the necessary photogrammetric results in this experiment because of too few number images to enable reconstruction of a 3D model. However, photogrammetric processing was achieved in both PhotoScan and VisualSfM & PMVS for 3D reconstruction from the same images. The different performance of each SfM software had a direct impact on the potential of photogrammetric processing. The comparison of results between the SfM outputs and the TLS data was calculated as distance errors to quantify the photogrammetric accuracy of each camera and SfM software (Table 4-1).

Table 4-1: Statistics of distance errors between SfM models and TLS data for direct registration and after applying the ICP algorithm.

Digital camera	Processing software	After geo-referencing			After applying ICP		
		Mean (m)	SD (m)	RMSE (m)	Mean (m)	SD (m)	RMSE (m)
Nikon D300	PhotoScan	0.022	0.020	0.021	0.000	0.022	0.025
	VisualSFM & PMVS	0.018	0.023	0.025	-0.002	0.030	0.031
iPhone 4	PhotoScan	0.032	0.034	0.035	0.015	0.030	0.032
	VisualSFM & PMVS	0.030	0.058	0.060	0.008	0.056	0.057

Following Table 4-1, the mean and root-mean-squared error (RMSE) values of both PhotoScan and VisualSFM and PMVS (using a direct registration) from a Nikon D300 camera were smaller than from an iPhone 4 camera. It is likely that the photogrammetric accuracy captured from a Nikon D300 camera was slightly better than from an iPhone 4 camera in both SfM software packages. Moreover, the photogrammetric results obtained from PhotoScan provided a higher accuracy than VisualSFM and PMVS for both cameras. After applying the ICP algorithm to photogrammetric results, the mean of distance errors between the SfM models and the TLS data decreased significantly to 0.0 and 1.5 cm. This mean value of distance error reveals a biased outcome after geo-referencing, whereas it does not show the quality of photogrammetric accuracy (Stumpf *et al.*, 2015). Clearly, the ICP algorithm helped reduce influences of geo-referencing errors for the SfM approach. The RMSE values of a Nikon D300 from PhotoScan and VisualSFM & PMVS increased to 0.4 and 0.6 cm, respectively after applying the ICP algorithm. Meanwhile, the RMSE values of an iPhone 4 from both software decreased to 0.3 cm after applying the ICP algorithm. Nonetheless, the use of the ICP algorithm does not always return better accuracy and the photogrammetric accuracy was not significantly improved. Due to uncertainties of vegetated surfaces, photogrammetric results still had some errors from the vegetation effects. To conclude, the SfM outputs captured from a smart phone camera and photogrammetric processing based on freely available software using VisualSFM & PMVS provided results of sub-dm-level accuracy (between 5.7 and 6.0 cm).

4.3 SfM-photogrammetric processing based on cloud computing

From the development of a photogrammetric measurement system on the cloud, as described in the previous chapter, this experiment was carried out to ensure efficient performance of the developed system. In particular, the SfM-results obtained using a state-of-the-art smart phone at the outset of the research were evaluated for the photogrammetric accuracy and compared to two other alternative SfM methods.

4.3.1 Experimental design

The smart phone tested in this experiment was a Nexus 6. Imagery was captured on 10 June 2015 with a maximum image resolution of 4160 x 3120 pixels (approximately 13 megapixels). This image dataset comprised 36 images captured around a natural landslide at the BGS's Hollin Hill landslide observatory. Markers for geo-referencing were located around the landslide, comprising six photo control targets printed on paper. The locations of markers, camera stations and viewing direction of the captured images are shown in Figure 4-2.

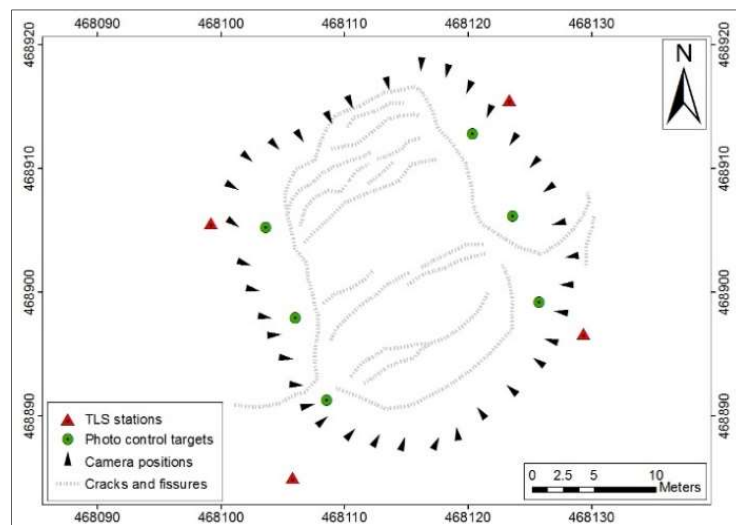


Figure 4-2: Illustration of camera positions for photogrammetric image capture.

Moreover, for validation of photogrammetric results, a high-resolution, high-accuracy TLS dataset was collected on the same date using a Leica ScanStation P20 to compare with each photogrammetric approach. The TLS data was captured from four scanner positions to ensure complete coverage of the full landslide area. Finally, the locations of

the six photo control targets and the four TLS stations were observed with GNSS at mm-level accuracy. The configuration of this experiment is outlined in Figure 4-3.

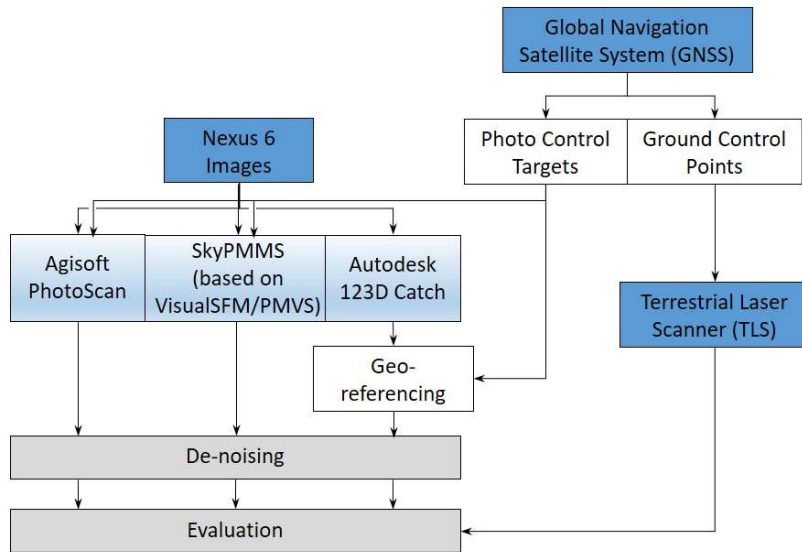


Figure 4-3: Methodology in the photogrammetric processing comparison experiment.

Following the methodology flowline illustrated in Figure 4-3, each SfM-photogrammetric processing workflow, conducted under laboratory conditions, used the same 36 image dataset. Photogrammetric processing with PhotoScan was performed on a desktop computer running on Windows 8 OS using an Intel Core i7-4770 Processor with 3.4 GHz CPU, 16 GB of RAM and an Intel HD Graphics 4600 with 1.4 GHz GPU. SkyPMMS (based on VisualSfM and PMVS) was run on the g2.2xlarge of Amazon EC2 instance under Windows Server 2012 with Intel Xeon E5-2670 Processor, 15 GB RAM and NVIDIA GPUs with 4GB of video memory. For data processing in Autodesk 123D Catch, the specification of the processing system is unknown because it is a web-based black box service for SfM.

For the geo-referencing step in VisualSfM and PMVS (implemented on the cloud) and Agisoft PhotoScan, the locations of targets were observed directly in the imagery, and this step was undertaken as part of the workflow. However, 123D Catch did not allow the user to undertake geo-referencing in the processing system. The SfM output from 123D Catch was georeferenced by identification of targets in the point cloud using the CloudCompare software. This step of the methodology for all SfM approaches required

manual input by the user. Next, the de-noising stage consisted of automatic and manual outlier removal was used to completely remove all gross errors for the photogrammetric results before the evaluation of SfM results from all three approaches. Finally, the comparison between photogrammetric results from each SfM approach and the TLS data, which was used for the evaluation of the SfM results, was carried out using the cloud-to-mesh distance tool in CloudCompare.

4.3.2 Test results

Visual comparison of the results provided by different SfM methods, as shown in Figure 4-4, shows Agisoft PhotoScan was able to produce a much denser point cloud than both Autodesk 123D Catch and the cloud-implemented VisualSFM & PMVS. Moreover, 123D Catch produced more uniform coverage than VisualSFM & PMVS, which was sparser, especially over vegetated surfaces. Nevertheless, the resultant point clouds generated by the latter two methods still provided the key information over landslide areas, especially fissures and cracks on the landslide body.

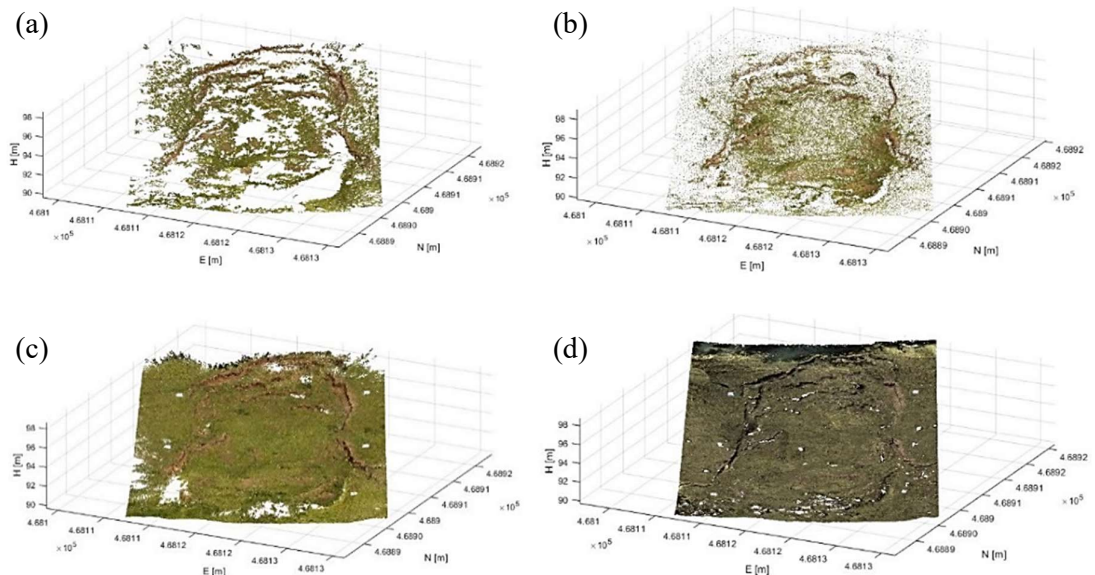


Figure 4-4: Photogrammetric point clouds obtained from the three adopted SfM approaches; (a) VisualSFM & PMVS, (b) Autodesk 123D Catch, (c) Agisoft PhotoScan, and the TLS validation data (d).

With regard to the assessment of photogrammetric accuracy from each SfM method with a high-resolution TLS dataset, statistics of the comparison between each SfM output and the TLS data are presented in Table 4-2. In addition, the distributions of distance difference are shown in Figure 4-5.

Table 4-2: Statistics of differences between the different SfM-outputs and the TLS data.

SfM method	TLS-SfM				
	Min (m)	Max (m)	Mean (m)	SD (m)	RMSE (m)
Agisoft PhotoScan	-0.545	0.463	0.022	0.034	0.036
Autodesk 123D Catch	-1.186	0.357	0.013	0.041	0.043
VisualSFM & PMVS	-0.406	0.461	0.027	0.050	0.053

Table 4-2 shows that minimum differences between 123D Catch and the TLS reference was noticeably higher than that of both PhotoScan and VisualSFM & PMVS. This is due to gross errors in the point cloud produced by 123D catch which have a greater impact on the range of differences, even though it was reduced by de-noising. Statistics of the results provided by PhotoScan showed the highest quality. This is further confirmed in Figure 4-5, which depicts the distribution of distance differences.

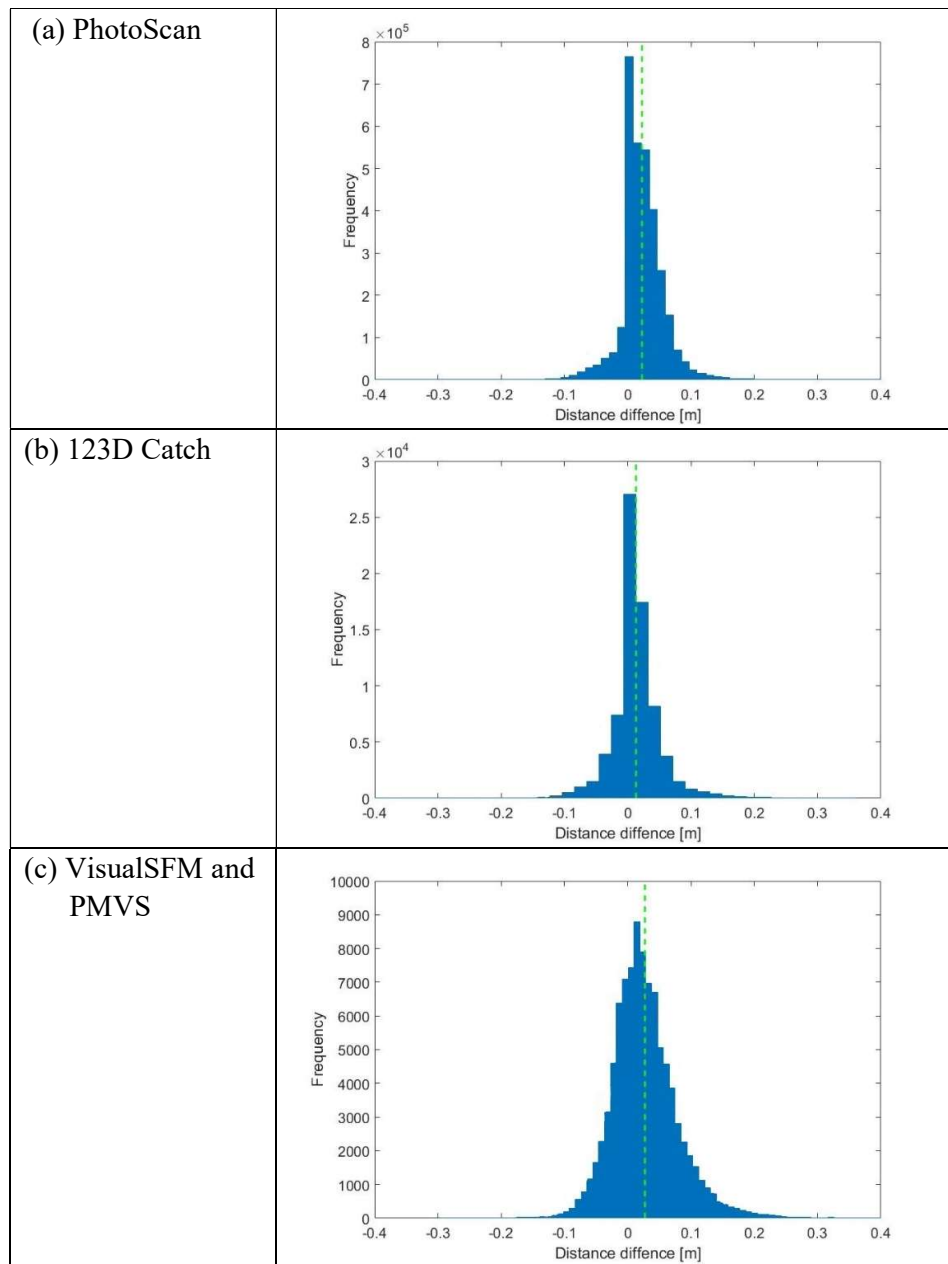


Figure 4-5: The distribution of distance differences between each SfM result and the TLS data; (a) PhotoScan, (b) 123D Catch and (c) VisualSFM & PMVS.

Based on the presented results, all means of the distance differences showed positive values, indicating that all SfM point clouds were slightly above the ground points of TLS data because the results from the SfM approach were often on top of vegetated surfaces. The RMSE values from PhotoScan, 123D Catch and VisualSFM & PMVS were 0.036, 0.043 and 0.053 m, respectively. Consequently, the photogrammetric approach using the SfM technique based on the development system can be deemed to provide results at sub-

dm level accuracy for this type of landslide surface in the same previous experiment (about 5.3 cm).

In terms of the application for photogrammetric processing, PhotoScan was not suited to on-site investigation of landslides because the software supports only a stand-alone system such as a desktop or laptop computer. On the other hand, Autodesk 123D Catch provides access for Internet-based processing, in a similar manner to SkyPMMS as cloud-implemented VisualSFM & PMVS. However, manual target geo-referencing in the point cloud (123D Catch) proves more difficult than target identification in imagery (SkyPMMS), which makes the process less convenient for the end user.

In the case of data transfer for photogrammetric processing on the cloud implemented SkyPMMS, this experiment required the uploading of 36 image files from a smart phone to the cloud server. The total file size of this image set was approximately 260 MB. Wi-Fi with an average upload speed of 40 Mbps was used to transfer the images from a smart phone to the cloud, with the total upload time taking approximately 1 minute. Table 4-3 summarizes the predicted upload time for such a dataset using different Internet networks on a smart phone. Transfer using a 3G network would take approximately 35 minutes, which is clearly unsuitable for a real-time photogrammetric measurement system. It is, however, anticipated that faster 4G internet will be more widespread in the future and would allow a near real-time response for such a system.

Table 4-3: Estimated data transfer time from a smart phone to the cloud server for 36 images (260MB in total).

Type of mobile networks	Average upload speed (Mbps)	Time for data upload (minutes)
3G	1	34.7
4G	10	3.5
Wi-Fi	40	0.9

As discussed above, the photogrammetric processing for SkyPMMS (based on VisualSFM and PMVS) could provide results achieving centimeter-level accuracy. However, from the completeness assessment of photogrammetric results, the main weakness of the photogrammetric processing using free and open SfM software was the low point density and data gaps (void areas) in the generated point cloud results when compared to that produced by commercial SfM software. Typically, an increase in the

number of images will increase the number of points, or point density, for photogrammetric results. However, the use of additional images will result in an increase in uploading and processing time. To overcome this issue, optimisation of the imaging network for photogrammetry was considered to find a suitable relationship between the number of camera stations and size of each image before uploading images to the cloud-based system.

4.4 Optimisation of imaging network

Due to a delay in real-time response for landslide monitoring when using SkyPMMS, time-consuming data transfer and processing on the cloud-based SfM-photogrammetric measurement system should be mitigated by optimising input data prior to uploading. This is necessary to mitigate 1) excessive amounts of image data used for processing on the cloud and 2) the inefficient performance of an Internet service via current mobile networks. Moreover, the completeness of photogrammetric results obtained from free SfM software was sometimes found to be insufficient to be used for landslide monitoring analysis. To deliver the appropriate quality of photogrammetric results for landslide monitoring, an optimal imaging network would provide an appropriate image size and a suitable number of camera stations prior to uploading data to the cloud.

4.4.1 Experimental design

As with the previous experiment, imagery was acquired on 10 June 2015 at the BGS's Hollin Hill landslide observatory using a Nexus6 smart phone camera. The image data tested comprises 74 images of 4160x3120 pixels (maximum resolution of the Nexus6). The validation for assessing photogrammetric accuracy was performed using a Leica ScanStation P20 from four scanner positions. The locations of the four laser scanning stations were observed using the GNSS survey.

For the optimal imaging network in this experiment, the two main factors assessed were the number of images and size of each image. Firstly, the different number of images in each approach was defined according to the condition of the location of camera station and a B/D ratio. As reviewed in the previous chapter, the optimal B/D ratio for such photogrammetric networks is between 0.1-0.3 for SfM-based 3D reconstruction. The values of B/D ratio were calculated as shown in Table 4-4.

Table 4-4: Comparison of B/D ratio used in each image dataset.

Number of images	Average base (m)	Average distance (m)	B/D ratio
24	3.811	15	0.254
28	3.271	15	0.218
32	2.869	15	0.191
36	2.558	15	0.171
40	2.302	15	0.153
44	2.097	15	0.140
48	1.925	15	0.128
52	1.775	15	0.118
56	1.649	15	0.110
60	1.540	15	0.103
64	1.443	15	0.096
68	1.361	15	0.091
72	1.286	15	0.086
74	1.251	15	0.083

For this experiment, the number of images used in each approach was selected from 24 to 60, increasing in steps of four images. The photogrammetric configuration of each approach is shown in Figure 4-6.

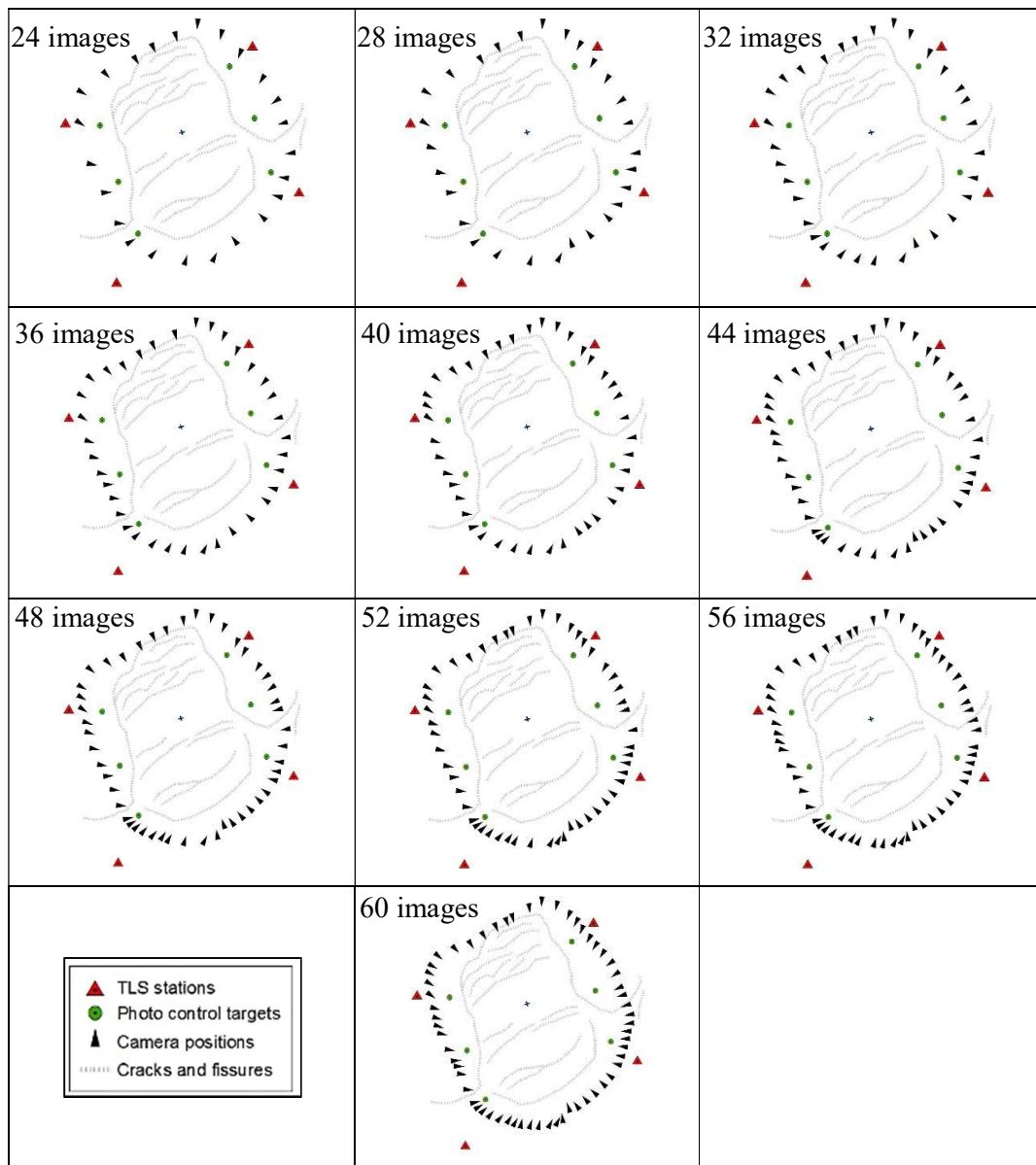


Figure 4-6: Comparison between photogrammetric configuration of each approach.

Secondly, the size of each image was sequentially reduced by 10%. However, resizing images of more than 70% of the original image size were not considered because it was lower than the essential requirement of image resolution for photogrammetric approach (>1 megapixels defined as a high resolution of digital camera). Thus, the details of each image were used in this experiment from original size to 70%, reducing in image resolution, as shown in Table 4-5.

Table 4-5: Comparison between image resolution and size used in each approach.

Size of image	Image resolution (Pixels)	Image size (MP)	Pixel size (μm)
Original size	4160x3120	13.0	1.12
Reducing 10%	3744x2808	10.5	1.24
Reducing 20%	3328x2496	8.3	1.40
Reducing 30%	2912x2184	6.4	1.60
Reducing 40%	2496x1872	4.7	1.87
Reducing 50%	2080x1560	3.2	2.24
Reducing 60%	1664x1248	2.1	2.80
Reducing 70%	1664x1248	1.2	3.36

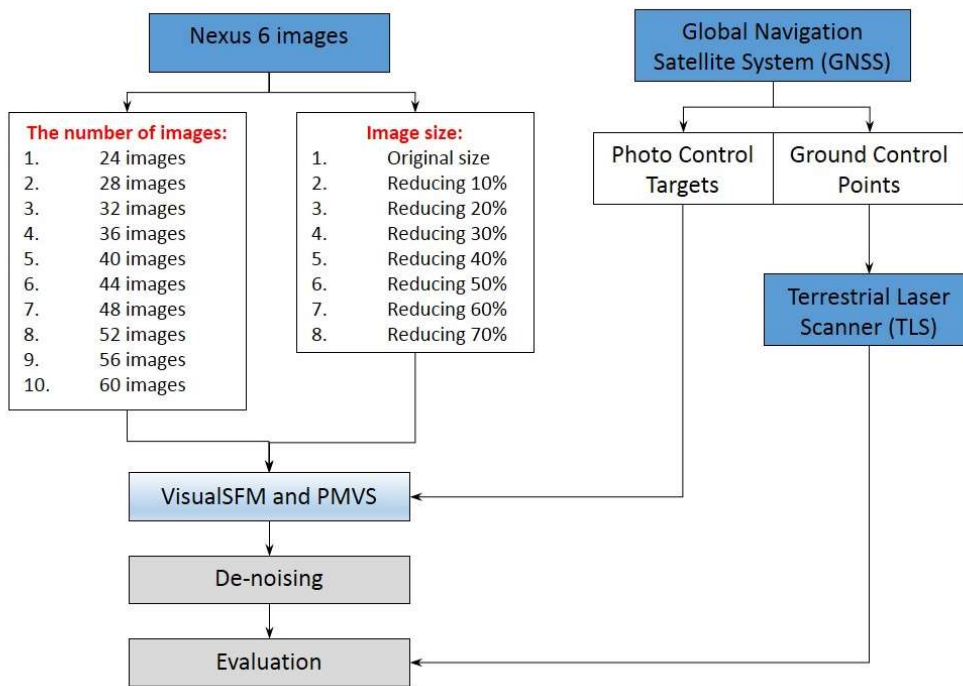


Figure 4-7: Methodology in the optimisation of imaging network experiment.

Figure 4-7 shows the methodology that used a different number of images and image size in order to optimise photogrammetric results for landslide monitoring. All photogrammetric processing was carried out using SkyPMMS (based on VisualSFM and PMVS) on the cloud server. For geo-referencing with the target-based observations, a pair list of coordinates between target location in the imagery and the GNSS-based target observation were exported to text file format for geo-referencing. Then, the de-noising step was carried out manually using CloudCompare software on a desktop computer.

Finally, in terms of the evaluation of photogrammetric results and the performance of photogrammetric processing at each approach, an accuracy assessment was performed between the SfM point clouds and TLS data using the cloud-to-mesh distance in CloudCompare.

4.4.2 Test results

Unfortunately, photogrammetric processing of SkyPMMS (based on VisualSfM and PMVS) could not successfully reconstruct 3D models when the number of images fell below 36. Because the overlaps were less than three images, the quality of the photogrammetric network in those images was unacceptable (as shown in Figure 4-8).

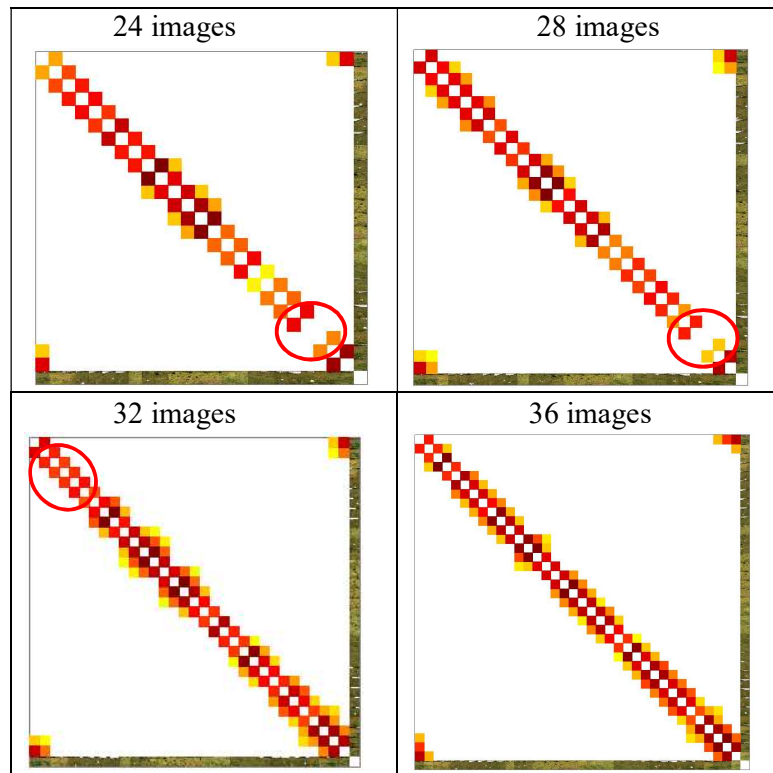


Figure 4-8: Comparison of image matching matrix for the relationship between each image in each approach.

In terms of the assessment of photogrammetric accuracy in this experiment, the statistics of the comparison between each SfM approach and a high resolution TLS survey are shown in Table 4-6 and Table 4-7.

Table 4-6: Comparison of mean value for the differences between each SfM approach and the reference TLS data.

Size of image	Mean (m)						
	36 images	40 images	44 images	48 images	52 images	56 images	60 images
Original images	0.027	0.028	0.028	0.025	0.026	0.024	0.026
Reducing 10%	0.028	0.026	0.029	0.030	0.025	0.028	0.024
Reducing 20%	0.036	0.028	0.030	0.027	0.027	0.025	0.024
Reducing 30%	0.032	0.030	0.038	0.027	0.028	0.029	0.026
Reducing 40%	0.036	0.028	0.031	0.029	0.024	0.027	0.025
Reducing 50%	0.040	0.030	0.026	0.031	0.029	0.031	0.028
Reducing 60%	0.038	0.033	0.030	0.030	0.033	0.031	0.033
Reducing 70%	0.041	0.036	0.038	0.038	0.034	0.031	0.036

Table 4-7: Comparison of RMSE value for the differences between each SfM approach and the reference TLS data.

Size of image	RMSE (m)						
	36 images	40 images	44 images	48 images	52 images	56 images	60 images
Original images	0.058	0.056	0.051	0.057	0.062	0.059	0.056
Reducing 10%	0.059	0.062	0.056	0.058	0.059	0.057	0.056
Reducing 20%	0.066	0.063	0.059	0.057	0.059	0.055	0.057
Reducing 30%	0.058	0.063	0.057	0.059	0.057	0.058	0.060
Reducing 40%	0.064	0.061	0.059	0.060	0.062	0.058	0.058
Reducing 50%	0.070	0.068	0.063	0.061	0.067	0.063	0.062
Reducing 60%	0.082	0.076	0.065	0.069	0.072	0.070	0.059
Reducing 70%	0.095	0.088	0.074	0.071	0.074	0.071	0.065

Table 4-6 and Table 4-7 reveal that the values of both mean and RMES of the differences between each SfM approach and the reference TLS data improved only very marginally when the number of images used for data processing increased. Meanwhile, reducing image resolution in each image led to the degraded values of both mean and RMSE of the differences between their results. This is to be expected as, in terms of photogrammetric accuracy, a lower-image resolution could directly affect the precision of image mensuration and geo-referencing. The lower quality of photogrammetric measurement therefore caused a decreased accuracy in the results. However, each SfM-photogrammetric approach provided results from sub-dm (5.1 cm) to dm (9.5 cm) level accuracy, in this type of landslide. The natural slope in this experiment was mainly

covered by vegetated surfaces. Vegetation effects therefore had an influence on this assessment of photogrammetric results.

With regard to the evaluation of completeness for photogrammetric results, the number of points and density of point cloud obtained from each approach were analysed and are showed in Figure 4-9.

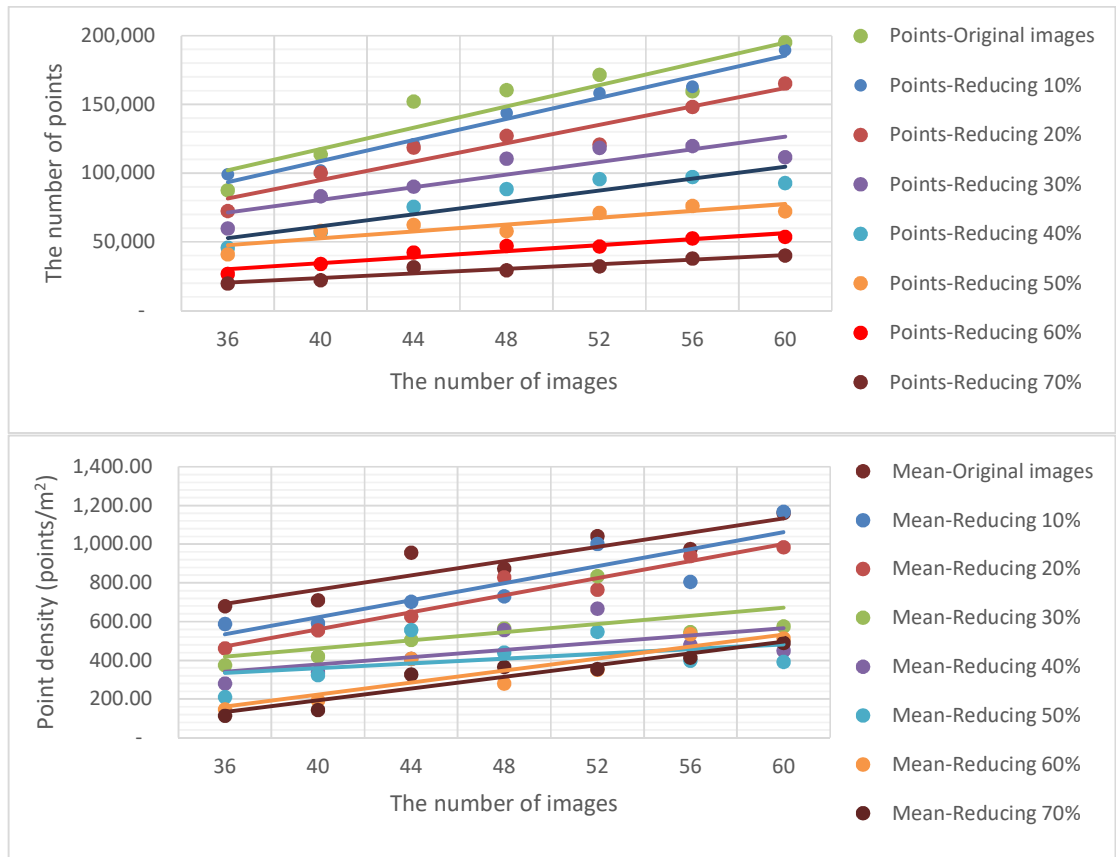


Figure 4-9: Comparison of the relationship between the number of points and point density of photogrammetric results obtained from each SfM approach.

Figure 4-9 shows an increasing number of points and point density when using more images for processing. It can be seen that an increase in the number of images results directly in a higher number of both points and density due to the increased overlapping areas for dense image matching in 3D reconstruction. On the other hand, decreasing image resolution for each image reduces both the number of points and point density. Although the completeness of results was improved by increasing the number of images (or camera stations) for photogrammetric processing, their point clouds still had void data,

as shown in Figure 4-10. Such a point cloud over bare-earth surfaces of each approach retains the key information, such as cracks or fissures, that might be used for assessing the landslide deformation.

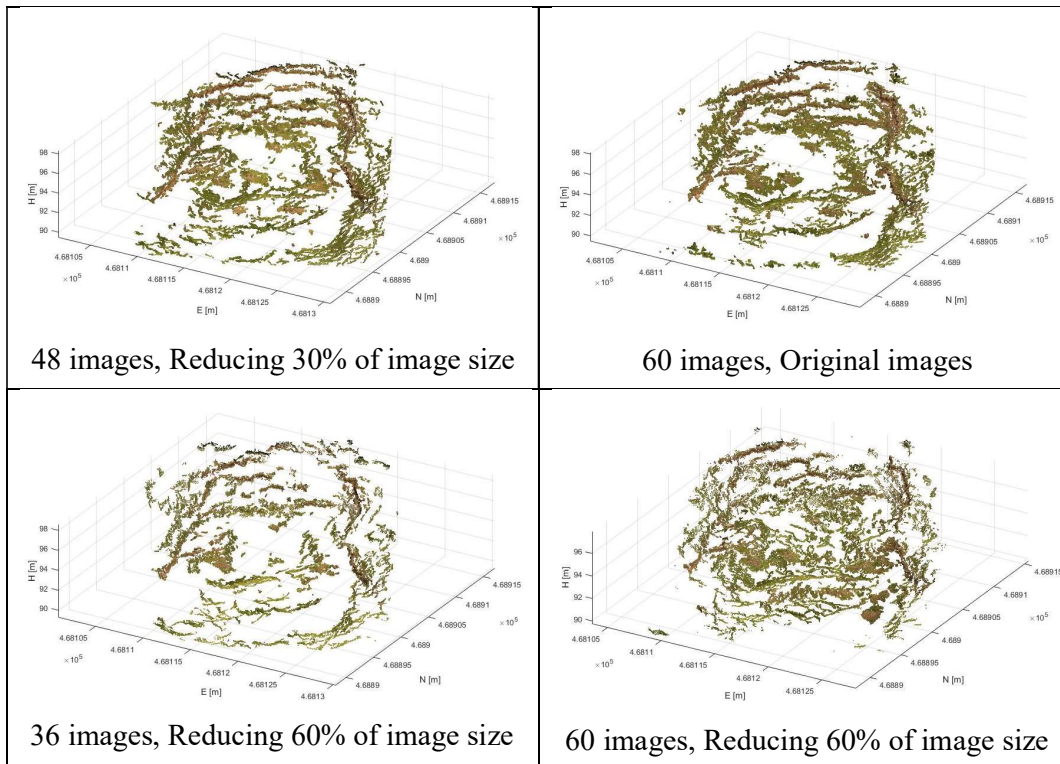


Figure 4-10: Comparison of photogrammetric point clouds obtained from different number of images and different image size.

Regarding the performance evaluation of photogrammetric processing on SkyPMMS, the results for the processing time at each approach are shown in Table 4-8. The estimation of file size and upload time for each approach was calculated from image data transfer to the cloud using a 4G and a Wi-Fi network (at approximately 10 and 40 Mbps of average upload speed, respectively), as shown in Table 4-9.

Table 4-8: Comparison of processing time between the different camera station and image resolution using SkyPMMS on the cloud.

Size of image	Data processing time (min)						
	36 images	40 images	44 images	48 images	52 images	56 images	60 images
Original images	8.58	9.63	11.78	13.65	14.70	16.13	17.58
Reducing 10%	6.47	9.02	9.47	11.10	11.93	12.97	15.40
Reducing 20%	5.93	6.90	7.65	8.77	9.05	10.67	11.70
Reducing 30%	6.00	7.58	8.22	8.95	10.67	11.68	12.80
Reducing 40%	5.58	6.55	8.13	8.88	10.35	11.02	11.88
Reducing 50%	5.32	6.35	7.27	8.22	9.15	10.42	11.57
Reducing 60%	3.70	4.40	4.82	5.63	6.15	6.83	7.50
Reducing 70%	3.18	4.06	4.65	5.04	5.85	6.40	6.85

Table 4-9: Comparison of image resolution between estimated file size and estimated upload time used in each approach. The data in brackets are estimated upload time using a 4G and a Wi-Fi network, respectively.

Size of image	Estimation of file size (MP) and upload time (min)						
	36 images	40 images	44 images	48 images	52 images	56 images	60 images
Original images	260 (3.5, 0.9)	289 (3.9, 1.0)	318 (4.2, 1.1)	347 (4.6, 1.2)	376 (5.0, 1.3)	404 (5.4, 1.3)	433 (5.8, 1.4)
Reducing 10%	234 (3.1, 0.8)	260 (3.5, 0.9)	286 (3.8, 1.0)	312 (4.2, 1.0)	338 (4.5, 1.1)	364 (4.9, 1.2)	390 (5.2, 1.3)
Reducing 20%	208 (2.8, 0.7)	231 (3.1, 0.8)	254 (3.4, 0.8)	277 (3.7, 0.9)	300 (4.0, 1.0)	324 (4.3, 1.1)	347 (4.6, 1.2)
Reducing 30%	182 (2.4, 0.6)	202 (2.7, 0.7)	222 (3.0, 0.7)	243 (3.2, 0.8)	263 (3.5, 0.9)	283 (3.8, 0.9)	303 (4.0, 1.0)
Reducing 40%	156 (2.1, 0.5)	173 (2.3, 0.6)	191 (2.5, 0.6)	208 (2.8, 0.7)	225 (3.0, 0.8)	243 (3.2, 0.8)	260 (3.5, 0.9)
Reducing 50%	156 (1.7, 0.4)	173 (1.9, 0.5)	191 (2.1, 0.5)	208 (2.3, 0.6)	225 (2.5, 0.6)	243 (2.7, 0.7)	260 (2.9, 0.7)
Reducing 60%	130 (1.4, 0.3)	145 (1.5, 0.4)	159 (1.7, 0.4)	174 (1.9, 0.5)	188 (2.0, 0.5)	202 (2.2, 0.5)	217 (2.3, 0.6)
Reducing 70%	104 (1.0, 0.3)	116 (1.2, 0.3)	127 (1.3, 0.3)	139 (1.4, 0.3)	150 (1.5, 0.4)	162 (1.6, 0.4)	173 (1.7, 0.4)

Based on the performance results of processing in Table 4-8, data processing time of SkyPMMS was inevitably longer when the number of images increased. Clearly the more images (camera stations) used for landslide photogrammetric monitoring, the longer time is required for both data transfer and data processing. The processing time from each approach dramatically increased from 3.18 to 17.58 minutes, whereas the estimation of

upload time of each approach (in Table 4-9) was slightly different (approximately 1.1 min ranging from 0.3 min to 1.4 min). Time for data transfer using a Wi-Fi network was relatively insignificant when compared to data processing time. On other hand, the estimation of upload time using a 4G network was dramatically different (about 4.8 min ranging from 1.0 min to 5.8 min).

With respect to decrease of the data processing time, reducing the resolution of each image can also critically help. For example, the relationship between the photogrammetric accuracy and data processing time of each approach was generated to find the optimal imaging network as in the results of this experiment, as shown in Figure 4-11.

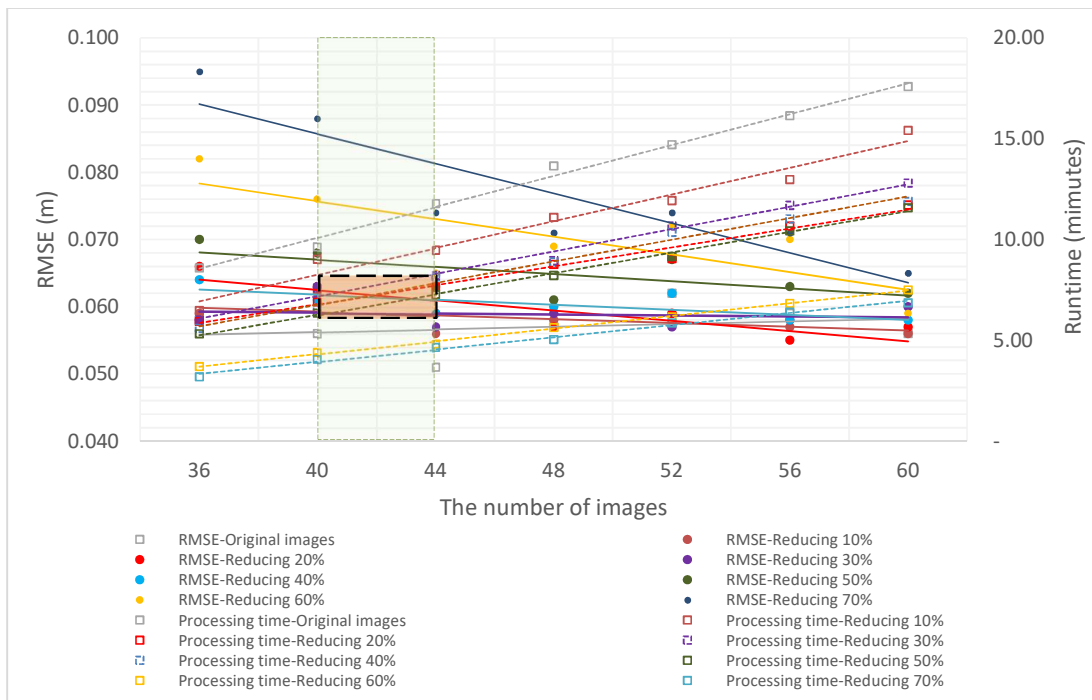


Figure 4-11: Comparison of the relationship between data processing time obtained from each SfM approach and the RMSE of differences between each SfM result and the TLS data in each approach.

For the optimisation of the imaging network, there are four crucial factors to balance the data processing time for a near real-time response for landslide monitoring: 1) the number of images, 2) image resolution, 3) photogrammetric accuracy and 4) data processing time. The optimal image resolution for each image was selected by consideration of resultant photogrammetric accuracy and data processing time. From Figure 4-11, the resolution of

each image in a photoset can be reduced between 20% and 30% of the original image size with only slight differences in photogrammetric accuracy and processing time when 40 and 44 images were processed. Referring to Table 4-4, the number of images (40 and 44 images) were assumed as a B/D ratio of 0.14-0.15. Thus, the recommended design of photogrammetric configuration should be a B/D ratio of approximately 0.1-0.2. Furthermore, data processing time of each approach was not significantly lowered when > 20% reduction of original image size was applied (Figure 4-12).

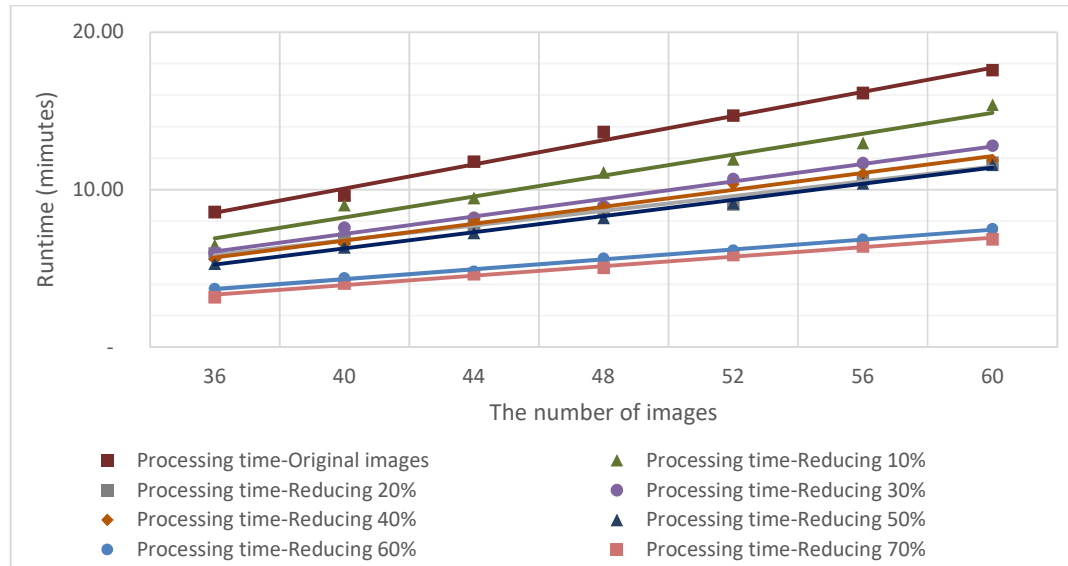


Figure 4-12: Data processing time obtained from each approach.

To conclude, firstly, although a larger number of images (or camera stations) helps improve the quality of imaging network for photogrammetric approach, the improvement of photogrammetric accuracy and completeness of results were insignificant (i.e. accuracy increased slightly at the mm level). Secondly, a decrease in image resolution also helps increase the speed of photogrammetric processing reducing the processing time, whereas the difference of time for image data transfer using Internet service via a Wi-Fi network was insignificant (i.e. approximately 0.9 min), and the accuracy of photogrammetric results decreased slightly. Finally, for optimising the imaging network, the recommended design of photogrammetric configuration in this experiment (using a B/D ratio of 0.1-0.2) can be confirmed and this configuration yields the appropriate photogrammetric results. In addition, already improved image data (i.e. 20%-30% of

image size reduction) before transferring or uploading to the cloud-based server can enhance the performance of data processing.

4.5 Performance evaluation of developed functions for photogrammetric processing

In this section, the experimental studies of the functions implemented in the photogrammetric measurement and monitoring system were evaluated to ensure the development of a low-cost, real-time solution for on-site investigation of landslide hazard analysis. A series of assessments for each developed function was performed comprising pre-processing and post-processing stages for the SfM-photogrammetric approach and landslide monitoring analysis.

4.5.1 Pre-image matching

For the SfM-photogrammetric approach to reconstruct 3D models from images, there are normally four main stages, including feature detection, image matching, sparse reconstruction and dense reconstruction. To clarify understanding of processing time in each stage for the SfM approach, an experiment in photogrammetric processing from three image datasets acquired at the Hollin Hill landslide was carried out using VisualSfM and PMVS on a desktop computer running on Windows 8 OS including an Intel Core i7-4770 Processor with 3.4 GHz CPU, Intel HD Graphics 4600 and 16 GB RAM of memory. The processing times in this experiment are shown in Table 4-10 and Figure 4-13.

Table 4-10: Data processing time of each stage in the SfM workflow obtained from different numbers of images.

The number of images	Data processing time (minutes)				
	Feature detection	Image matching	Sparse reconstruct-ion	Dense reconstruct-ion	Total
36	0.2	3.0	2.5	3.3	9.0
48	0.3	5.3	2.8	5.4	13.8
60	0.3	8.3	2.6	6.7	17.9

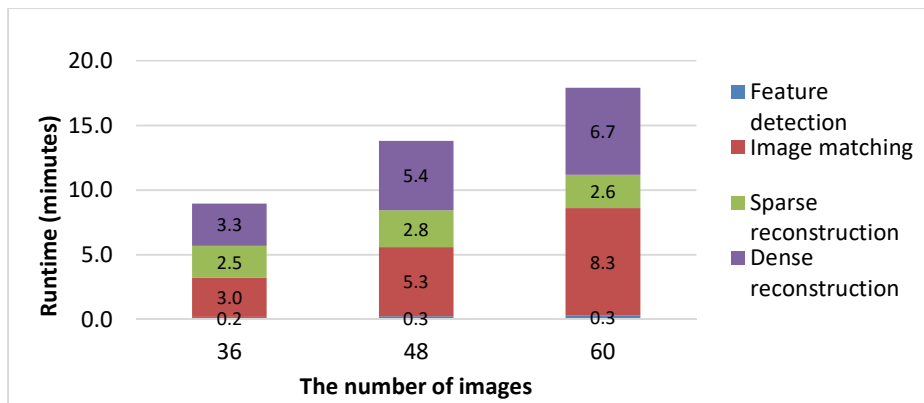


Figure 4-13: Comparison of data processing time at each stage obtained from the SfM-photogrammetric processing using VisualSfM and PMVS.

Considering Table 4-10 and Figure 4-13, the number of images used for processing had a direct effect on processing time. When the number of images increased from 36 images to 48 images and 60 images, matching time increased 77% and 176%, respectively. Clearly, the more images that were processed, the longer image matching took. The image matching stage in the SfM approach needs to be investigated.

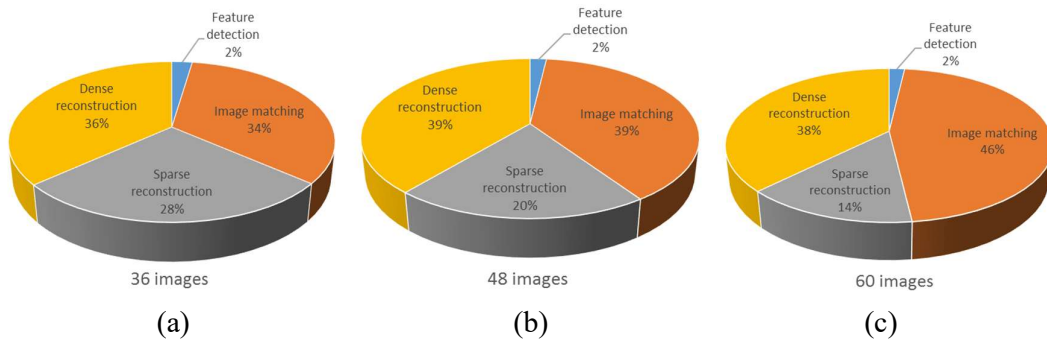


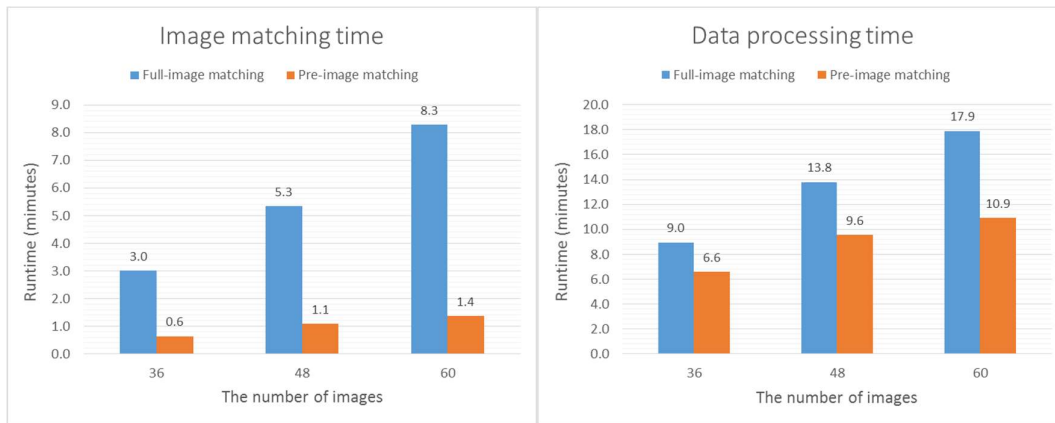
Figure 4-14: Percentage comparisons of data processing time in each stage of the SfM-photogrammetric approach using VisualSfM and PMVS with three image datasets; (a) 36 images, (b) 48 images and (c) 60 images.

Figure 4-14 shows the proportion of each stage for 3D reconstruction using VisualSfM and PMVS. The two stages that took the majority of data processing time were image matching and dense reconstruction. In this experiment, image matching time based on the method of full-image matching for 36, 48 and 60 images were approximately 34%, 39% and 46% of the total data processing time, respectively. As mentioned in Section 3.4.1, the algorithm developed for pre-image matching was used to reduce time in the image matching stage for the SfM approach. The comparison of image matching and data

processing times between pre-image matching and full-image matching are presented in Table 4-11 and Figure 4-15.

Table 4-11: Comparison of image matching time and data processing time using full- and pre-image matching method.

Number of images	Image matching time (minutes)		Percentage of reduced time for image matching	Total of data processing time (minutes)		Percentage of reduced time for data processing
	Full-image matching	Pre-image matching		Full-image matching	Pre-image matching	
36	3.0	0.6	79%	9.0	6.6	27%
48	5.3	1.1	80%	13.8	9.6	31%
60	8.3	1.4	84%	17.9	10.9	39%



(a)

(b)

Figure 4-15: Comparison of processing time from different image matching methods and the number of images; (a) image matching time and (b) data processing time.

However, the method of pre-image matching needs to be processed using the developed function before image matching in the SfM workflow. Pre-image matching took only a few seconds of processing time and was insignificant compared to image matching time.

To conclude, the function developed for pre-image matching from image sequences can help to reduce image matching time in the SfM workflow by around 80%. As a result, total data processing time of the SfM workflow using pre-image matching in this experiment can be reduced by approximately 30% compared to image matching based on

the standard method. The developed pre-image matching algorithm can therefore lead to improved performance in achieving a real-time landslide monitoring system.

4.5.2 Lens distortion correction

Imagery captured by a digital camera usually incorporates effects of lens distortion. To provide precise measurement from SfM-photogrammetry, this should be eliminated from the imagery before photogrammetric processing. Lens distortion correction is performed using a developed function with the calibrated camera modelling. The parameters of the camera model were derived from camera calibration tool in Matlab software. An example of imagery before and after applying lens distortion correction is illustrated in Figure 4-16.

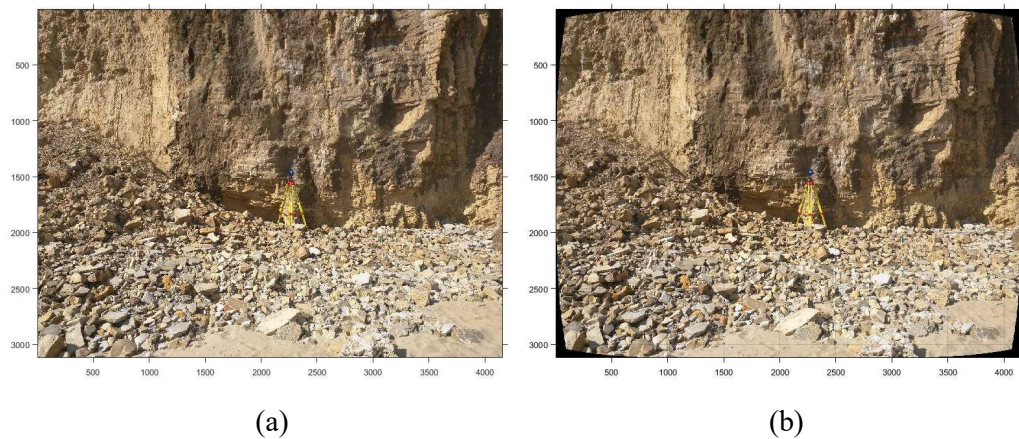


Figure 4-16: Comparison between original image and image after applying lens distortion correction; (a) before and (b) after.

In terms of accuracy assessment of photogrammetric results from raw and images corrected for lens distortion, the imagery was acquired using a Nexus6 smart phone camera. Photogrammetric processing used VisualSFM & PMVS. The validation data for assessing photogrammetric accuracy was captured using a Leica ScanStation P20. The comparison results of photogrammetric accuracy between the use of raw images and lens distortion correction are shown in Table 4-12.

Table 4-12: Statistics of distance differences between the different SfM results and the TLS data.

Pre-processing	TLS-SfM				
	Min (m)	Max (m)	Mean (m)	SD (m)	RMSE (m)
Raw images	-0.958	0.866	-0.419	0.264	0.269
Images corrected for lens distortion and fixed calibration	-0.275	0.257	0.004	0.043	0.046

Table 4-12 reveals that the mean and RMSE values of the differences between SfM output using undistorted images with fixed calibration and the TLS data decreased considerably when compared to the original images. The quality of photogrammetric results was improved using the function developed for lens distortion correction, provided a higher accuracy of photogrammetric results.

4.5.3 Geo-referencing

Geo-referencing, an important stage of post-processing for photogrammetric results, is used to provide a real-world coordinate system for comparison and analysis of landslide monitoring. For geo-referencing with GCPs or targets, their locations are normally observed using a high-precision survey (e.g. GNSS or TLS). However, a solution for geo-referencing based on both real-time processing and low-cost observation is important for on-site investigation. This experiment focused only on geo-referencing without GNSS or TLS observation for the location of GCPs or targets. The solution developed for geo-referencing with dimensions of known objects was evaluated to determine the suitability of a low-cost choice of geo-referencing for the user.

Following the geo-referencing routine explained in Section 3.4.3.2, the dimension of known objects was firstly carried out using a high-precision distance measurement with a Leica Disto D510 (with precision ± 1 mm) to find the distances between each photo control target (Figure 4-17). The details of measuring these distances are shown in Table 4-13.

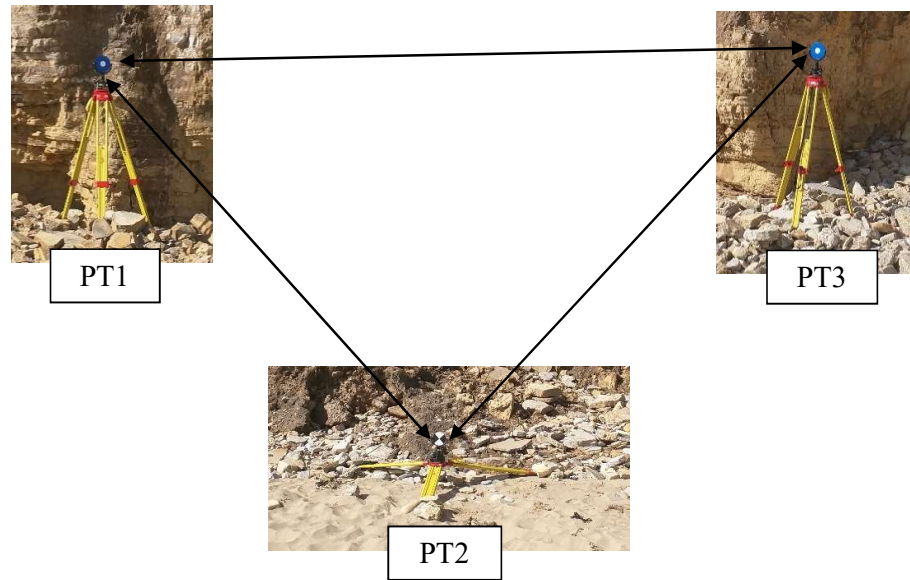


Figure 4-17: Configuration for photo control targets.

Table 4-13: Statistics of measuring distances between each photo control target.

From	To	Distance measurements (m)			Average of distances (m)
		#1	#2	#3	
PT1	PT2	14.11	14.11	14.12	14.11
PT2	PT1	14.13	14.13	14.12	14.13
PT2	PT3	14.37	14.38	14.39	14.38
PT3	PT2	14.38	14.38	14.38	14.38
PT1	PT3	28.13	18.13	28.13	28.13
PT3	PT1	28.14	28.14	28.14	28.14

The use of pseudo coordinates for the three points enables precise scaling in the 3D model of the photogrammetric results. Prior to scaling, the pseudo coordinates are generated as follows. Firstly, the coordinates of the PT1 point are set to (0, 0, 0). Next, the coordinates of PT2 are generated by (0, P1P2, 0) where P1P2 is the mean distance between PT1 and PT2. Finally, the coordinates of PT3 point are determined at the intersection of arc of length PT1 to PT3 and PT2 to PT3 in a 2D plane in which the Z coordinate of PT3 is set at 0. Note that points (PT1, PT2, PT3) lie in a 3D plane for which the Z coordinates are always 0. Thus, the photogrammetric results at each epoch are referenced using three pseudo points.

The scaling of photogrammetric results thus uses a pair list of three targets with photo coordinates and pseudo coordinates based on three distances measured between the target, as presented in Table 4-13. After scaling the photogrammetric results using the developed function, the next stage was manual alignment of photogrammetric results with the TLS data. Then, the application of the ICP algorithm without scaling was performed using the CloudCompare software on a desktop computer. To assess the photogrammetric accuracy from this method, comparison of photogrammetric results and the TLS data was carried out using the cloud-to-mesh distance tool in CloudCompare. The results of accuracy assessment for this photogrammetric approach are presented in Table 4-14.

Table 4-14: Statistics of distance differences between the SfM results obtained from different geo-referencing with the dimensions of known objects and applying ICP and the TLS data.

Pre-/Post-processing	TLS-SfM				
	Min (m)	Max (m)	Mean (m)	SD (m)	RMSE (m)
Original images, Direct geo-referencing and ICP	-0.574	1.602	-0.017	0.082	0.084
Original image, Scaling, Alignment & ICP	-0.282	0.297	0.010	0.045	0.047

From Table 4-14, the values of the mean and RMSE of the differences between the SfM approach using geo-referencing with the dimensions of known object and applying ICP and the TLS data were slightly lower when compared to a normal SfM approach. Also, the quality of the photogrammetric accuracy using the function of geo-referencing and applying ICP was similar to a normal SfM approach.

4.5.4 Automatic de-noising

The development of a function for automatic de-noising is used for gross outlier detection and removal in point clouds to improve the quality of photogrammetric results before landslide monitoring analysis. This algorithm for automatic de-noising is based on the statistical outlier removal (SOR) filter. To clarify understanding of this method, the experiment used the photogrammetric results acquired on 10 June 2015 at the Hollin Hill landslide and processed using VisualSfM and PMVS. For the development of the automatic de-noising function, the settings of parameters consist mainly of the number of

points (N) considered and the number of multipliers (n) with a standard deviation to identify the threshold of classification for outlier detection. However, the solution for automatic de-noising can be changed from case to case since the values of these parameters were variable. For example, in the case of inappropriate n and N , manual cleansing may be required after automatic de-noising.

In this experiment, the mean distances of K-nearest neighbours for each point from photogrammetric results were calculated according to two sets of n and N as illustrated in Figure 4-18. The points which had a mean distance greater than the threshold of outlier classification (above the red line in Figure 4-18) were eliminated from the point cloud. The use of different parameters in the number of K-nearest points and the number of multipliers caused different results for automatic de-noising (Figure 4-19).

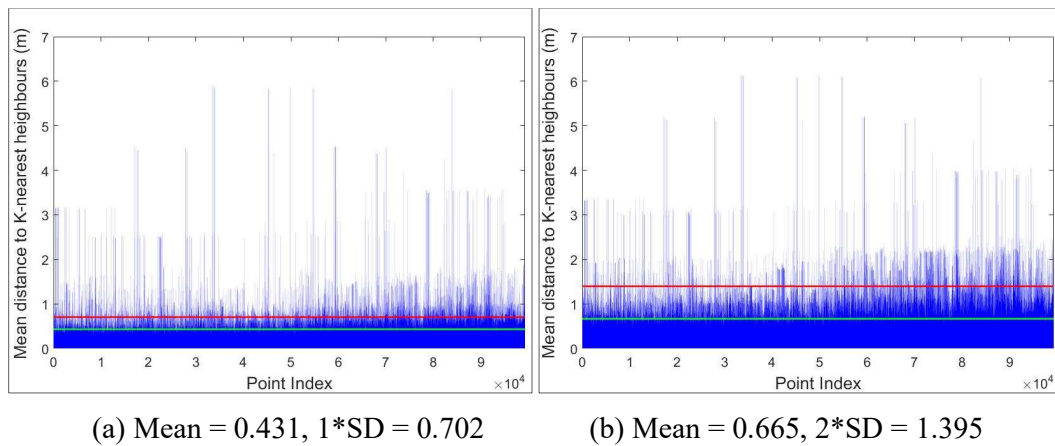


Figure 4-18: Comparison of the mean distances of K-nearest neighbours using different parameters for automatic de-noising; (a) $N = 500$, $n = 1$ and (b) $N = 1000$, $n = 2$. The green and red lines show the mean distance and the threshold of outlier classification, respectively.

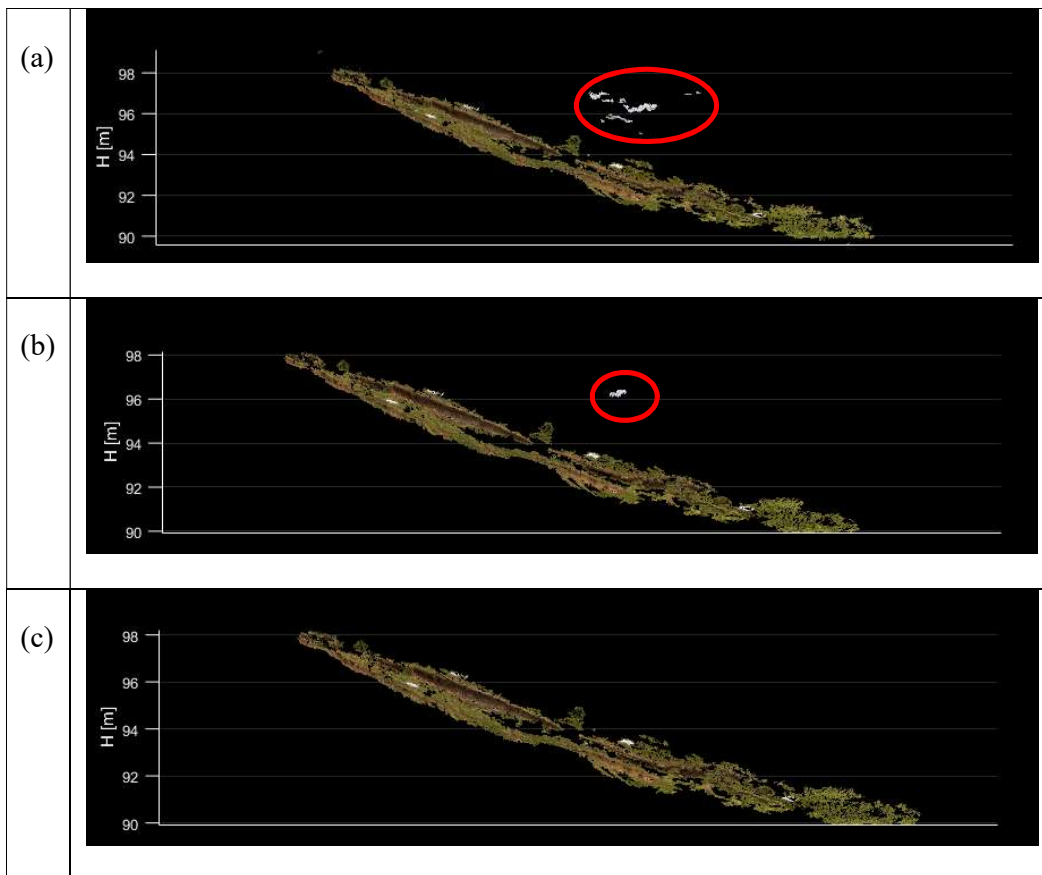


Figure 4-19: Comparison of photogrammetric results when using different parameters for automatic de-noising; a) original point cloud, b) point cloud after automatic de-noising using $N = 500$, $n = 1$ and (c) point cloud after automatic de-noising using $N = 1000$, $n = 2$. The red circles show the outliers in the point cloud.

Figure 4-19 shows the photogrammetric results before and after automatic de-noising. It is likely these outliers in the point cloud were noise, which are clearly located higher than the ground points. To ensure improved results after automatic de-noising, the accuracy assessment of photogrammetric results was performed using the cloud-to-mesh distance tool in CloudCompare with high-resolution, high-accuracy data from the TLS survey. Comparison of the photogrammetric accuracy before and after automatic de-noising is presented in Table 4-15.

Table 4-15: Comparison for statistics of differences between the TLS data and the SfM point clouds before and after automatic de-noising.

Automatic de-noising	Parameters of automatic de-noising	TLS-SfM				
		Min (m)	Max (m)	Mean (m)	SD (m)	RMSE (m)
Before	-	-2.191	5.602	0.051	0.301	0.305
After	$N = 500, n = 1$	-0.252	2.958	0.031	0.132	0.137
	$N = 1000, n = 2$	-0.252	0.433	0.026	0.045	0.048

From Table 4-15, mean and RMSE values of the differences between the TLS data and the SfM point clouds after automatic de-noising of the two approaches clearly decreased when compared to before automatic de-noising. In the comparisons using different parameters, the statistics using a higher degree of both n and N decreased, especially the maximum, mean and RMSE. The photogrammetric results were likely to provide a higher accuracy after automatic de-noising in this case.

In summary, the function developed for automatic de-noising aims to remove gross outliers from the photogrammetric results, especially air points. Automatic de-noising can also improve the quality of photogrammetric results in terms of accuracy. However, due to the need for threshold determination, manual interaction may still often be required for de-noising.

4.5.5 Vegetation filtering

The vegetation filtering function was developed to remove points over vegetated surfaces from photogrammetric results before landslide monitoring analysis. In this experiment, two point clouds were obtained from the imagery acquired on 20 March 2015 and 10 June 2015 at the Hollin Hill landslide using VisualSfM and PMVS. With regard to the vegetation filtering algorithm, points which had green vegetation index above the threshold for classification were eliminated from the point cloud. However, the threshold used for classification of vegetation depended on the weather and season. To find a suitable threshold for point cloud classification, histograms of the green vegetation index were considered, as shown in Figure 4-20.

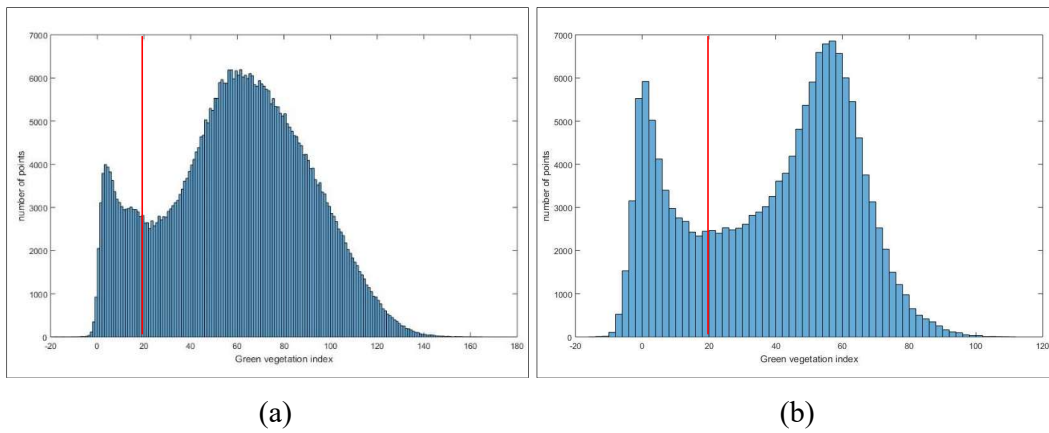


Figure 4-20: The histograms of green vegetation index from two point clouds acquired on (a) 20 March 2015 and (b) 10 June 2015.

In this experiment, both histograms of green vegetation index were assumed as a bimodal frequency distribution. The appropriate threshold was selected by the operator at approximately point 20 of the green vegetation index value. After vegetation filtering, the results of the point clouds are shown in Figure 4-21.

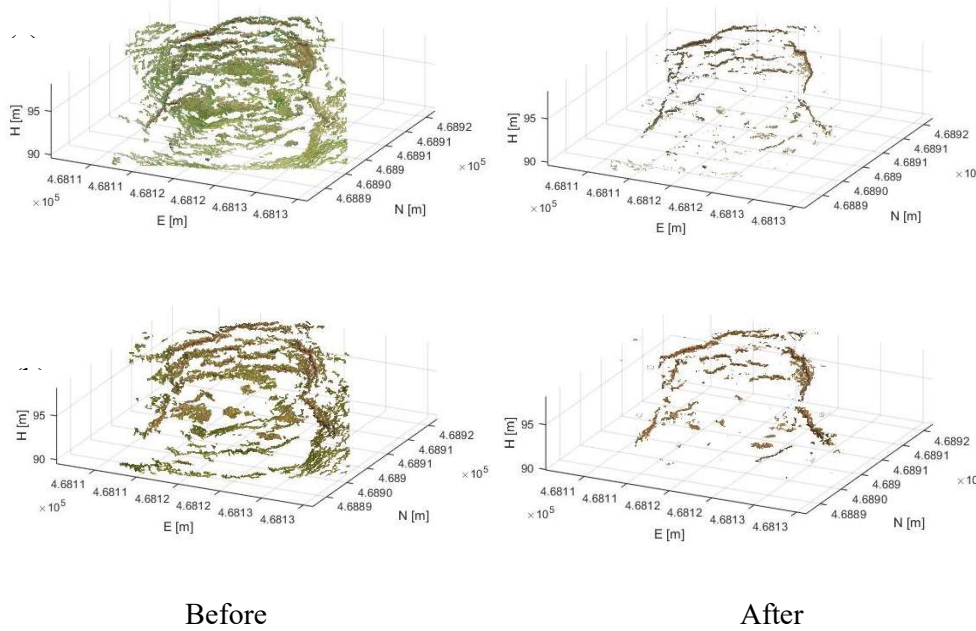


Figure 4-21: Comparison of point clouds before and after vegetation filtering acquired on (a) 20 March 2015 and (b) 10 June 2015.

To evaluate the photogrammetric accuracy before and after vegetation filtering, a comparison between photogrammetric results from the SfM point clouds and the TLS data was carried out using the cloud-to-mesh distance tool in CloudCompare. The assessment of photogrammetric accuracy in this experiment is presented in Table 4-16.

Table 4-16: Statistics of differences between the SfM point clouds and reference TLS data and the comparison between before and after vegetation filtering.

Images acquired on	Vegetation filtering	TLS-SfM				
		Min (m)	Max (m)	Mean (m)	SD (m)	RMSE (m)
20 March 2015	Before	-0.287	0.288	0.017	0.024	0.026
	After	-0.168	0.169	0.010	0.023	0.025
10 June 2015	Before	-0.332	0.372	0.008	0.069	0.070
	After	-0.286	0.310	0.004	0.046	0.048

The statistical values of differences between the TLS data and the SfM point clouds after vegetation filtering of both epochs were obviously reduced. It could be that the photogrammetric accuracy achieved after vegetation filtering was higher. In comparison with two photogrammetric results at different times, the RMSE value of the results after vegetation filtering acquired on 20 March 2015 improved from 0.026 m to 0.025 m (approximately 4%), whereas the results acquired on 10 June 2015 improved by 40% when using vegetation filtering (from 0.070 m to 0.048 m). The seasonal changes for a natural landslide monitoring had a noticeably influence over the height of the vegetated surface.

To conclude, the SfM-photogrammetric approach was only able to capture the visible surface, and hence was unable to penetrate vegetated surfaces. The photogrammetric accuracy could be improved using the developed function of vegetation filtering, especially for landslide monitoring in a natural terrain covered by the variety of vegetated surfaces. Vegetation has a direct impact on the assessment of landslide deformation. Before landslide monitoring analysis, this factor should be considered and eliminated. However, after vegetation filtering, some outliers still remained in the point cloud and needed to be removed manually by the operator.

4.5.6 Change assessment

Change assessment was the crucial final step of the workflow to detect the deformation of the landslide over time. This experiment used photogrammetric results at different epochs using the PhotoScan software because the results had higher point density than those from SkyPMMS. The comparison of multi-epoch analysis was carried out using two methods of point cloud comparison: M3C2 and C2M. For the M3C2 method, based on the study of Stumpf *et al.* (2015) involving landslide monitoring using ground-based photogrammetry, the recommended parameter settings for change assessment are shown in Table 4-17.

Table 4-17: The appropriate parameters based on a point cloud comparison method using M3C2 (Stumpf *et al.*, 2015).

M3C2 parameters	Value (m)
D	5.0
d	0.5
p_{max}	5.0
Registration error	0.1

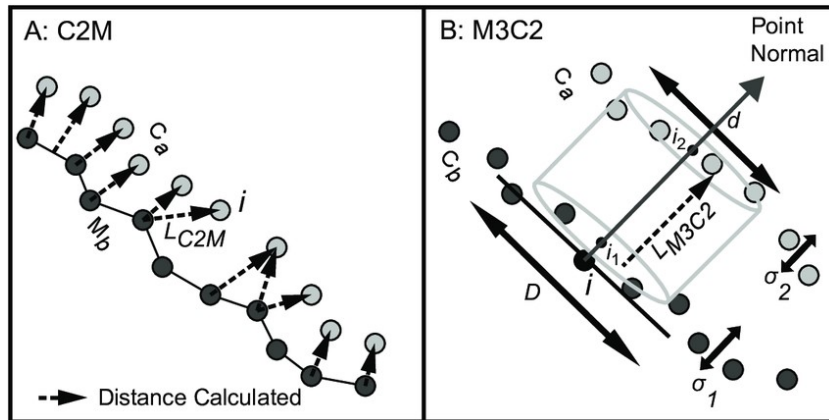


Figure 4-22: Comparison of conceptual diagrams for cloud comparison method (a) C2M and (b) M3C2 (Barnhart and Crosby, 2013).

Figure 4-22 presents conceptual diagrams of point cloud comparison methods for multi-epoch analysis using M3C2 and C2M to assess landslide deformations at different times. In particular, a limitation of C2M point cloud comparison, is that it is possible that

variable values for landslide deformation are a result of extreme distance between two points used for assessing change detection (Figure 4-22(a)). In contrast, the M3C2 algorithm can estimate the maximum difference between two point clouds within just a cylinder (Figure 4-22(b)).

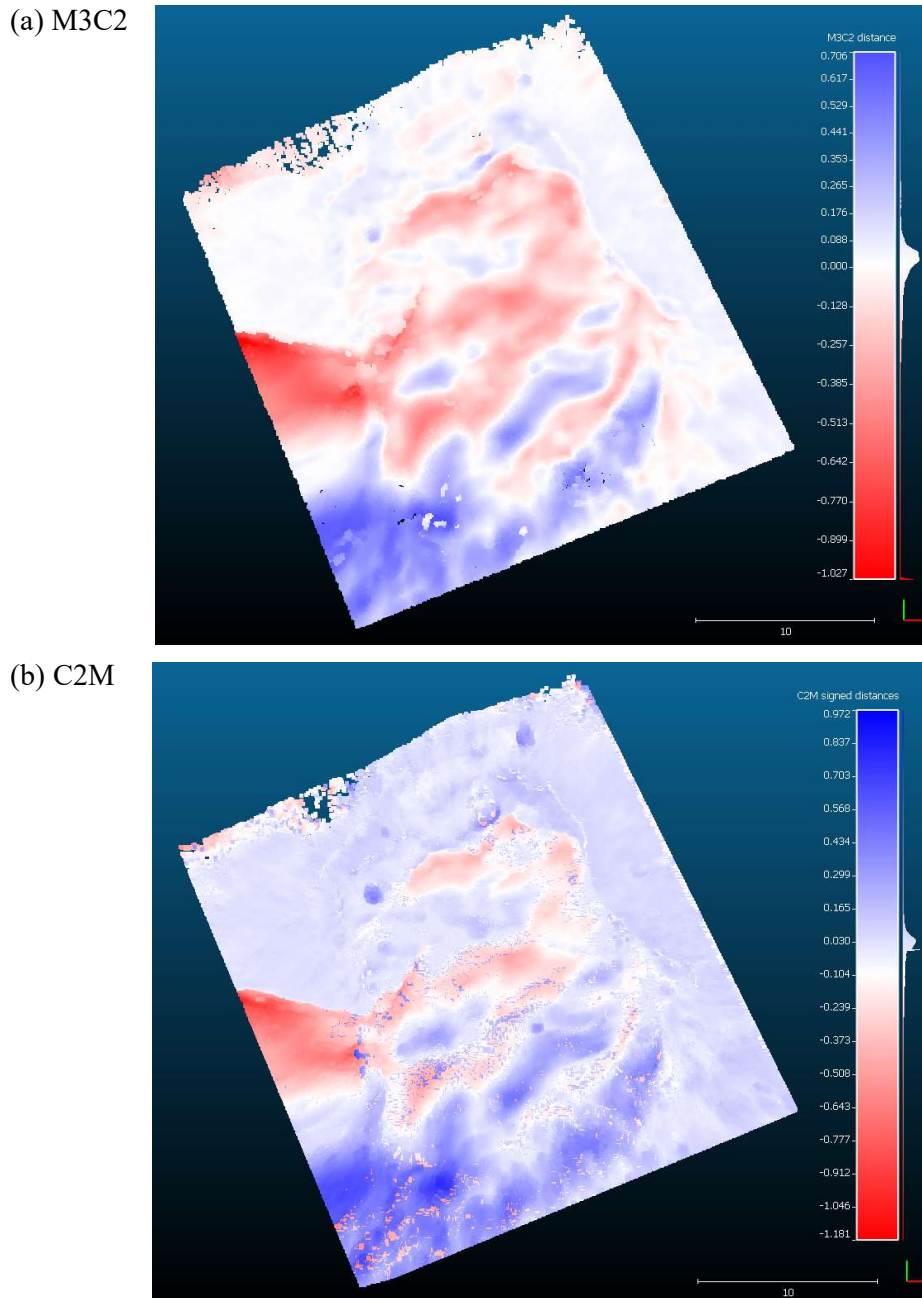


Figure 4-23: Comparison results of change assessment using cloud comparison method based on (a) M3C2 and (b) C2M.

Table 4-18: Statistics of differences between two photogrammetric results using M3C2 and C2M cloud comparison method.

Comparison method	Differences				
	Min (m)	Max (m)	Mean (m)	SD (m)	RMSE (m)
M3C2	-1.027	0.706	-0.005	0.212	0.215
C2M	-1.181	0.972	-0.012	0.195	0.200

The results of multi-epoch analysis from the M3C2 method (Figure 4-23(a)) showed the delicately detected changes of landslide monitoring, whereas the C2M method (Figure 4-23(b)) provided discontinuous values for landslide deformation that might result from non-overlapping areas of both point clouds at different times of the multi-epoch analysis. However, the statistics of differences obtained from the two cloud comparison methods (as shown in Table 4.18) were slightly different.

4.6 Summary

This chapter has presented the photogrammetric potential for landslide monitoring using a mobile device. Also, it has described a series of experiments used in the investigation of performance for developed functions of the mobile cloud based photogrammetric measurement and monitoring system for landslide hazards. The main details of these experiments are highlighted in Table 4-19.

Table 4-19: Summary of findings from Chapter 4 experimentation.

	Experiments	Main findings
§4-2	Investigation of the potential for photogrammetric landslide monitoring.	<ul style="list-style-type: none"> The photogrammetric precision was reliable and useful for measuring landslide movement at sub-decimeter-level accuracy.
§4-3	Investigation of the developed system implemented on the cloud.	<ul style="list-style-type: none"> The time-consuming process of image data transfer from mobile device to the cloud was solved by Internet service with high bandwidth connectivity. If a modern 4G/5G network is available in the future for Internet service, data transfer will be less troublesome.
§4-4	Investigation of relationship between the number of images and image size for optimal imaging network.	<ul style="list-style-type: none"> The suitable number of camera stations (or the number of images) was recommended by the design of photogrammetric configuration using a B/D ratio of 0.1-0.2. Improved image data (i.e. 20%-30% of image size reduction) prior to upload enhanced the performance of both data transfer and processing.
§4-5	Investigation of developed functions on the system	<ul style="list-style-type: none"> Pre-image matching from image sequences can help reduce the overall processing time by approximately 30%. Scaling the photogrammetric results with the distances between targets can avoid the limitations of a conventional approach in geo-referencing with GNSS or TLS observation. However, manual alignment and application of the ICP algorithm to the photogrammetric results between epochs is performed later to ensure referencing into the same coordinate system. Automatic de-noising helps remove gross outliers from the photogrammetric results, especially air points. The application of vegetation filtering for natural landslide monitoring can eliminate vegetated effects over photogrammetric results.

With regard to the data collection for landslide monitoring, a TLS survey usually takes longer than a photogrammetric approach due to the nature of laser-based data capture. Moreover, the post-processing of TLS data can also be complex and normally involves significant manual interaction by an expert user. In contrast, SfM data collection is considerably faster than TLS, and the SfM method is arguably also better suited to

automation. However, the post-processing of the SfM approach based on the developed system does still require manual interaction, especially the geo-referencing and denoising stages.

In terms of geo-referencing for photogrammetry, the aforementioned photo control targets, precisely measured by GNSS, enabled straightforward comparison of the photogrammetric results for each epoch in a common coordinate system. In contrast, geo-referencing without GNSS based target observation was proposed using a solution with a function for geo-referencing which involved measuring the distances between points. This solution can provide low-cost observations to support on-site investigation of landslide monitoring. To ensure the efficiency of the cloud-based photogrammetric landslide monitoring system, the next chapter describes the validation of the developed system at two existing test sites with different types of landslide hazard.

Chapter 5. System implementation

5.1 Introduction

The development stages of the proposed measurement and monitoring system for on-site landslide investigation were described in the previous chapter. To assess the potential of the system for monitoring landslides, two experimental studies were performed: 1) one on a natural earth-flow landslide deformation and 2) one on an area of coastal cliff erosion. This chapter describes these two monitoring experiments and evaluates the performance of the low-cost, real-time approach for landslide hazard analysis.

5.2 Natural earth-flow landslide monitoring experiment

Earth-flows are one of the most common ground movements occurring in natural landslides. They typically have a wide range of movement speeds. In the case of very slow earth-flows, the ground movements can sometimes reveal clues on their slope areas, such as cracks and fissures. To understand the behaviour of this landslide type and evaluate the performance of the photogrammetric landslide monitoring system, the system was used to monitor an active landslide.

5.2.1 Study area

The study area was located at the BGS's Hollin Hill landslide observatory in North Yorkshire, UK. A number of in-situ monitoring systems are already installed at the site, including those based on geotechnical and geophysical techniques, such as ERT which is used for real-time monitoring of sub-surface deformation (Merritt *et al.*, 2014). In addition, geomatics techniques (such as GNSS, lidar) were used to investigate the landslide movements and changes compared to both methods. The focus of this experiment was the main scarp at the top of the slope (red box in Figure 5-1), which extends for 25 m in an approximately east-west direction, and 25 m from north to south, with 8 m elevation difference between the top and bottom of the scarp as shown in Figure 5-2.

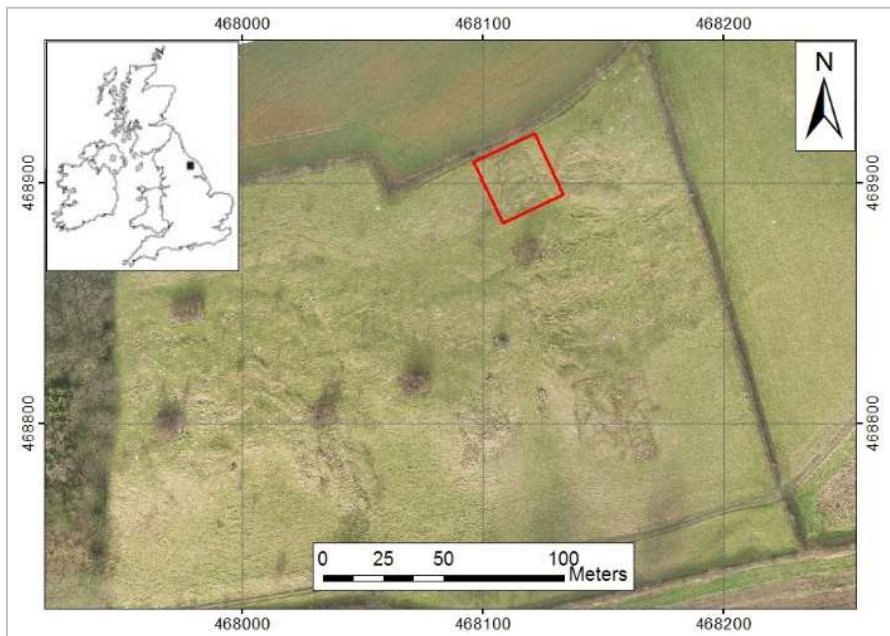


Figure 5-1: Overview of test site location at Hollin Hill landslide observatory: the red box shows the area used for this experiment.



Figure 5-2: Photograph of the main scarp at the top of the Hollin Hill landslide used for the photogrammetric monitoring experiment.

The Hollin Hill landslide consists of a shallow rotational failure at the top of the slope and then moving through an area of translational landslide movement at the middle of the slope. The landslide extends as flow lobes towards the bottom of the slope. The landslide is mostly caused by the movement of the Whitby mudstone formation over the Cleveland ironstone and Staithes sandstone formations, which are highly prone to land sliding (Figure 5-3). The Hollin Hill landslide is vegetated with short grass, which is pasture land for sheep.

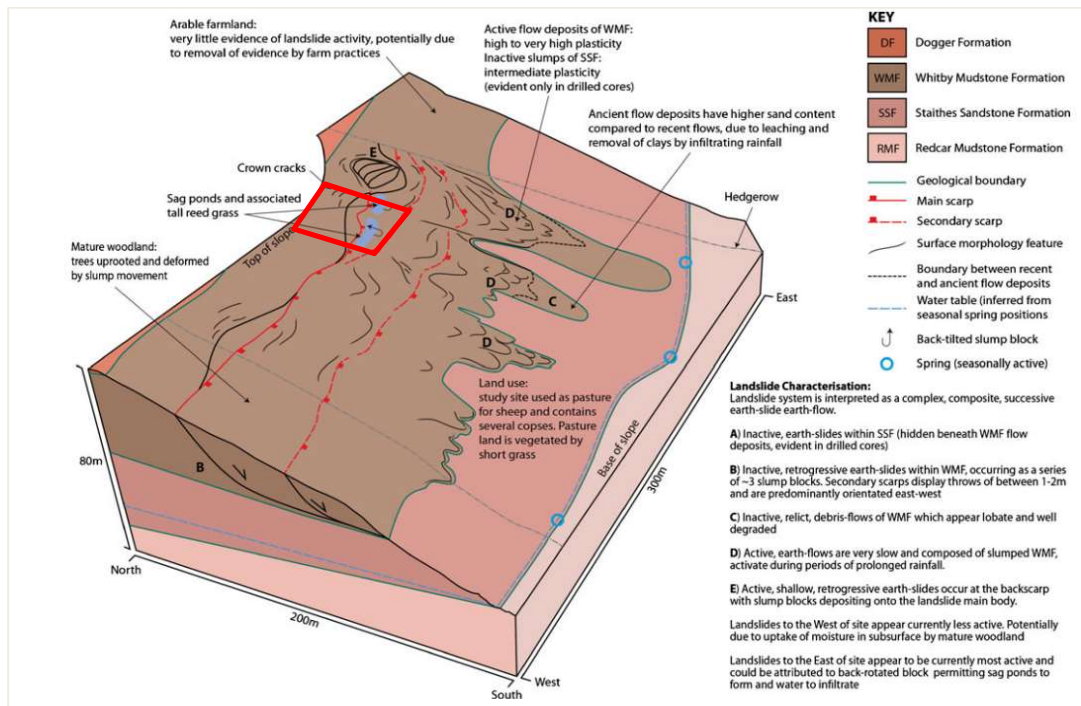


Figure 5-3: Illustration of landslide characteristics at Hollin Hill landslide: the red box shows the area used for the landslide monitoring experiment (Merritt *et al.*, 2014).

5.2.2 Experimental design

In terms of image acquisition for photogrammetric monitoring, suitable camera locations were chosen using photogrammetric network design parameters (as reviewed in section 3.2.3). Imaging configuration was based on a B/D ratio of 0.1-0.2, the maximum allowable camera-to-object distance was < 15 m and the maximum distance between each camera station was approximately 2-3 m. During the survey, those estimated distances were roughly measured by pacing. In order to obtain full coverage of the landslide monitoring area, images were taken around the main scarp in a 360° loop, providing a convergent imaging network. When ground-based photogrammetry was performed, images were captured obliquely depending on the height of operator, the viewing angle of camera and the angle of landslide slope.

To inspect changes in landslide slopes, image data should be regularly collected. The experiment envisaged image collection every three months following seasonal changes in the UK. However, the frequency of image collection was restricted by the need for survey assistance. As a result, three image datasets were acquired using the same Nexus 6 smart phone camera on 1) 10 June 2015, 2) 12 February 2016, and 3) 26 May 2016. Each photoset comprised 36 images of 4160 x 3120 pixels (\approx 13 megapixels). The photo control targets were established around the landslide for geo-referencing of the photogrammetric results. The camera position and viewing direction of each epoch is shown in Figure 5-4. The values of B/D ratio from the photogrammetric configuration at each epoch were calculated as shown in Table 5-1.

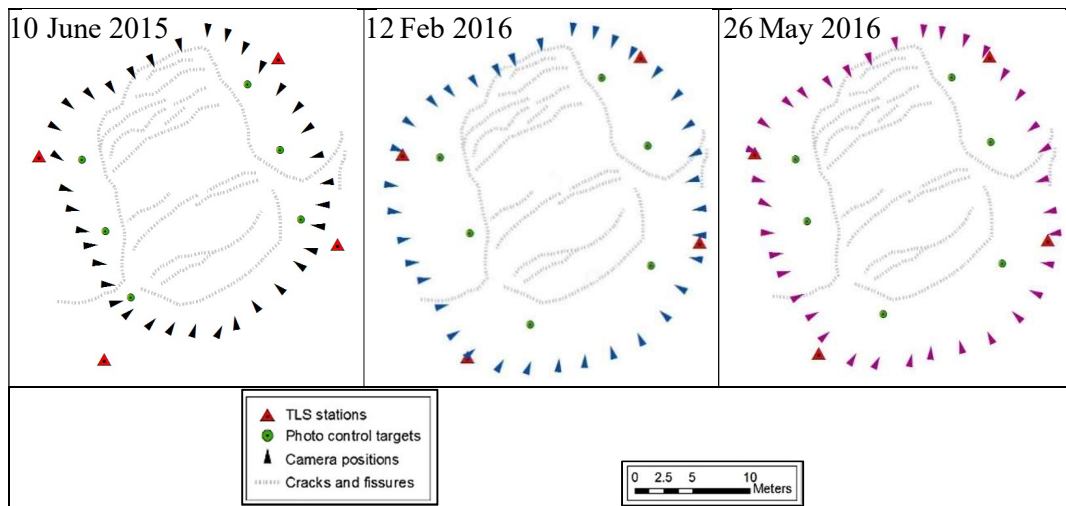


Figure 5-4: Illustration of photogrammetric configuration for each epoch.

Table 5-1: Comparison of a B/D ratio used in each epoch.

	10 June 2015	12 February 2016	26 May 2016
Average base, B (m)	2.56	2.96	2.92
Average distance, D (m)	15	15	15
B/D ratio	0.170	0.197	0.195

To assess the accuracy of photogrammetric results at different epochs, TLS survey was used to provide reference data that could be used for validation. The locations of six photo control targets and four TLS scanning stations were determined using a rapid-static GNSS technique at mm-level accuracy. However, in terms of data processing for each epoch (as shown in Figure 5-5), this experiment was carried out under laboratory simulation because of the inefficient performance of Internet service via current mobile networks in the study area, which was unsuitable for data transfer from mobile device to cloud.

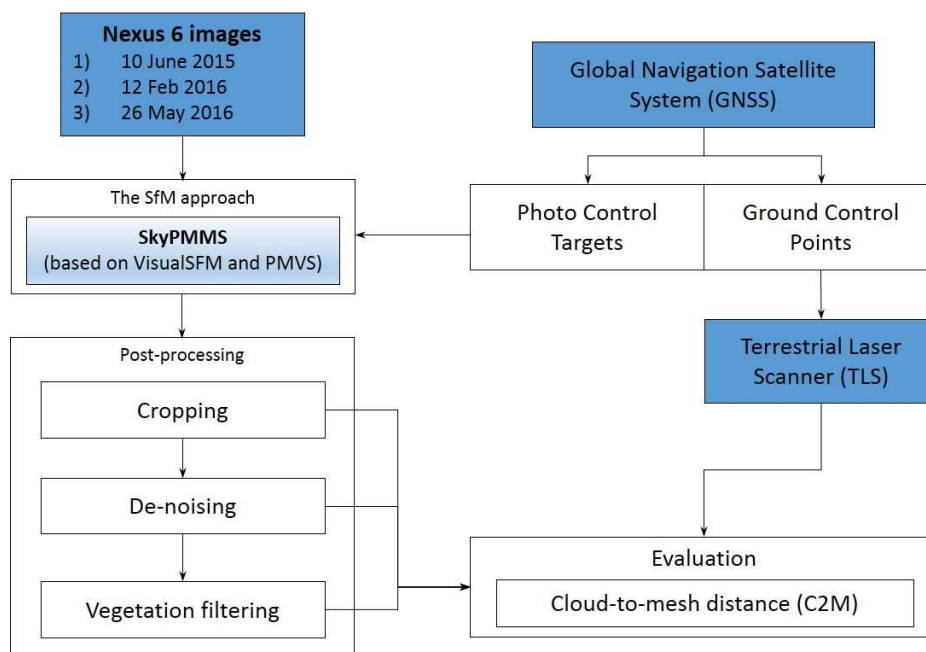


Figure 5-5: The methodology scheme for the accuracy assessment of photogrammetric results at different epochs.

Photogrammetric results for each date were generated using original image datasets that did not adjust the lens distortion in the imagery. The pre-processing stage was unnecessary thanks to a strongly convergent imaging network and a sufficient number of GCPs for the bundle adjustment. For geo-referencing, the target locations on the imagery were directly observed using the developed smart phone function. The quality of transformation for target-based geo-referencing (comprising rotation and translation components only) was computed as the RMSE of transformation from VisualSfM, as shown in Table 5-2.

Table 5-2: Results after target-based geo-referencing of each epoch.

Date	Geo-referencing	
	No. of targets (points)	RMSE of transformation (m)
10 June 2015	5	0.089
12 February 2016	6	0.064
26 May 2016	6	0.042

The RMSE value for the first epoch was higher than for other epochs because a lower quality target was used. Due to the different types of targets used for geo-referencing at each epoch, the small coloured plastic balls utilised as targets for the last two epochs provided a higher precision of mensuration in the imagery. Whereas, the first epoch utilised large markers printed on paper as targets for geo-referencing (Figure 5-6).

		
Physical target	A circular marker printed on paper	A coloured plastic ball
Date of epoch	10 June 2015	12 February 2016, 26 May 2016
Ø of target size	18 cm	6 cm

Figure 5-6: Illustrations of the different types of targets used for geo-referencing.

After photogrammetric processing and geo-referencing of each epoch, photogrammetric results were improved through three stages of post-processing, including 1) cropping, 2) de-noising, and 3) vegetation filtering. Firstly, three point clouds obtained from each epoch were selected using an automatic segmentation in the CloudCompare software. The same extents were chosen in order to avoid non-overlapping areas to allow for an effective comparison. Secondly, to reduce noise in those point clouds, outlier removal was performed using both automatic and manual de-noising in the CloudCompare software. Finally, vegetation filtering was used to extract bare-earth points in the photogrammetric results before assessing the photogrammetric accuracy through the developed function of the system.

5.2.3 Test results

The performance of photogrammetric processing on the developed system was assessed through data processing time, which depended on the performance of cloud computing. Although the higher-performance GPU cloud server (comprising a higher CPU memory size and multiple GPUs) was used to enhance the processing performance and achieve

real-time processing capability, it was revealed that the use of multiple GPUs on a cloud server insignificantly decreased the processing time when compared to the use of PhotoScan software (Table 5-3). Because PhotoScan can support parallel data processing based on multicore-GPU platforms, processing time decreased dramatically by around 46%. The limitation of photogrammetric processing with VisualSfM and PMVS is that they only utilised a single-core processing of GPU. Moreover, the use of the higher-performance GPU cloud server resulted in a higher financial cost of photogrammetric processing.

Table 5-3: Comparison of processing time between the different SfM software and the different performance of GPU cloud server.

SfM software	GPU cloud server		Data processing time (min)
	memory size on GPU	No. of GPUs	
VisualSfM and PMVS	4 GB	1	8.58
	4 GB	2	8.29
PhotoScan	4 GB	1	4.16
	4 GB	2	2.85

To compare photogrammetric results achieved at different times, the details of point clouds were obtained after each post-processing step using the developed photogrammetric measurement system (SkyPMMS) and the validation data from TLS survey (Table 5-4 and Figure 5-7).

Table 5-4: Point cloud comparisons of photogrammetric results at different times and the TLS data.

Date	Ground points of TLS survey (points)	Point cloud of SfM results (points)		
		after cropping	after de-noising	after vegetation filtering (points)
10 June 2015	12,434,476	109,308	104,004	33,377
12 February 2016	10,626,995	157,564	149,007	25,554
26 May 2016	14,111,055	155,275	150,019	36,292

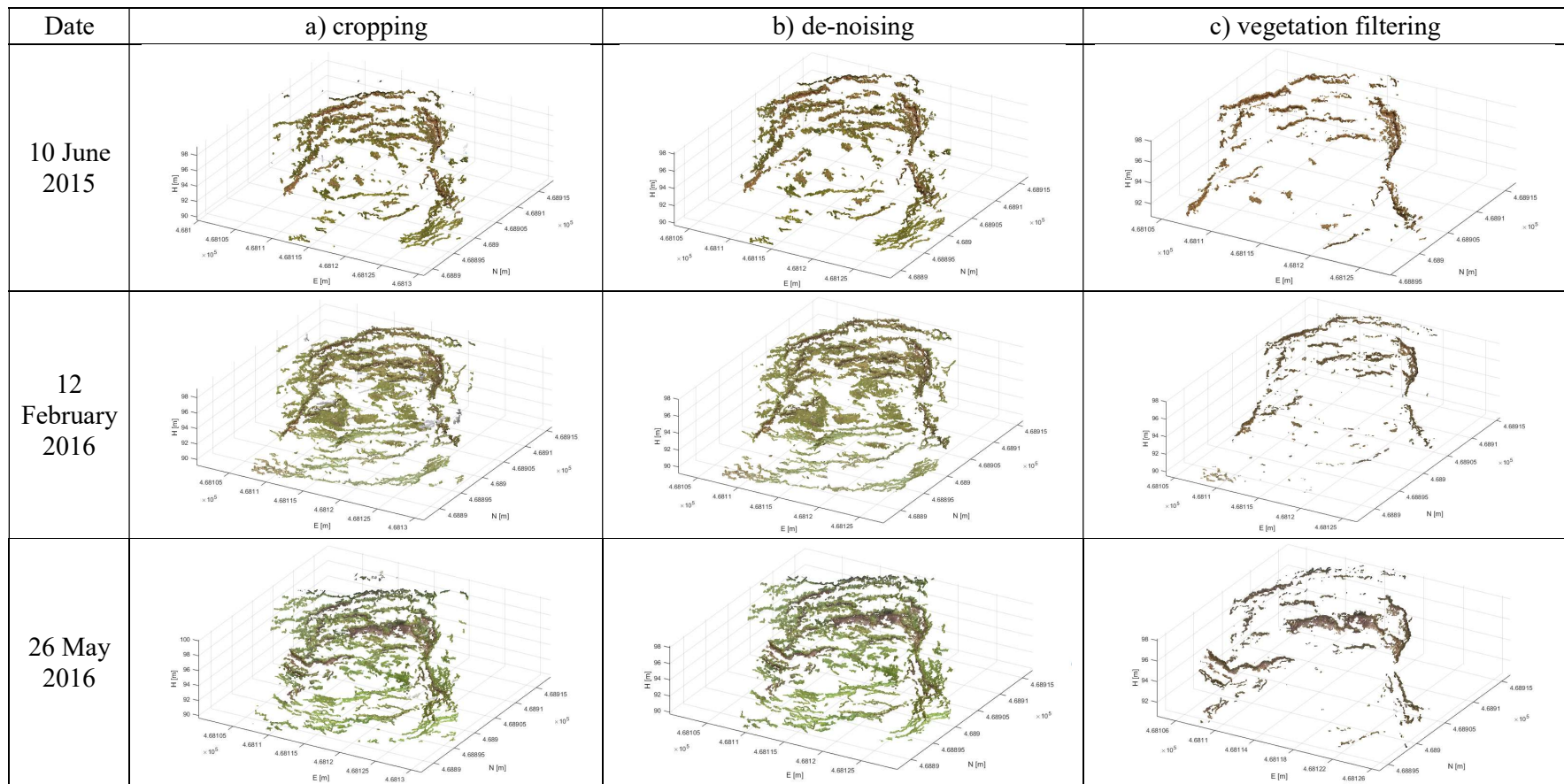


Figure 5-7: Photogrammetric point clouds obtained after applying each post-processing step; a) cropping, b) de-noising, and c) vegetation filtering.

The resultant point cloud from the first epoch after cropping and de-noising was sparser than the point clouds generated at the two last epochs. Because this epoch had varying image quality due to the brightness changes at time of image capture (Figure 5-8), the low quality of dense matching directly affected the quality of the photogrammetric result by producing a fewer number of points. On the other hand, after vegetation filtering the number of bare-earth points from each epoch were very similar (Table 5-4). It is likely that bare-earth points from each epoch represent the key information on landslide areas such as cracks or fissures, although the landslide deformation had changed over time.

	<p>Images acquired on: 10 June 2015 Weather condition: sunny and light cloud</p>
	<p>Images acquired on: 12 February 2016 Weather condition: cloudy</p>
	<p>Images acquired on: 26 May 2016 Weather condition: cloudy</p>

Figure 5-8: Comparison of each image dataset used in the SfM photogrammetric approach at different times: the red boxes distinctly show the different brightness of images.

5.2.4 Assessment of photogrammetric accuracy

To assess the accuracy of the photogrammetric approach for each epoch, point cloud comparisons between TLS data and photogrammetric results following each post-processing stage were performed using the cloud-to-mesh distance tool in the CloudCompare software. The statistical results of the differences are as shown in Table 5-5.

Table 5-5: Statistics of the differences between TLS data and SfM-photogrammetric results for each epoch after post-processing stages using C2M.

Post-processing	Statistics of distance errors	Photogrammetric results at different times		
		10 June 2015	12 Feb 2016	26 May 2016
Point cloud after cropping	Min (m)	-0.297	-0.945	-0.394
	Max (m)	5.605	5.550	6.539
	Mean (m)	0.060	0.139	0.106
	SD (m)	0.320	0.730	0.482
	RMSE (m)	0.322	0.733	0.486
Point cloud after de-noising	Min (m)	-0.297	-0.382	-0.359
	Max (m)	0.442	0.440	0.549
	Mean (m)	0.027	0.009	0.051
	SD (m)	0.051	0.058	0.065
	RMSE (m)	0.053	0.061	0.069
Bare-earth points after vegetation filtering	Min (m)	-0.298	-0.381	-0.333
	Max (m)	0.272	0.393	0.412
	Mean (m)	0.019	0.022	0.033
	SD (m)	0.045	0.056	0.058
	RMSE (m)	0.048	0.058	0.060

The RMSE values for each epoch after cropping and de-noising varied between 5.3 and 6.9 cm. Vegetation filtering provided slightly higher accuracy (RMSE of 4.8 – 6.0 cm). It is likely that photogrammetric accuracy can be improved using the functions developed for post-processing. The vegetated surfaces had an effect on the quality of the results because photogrammetric approaches cannot penetrate vegetated surfaces unlike TLS. SfM-photogrammetric approach based on the developed system (SkyPMMS) using a Nexus 6 smart phone camera can yield sub-dm accuracy level (from 4.8 cm to 6.0 cm) in this type of landslide.

5.2.5 Inspection of landslide monitoring analysis

It was shown by the photogrammetric results in the previous section that the bare-earth point cloud after vegetation filtering can provide a higher accuracy for measuring landslide movement. Based on multi-epoch analysis, each point cloud after vegetation filtering should have been used to assess the changes of landslide deformation over time. However, bare-earth point cloud from SkyPMMS in this experiment revealed only sparse points (in Figure 5.7(c)) because this landslide site was mostly covered by vegetated surfaces; and the majority of points over those surfaces was eliminated though vegetation removal. Although bare-earth points can reveal the key information on landslide areas such as cracks or fissures, the insufficient point clouds used for landslide monitoring analysis might be more prone to fail in the recognition of landslide changes. Therefore, in this case the use of each point cloud after the de-noising stage was more suitable to analyse landslide monitoring.

For the assessment of landslide changes, the comparison between three point clouds at different times was performed using the M3C2 technique based on the developed landslide monitoring system (SkyPMMS), which generates the elevation difference of landslide deformation for on-site investigation. Moreover, this experiment utilised three point clouds at different epochs obtained from PhotoScan software (as shown in Figure 5-9) to compare with those results from the developed system. The results of multi-epoch analysis for the photogrammetric approaches (SkyPMMS and PhotoScan) are illustrated in Figure 5-10 and Figure 5-11, whilst the statistics of elevation differences for assessing landslide changes are presented in Table 5-6.

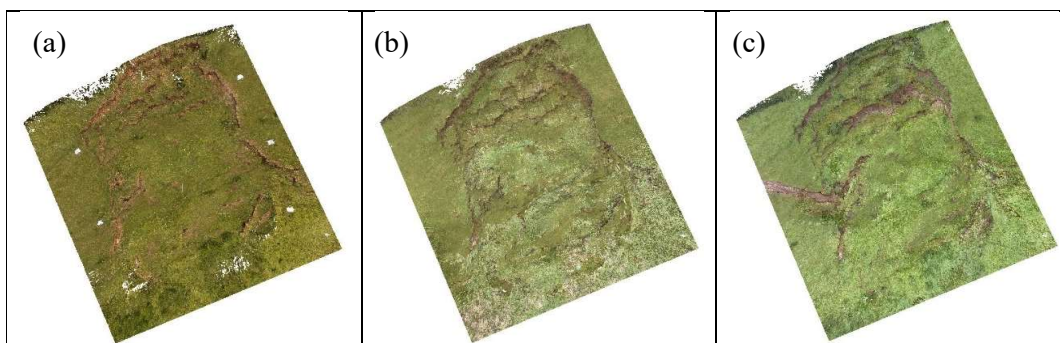


Figure 5-9: Three point clouds of photogrammetric results at different epochs from PhotoScan software acquired on: (a) 10 June 2015, (b) 12 February 2016 and (c) 26 May 2016.

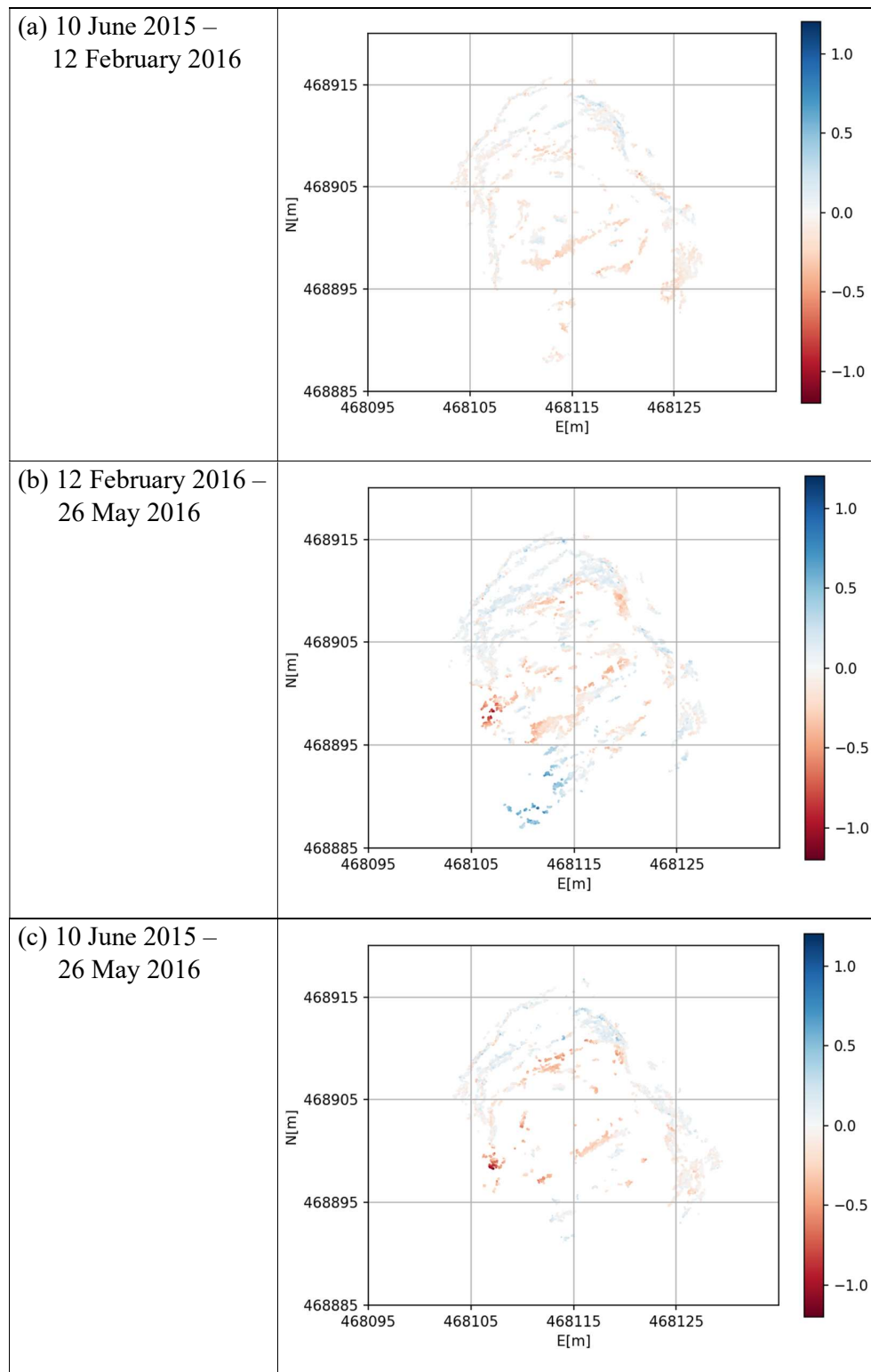


Figure 5-10: Elevation difference of photogrammetric results at different times from the developed system (SkyPMMS) used in the assessment of landslide changes.

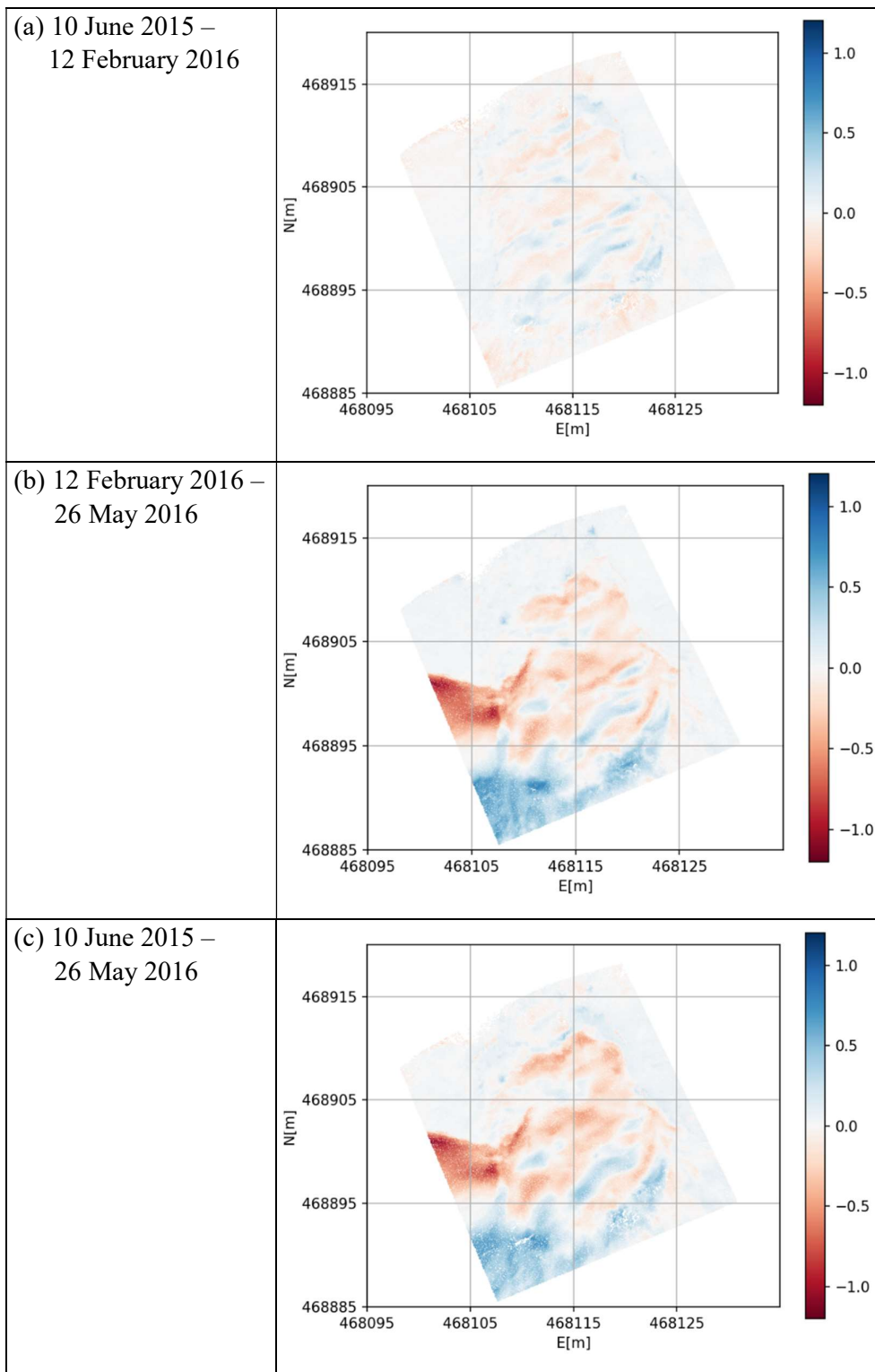


Figure 5-11: Elevation difference of photogrammetric results at different times from PhotoScan software used in the assessment of landslide changes.

Table 5-6: Comparison statistics of elevation changes from TLS data and different SfM-photogrammetric approach (SkyPMMS and PhotoScan).

Epochs	Statistics of elevation changes	Method/SfM approach		
		TLS	SkyPMMS	PhotoScan
10 June 2015 to 12 Feb 2016 (242 days)	Min (m)	-0.347	-0.594	-0.343
	Max (m)	0.356	0.493	0.424
	Mean (m)	-0.049	-0.041	0.001
	SD (m)	0.070	0.120	0.076
12 Feb 2016 to 26 May 2016 (104 days)	Min (m)	-1.111	-1.076	-1.100
	Max (m)	0.821	0.956	0.812
	Mean (m)	-0.014	-0.015	0.005
	SD (m)	0.213	0.180	0.234
10 June 2015 to 26 May 2016 (346 days)	Min (m)	-1.150	-1.109	-1.099
	Max (m)	0.814	0.614	0.801
	Mean (m)	-0.066	-0.044	-0.008
	SD (m)	0.228	0.175	0.233

Three analyses were performed to assess elevation changes shown by each different approach: 1) between 10 June 2015 and 12 Feb 2016 (242 days), 2) between 12 Feb 2016 and 26 May 2016 (104 days), and 3) between 10 June 2015 and 26 May 2016 (346 days). Visual comparison of the landslide changes detected using different SfM approaches (as shown in Figure 5-10 and Figure 5-11) reveals that the changes of landslide deformation were clearer for the point clouds processed in PhotoScan. This is due to a much denser point cloud provided by PhotoScan. Nevertheless, the results obtained from SkyPMMS still highlighted the landslide changes near cracks or fissures over landslide areas.

The elevation difference results using multi-epoch analysis (Table 5-6) showed that the values of minimum, maximum and standard deviation for elevation changes of TLS data and PhotoScan were slightly different (for both the first 242 days epochs and the second 104 days epochs). In contrast, the mean values of TLS data and SkyPMMS were negative and differed slightly in terms of magnitude. As mentioned above, point clouds provided by PhotoScan were mostly above the vegetated surfaces, while point clouds from TLS data and SkyPMMS were mainly over the bare-earth surfaces. As a result, the mean value of elevation changes from PhotoScan was substantially different from TLS data and SkyPMMS because of vegetation effects.

However, due to vegetation effects, the main drawback of photogrammetric monitoring for landslide hazards is the inability to penetrate vegetated surfaces. The height of vegetation during an annual cycle can directly impact on assessing landslide deformation. It is likely that positive changes in stable areas of landslide will be found, as shown in Figure 5-11. However, the uncertainty of this factor should be considered for evaluating elevation changes using a point cloud comparison method based on the M3C2 technique. In ideal experiments into landslide monitoring, it can be reasonably assumed that the comparison of point clouds over bare-earth surfaces only would eliminate the effects of vegetation when assessing landslide deformation.

Due to the extremely different number of points and point density from SkyPMMS, the values of minimum, maximum and standard deviation of elevation changes were considerably different from both TLS data and PhotoScan. Nevertheless, the photogrammetric approach based on the developed system still had sufficient potential for quantitative analysis of landslide movement. It was shown that SkyPMMS photogrammetric results acquired at different times might be utilised for initial assessment of landslide monitoring.

To further validate the landslide analysis, GNSS observations for the position of BGS pegs were regularly used to measure 3D displacement of this landslide site over 346 days. The location of three BGS' pegs used in this validation are shown in Figure 5-12. The comparison results of change detection for landslide deformation using different geomatics technique are shown in Table 5-7.

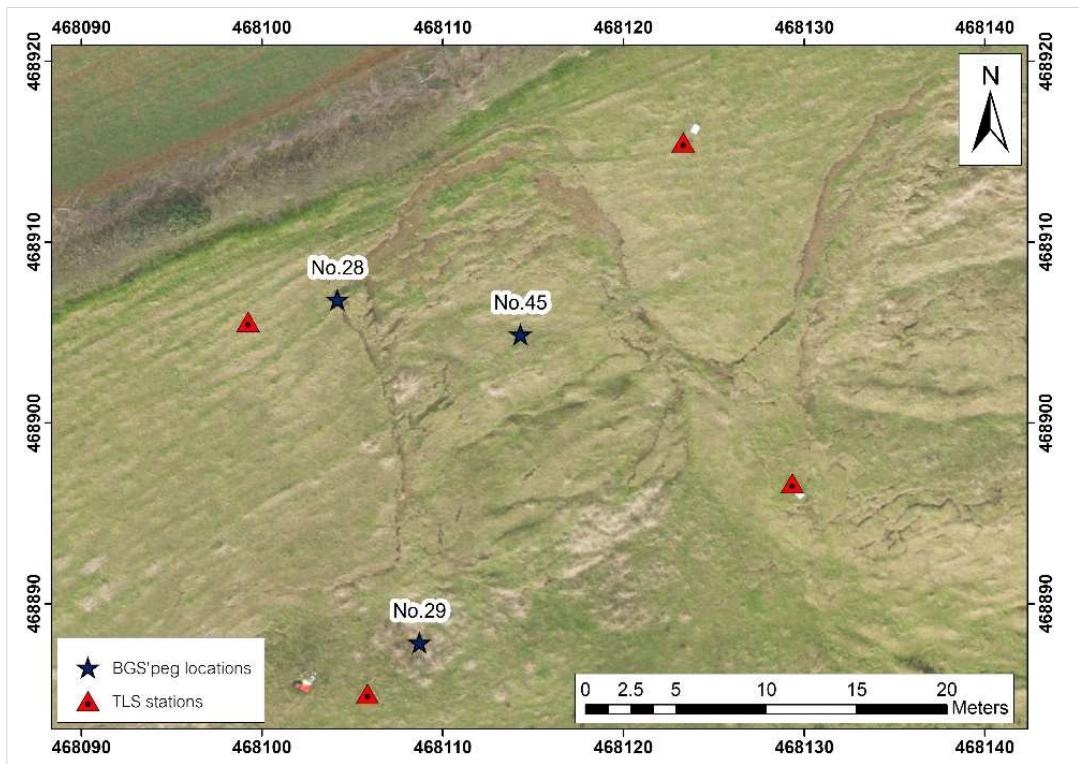


Figure 5-12: Illustration of the location of BGS pegs used in landslide monitoring.

Unfortunately, this validation step could not utilise photogrammetric results obtained from SkyPMMS because of the insufficient number of points in the point cloud. Inspection of landslide movement from this data at the location of the BGS pegs proved impossible.

Table 5-7: Comparison between cumulative displacement of GNSS survey and elevation changes of TLS data and SfM approach.

Epochs	No. of pegs	Method/ SfM approach	Cumulative displacement (cm)			
			ΔE	ΔN	ΔH	Δ
10 June 2015 till 12 Feb 2016 (242 days)	28	GNSS	6.8	-2.7	-1.4	7.4
		TLS			-4.6	
		PhotoScan			0.8	
	29	GNSS	6.2	-6.6	-5.0	10.3
		TLS			-3.1	
		PhotoScan			-1.4	
	45	GNSS	19.3	-61.9	-27.7	70.5
		TLS			-23.4	
		PhotoScan			-14.9	
12 Feb 2016 till 26 May 2016 (104 days)	28	GNSS	-1.7	-4.3	6.3	7.8
		TLS			2.7	
		PhotoScan			1.9	
	29	GNSS	51.3	-89.8	18.4	105.0
		TLS			25.9	
		PhotoScan			24.8	
	45	GNSS	28.6	-85.5	-36.4	97.3
		TLS			-21.2	
		PhotoScan			-25.1	

It can be seen from the cumulative displacement in Table 5-7 that GNSS-based observations showed significantly more information on displacement than both TLS survey and SfM approaches, in particular for the 3D displacements. Measuring the landslide changes using TLS survey and SfM approaches yielded only relative movement in terms of the elevation differences over time. The elevation changes over landslide areas using the three geomatics techniques showed significantly positive correlation, although slightly different values were recorded ($\approx 3.2 - 12.8$ cm of the first 242 days and $\approx 4.4 - 11.3$ cm of the second 104 days). The assessment of landslide monitoring analysis using photogrammetric results indicated that PhotoScan can provide measurement of landslide movement at dm-accuracy level (based on comparison to the GNSS observations). Although SkyPMMS could not deliver the elevation changes in this experiment due to a dramatically different density of point cloud, bare-earth points (e.g. cracks and fissures on landslides areas) might reasonably be used for tracking landslide deformations using the developed algorithm in future work.

5.3 Coastal cliff monitoring experiment

This experiment aimed to investigate the performance of the SfM photogrammetric approach using the developed landslide monitoring system for change detection of coastal cliff deformation. In particular, geo-referencing without GNSS/TLS-based target observation was proposed and tested in order to provide a low-cost approach for on-site investigation of landslide monitoring for cliff deformation.

5.3.1 Study area

Coastal cliff monitoring mainly consists of inspection of the changes of cliff deformation or rock falls due to coastal erosion. In this experiment, the study site was located at Marsden Bay in South Shields, near Newcastle upon Tyne, UK. The deformation of coastal cliff was mostly caused by the crushed rock and natural aggregates of limestone or dolomite formations. To assess the changes occurring at this type of landslide hazard, visual comparison of the coastal cliff site was performed on 27 November 2016 and 13 April 2017 (Figure 5-13). The section of coastal cliff to study erosion was over 5-m high by 20-m long.



Figure 5-13: Illustrations of coastal cliff site at two epochs acquired on: (a) 27 November 2016 and (b) 13 April 2017.

5.3.2 Experimental design

The photogrammetric configuration used for the previous experiment could not be applied due to the high and steep geometry of the coastal cliff site. The block configuration was more suitable than a conventional configuration because images were taken in the front of the cliff in a linear sequence (as illustrated in Figure 5-14). The photogrammetric configuration design still utilised the same main factors according to the previous experiment using a B/D ratio of 0.1-0.2.

Two datasets were acquired on 27 November 2016 and 13 April 2017 using a Nexus 6 smart phone camera. Each photoset comprised 26 images with a maximum image size of 4160 x 3120 pixels (approximately 13 MP). For geo-referencing, five photo control targets were located in front of the coastal cliff. The camera positions and viewing directions for each epoch are shown in Figure 5-14.

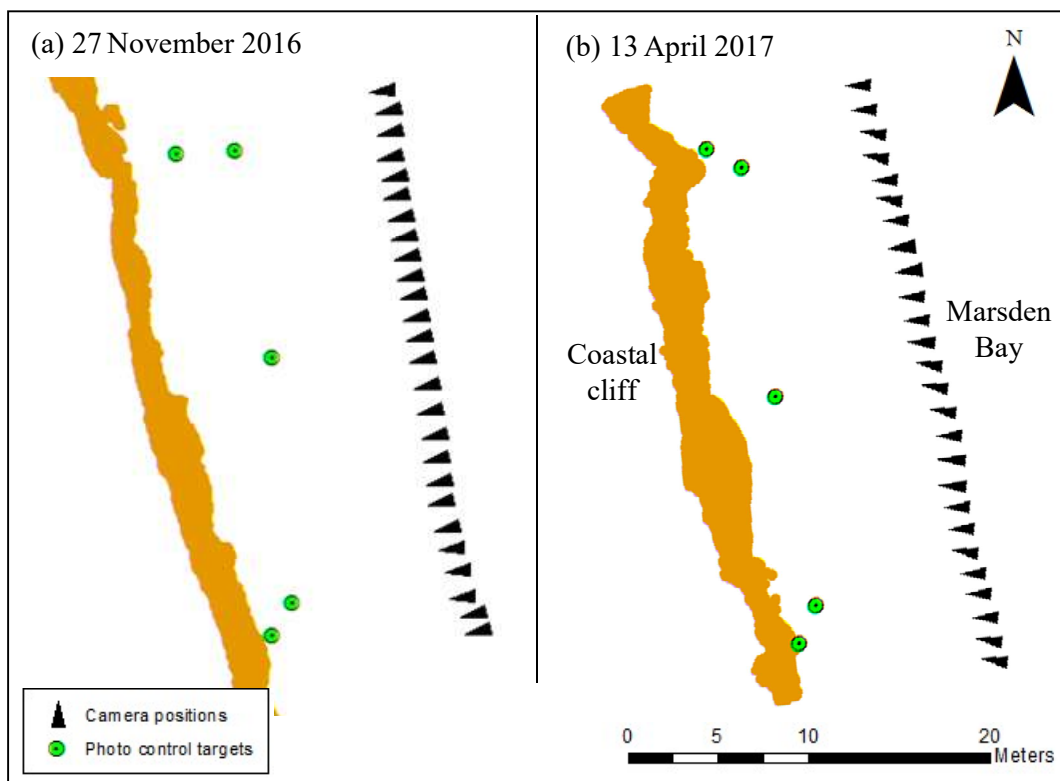


Figure 5-14: Camera positions and viewing directions between two epochs acquired on (a) 27 November 2016 and (b) 13 April 2017.

From Figure 5-14, a B/D ratio of each epoch was calculated as shown in Table 5-8.

Table 5-8: Comparison of B/D ratio used at each epoch.

	27 November 2016	13 April 2017
Average base, B (m)	1.24	1.33
Average distance, D (m)	12.10	10.85
B/D ratio	0.102	0.122

A Leica ScanStation P40 was used to acquire TLS data from a single scanner position on the same date as imaging observation to validate the photogrammetric results. To clarify the workflow used in the assessment of photogrammetric results, the design of this experiment is shown in Figure 5-15. Due to the unavailability of a mobile network at this study site, Internet service under real-world conditions was unavailable for data transfer and processing. Thus, laboratory experimentation was conducted using the data collected at the coastal cliff site.

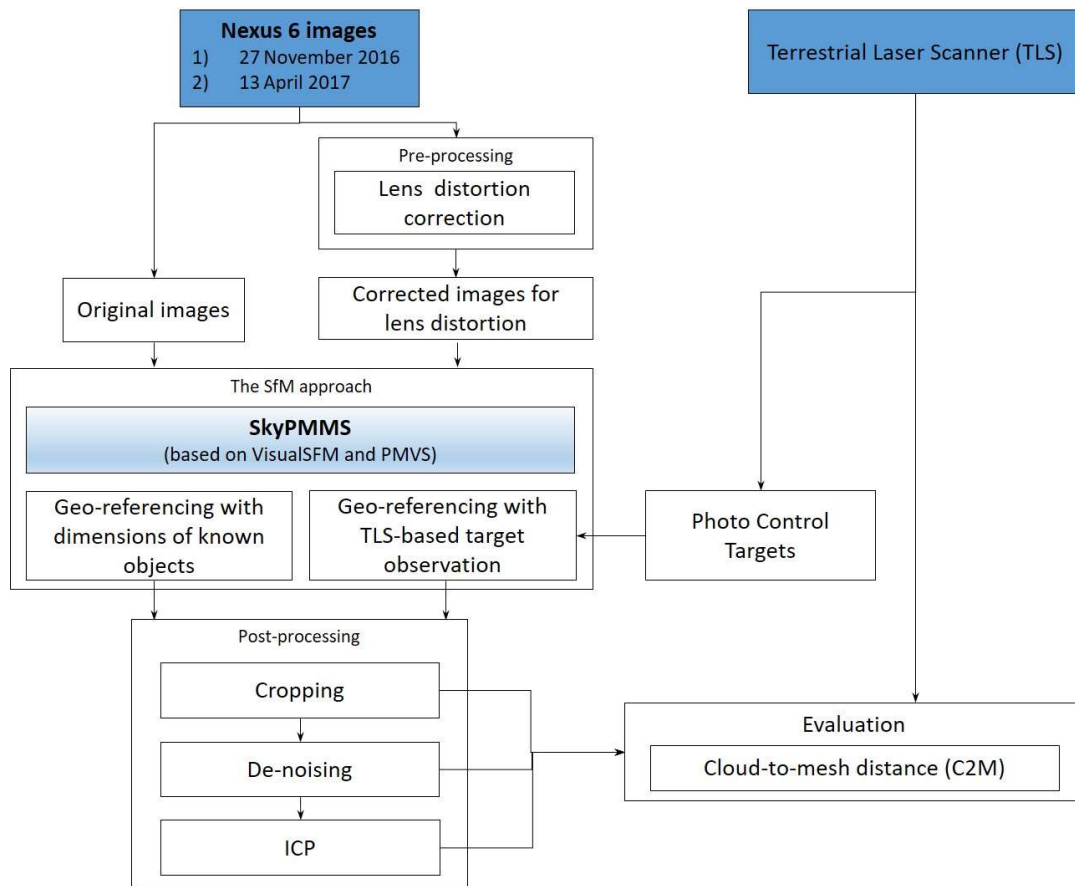


Figure 5-15: The methodology scheme for the accuracy assessment of photogrammetric results at different epochs.

In this experiment, photogrammetric results were generated from both raw images and images corrected for lens distortion with fixed calibration. The Nexus 6 smart phone camera was calibrated using the camera calibrating application in Matlab. Imagery was then corrected using a Python script with OpenCV library based on the developed function of SkyPMMS. For geo-referencing with TLS- based GCPs, the targets could be measured directly in the imagery to provide a pair list of targets with photo coordinates and the real-world coordinates acquired from TLS survey. The other geo-referencing approach without TLS observations, however, used a pair list of three targets with photo coordinates and pseudo coordinates from three distances measured between each target and then aligned manually with TLS data using four key features on the coastal cliff. The details of both geo-referencing approaches were described in Section 4.5.3. The quality of geo-referencing using photo control targets of each epoch was computed in the form of RMSE for transformation (comprising a rotation and translation only), as shown in Table 5-9.

Table 5-9: Statistics of the results from geo-referencing using photo control targets and after applying ICP.

Epoch	Photoset	After geo-referencing		RMSE of transformation after applying ICP (m)
		The number of GCPs (points)	RMSE (m)	
27 November 2016	Raw images	5	0.104	0.091
	Images corrected for lens distortion with fixed calibration mode	5	0.069	0.050
13 April 2017	Raw images	5	0.148	0.082
	Images corrected for lens distortion with fixed calibration mode	5	0.030	0.030

Photogrammetric results were processed by cropping and de-noising in order to improve their quality. However, after geo-referencing, the SfM-approach might be prone to transformation errors. To reduce this problem, the ICP algorithm was applied in the experiment. To investigate the photogrammetric accuracy, the comparison between photogrammetric results at different times and TLS data was carried out using the C2M method in the CloudCompare software.

5.3.3 Test results

The performance of the developed system for photogrammetric landslide monitoring was assessed in the previous experiment. This experiment tested the transferability to coastal cliff monitoring. In the first part of this experiment, the details of photogrammetric results obtained from SkyPMMS using a Nexus 6 smart phone camera before and after applying lens distortion corrections are shown in Table 5-10. Figure 5-16 and Figure 5-17 compare the point clouds at different times obtained from different SfM approaches (SkyPMMS, PhotoScan) and TLS survey.

Table 5-10: Comparison between the SfM-photogrammetric results and TLS data acquired on 27th November 2016 and 13th April 2017.

Date	Ground points of TLS data (points)	Photoset/Pre-processing	SfM-photogrammetric results	
			Point cloud (points)	Point cloud after cropping and de-noising (points)
27 November 2016	10,052,978	Raw images	864,944	384,611
		Images corrected for lens distortion with fixed calibration mode	879,795	442,656
13 April 2017	11,609,458	Raw images	758,241	537,576
		Images corrected for lens distortion with fixed calibration mode	956,091	647,061

As shown in Table 5-10, photogrammetric processing which utilised images corrected for lens distortion with the fixed calibration mode, provided a higher number of points; a denser point cloud and fewer void areas can be seen for those photosets in both Figure 5-16 and Figure 5-17. Applying this method based on the developed system could significantly improve the quality of photogrammetric results for this type of coastal cliff surface. However, the bottom part of this coastal cliff point cloud obtained from SkyPMMS showed large areas of voids when compared to TLS data and the SfM approach using PhotoScan. Due to the insufficient dense matching in the developed system based on VisualSfM and PMVS, points were not generated in this area. The free SfM software was not able to produce as large a number of points as the SfM-commercial software (PhotoScan).

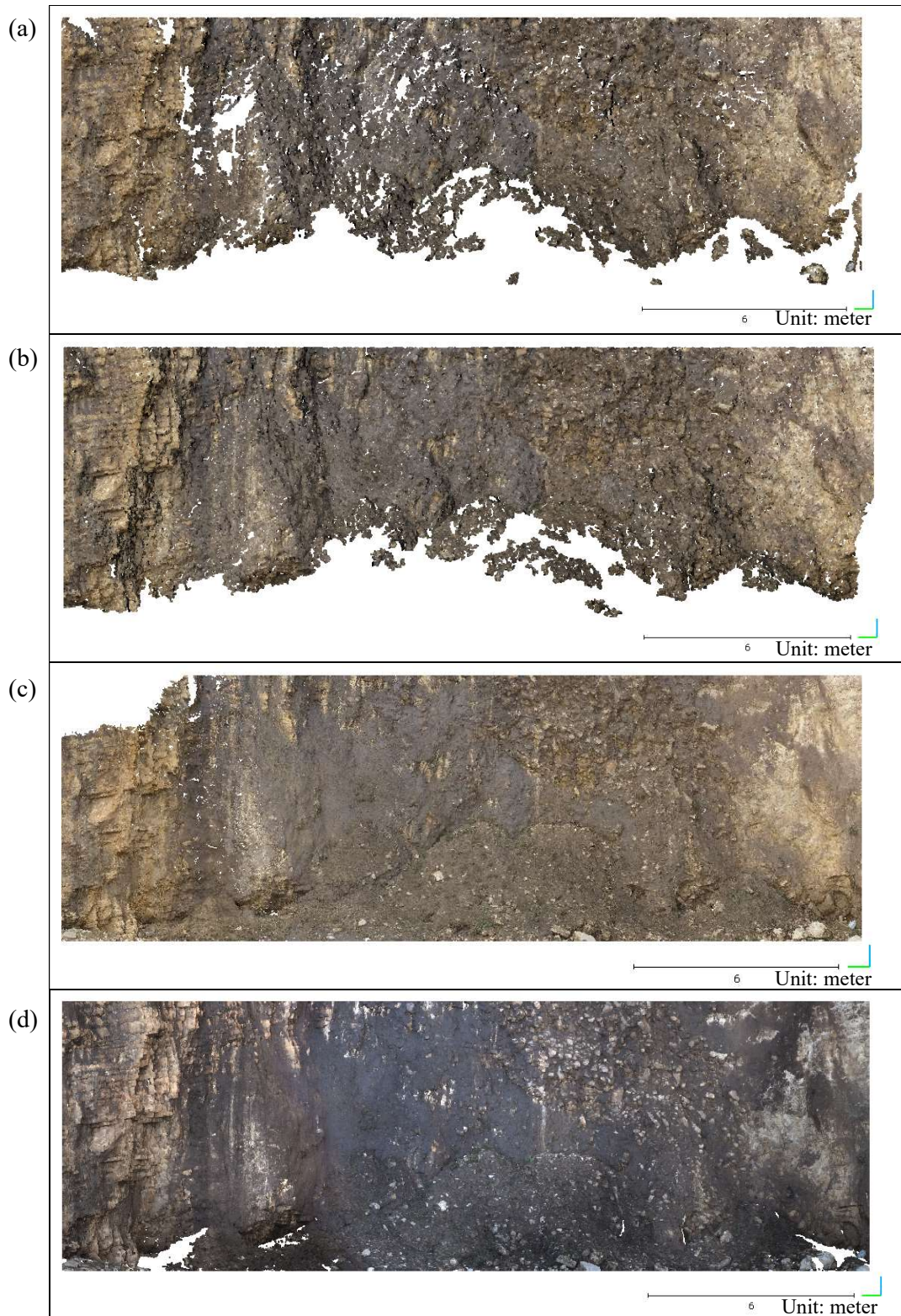


Figure 5-16: Comparison of four point clouds obtained using (a) raw images (SkyPMMS), (b) images corrected for lens distortion with the fixed calibration mode (SkyPMMS), (c) PhotoScan (d) and TLS survey (27 November 2016).

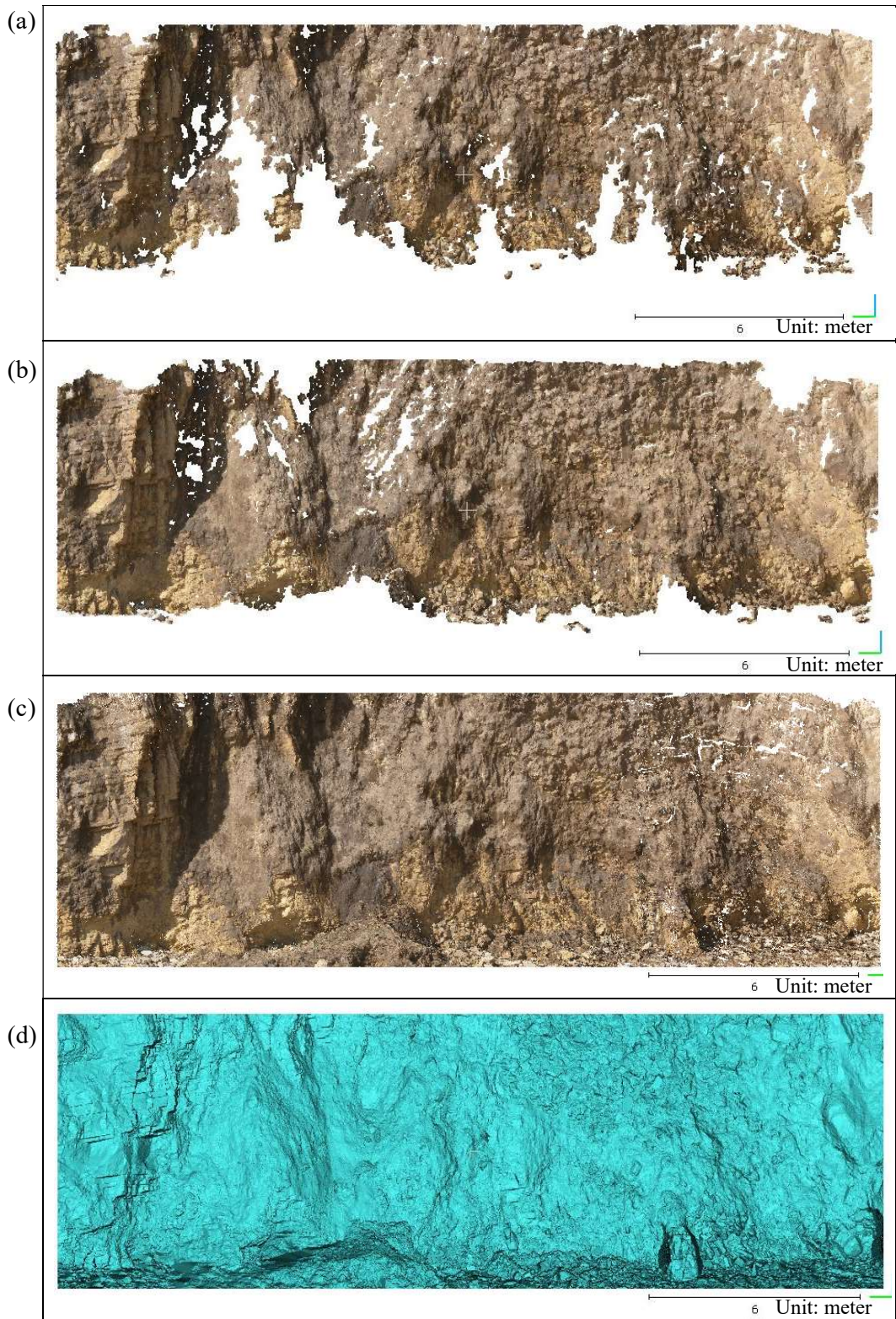


Figure 5-17: Comparison of four point clouds obtained using (a) raw images (SkyPMMS), (b) images corrected for lens distortion with the fixed calibration mode (SkyPMMS), (c) PhotoScan (d) and TLS survey (13 April 2017).

5.3.4 Assessment of photogrammetric accuracy

Following the lens distortion correction of images, photogrammetric results were generated from images corrected for lens distortion with the fixed calibration mode using the developed system. To inspect the photogrammetric accuracy, the results at different times from original and improved image data were compared to the TLS data, as shown in Table 5-11.

Table 5-11: Statistics of distance differences between TLS data and SfM results from original and images corrected for lens distortion with fixed calibration mode.

Date	Photoset/Pre-processing	TLS-SfM using C2M method				
		Min (m)	Max (m)	Mean (m)	SD (m)	RMSE (m)
27 November 2016	Raw images	-0.958	0.866	-0.419	0.266	0.269
	Images corrected for lens distortion with the fixed calibration mode	-0.275	0.257	0.004	0.044	0.046
13 April 2017	Raw images	-0.735	0.684	-0.279	0.202	0.205
	Images corrected for lens distortion with the fixed calibration mode	-0.191	0.257	0.022	0.040	0.042

In Table 5-11, the minimum, maximum, mean and RMSE values of distance errors between the TLS reference and SfM approach using images corrected for lens distortion with the fixed calibration mode were noticeably smaller than for SfM using raw images. The results suggest applying lens distortion correction with the fixed calibration mode used in processing can help significantly improve the photogrammetric accuracy and provide a better quality of results in terms of a denser point cloud, as explained in the previous section. This is most probably related to the fact that 3D reconstruction with the fixed camera model from images corrected for lens distortion did not generate an error along the image sequence. Furthermore, lens distortion correction was applied to the imagery, which provided a higher accuracy of imaging mensuration.

The mean errors of both epochs can represent the quality of transformation for photogrammetric results after geo-referencing. Table 5-12 shows the summary statistics for the accuracy assessment when applying ICP for photogrammetric results at each epoch with the TLS reference acquired at the same time.

Table 5-12: Statistics of distance differences between TLS data and SfM results from images corrected for lens distortion with the fixed calibration mode after applying ICP.

Date	Photoset/Pre-processing	Post-processing	TLS-SfM using C2M method				
			Min (m)	Max (m)	Mean (m)	SD (m)	RMSE (m)
27 November 2016	Images corrected for lens distortion with fixed calibration mode	-	-0.275	0.257	0.004	0.044	0.046
		applying ICP	-0.236	0.223	0.000	0.025	0.028
13 April 2017	Images corrected for lens distortion with fixed calibration mode	-	-0.191	0.257	0.022	0.040	0.042
		applying ICP	-0.204	0.234	0.000	0.028	0.030

As shown in Table 5-12, the mean and RMSE values of distance errors between TLS data and photogrammetric results from both epochs decreased significantly after applying ICP algorithm. It is likely that the ICP adjustment in this experiment might help to reduce a potential bias after geo-referencing. However, point clouds in this type of landslide monitoring were mostly over bare-earth surfaces. Therefore, the use of ICP algorithm may be more suitable for stable areas and over surfaces without vegetation.

The accuracy assessment of photogrammetric results for the geo-referencing solution without GNSS/TLS-based target observations is shown in Table 5-13. However, the last epoch was only processed by this solution because it was developed after the first data collection.

Table 5-13: Statistics of distance differences between TLS data and SfM results from images corrected for lens distortion with the fixed calibration mode, different geo-referencing.

Date	Photoset/Pre-processing	Method of geo-referencing	TLS-SfM using C2M method				
			Min (m)	Max (m)	Mean (m)	SD (m)	RMSE (m)
13 April 2017	Images corrected for lens distortion with the fixed calibration mode	with TLS-based target observation and applying ICP	-0.204	0.234	0.000	0.028	0.030
		Scaling with the dimensions of known object, manual alignment and applying ICP	-0.256	0.265	0.000	0.026	0.027

The minimum, maximum, mean and RMSE values of distance errors between the TLS reference and photogrammetric results after applying ICP obtained from geo-referencing with the dimensions of known object and manual alignment were approximately the same as when geo-referencing with TLS-based target observation. Surprisingly, the photogrammetric results using the geo-referencing solution without GNSS/TLS-based target observations still provided an accuracy commensurate to conventional geo-referencing.

5.3.5 Cliff erosion monitoring analysis

Monitoring analysis was performed by comparing two point clouds acquired at different times between 27 November 2016 and 13 April 2017 (135 days). To ensure the photogrammetric results were in the same reference coordinates before analysis, the point cloud from the second epoch (acquired on 13 April 2017) was georeferenced to the first epoch. The method of geo-referencing consisted of two main stages; 1) alignment with each other using four key features on the coastal cliff, and 2) application of the ICP algorithm. The assessment of cliff erosion was performed using the system developed for landslide monitoring analysis over the 135 day intervening period. Figure 5-18 compares the results of change assessment for cliff erosion obtained from TLS survey and different SfM approaches (SkyPMMS and PhotoScan) using M3C2.

In terms of the additional results after point cloud comparison using the M3C2 method, the distance uncertainty and statistically significant change of differences between two point clouds at different times were calculated. Due to the uncertainty in different roughness of both point clouds, change significance should be considered for the differences in case of a real change (Lague *et al.*, 2013). Significant change (value = 1) refers to situation where the value of differences from M3C2 is more than the distance uncertainty calculated with M3C2. On the other hand, insignificant change (value = 0) means that the differences between two point clouds is less than the distance uncertainty.

The preliminary analyses of the three approaches showed significant changes at the toe of the cliff. The most active part in this coastal surface was significantly eroded during the investigated period. Based on initial visual assessment of Figure 5-18, the surface changed by between approximately -0.5 and -2.0 m. Figure 5-19 shows significant

changes within the analysis results obtained from TLS survey and different SfM approaches. It can be seen that no significant differences were found in the upper and central part of coastal cliff; in those parts the coastal surface remained predominantly stable.

As shown in Figure 5-19(c), PhotoScan detected larger amounts of significant change in the left- and right-hand side of coastal cliff than both TLS and SkyPMMS. Moreover, those were not actual changes, but artefacts most probably related to the fact that point clouds from PhotoScan had greater errors due to the known problem of the doming effect. As SfM-photogrammetric PhotoScan processing was performed with many adverse conditions, systematic errors were often found in the results. For example, the use of independent camera models with poor photogrammetric network configuration could result in distorted reconstruction that was always found in the linear sequences of images. In addition, the number and distribution of GCPs was insufficient in bundle adjustment (Eltner and Schneider, 2015).

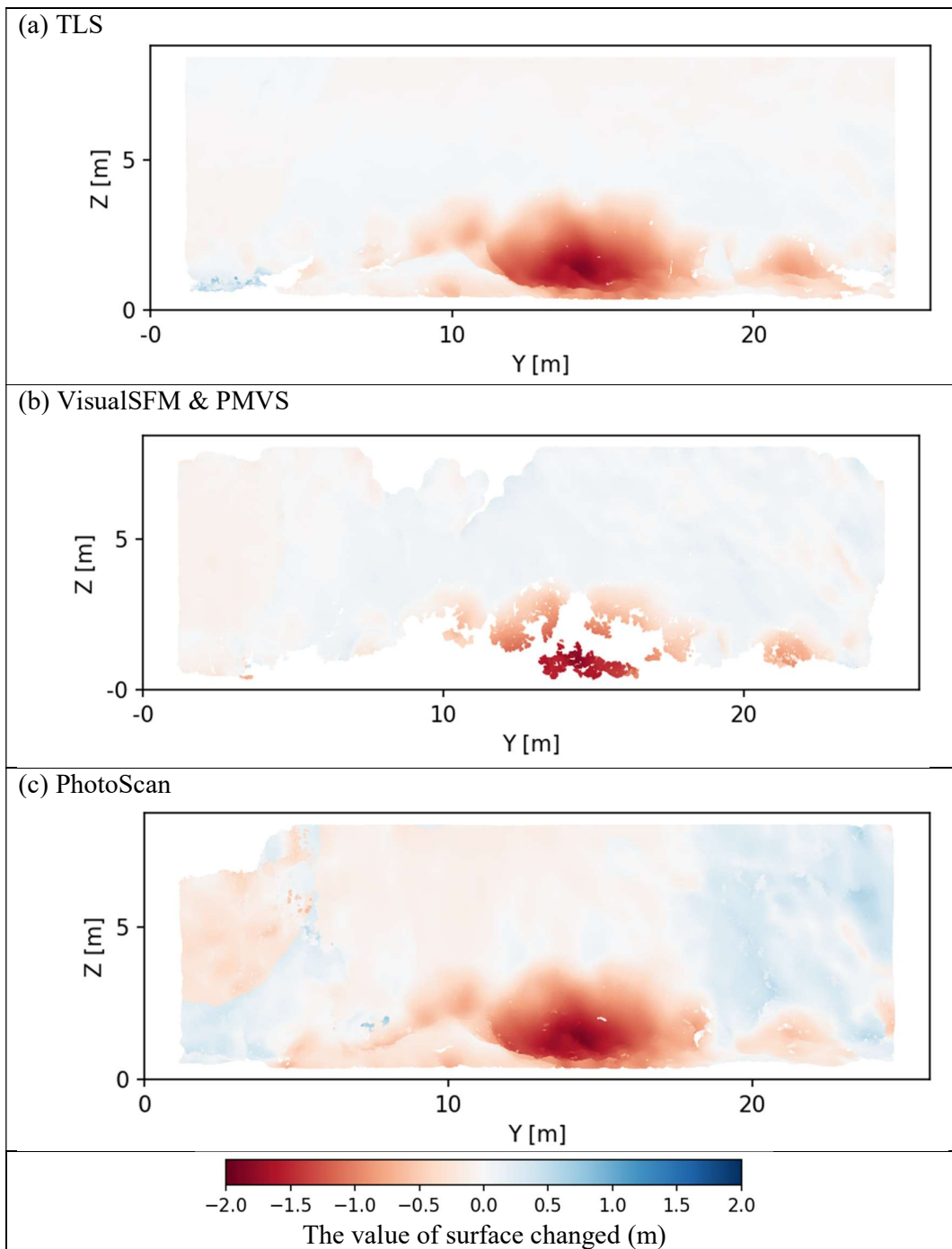


Figure 5-18: Comparison of distance differences between two datasets acquired on 27 November 2016 and 13 April 2017 from (a) the TLS approach, (b) the photogrammetric results using VisualSFM & PMVS and (c) PhotoScan using M3C2.

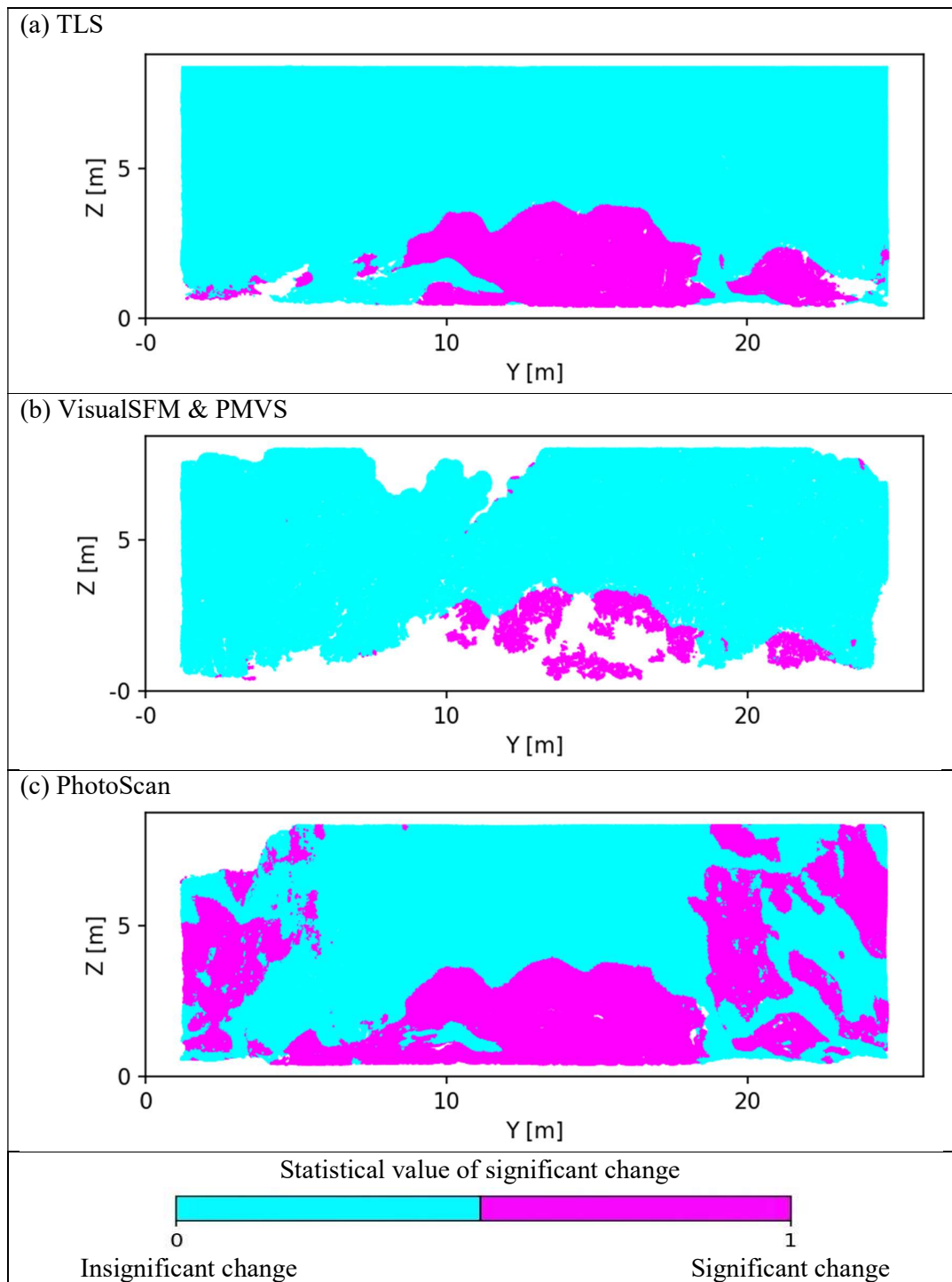
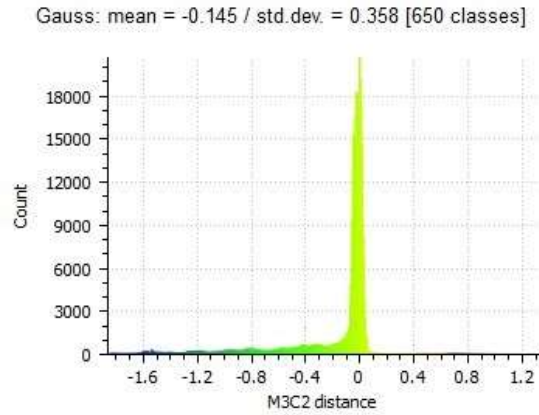
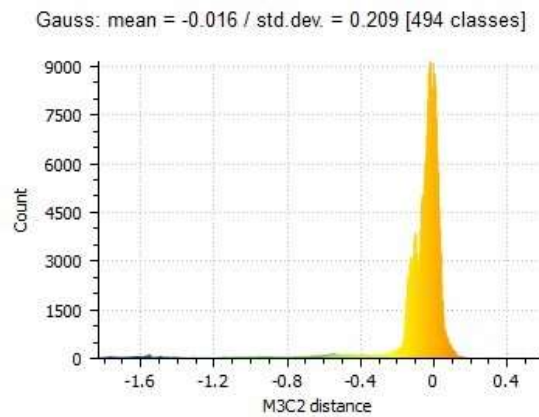


Figure 5-19: The comparison of statistically significant change between two datasets acquired on 27 November 2016 and 13 April 2017 from (a) the TLS approach, (b) the photogrammetric results using VisualSFM & PMVS and (c) PhotoScan using M3C2.

(a) TLS



(b) VisualSFM & PMVS



(c) PhotoScan

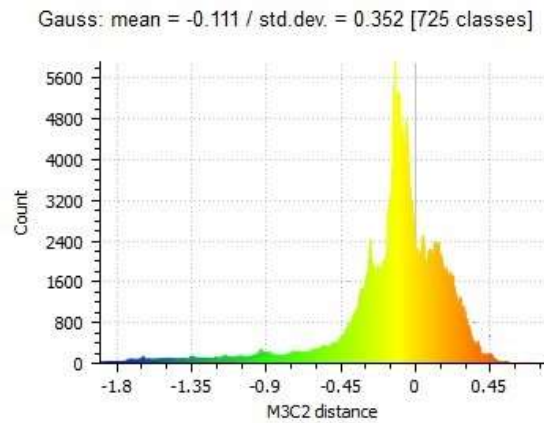


Figure 5-20: Histograms of the distance differences between two point clouds acquired on 27 November 2016 and 13 April 2017 using M3C2 from (a) TLS survey, (b) photogrammetric results using VisualSFM & PMVS and (c) PhotoScan.

Table 5-14: Statistics of the distance differences between two epochs acquired on 27 November 2016 and 13 April 2017 from (a) TLS survey, (b) SfM-photogrammetric approach of VisualSfM & PMVS and (c) PhotoScan using M3C2.

Method/ SfM-approach	Multi-epoch analysis			
	Min (m)	Max (m)	Mean (m)	SD (m)
TLS	-1.862	1.327	-0.145	0.358
VisualSfM & PMVS	-1.830	0.576	-0.016	0.209
PhotoScan	-1.901	0.799	-0.111	0.352

The mean of the differences between two point clouds at different epochs (135 days apart) obtained from all approaches showed negative values (Table 5-14), indicating that the majority of surface changes of the coastal cliff monitoring at Marsden was caused by erosion. This was confirmed by the distribution of elevation differences (in Figure 5-20), which mostly displayed a negative bias of detected changes. The minimum, maximum and standard deviation values of the distance differences were slightly different for the different approaches. Whereas, the maximum value for the distance differences was significantly different because the point density of photogrammetric results from both PhotoScan and VisualSfM & PMVS had an insufficiently dense point cloud and more void areas when compared to the corresponding TLS survey. Nevertheless, the accuracy of photogrammetric results was shown to be sufficient for the initial assessment of change for this type of coastal cliff.

Unfortunately, in this experiment images from a ground-based approach cannot be captured entirely due to the high cliff. The processing therefore mostly focused on the bottom part of the coastal cliff. Consequently, the change assessment was not able to comprehensively determine the volume balance in this experiment.

5.4 Summary

In this chapter, two experiments were performed to inspect the photogrammetric potential of the cloud-based system for initial assessment of two types of landslide hazard. The study sites at a natural earth-flow landslide and a coastal cliff were used to examine the developed approach using different imaging configurations and geo-referencing approaches. The photogrammetric approach achieved moderate accuracy for the initial assessment of landslide monitoring at both sites. The improved photogrammetric processing with the developed functions solved many of the disadvantages associated with the implementation of a low-cost photogrammetric monitoring system (using a smart phone and a free-SfM Software). The test results for on-site investigation proposed a reliable method for geo-referencing without the need for high accuracy GNSS/TLS observation. The photogrammetric approach using the developed system was sufficiently accurate for assessing landslide changes and measuring landslide deformation at the dm-level.

Chapter 6. Discussion of results

6.1 Introduction

A mobile device-based photogrammetric measurement and monitoring system for the initial assessment of landslide hazards has been developed in this research. Close-range photogrammetric approaches using imagery from a modern smartphone were investigated for use in a low-cost, non-contact monitoring approach for on-site landslide investigation. The system was implemented with mobile cloud computing technology to enable the potential for real-time processing. The developed system integrated with additional functions for the improved photogrammetric processing and landslide monitoring analysis was evaluated through a series of experiments to assess its potential. The landslide monitoring system was investigated using data collected from two different real-world sites in the UK. An additional discussion of the experiments and of the limitations of the developed system is presented in this chapter.

6.2 System inspection

Close-range photogrammetric techniques can be practically adopted for the purpose of monitoring landslide hazards, and offer a potentially low-cost approach in terms of implementation and operation for ground-based platforms, as explained in Chapter 2. In particular, for initial assessments in on-site investigations for landslide monitoring, close-range photogrammetry has the capability to be used in surveying to avoid the need for time-consuming data collection. Moreover, the digital camera technology in mobile devices can be widely utilised for image acquisition as part of a photogrammetric monitoring approach. However, due to the limited computational power of mobile devices, it is difficult to manage the intensive data processing required in photogrammetry. Cloud-based processing is used here to overcome the drawbacks of mobile computing. In this research, a photogrammetric measurement and monitoring system based on a mobile platform was developed and implemented using cloud computing technology to deliver a low-cost, near real-time solution for an in-situ landslide monitoring approach, as illustrated in Chapter 3. This section considers advantages and disadvantages of the developed system and provides recommendations for improvements.

The architecture of the developed system is mainly based on client-server communication with a mobile cloud computing service. The system comprises a front-end service on a mobile application controlled by the operator and a back-end service on the cloud-based server employed for photogrammetric measurements and landslide monitoring analysis. In this solution, the crucial concept in system development was based on design simplicity associated with two components involving a controller and processor, as illustrated in Figure 3.25. Furthermore, the system has more flexibility in managing the resources of both the mobile device and cloud server. For example, data processing in the photogrammetric approach can be utilised on a multi-cloud server to optimize the low financial costs of cloud computing, as presented in section 3.5.2.

In terms of the flexibility in the front-end part of the system, although an Android mobile application was developed to be controlled remotely by the user, the operation of the system can be independently employed on multiple platform types, including tablets, laptop computers and PCs, using a standard Web-based browser, as shown in Figure 6.1.

One of the benefits of the use of an independent platform is to reduce the need for the developer to design mobile applications.



Figure 6-1: Front-end service: (a) mobile application; (b) web browser.

The evaluation of the development of a low-cost, real-time photogrammetric landslide monitoring system based on a mobile platform for on-site investigation can be divided into two main aspects, as follows:

6.2.1 Mobile devices (smart phone case)

In this research, the close-range photogrammetric approach has mainly utilised images captured from a modern smart phone camera (i.e. a Nexus 6 mobile phone) for landslide monitoring. Typically, smart phone technology can provide more convenience in image acquisition for on-site investigations. Moreover, images can be uploaded to a cloud-based server for data processing and the results of photogrammetric landslide monitoring displayed in order to facilitate an efficient initial assessment of landslide hazards.

The digital camera technology in mobile devices has become increasingly advanced in recent years, in terms of the high-resolution capabilities of the imaging sensors. On other hand, the quality of images produced is still lower than in images captured from DSLR cameras or consumer-grade digital cameras, as explained in section 3.2.1. Comparison of photogrammetric results obtained from a DSLR camera and a smart phone camera, as shown in the experiment of section 4.2, revealed that the photogrammetric accuracy of a DSLR camera was better than that of the smart phone camera. In the same situation (e.g. using the SfM photogrammetric software), a DSLR camera of Nikon D300 can provide more accurate photogrammetric results (between 0.0 ± 2.5 and -0.2 ± 3.1 cm) than that of an iPhone 4 smart phone camera (between 0.8 ± 5.7 and 1.5 ± 3.2 cm). It is likely that the quality of both cameras was not significantly different for the initial assessment of landslide monitoring.

For highly precise photogrammetry using both UAV and ground-based platforms, DSLR and consumer-grade cameras are intensively used for image acquisition for monitoring purposes in geoscience applications (James and Robson, 2012; Micheletti *et al.*, 2015a). However, images from DSLR or consumer-grade cameras can be used in the developed system in assessing landslide deformations. The system can support the uploading of images not only from the camera in a mobile device, but also images from multiple other cameras, thus increasing the opportunities for image acquisition from enhanced sensors.

For instance, modern DSLR and off-the-shelf digital cameras have built-in wireless connectivity, such as Wi-Fi or Bluetooth, that can be used for direct connection to a smart phone for image transfer. In the case of on-site investigations using a DSLR or consumer-grade camera, Figure 6-2 illustrates image acquisition through a mobile application for uploading to the landslide monitoring system.

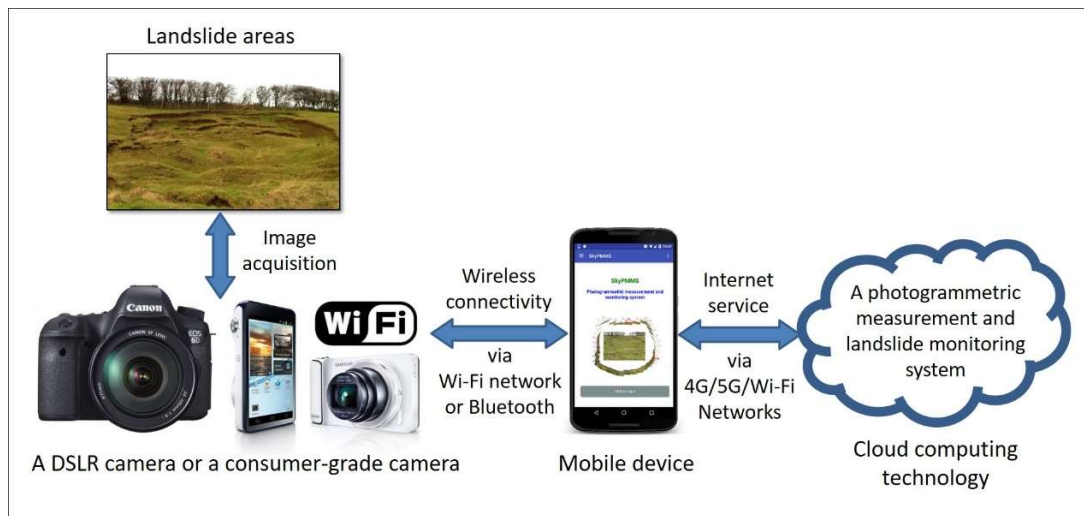


Figure 6-2: The implementation of a DSLR or consumer-grade camera for image acquisition applied in the developed system.

6.2.2 The cloud-based server

For development of the back-end service of the system, all processing of photogrammetric measurement and landslide monitoring was implemented on cloud computing technology. The cloud-based server was used for the SfM-based photogrammetric processing of the image data from the smart phone and the assessment of landslide deformations from photogrammetric results at different times. Although the cloud computing technology is based on virtual machine (VM), the cloud-based server can operate the same as a hardware platform. Furthermore, the advantages of a cloud-based server include the low financial investment in the system development for the end user and the flexibility in management and monitoring of the system. For instance, technical skills in the maintenance of the server are not required in developing the system.

Currently, commercial SfM software such as Pix4D can be used on a desktop computer or with cloud computing technology for the SfM-photogrammetric services allowing 3D reconstruction from images. Unfortunately, a free Internet-based SfM system, such as Microsoft Photosynth or Autodesk 123D catch, is no longer available. Those SfM services offer full photogrammetric processing workflows, but some advanced functions lack details and are treated as a black box for processing. Moreover, the requirement of additional functions in terms of post-processing is necessary to achieve the appropriate

photogrammetric results for landslide monitoring purposes. Therefore, it is difficult for an Internet-based SfM service that had been implemented with low-cost landslide monitoring to be used in the photogrammetric processing.

The proposed system has various strengths for initial assessments in in-situ landslide monitoring. It can offer visualisation of a three-dimensional scene of the photogrammetric results in near real-time after data processing. Consequently, the results can be instantly verified by the operator using 3D visualisation of a point cloud on a mobile device (such as a tablet), before assessing landslide deformations, as shown in Figure 3-29. Moreover, the system can back-up the image data, along with the photogrammetric results, as well as the results of the analysis of landslide monitoring using cloud storage technology with Amazon S3 to avoid data loss, and support subsequent multi-temporal comparisons.

However, there are still some weaknesses of the developed system where improvements are needed. Firstly, the design of the system does not support multi-tasking, and the system can be operated only by a single user at one time. To support simultaneous use of the system by multiple users, a queuing management system would be required to facilitate access. Secondly, the security of the developed system for landslide monitoring was considered to be outside the scope of this study, but should be considered in any future development. Finally, feedback concerning system usability from geotechnical or geological engineers would be useful to evaluate practical applicability to the user community and steer further improvements in the system.

6.3 Performance assessment

The performance of the cloud-based system was assessed for its ability to deliver real-time photogrammetric measurement and monitoring for use in on-site investigations assessing landslide hazards using mobile device technology. Evaluation of advanced functions for improved photogrammetric processing and the effectiveness for landslide monitoring is highlighted in this section.

The proposed system requires an Internet service with high bandwidth connectivity in order to provide necessary connection speed for image data transfer from a smart phone to a cloud server for photogrammetric processing. As is often the main problem with

mobile cloud computing technology, successful upload of images from a smart phone is subject to variation given the inefficient performance of Internet services via current mobile networks. Service coverage is often a serious issue for the countryside or rural areas, as discussed in section 4.3. In the near future, mobile network operators are expected to deliver advances in both coverage and performance of mobile data technology. In summary, the cloud-based system requires Internet services via a modern 4G/5G network to operate effectively.

The state-of-the-art mobile device-based SfM photogrammetry avoid only the cloud-based processing. In order to facilitate a real-time response capability, various processes in the SfM-based photogrammetric workflow can be performed on the mobile device, such as feature detection or image matching. As shown in Figure 6-3, photogrammetric processing can be carried out using the resources of both mobile devices and cloud computing in order to help reduce the demands for bandwidth connectivity (Nocerino *et al.*, 2017). Moreover, an innovative approach to real-time 3D surface reconstruction on mobile devices has been developed using a new pipeline for image processing on GPU/CPU integrated with an inertial measurement unit (IMU) in order to eliminate the cloud-based processing (Ondrůška *et al.*, 2015).

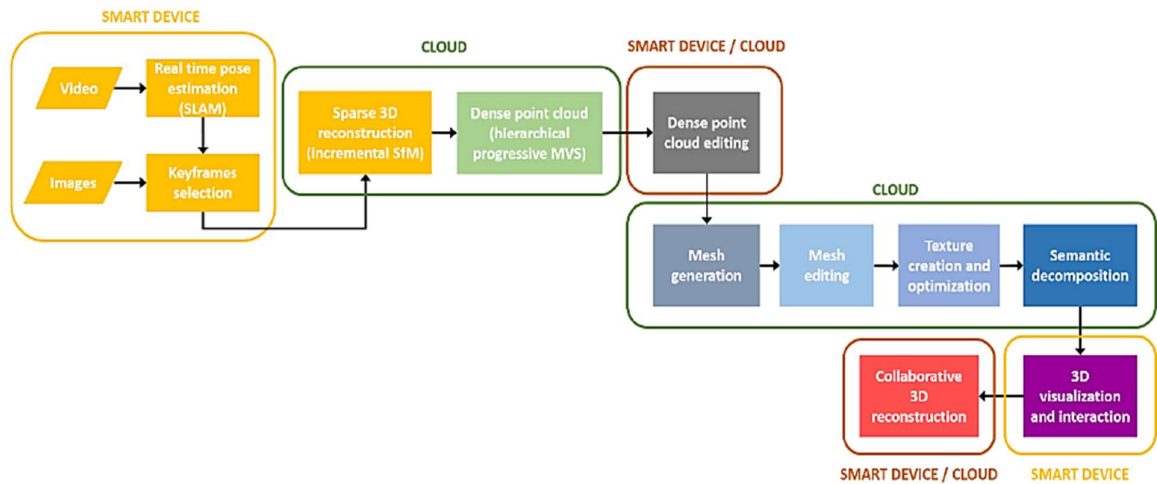


Figure 6-3: Workflow of data processing for SfM-photogrammetry based on mobile devices and cloud computing (Nocerino *et al.*, 2017).

These approaches can address the issue of the bandwidth demand for Internet connectivity between a smart phone and a cloud server. Nevertheless, an in-situ landslide monitoring approach based on the SfM technique is still more appropriate for cloud-based processing. That is because such approaches cannot deal with the photogrammetric processing with the requirement of large numbers of high resolution images to maintain the accuracy and resolution of results in real time.

In this study, for example, the process of dense image matching from large numbers of images employed in generating the point cloud might be time-consuming. To deliver photogrammetric results with the appropriate quality for in-situ landslide monitoring, the relationship between the number of images and image size has been investigated to optimise data processing in real-time. Consequently, an optimal imaging network would deliver an appropriate image size and a suitable number of camera stations prior to uploading data to the cloud, as explained in section 4.4. The recommendation for photogrammetric configuration using a B/D ratio of 0.1-0.2 determines the number of camera stations or images for a close-range photogrammetric approach. Furthermore, improved image data (i.e. 20%-30% of image size reduction) before transfer may help in reducing both the uploading and processing time in order to achieve a near real-time response for landslide monitoring.

In terms of the functions developed to improve photogrammetric processing in the system, a pre-image matching stage is used to reduce the image matching time using image sequences. In the experiment concerning pre-image matching, the time required for image matching can be decreased by approximately 80%, compared to using full matching, and this can help reduce the overall photogrammetric processing time by approximately 30%. In addition, the pre- and post-processing procedures, such as lens distortion correction, automatic de-noising and vegetation filtering, can help to improve the quality of photogrammetric results before assessment of landslide behaviour. Geo-referencing is another important stage of post-processing for photogrammetric results, generally used to provide a real-world coordinate system for comparison and analysis of landslide monitoring. For this study, additional functions developed for geo-referencing can be directly employed on mobile devices in order to provide a highly precise geo-referencing for photogrammetry. The development of additional functions can achieve the basic requirements for on-site investigations, as proposed in section 3.3.3. However,

although the advanced functions of the system can enhance the potential for photogrammetric measurement and automated landslide analysis, human interaction may be required in post-processing, such as for geo-referencing and de-noising.

Although development of additional functions in the system can facilitate the automated and straightforward workflows of photogrammetric processing and landslide monitoring analysis for non-expert users, basic knowledge of the use and understanding of each function is necessary to utilise the system appropriately for fieldwork. In particular, the settings of appropriate parameters for some functions is one of the greatest challenges faced by non-expert users. For example, the additional functions of automatic de-noising, vegetation filtering and assessing landslide deformations using M3C2 needs experimental study before fieldwork for specification of appropriate parameters. Moreover, the selection of suitable parameters depends on the different types of landslide hazard for monitoring. Therefore, the parameters for each function should be carefully chosen to achieve sensible results in photogrammetric landslide monitoring.

6.4 Assessment of photogrammetric accuracy

In considering photogrammetric approaches for monitoring purposes, accuracy is the first concern. In particular, sources of reconstruction errors, which have a strong influence on photogrammetric precision, should be identified and tackled to optimise measurement quality, as highlighted in section 3.2. The accuracy of photogrammetric measurement in this research was investigated using two experimental studies in different landslide areas. The accuracy of the photogrammetry used in in-situ landslide monitoring is discussed in this section.

The design of the photogrammetric network configuration for landslide monitoring should be determined by the characteristics of the area monitored. Firstly, the accessibility and steepness of landslide area should be considered. Convergent imaging networks and image acquisition with a full 360° coverage of the monitoring area are usually employed to deliver effectively a 3D reconstruction (Gómez-Gutiérrez *et al.*, 2014), as shown in Figure 5-4. However, if the monitoring area is inaccessible or too steep, such as a coastal cliff, a block configuration is more suitable for the photogrammetric imaging network, and images should be taken from the front of the monitoring area in a linear sequence.

Therefore, the optimal quality of photogrammetric measurement can be achieved by choosing the most appropriate configuration for landslide monitoring in a specific site.

In terms of photogrammetric processing software, point clouds obtained from free SfM software such as VisualSfM and PMVS produce relatively low-quality results in terms of both point density and accuracy when compared to results from commercial SfM software such as PhotoScan, as shown in section 4.2 and 4.3. Moreover, the different algorithms used in each type of SfM software (for example when conducting feature detection using SIFT or SURF) have an influence on the precision of image measurement and thus on photogrammetric accuracy (James and Robson, 2012). The RMSE of measurement using SIFT is assumed to be approximately one half of a pixel (Barazzetti *et al.*, 2010), but it is likely that SfM photogrammetry involves lower precision of image mensuration compared to traditional digital photogrammetry. Consequently, photogrammetric precision in 3D reconstruction from the imagery is further degraded due to these factors. Thus, the choice of photogrammetric processing software implemented in the developed system has an influence on accuracy in assessing landslide deformations.

In geo-referencing, the use of photo control targets is essential for highly precise photogrammetric measurement. In general, control points should be distributed to cover the whole area to be monitored. If the distribution of targets is not good enough as described in the experiment of section 4.5.3, this will result in a low quality of geo-referencing. For geo-referencing with GNSS/TLS-based target observations, the photogrammetric results for each epoch were determined so as to enable a straightforward comparison in a common coordinate system. In contrast, to avoid measurement using GNSS/TLS observations, an innovative solution with a newly-developed function was utilised for highly precise scaling of photogrammetric results. This application of scaling was performed using distances of known objects, such as with a scale bar (Kaiser *et al.*, 2014). However, after scaling, manual alignment of photogrammetric results at different epochs was required. This solution can also offer low-cost observations to support the on-site investigation of landslide monitoring. As shown in the experiment described in section 5.3.4, the test results confirmed that this is a reliable method for geo-referencing without the need for highly accurate GNSS/TLS observation data. Thus, the development of automated alignment should be proposed for an additional study in the future. This automated alignment of results from different epochs would be definitely better than the

manual approach, especially for practical application by engineers. For example, the study on markerless point cloud registration (Theiler *et al.*, 2013) and point cloud coarse registration (Bueno *et al.*, 2016) may be utilised with an automated alignment.

Compared with the accuracy of results for close-range photogrammetry in the experimental studies described in chapter 5, the photogrammetric measurement system based on a mobile-platform can yield a sub-dm accuracy level, especially over surfaces without vegetation. In the case of natural earth-flow landslide monitoring, photogrammetric precision was noticeably degraded due to the effect of vegetation. In the case of monitoring of coastal cliff erosion, the photogrammetric accuracy was at the level of centimetres (from 2.7 to 3.0 cm) due to the monitoring area consisting of a bare-earth surface.

However, due to the different types of landslide hazard being monitored, the conditions adopted in the photogrammetric approach have a direct impact on the quality of final results, i.e. the quality of camera for image acquisition, photogrammetric network configuration, the number and distribution of ground control points, etc. As shown in the experiment described in section 5.3.5, the problem of the doming effect can cause systematic errors in the results due to SfM-photogrammetric processing under adverse conditions. Firstly, the use of raw (un-calibrated) images with weak photogrammetric network geometry (the linear sequences of images) for processing could result in distorted reconstruction (James and Robson, 2012). Secondly, the number of ground control points were insufficient and they were poorly distributed. Consequently, a bundle adjustment has been insufficiently strong (Eltner and Schneider, 2015). Therefore, photogrammetric processing should be carefully performed to reduce these systematic errors and minimise any doming effect.

6.5 Assessment of landslide monitoring analysis

After improving and evaluating photogrammetric accuracy, the enhanced results at different epochs can be utilised for assessment of landslide deformation. The proposed analysis of landslide monitoring is performed using a point-based approach with the comparison of 3D models from two point clouds. As shown in the experiment results presented in section 4.5.6, the M3C2 method reveals fine-scale changes occurring due to landslide activity. Furthermore, the levels of uncertainty in point clouds have been taken into consideration in this comparison method in order to provide an efficient analysis for landslide monitoring. In particular, for the initial assessment in an on-site investigation, the function developed for landslide monitoring analysis is based on the M3C2 technique comparing point clouds. The results of this function can be displayed directly on a smart phone through visualisation or statistical quantification by the developed system for the analysis of landslide monitoring, as shown in Figure 3-29.

Before assessing landslide deformations, the photogrammetric results at different epochs should be aligned to a common reference system. In the case of geo-referencing without a highly precise GNSS survey for the observation of control point locations, improved referencing is essential to ensure that the results are well-aligned. In general, all epochs should be georeferenced to the first epoch. The primary method of improved referencing consists of an alignment of point clouds with each other using at least four key features in the monitored area, with application of the ICP algorithm.

Comparing results of the landslide monitoring analysis in the two experimental studies described in chapter 5, the sources of uncertainty which might have an influence on the assessment of landslide changes should be taken into consideration when delivering the results. In the case of natural earth-flow landslide monitoring, the surfaces covered in vegetation can affect the accuracy of landslide measurements because the heights of vegetation surfaces change seasonally. Vegetation filtering is used over vegetated surfaces to deliver bare-earth point clouds so as to detect landslide movement over time. Typically, vegetation filtering is carried out using the green vegetation index to eliminate point clouds assumed over the vegetated surfaces. However, vegetated surfaces that are not coloured green, such as in the presence of brown grass, often appears in summer. Consequently, the point cloud over these vegetated surfaces remains and is used for

assessing landslide change. Furthermore, point clouds obtained from photogrammetric processing using VisualSFM and PMVS showed sparse points and large void areas. As a result, insufficient detail at each epoch might be more prone to fail in the recognition of the landslide deformation, as shown in Figure 5-10 and 5-18(b).

Considering the sparse point clouds and large void areas, completeness of coverage of the results can be slightly improved by increasing the number of images (or camera stations) in photogrammetric processing. However, the results still contain void data because of the insufficient potential of free SfM software for generating the point cloud, as shown in Figure 4-10. Consequently, the use of dense image matching for a large number of images to increase the number of points might be too time-consuming, and thus would be inappropriate for initial assessments in on-site investigations. However, although a low-quality point cloud (such as one with sparse points and void areas) might be inappropriate in the analysis of landslide monitoring, the extraction of bare-earth point clouds after vegetation filtering can allow the key information in landslide areas, such as cracks or fissures, to be presented. Therefore, landslide monitoring using a point-based approach (i.e. point cloud comparison method) might not be suitable in the case of landslide areas covered by vegetation.

For 3D point-based analysis, bare-earth point clouds might have the potential to allow feature extraction, such as of cracks or fissures, in the scarp of landslides. The extraction of features is performed using the analysis of geomorphological factors, such as the surface roughness index, as shown in Figure 6-4. However, although this approach can be automatically performed, the tracking of features might be complicated and time-consuming in evaluating landslide movements over time. Therefore, the 3D features have to be degraded into 2D information from the imagery in order to analyse landslide monitoring using an image correlation method.

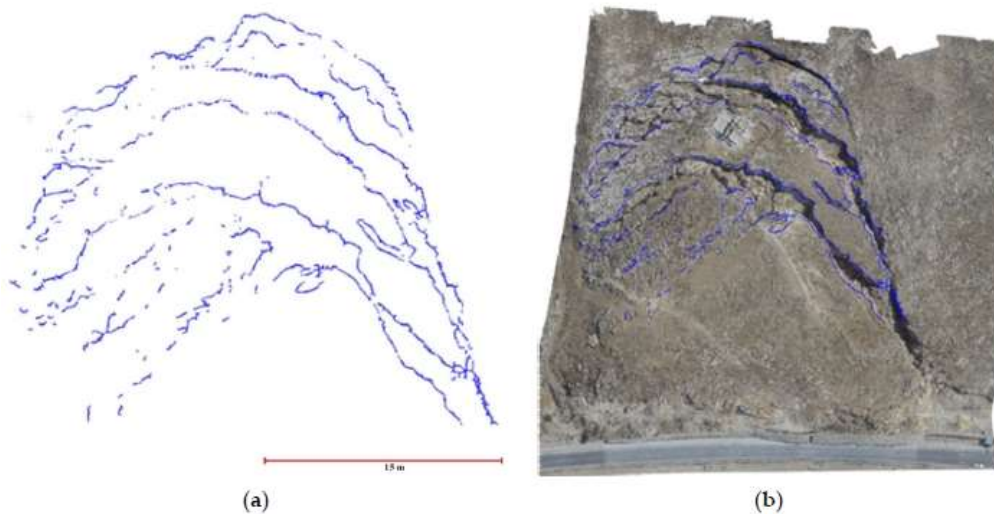


Figure 6-4: Extraction of (a) landslide scarp using analysis of the surface roughness index, and (b) orthophoto derived from UAV approach (Al-Rawabdeh *et al.*, 2016).

Although the developed system was not implemented in the actual area, conditions in the simulation was equally assigned. The image data was collected from the study area. The experiments were carried out under laboratory simulation because of the inefficient performance of Internet service via current mobile networks, which was unsuitable for data transfer from mobile device to the cloud. Consequently, the photogrammetric approach using the developed system was sufficiently accurate to assess landslide movements and measuring landslide deformations at the dm-level.

6.6 Potential challenges of operation

As mentioned above, the main drawback of mobile devices is usually their low computing power when compared to PCs or laptop computers. The use of cloud-based processing is essential to overcome the problems of insufficient resources on mobile devices in order to manage data-intensive processing. In the development of a photogrammetric measurement and landslide monitoring system, the architecture is based on client-server communication using Internet services. Thus, the appropriate Internet connectivity between a smart phone and the cloud server is essential for the system to operate continuously.

Deficiencies in Internet connections are one of the main limitations of the proposed system. If a landslide occurs in the countryside, connection to the Internet might not be possible due to poor coverage of mobile networks, as found in the two experimental studies described in chapter 5. Furthermore, the Internet services may not perform well. If Internet connectivity is temporarily unavailable for data processing, the system cannot operate. When Internet connectivity is not available, it is essential to develop additional functions on the system to provide the synchronisation of both data and state for data processing (i.e. specifying status for the steps of data processing before Internet disconnection). In addition, the system could be improved to support offline data processing whereas it may become possible for the development of smart phone technology to undertake all processing.

There are other factors affecting the photogrammetric measurement: 1) insufficient image matching and 2) presence of vegetation over the monitoring areas. Image matching, when overlaps were less than three images, may lead to failure in 3D model reconstruction from images. In this case, the recommendation for photogrammetric configuration should be a B/D ratio of 0.1-0.2 to provide a suitable number of camera stations or images for a close-range photogrammetric approach. As for the presence of vegetation, this can have a direct impact on the accuracy of photogrammetric results due to the unreliability of photogrammetric measurement over these surfaces, which is discussed in the next chapter.

6.7 Summary

Following the evaluation of the developed system in chapter 4 and the results of the experiments described in chapter 5, an additional discussion has been presented in this chapter to assess the performance of the system. The proposed mobile platform-based system was investigated using the photogrammetric solution for landslide monitoring purposes that was explained in chapters 2 and 3. The experimental results have revealed the potential of mobile cloud-based processing, and the levels of photogrammetric accuracy and the quality of landslide monitoring analysis for on-site investigation. The experiments have confirmed that the developed low-cost, real-time system can be utilised for initial assessments of on-site investigation in landslide monitoring.

Chapter 7. Conclusions and future work

7.1 Introduction

This research has presented the development of a cost-effective photogrammetric monitoring system based on a mobile platform for real-time on-site investigation in order to aid initial geotechnical interpretation and assessment of landslide hazards. The potential of the developed system for monitoring landslides has been confirmed through exploitation at recognised real-world test sites, comprising a natural earth-flow landslide and an area of coastal cliff erosion. To conclude the findings and discussions of the implementation and the experimental studies in this research, the overall study, research contributions, and recommendations for future work are summarised in this chapter.

7.2 Summary of work

The research aimed to exploit mobile devices and modern ICT in order to develop a photogrammetric measurement and monitoring system for real-time on-site investigation of landslide hazards. The development and implementation of a system was accomplished in order to achieve the goal for this research that was divided into four stages. Thus, the review of the overall studies are summarized in this section following the research objectives, as originally presented in Chapter 1.

Objective 1: To investigate the potential of commonly used approaches and technologies in landslide monitoring and to propose the basic requirements of a low-cost photogrammetric solution for initial landslide assessment during on-site investigations by non-photogrammetrists;

Regarding the first stage of this research, as presented in chapter 2, landslide hazards have been reviewed. This includes the occurrence, types, causes, factors and behaviour of landslides in order to understand key parameters required for landslide assessment and monitoring. Many of the more common geomatics, geotechnical and geophysical engineering approaches for landslide monitoring were inspected and the advantages and disadvantages relating to their adoption for on-site investigation purposes assessed. According to the assessment, many geomatics, geotechnical and geophysical approaches present restrictions in usability for landslide monitoring due to the often labour-intensive and costly methods used. For initial assessment, the technique of modern close-range photogrammetry was deemed to offer a flexible, cost-effective approach to landslide monitoring. Taking this assessment into consideration, a photogrammetric measurement and monitoring solution that employed a mobile device and cloud computing technology was pursued, which thereby achieved Objective 1.

Objective 2: To develop the mobile platform-based photogrammetric services associated with cloud-based computing technology for the provision of real-time slope monitoring information;

Following the findings of Objective 1, the proposed photogrammetric landslide monitoring system was developed based on a mobile platform implemented with cloud computing technology to enable the potential for real-time processing, as proposed in Chapter 3. The components of the system comprised a front-end service of a mobile application controlled by the operator and a back-end service employed for cloud-based processing. In the case of smart phone technology, such a device can provide more convenience in image acquisition for on-site investigations, and can upload imagery for processing, as well as display the results. In developing a back-end service for the system, cloud-based processing using free SfM software has provided near-real-time, fully-automated processing within a user-friendly, cost-effective photogrammetric framework for non-expert use. This was augmented with additional functions for pre- and post-

processing of SfM photogrammetry, such as lens distortion correction, pre-image matching, geo-referencing, automatic de-noising and vegetation filtering, that were used to enhance the processing performance and deliver appropriate photogrammetric results prior to the assessment of landslide deformations.

Objective 3: To exploit the photogrammetric results by developing appropriate functionality to assess landslide temporal change directly using a mobile device;

This stage focused on the development of landslide monitoring analysis that utilised the enhanced photogrammetric results from different epochs. The proposed landslide analysis was performed using a point-based approach using the M3C2 technique for efficient 3D point cloud comparison. This additional system functionality was developed and carried out using cloud-based processing, as presented in Chapter 3. The results of landslide analysis were retrieved and displayed directly on a smart phone through the mobile application developed for visualisation and the statistical quantification of landslide deformations.

Objective 4: To ensure the accuracy and reliability of the results and the capabilities of the low cost sensors found on common mobile devices for landslide monitoring applications by validating the developed system at real-world test sites;

Prior to the experimental study at an existing landslide test site, the capabilities of functions developed for improved photogrammetric processing and landslide monitoring on the cloud were evaluated and inspected to ensure the accuracy and reliability of the results, as presented in Chapter 4. The potential of the developed system for monitoring landslides was investigated at two different real-world UK sites, comprising a natural earth-flow landslide and an area of coastal cliff erosion. These experiments and evaluations confirmed the performance of the developed low-cost, real-time approach for landslide hazard analysis, as presented in Chapter 5. These investigations demonstrated that the cloud-based photogrammetric measurement system was capable of providing three-dimensional results with sub-decimeter level accuracy. However, for coastal cliff erosion monitoring, it is necessary to consider the possibility of systematic errors from the doming effect due to weak geometry in the network configuration or inappropriate photogrammetric processing based on the raw imagery. As a solution to this problem, a convergent imaging network and multi-scale imaging could have been adopted, as well

as better distributed control points. The results of the initial assessments for on-site investigation could therefore effectively detect landslide deformations at a local-scale.

7.3 Research contributions

The initial assessment for on-site investigations of landslide hazards is important in geophysical and geotechnical engineering to reduce the risk of landslides. Improvements to existing geomatics approaches based on ground platforms are essential to reduce the financial costs of both instrumentation and labour, as well as saving time for conventional landslide monitoring. In this research, the development of an appropriate monitoring system for use in real-time on-site investigation aids initial geotechnical interpretation and assessment of landslides. In comparison with conventional geomatics approaches, affordable mobile devices (such as smart phones and tablets) have been used to offer the potential for cost-effective, close-range photogrammetry. The immediate noticeable benefit of a smart phone is convenience in image acquisition. Another advantage is that a smart phone can upload the image data for data processing and it can display the results of photogrammetric landslide monitoring in order to facilitate an efficient initial assessment of landslide hazards.

In terms of the proposed system to achieve a low-cost solution, the development of a system in this research was based solely on open-source or free software. Moreover, cost-effective cloud computing services were implemented for data storage, processing and analysis in the system. The development of a cloud-based system was particularly utilised for SfM-based photogrammetric processing of the image data from the smart phone and the assessment of landslide deformations from photogrammetric results at different epochs. The implemented SfM workflow involved a high degree of automated processing. Furthermore, the development of additional functions for the SfM-photogrammetric approach was utilised to enhance the processing performance and improve the quality of results. According to the workflow for photogrammetry-based landslide monitoring, as shown in Figure 3-13, the system utilises automated workflows to offer user-friendliness for non-experts.

To provide a photogrammetric solution suitable for non-expert users and to achieve the necessary quality of photogrammetric results for landslide monitoring, photogrammetric

network design is an essential consideration for close-range photogrammetry (Luhmann et al., 2006). The imaging plan was calculated using four main factors, as follows: (1) base to depth (B/D) ratio of imaging geometry in the range of 0.1-0.3 to provide accurate ray intersection for 3D reconstruction (Hullo et al., 2009; Waldhäusl and Ogleby, 1994); (2) the maximum distance between the camera and the object (in this research it was kept at less than 30 m), because image scale, a function of the focal length of the camera lens, has a direct impact on the measurement precision; (3) a camera field of view (FOV) of $\sim 40^\circ$ to 80° is generally required in deformation monitoring for engineering applications (Fryer et al., 2007), which is applicable here, given the requirement to capture detailed surface information; (4) images should fully cover the study area (360° coverage), with necessary overlaps, to enable effective 3D reconstruction. Therefore, it is crucial that the guideline for image capture should be determined following these basic requirements and should be considered prior to data collection.

In terms of the implemented system's capability to deliver a near real-time response, image upload and processing time are crucial factors to be considered. The GPU cloud server was required for dealing with the computationally-intensive modules of the SfM workflow. Moreover, the management of the image data upload from a smart phone to a cloud server is critical for achieving on-site investigation. The cloud-based system required data transfer using Internet services such as modern 4G/5G (future) networks in order to provide satisfactory connection speeds due to the need for high bandwidth connectivity. Reducing the workload for image data upload can help decrease the demand for high Internet connection speeds. The relationship between the number of images or camera stations and image size was investigated to optimize data processing, as presented in Chapter 4. The recommendation for the photogrammetric configuration (i.e. using a B/D ratio of 0.1-0.2) can offer a suitable number of camera stations or images for a close-range photogrammetric approach. Moreover, reducing image resolution (i.e. 20%-30% of image size reduction) before data transfer may help reduce both the uploading and processing time in order to achieve a response closer to real-time.

Focusing on the accuracy assessment of results obtained from the mobile platform-based photogrammetric measurement system, this approach can yield a sub-dm accuracy level, especially over surfaces without vegetation. In the case of natural earth-flow landslide monitoring, photogrammetric precision was noticeably degraded due to the effect of

vegetation. Meanwhile, in the case of monitoring coastal cliff erosion, photogrammetric accuracy was at the cm-level due to the monitoring area consisting of a bare-earth surface. Regarding the application of landslide monitoring, the photogrammetric results provided sufficient accuracy for initial assessment with measurements at the dm-level.

7.4 Suggestions for future work

The system developed as part of this research can provide a solution for low-cost, near real-time photogrammetric measurement and automated landslide analysis by non-experts. However, human interaction is required at some stages of processing. Moreover, higher-performance in processing and highly precise photogrammetric measurements are required to increase user satisfaction. Taking into account some existing drawbacks of the developed system, potential improvements of the system are recommended in this section.

7.4.1 Precision improvement of SfM-photogrammetric processing

In the case of natural earth-flow landslide monitoring, the surfaces covered in vegetation can significantly degrade the quality of photogrammetry because of variation in the heights of vegetation. This can have a direct impact on the accuracy of photogrammetric results due to the unreliability of photogrammetric measurement over these surfaces. The masking of the vegetated surfaces in the imagery is proposed to improve the quality of photogrammetric measurement. The algorithm for this additional functionality might employ the green vegetation index, as calculated in equation (3-7), to remove pixels assumed as vegetated surfaces from the original imagery. As a result, images without vegetated surfaces are uniquely used for SfM photogrammetric processing, as shown in Figure 7-1(b).



(a)

(b)

Figure 7-1: Example of imagery used for photogrammetric landslide monitoring between (a) before and, (b) after masking of vegetation (Zhan and Lai, 2015).

7.4.2 Automated target detection for geo-referencing

The development of SfM techniques has improved the accessibility of photogrammetric processes for use by non-experts, and it can increase automation (Westoby *et al.*, 2012; Javernick *et al.*, 2014). In particular, a target-less approach based on SfM photogrammetry can offer fully-automated processing in the image matching stage. Consequently, the benefit from this approach is that there is no requirement for any markers or targets when compared to conventional digital photogrammetry. However, in this research, the use of photo control targets is still necessary to achieve high quality geo-referencing of photogrammetric results, as proposed in Section 3.4.3. The additional function of target detection could be developed to enable fully-automated geo-referencing as part of the system. Coded target detection would then be automatically carried out using the template matching method, for example by the Python script within OpenCV library, as shown in Figure 7-2.

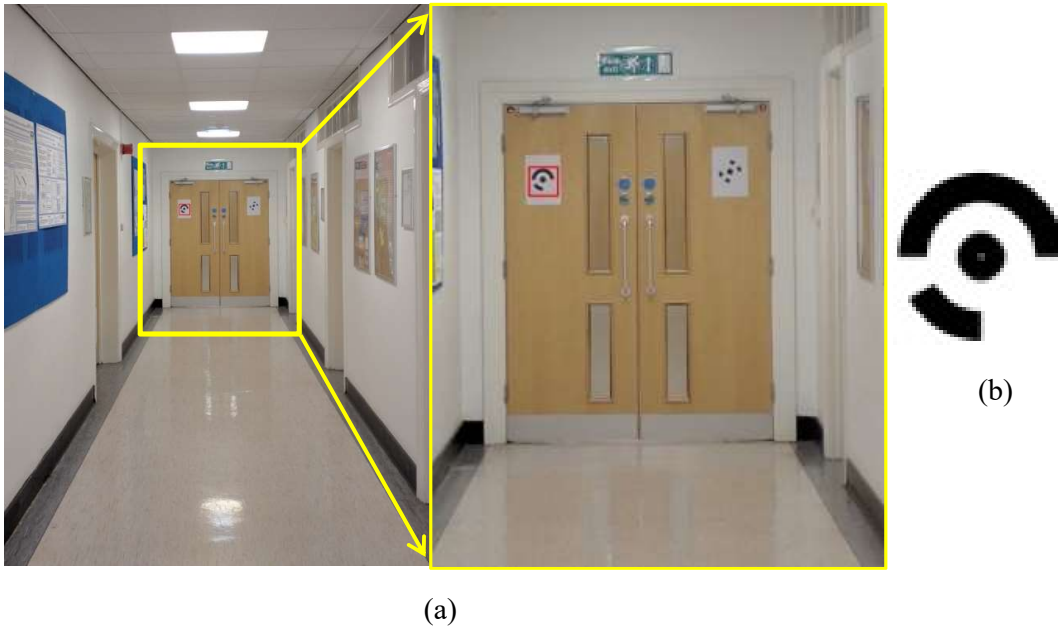


Figure 7-2: Example of (a) automatic detection of (b) coded target used for geo-referencing: the coded target is automatically found in the red boxed area.

However, when using coded targets for geo-referencing of photogrammetric results at different epochs, the size of the coded target should be considered. Due to image scale, the distance between the camera and the target has a direct impact on the size of target in the resultant imagery. If a coded target is not large enough, it might be difficult to automatically detect and identify its location, in particular for landslide monitoring over large areas. Achieving the optimal size of coded target is still challenging for practical applications and the potential use of coded targets might therefore be impracticable for fieldwork.

7.5 Concluding remarks

This research has demonstrated the potential of mobile and cloud computing in order to provide a cost-effective photogrammetric measurement solution on a mobile device for the purposes of small-area landslide monitoring. In particular, this approach supports off-the-shelf hardware (including affordable smartphone cameras) and open source software in order to deliver a low-cost monitoring system. Alternatively, SfM-commercial software (e.g. PhotoScan) can effectively provide sufficient quality of photogrammetric results for assessing landslide deformations. In future work, the mobile application should therefore be improved and developed to support the additional photogrammetric results obtained from other SfM software packages. However, Internet services in the monitored areas of landslides is a critical problem that hinders the full implementation of such a system. Furthermore, manual intervention is inevitably required for preparing photogrammetric results in point cloud processing before landslide monitoring analysis. Based on the assessment of this system, the presented experiments utilising cloud-implemented SfM photogrammetry show substantial potential in terms of landslide monitoring over limited spatial extents.

In the case of the implementation for on-site landslide investigation, the developed system has taken into account a solution for near real-time processing. Two crucial factors are required to enable a near real-time response, including the use of a modern 4G/5G mobile network for data transfer and the GPU-based cloud server for SfM photogrammetric processing. Moreover, multi-epoch analysis needs to be considered in order to assess the photogrammetric results over time, thereby yielding information on landslides and hazard assessment. The additional functions of landslide monitoring analysis can automatically detect the landslide deformation at dm-level.

Appendix A

Camera calibration results (Section 3.2.2)

Table A-1: Camera calibration results for the Nikon D300 DSLR camera using three different calibration routines.

Parameter	Nikon D300					
	PhotoModeler		MATLAB		OpenCV	
	Mean	σ	Mean	σ	Mean	σ
Focal Length (mm)	30.300	0.009	30.165	0.038	30.183	N/A
Xp - principal point x (mm)	12.120	0.007	12.125	0.023	12.168	N/A
Yp - principal point y (mm)	8.130	0.005	8.132	0.020	8.157	N/A
Fw - format width (mm)	24.002	0.001	Not calculated			
Fh - format height (mm)	15.940	N/A				
K1 - radial distortion 1	-1.35×10^{-04}	1.52×10^{-06}	-1.34×10^{-04}	4.57×10^{-05}	-1.22×10^{-04}	N/A
K2 - radial distortion 2	1.04×10^{-07}	1.48×10^{-08}	1.24×10^{-07}	4.68×10^{-07}	1.85×10^{-08}	N/A
K3 - radial distortion 3	$0.00 \times 10^{+00}$	$0.00 \times 10^{+00}$	$0.00 \times 10^{+00}$	$0.00 \times 10^{+00}$	$0.00 \times 10^{+00}$	N/A
P1 - tangential distortion 1	4.14×10^{-06}	2.07×10^{-06}	1.94×10^{-07}	1.94×10^{-06}	-1.89×10^{-07}	N/A
P2 - tangential distortion 2	-4.28×10^{-07}	9.30×10^{-07}	1.89×10^{-07}	2.15×10^{-06}	2.30×10^{-07}	N/A
Image measurement precision: Overall RMS (pixels)	0.973		1.042		1.078	

Table A-2: Camera calibration results for the iPhone4 smart phone camera using three different calibration routines.

Parameter	iPhone4					
	PhotoModeler		MATLAB		OpenCV	
	Mean	σ	Mean	σ	Mean	σ
Focal Length (mm)	3.808	0.003	3.816	0.007	3.829	N/A
Xp - principal point x (mm)	1.983	0.002	1.987	0.005	1.990	N/A
Yp - principal point y (mm)	1.484	0.002	1.468	0.006	1.469	N/A
Fw - format width (mm)	3.959	0.000	Not calculated			
Fh - format height (mm)	2.958	N/A				
K1 - radial distortion 1	-8.33×10^{-03}	1.77×10^{-04}	-8.99×10^{-03}	2.04×10^{-03}	-8.97×10^{-03}	N/A
K2 - radial distortion 2	2.07×10^{-03}	4.74×10^{-05}	2.28×10^{-03}	7.73×10^{-04}	2.26×10^{-03}	N/A
K3 - radial distortion 3	$0.00 \times 10^{+00}$	$0.00 \times 10^{+00}$	$0.00 \times 10^{+00}$	$0.00 \times 10^{+00}$	$0.00 \times 10^{+00}$	N/A
P1 - tangential distortion 1	-2.67×10^{-04}	3.93×10^{-05}	-1.26×10^{-04}	1.27×10^{-04}	-1.16×10^{-04}	N/A
P2 - tangential distortion 2	-2.77×10^{-04}	3.80×10^{-05}	5.97×10^{-05}	1.47×10^{-04}	6.40×10^{-05}	N/A
Image measurement precision: Overall RMS (pixels)	0.982		1.255		1.351	

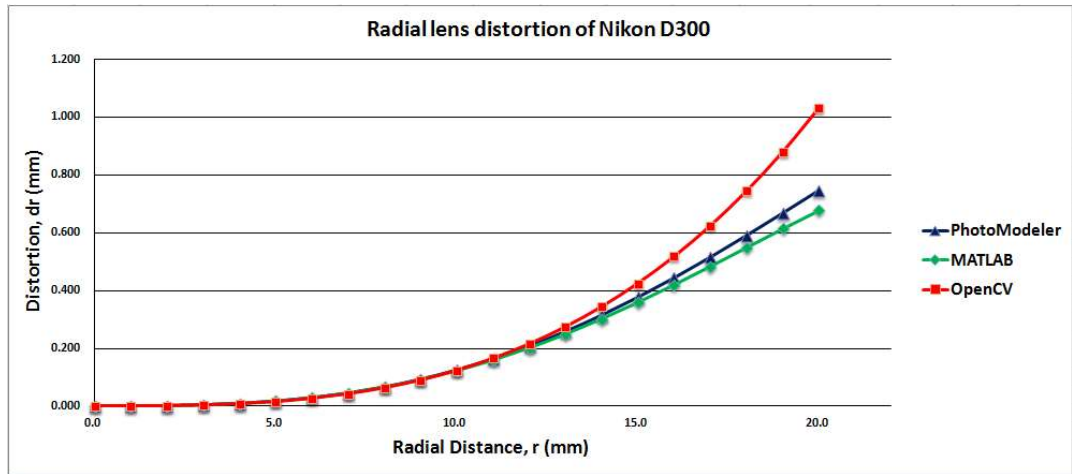


Figure A-1: Radial lens distortion of the Nikon D300, as determined from the three different calibration routines.

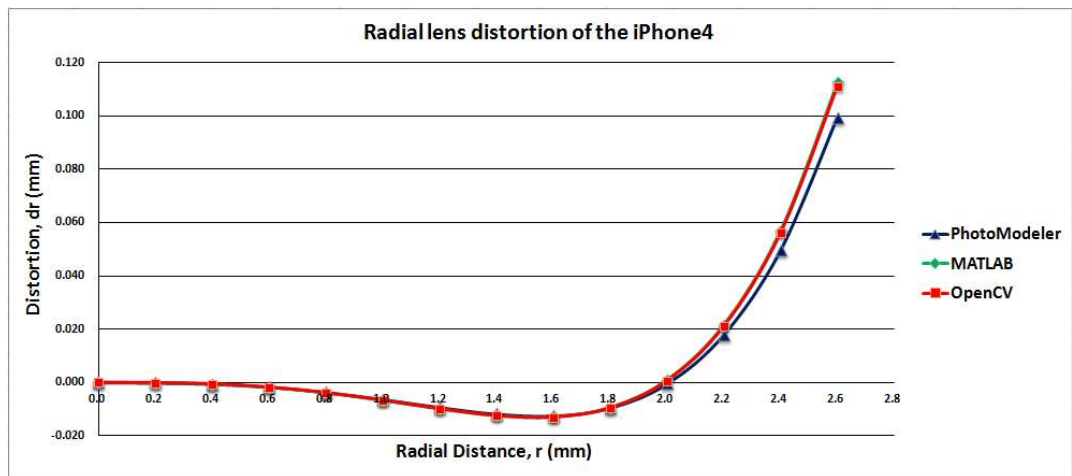


Figure A-2: Radial lens distortion of the iPhone4, as determined from the three different calibration routines.

Appendix B

Calculations of the maximum allowable camera-to-object distance and field of view of the camera (Section 3.2.3)

Table B-1: Maximum allowable camera-to-object distance (d_{max}) using the Nexus 6 smart phone camera for image acquisition.

Digital camera	Standard error in the object point, σ_c (m)	Focal length, c (mm)	Average number of exposure at/near each station, k	Design factor, q	Standard error in the image coordinate, σ (μm)	Maximum allowable camera-to-object distance, d_{max} (m) $d_{max} = \frac{\bar{\sigma}_c c \sqrt{k}}{q \sigma}$
Nexus 6	0.005	4	1	0.9	1.58	14.03

Table B-2: Field of view (FOV) of iPhone 4, Nexus 6 and Nikon D300 digital cameras.

Digital camera	Focal length, c (mm)	Format width, w (mm)	Format height, h (mm)	Image format diagonal, s' (mm)	Field of view, 2Ω (Degree)
iPhone4	3.8	4.0	3.0	5.0	66.68
Nexus 6	3.8	4.7	3.5	5.9	75.27
Nikon D300	28.0	23.6	15.8	28.4	53.78

Appendix C

SkyPMMS instructions (Section 3.5.3)

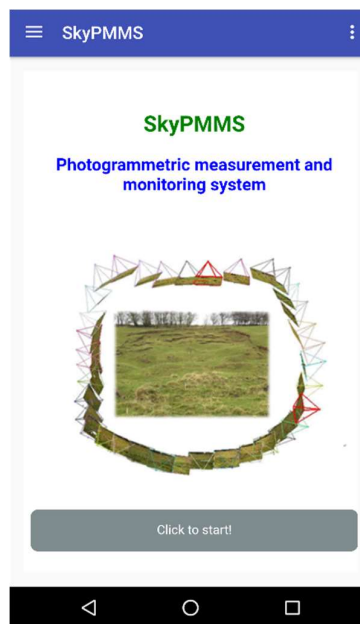
As a user guide of the SkyPMMS application for photogrammetric landslide monitoring, a user guide is divided into two modules, as follows:

Module 1: Photogrammetric measurement

This module is used to upload images from a mobile device to a cloud server, process imaging data on the system and display the point cloud results for photogrammetric measurement.

1) Create a new project or select an existing project

- Click to start the SkyPMMS application



- Choose either to create a new project or to select an existing project.

The screenshot shows the SkyPMMS interface with a blue header bar containing a menu icon and the text 'SkyPMMS'. Below the header, there is a section titled 'Project:' with two radio button options: 'Select an existing project:' (which is selected) and 'Create a new project:'. Below these options is a grey button with the text 'Please, click to next stage.'

2) Create a new epoch for photogrammetric measurement

- Click to start the module of photogrammetric measurement for generating results.

The screenshot shows the SkyPMMS interface with a blue header bar containing a menu icon and the text 'SkyPMMS'. Below the header, there is a section titled 'Project: HollinHill' with a bullet point 'Select a system for processing:'. Below this are three buttons: 'Photogrammetric measurement system' (highlighted with a red box), 'Landslide monitoring analysis', and 'Back to start a new Project'.

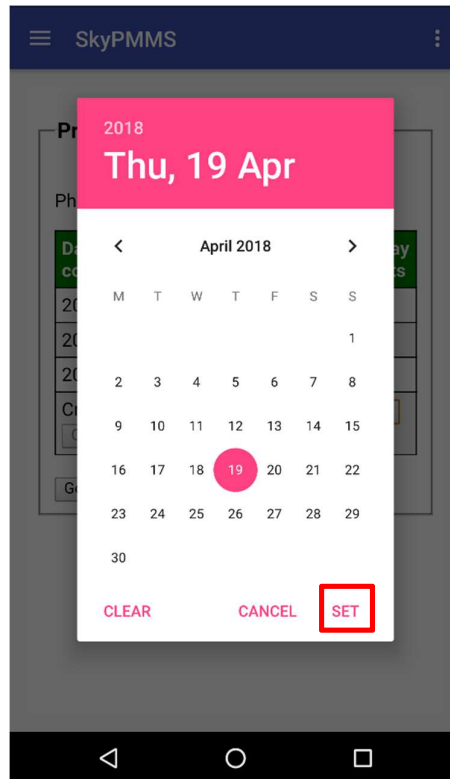
- Click to add a new epoch of measurement.

The screenshot shows the SkyPMMS interface with a blue header bar containing a menu icon and the text 'SkyPMMS'. Below the header, there is a section titled 'Project: HollinHill' with the text 'Photogrammetric measurement system:'. Below this is a table with the following data:

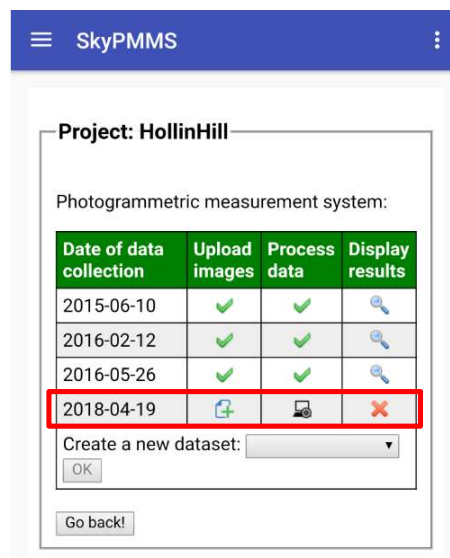
Date of data collection	Upload images	Process data	Display results
2015-06-10	✓	✓	🔍
2016-02-12	✓	✓	🔍
2016-05-26	✓	✓	🔍

Below the table, there is a 'Create a new dataset' dropdown menu (highlighted with a red box), an 'OK' button, and a 'Go back!' button.

- Select and set the date of data collection.

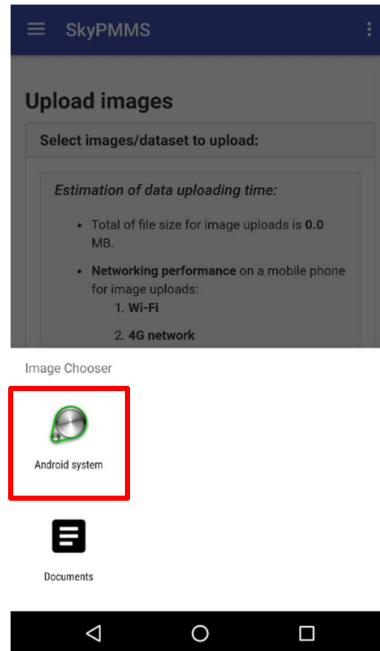


- Click to create a new epoch of photogrammetric measurement.

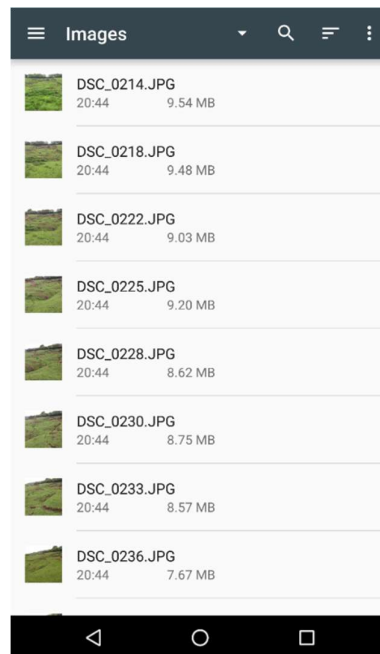


3) Upload a new image dataset

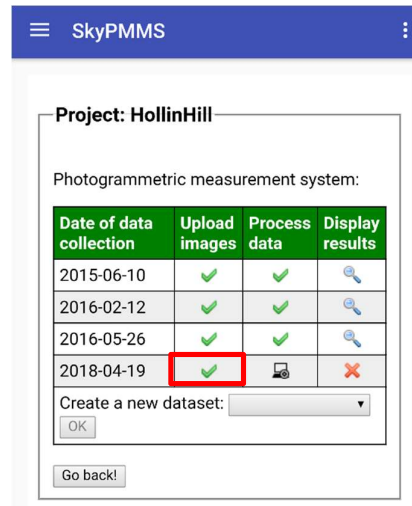
- Click  to add a new image dataset.
- Click  and select a path of image dataset.



- Select image files from a list of images.



- Click  to upload images from a mobile device to a cloud server.
- After uploading image data, the status of image upload  appears.



4) *Settings for data processing*

- Click  for settings of photogrammetric processing.
- These settings include three parts: 1) pre-processing, 2) geo-referencing, and 3) post-processing.

4.1) *Pre-processing*

In pre-processing, the user has two options to enhance the performance of data processing and improve the quality of photogrammetric results.

Pre-processing	
<input type="checkbox"/>	Making a pair-list of image matching from image sequence <ul style="list-style-type: none"> Number of matching neighbor frames: <input type="text" value="3"/>
<input type="checkbox"/>	Lens distortion correction <ul style="list-style-type: none"> select an existing camera model from a text file: <input type="button" value="Choose file"/> No file chosen

4.1.1) Lens distortion correction

- Check to use the images corrected for lens distortion for processing.
- The user has to import a TXT file of the parameters for a camera model.

4.1.2) Pre-image matching

- Check to use the pre-image matching.
- The user has to select the number of overlaps for image matching.
- In general, the user should select the appropriate number of overlaps for at least three images.

4.2) Geo-referencing

In the settings of geo-referencing for photogrammetric results, the user has four options, as follows:

Georeferencing	
<input checked="" type="radio"/>	None
<input type="radio"/>	with GCPs/targets ■ from a GCP file of observations: <input type="button" value="Choose file"/> No file chosen
<input type="radio"/>	with a real-time GCP observation on imagery <input type="button" value="Click to measurement"/>
<input type="radio"/>	with dimensions of known objects <input type="button" value="Click to process"/>

4.2.1) None

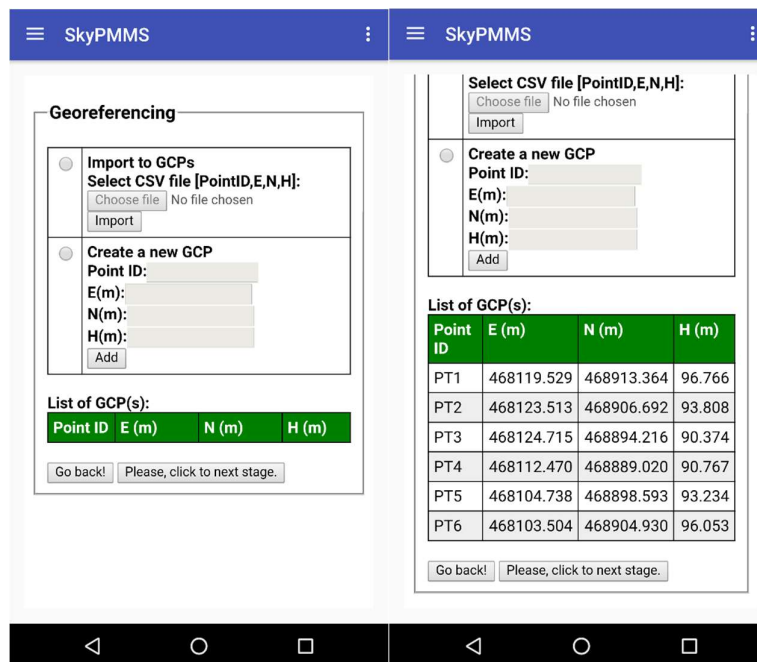
- Select not to provide any spatial information for photogrammetric results.

4.2.1) With GNSS-based target observations

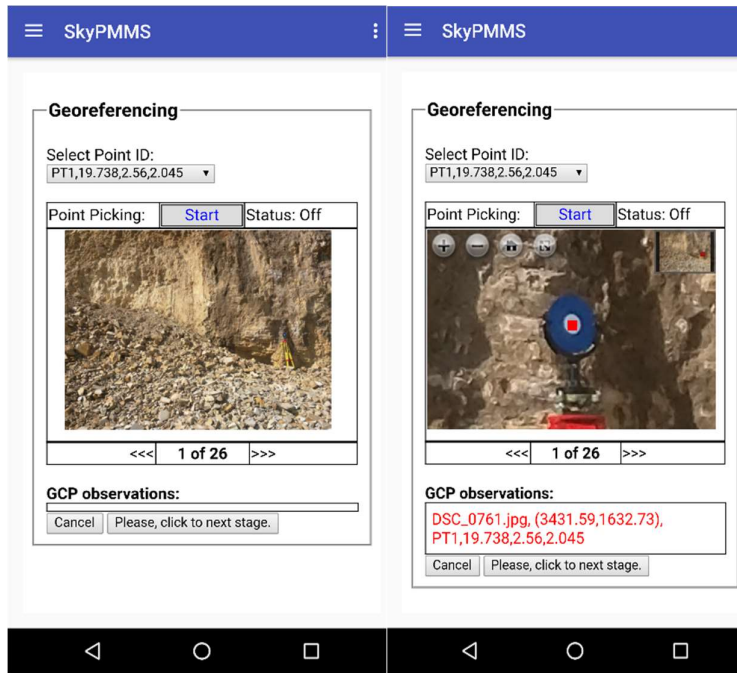
- The user has to import a TXT file for a pair list of targets with photo coordinates and the real-world coordinates acquired from GNSS survey for geo-referencing.

4.2.1) With real-time, GNSS-based target observations

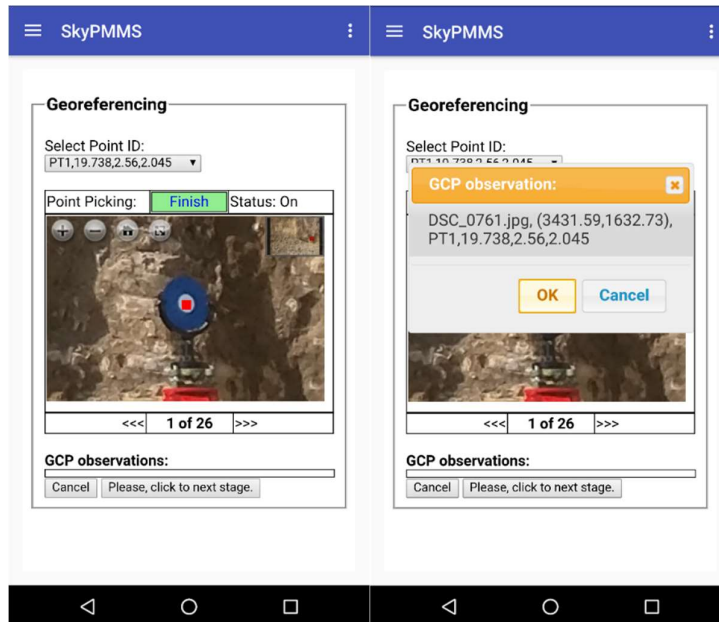
- The user has to measure the photo coordinates of targets on imagery and input the real-world coordinates acquired from GNSS survey.
- Select to import or input the real-world coordinates of targets.



- Select the target for measuring the photo coordinates.
- Click  to measure the photo coordinates of target.

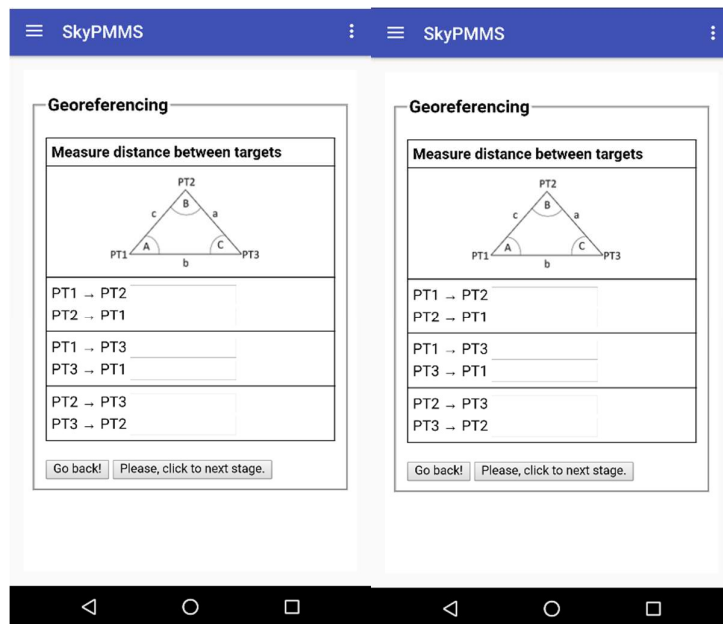


- Click Finish to identify and get the photo coordinates of target.



4.2.2) With distances between points

- The user has to measure the photo coordinates of three targets on imagery and input three distances between targets.
- This method is used for scaling the photogrammetric results. However, after scaling, manual alignment of photogrammetric results at different epochs is required on PC or laptop computer.
- Input the three distances between points or targets, and click to next stage.



- This function will automatically generate the three pseudo coordinates of points or targets.
- Click to next stage for measuring the photo coordinates of targets.

4.3.1) Cropping

- Check to provide the point cloud of photogrammetric results within the boundary of the area of interest.
- The user has to import a TXT file of the boundary of the area and select the orthogonal dimension in X, Y or Z axis.

4.3.2) De-noising

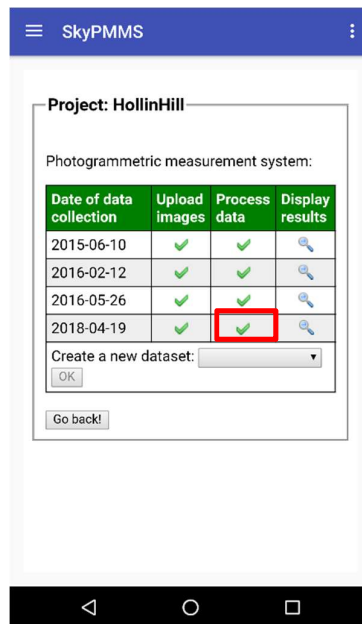
- Check to remove noise from the point cloud of photogrammetric results.
- The user has to input two parameters including the number of points (N) considered and the number of multipliers (n) with a standard deviation to identify the threshold of classification for outlier detection.

4.3.3) Vegetation filtering

- Check to remove point cloud over vegetated surfaces.
- The user has to input a parameter of the green vegetation index value. Points of photogrammetric results which have green vegetation index above the threshold for classification are eliminated from the point cloud. The threshold used for classification of vegetation depends on the weather and season.

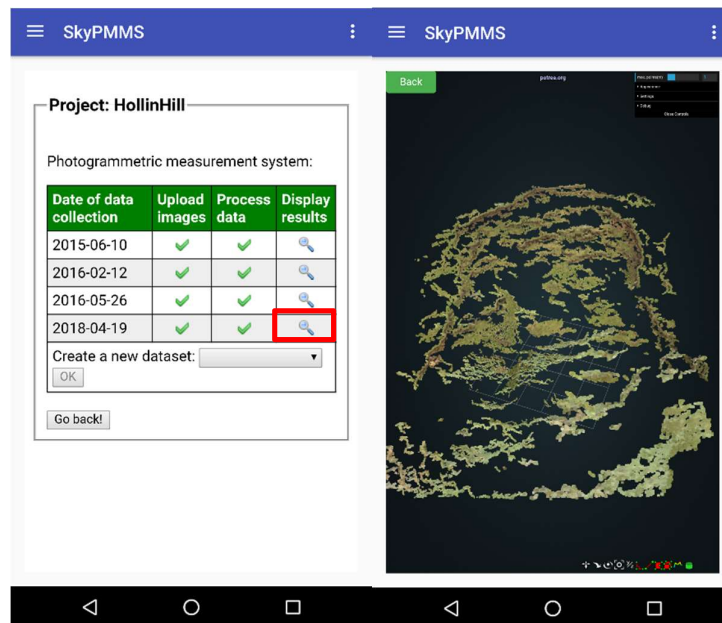
5) *Process the photogrammetric measurement*

- Click to next stage for photogrammetric processing.
- After photogrammetric processing, the status of data processing  appears.



6) *Display the photogrammetric results*

- Click 🔍 to display the point cloud of photogrammetric results.



Module 2: Landslide monitoring analysis

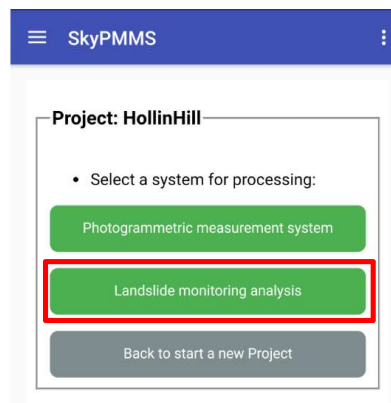
This module is used to select datasets for assessing landslide deformation, process and analyse the landslide and show the results of landslide monitoring analysis.

1) Select the project

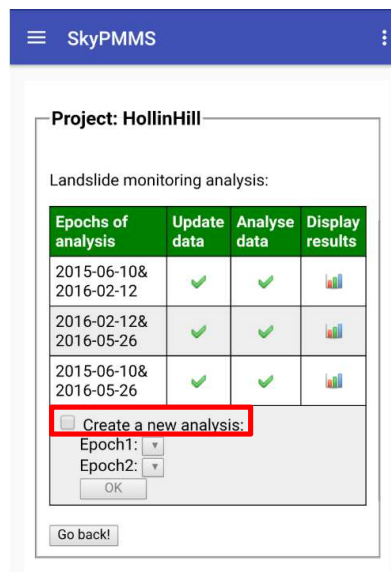
- Select an existing project of photogrammetric landslide monitoring.

2) Select the epochs for a multi-epoch analysis

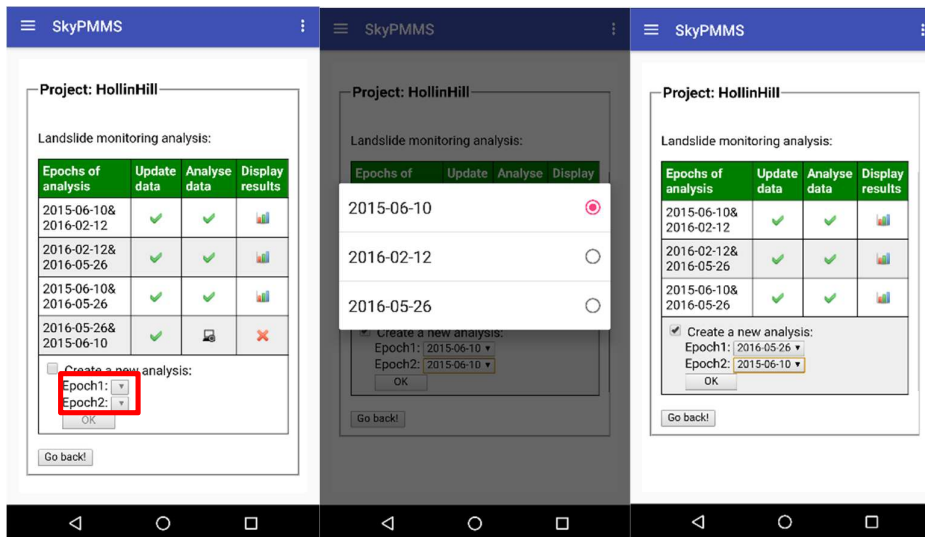
- Click to start the module of landslide monitoring analysis.



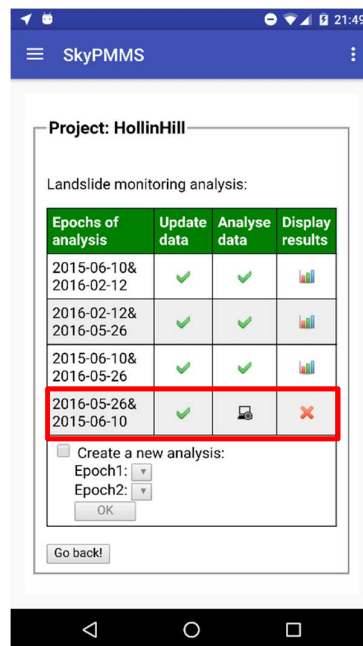
- Check to create a new analysis of landslide monitoring.



- Click to select each epoch of photogrammetric results used for assessing landslide deformation.

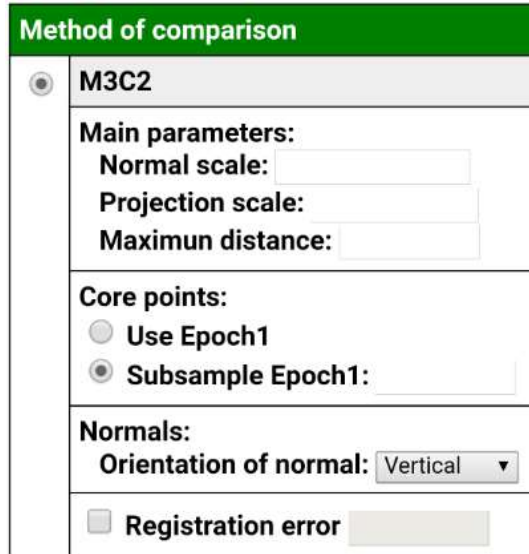


- Click  to create the landslide monitoring analysis.



3) *Setting of cloud comparison method using M3C2 technique*

- Click  for settings of landslide monitoring analysis.
- For landslide monitoring analysis, the settings have four parts to identify the parameters of cloud comparison method using M3C2 technique.



Method of comparison	
<input checked="" type="radio"/>	M3C2
Main parameters:	
Normal scale:	<input type="text"/>
Projection scale:	<input type="text"/>
Maximum distance:	<input type="text"/>
Core points:	
<input type="radio"/>	Use Epoch1
<input checked="" type="radio"/>	Subsample Epoch1: <input type="text"/>
Normals:	
Orientation of normal:	Vertical ▼
<input type="checkbox"/>	Registration error <input type="text"/>

3.1) *Main parameters*

- The main parameters of the M3C2 method for multi-epoch analysis are used for the change detection of landslides, including:
 - D - the scale factor or normal scale;
 - d - the project scale;
 - p_{max} - the height of the projection cylinder or the maximum distance;

3.2) *Core points*

- The setting of core points is used to enhance the performance of the computation for point cloud comparison. A very high density of point cloud requires longer data processing for analysis.
- In particular, the user should select the subsampling point cloud and input the distance between each point to decrease the number of points for timesaving analysis.

3.3) Normals

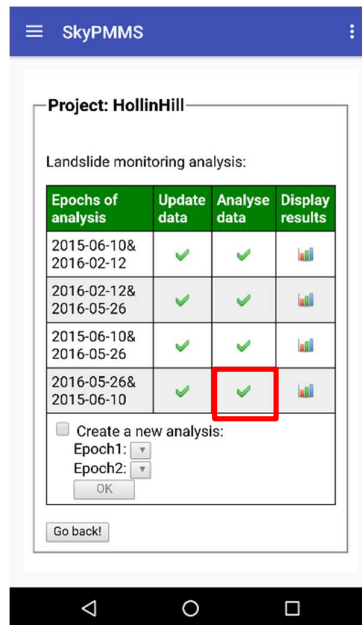
- This setting is used to compute a normal vector in the vertical or horizontal direction of the projection cylinder.
- In particular, the user should select the vertical direction to be used for detection of the elevation changes.

3.4) Registration error

- For point cloud comparison from different approaches, the user can input this error.
- However, with point cloud comparison from the same photogrammetric approach for landslide monitoring analysis, the user should not input the registration error.

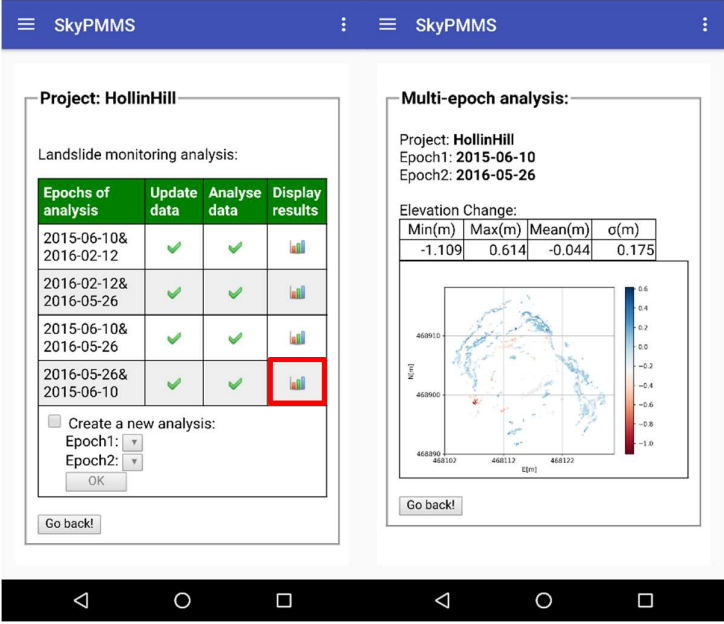
4) Process the landslide monitoring analysis

- Click to next stage for landslide monitoring analysis.
- After analysis, the status of data processing  appears.



5) Display the results of landslide monitoring analysis

- Click  to display the results of landslide monitoring analysis.



The screenshot displays the SkyPMMS mobile application interface. The top navigation bar is blue with the text 'SkyPMMS' and a hamburger menu icon on the left, and a vertical ellipsis menu icon on the right. The main content area is divided into two panels.

Project: HollinHill

Landslide monitoring analysis:

Epochs of analysis	Update data	Analyse data	Display results
2015-06-10&2016-02-12	✓	✓	
2016-02-12&2016-05-26	✓	✓	
2015-06-10&2016-05-26	✓	✓	
2016-05-26&2015-06-10	✓	✓	

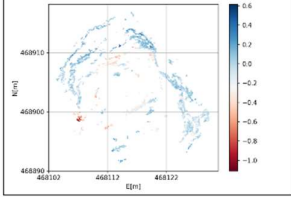
Create a new analysis:
Epoch1:
Epoch2:

Multi-epoch analysis:

Project: **HollinHill**
Epoch1: **2015-06-10**
Epoch2: **2016-05-26**

Elevation Change:

Min(m)	Max(m)	Mean(m)	σ (m)
-1.109	0.614	-0.044	0.175



The bottom of the screen shows the standard Android navigation bar with back, home, and recent apps icons.

References

- Agisoft, L.L.C. (2016) *Agisoft PhotoScan User Manual: Professional Edition, Version 1.2*.
- Agliardi, F., Crosta, G.B., Sosio, R., Rivolta, C. and Mannucci, G. (2013) 'In situ and remote long term real-time monitoring of a large alpine rock slide', in *Landslide Science and Practice*. Springer, pp. 415-421.
- Akca, D. (2013) 'Photogrammetric Monitoring of an Artificially Generated Shallow Landslide', *The Photogrammetric Record*, 28(142), pp. 178-195.
- Al-Rawabdeh, A., He, F., Moussa, A., El-Sheimy, N. and Habib, A. (2016) 'Using an unmanned aerial vehicle-based digital imaging system to derive a 3D point cloud for landslide scarp recognition', *Remote sensing*, 8(2), p. 95.
- Alsadik, B.S.A. (2014) *Guided Close Range Photogrammetry for 3D Modelling of Cultural Heritage Sites*. PhD thesis. University of Twente.
- Amazon Web Services, I. (2016) *Amazon EC2 - Virtual Server Hosting*.
- Antolini, F., Tofani, V., Del Ventisette, C., Luzi, G., Casagli, N. and Moretti, S. (2013) 'SAR interferometry for landslides risk assessment at local scale: the case study of Castagnola (Northern Apennines, Italy)', in *Landslide science and practice*. Springer, pp. 407-414.
- Arosio, D., Longoni, L., Mazza, F., Papini, M. and Zanzi, L. (2013) 'Freeze-thaw cycle and rockfall monitoring', in *Landslide science and practice*. Springer, pp. 385-390.
- Ayad, M., Taher, M. and Salem, A. (2015) *Energy Aware Computing Systems & Applications (ICEAC), 2015 International Conference on*. IEEE.
- Bandara, R.M.S., Bhasin, R.K., Kjekstad, O. and Arambepola, N. (2013) 'Examples of cost effective practices for landslide monitoring for early warning in developing countries of Asia', in *Landslide Science and Practice*. Springer, pp. 581-588.
- Barazzetti, L., Scaioni, M. and Remondino, F. (2010) 'Orientation and 3D modelling from markerless terrestrial images: combining accuracy with automation', *The Photogrammetric Record*, 25(132), pp. 356-381.
- Bardi, F., Frodella, W., Ciampalini, A., Bianchini, S., Del Ventisette, C., Gigli, G., Fanti, R., Moretti, S., Basile, G. and Casagli, N. (2014) 'Integration between ground based and satellite SAR data in landslide mapping: The San Fratello case study', *Geomorphology*, 223(0), pp. 45-60.
- Barnhart, T.B. and Crosby, B.T. (2013) 'Comparing two methods of surface change detection on an evolving thermokarst using high-temporal-frequency terrestrial laser scanning, Selawik River, Alaska', *Remote Sensing*, 5(6), pp. 2813-2837.

- Bay, H., Ess, A., Tuytelaars, T. and Van Gool, L. (2008) 'Speeded-Up Robust Features (SURF)', *Computer Vision and Image Understanding*, 110(3), pp. 346-359.
- Bednarczyk, Z. (2013) 'New real-time landslide monitoring system in Polish Carpathians', in *Landslide Science and Practice*. Springer, pp. 3-14.
- Behling, R., Roessner, S., Kaufmann, H. and Kleinschmit, B. (2014) 'Automated spatiotemporal landslide mapping over large areas using rapideye time series data', *Remote Sensing*, 6(9), pp. 8026-8055.
- Bouguet, J.-Y. (2000) 'Matlab camera calibration toolbox', *Caltech Technical Report*.
- Bozzano, F., Cipriani, I., Mazzanti, P. and Prestininzi, A. (2011) 'Displacement patterns of a landslide affected by human activities: insights from ground-based InSAR monitoring', *Natural Hazards*, 59(3), pp. 1377-1396.
- Bradski, G. and Kaehler, A. (2008) *Learning OpenCV: Computer vision with the OpenCV library*. Oreilly & Associates Inc., USA.
- Brown, D.C. (1971) 'Close-range camera calibration', *Photogramm. Eng.*, 37(8), pp. 855-866.
- Bueno, M., Martínez-Sánchez, J., González-Jorge, H. and Lorenzo, H. (2016) 'DETECTION OF GEOMETRIC KEYPOINTS AND ITS APPLICATION TO POINT CLOUD COARSE REGISTRATION', *International Archives of the Photogrammetry, Remote Sensing & Spatial Information Sciences*, 41.
- Caduff, R. and Rieke-Zapp, D. (2014) 'Registration and visualisation of deformation maps from terrestrial radar interferometry using photogrammetry and structure from Motion', *The Photogrammetric Record*, 29(146), pp. 167-186.
- Caduff, R., Schlunegger, F., Kos, A. and Wiesmann, A. (2015) 'A review of terrestrial radar interferometry for measuring surface change in the geosciences', *Earth surface processes and landforms*, 40(2), pp. 208-228.
- Carbonneau, P.E. and Dietrich, J.T. (2017) 'Cost-effective non-metric photogrammetry from consumer-grade sUAS: implications for direct georeferencing of structure from motion photogrammetry', *Earth Surface Processes and Landforms*, 42(3), pp. 473-486.
- Castillo, C., James, M.R., Redel-Macías, M.D., Pérez, R. and Gómez, J.A. (2015) 'SF3M software: 3-D photo-reconstruction for non-expert users and its application to a gully network', *Soil*, 1(2), pp. 583-594.
- Chambers, J., Meldrum, P., Gunn, D., Wilkinson, P., Merritt, A., Murphy, W., West, J., Kuras, O., Haslam, E. and Hobbs, P. (2013) 'Geophysical-geotechnical sensor networks for landslide monitoring', in *Landslide Science and Practice*. Springer, pp. 289-294.
- Chidburee, P., Mills, J.P., Miller, P.E. and Fieber, K.D. (2016) 'Towards a low-cost, real-time photogrammetric landslide monitoring system utilising mobile and cloud

computing technology', *International Archives of the Photogrammetry, Remote Sensing & Spatial Information Sciences*, 41.

- Chih-Lin, I., Han, S., Xu, Z., Sun, Q. and Pan, Z. (2016) '5G: rethink mobile communications for 2020+', *Phil. Trans. R. Soc. A*, 374(2062), p. 20140432.
- Corominas, J., Moya, J., Lloret, A., Gili, J.A., Angeli, M.G., Pasuto, A. and Silvano, S. (2000) 'Measurement of landslide displacements using a wire extensometer', *Engineering Geology*, 55(3), pp. 149-166.
- Corral, L., Sillitti, A. and Succi, G. (2012) 'Mobile multiplatform development: An experiment for performance analysis', *Procedia Computer Science*, 10, pp. 736-743.
- Cruden, D. and Lan, H.-X. (2015) 'Using the Working Classification of Landslides to assess the danger from a natural slope', in *Engineering Geology for Society and Territory-Volume 2*. Springer, pp. 3-12.
- Daponte, P., De Vito, L., Picariello, F. and Riccio, M. (2013) 'State of the art and future developments of measurement applications on smartphones', *Measurement*, 46(9), pp. 3291-3307.
- Datar, A., Liu, J., Linnemayr, S. and Stecher, C. (2013) 'The impact of natural disasters on child health and investments in rural India', *Social Science & Medicine*, 76, pp. 83-91.
- Davies, T. (2015) 'Chapter 1 - Landslide Hazards, Risks, and Disasters: Introduction', in *Landslide Hazards, Risks and Disasters*. Boston: Academic Press, pp. 1-16.
- Denora, D., Romano, L. and Cecaro, G. (2013) 'Terrestrial laser scanning for the Montaguto landslide (Southern Italy)', in *Landslide Science and Practice*. Springer, pp. 33-38.
- Devoto, S., Forte, E., Mantovani, M., Mocnik, A., Pasuto, A., Piacentini, D. and Soldati, M. (2013) 'Integrated monitoring of lateral spreading phenomena along the north-west coast of the Island of Malta', in *Landslide Science and Practice*. Springer, pp. 235-241.
- Di Maio, C., Vassallo, R., Vallario, M., Calcaterra, S. and Gambino, P. (2013) 'Surface and deep displacements evaluated by GPS and inclinometers in a clayey slope', in *Landslide Science and Practice*. Springer, pp. 265-271.
- Eltner, A., Kaiser, A., Castillo, C., Rock, G., Neugirg, F. and Abellán, A. (2016) 'Image-based surface reconstruction in geomorphometry – merits, limits and developments', *Earth Surf. Dynam.*, 4(2), pp. 359-389.
- Eltner, A. and Schneider, D. (2015) 'Analysis of different methods for 3D reconstruction of natural surfaces from parallel-axes UAV images', *The Photogrammetric Record*, 30(151), pp. 279-299.

- Fernando, N., Loke, S.W. and Rahayu, W. (2013) 'Mobile cloud computing: A survey', *Future generation computer systems*, 29(1), pp. 84-106.
- Fraser, C.S. (2013) 'Automatic camera calibration in close range photogrammetry', *Photogrammetric Engineering & Remote Sensing*, 79(4), pp. 381-388.
- Fryer, J., Mitchell, H. and Chandler, J.H. (2007) *Applications of 3D measurement from images*. Dunbeath, Scotland, UK: Whittles Publishing.
- Furukawa, Y., Curless, B., Seitz, S.M. and Szeliski, R. (2010) *Computer Vision and Pattern Recognition (CVPR), 2010 IEEE Conference on*. IEEE.
- Furukawa, Y. and Ponce, J. (2010) 'Accurate, dense, and robust multiview stereopsis', *Pattern Analysis and Machine Intelligence, IEEE Transactions on*, 32(8), pp. 1362-1376.
- Furuya, G., Katayama, T., Suemine, A., Kozato, T., Watanabe, T. and Marui, H. (2013) 'Application of the newly frequency domain electromagnetic method survey in a landslide area', in *Landslide science and practice*. Springer, pp. 169-175.
- Gómez-Gutiérrez, Á., Schnabel, S., Berenguer-Sempere, F., Lavado-Contador, F. and Rubio-Delgado, J. (2014) 'Using 3D photo-reconstruction methods to estimate gully headcut erosion', *CATENA*, 120(0), pp. 91-101.
- Hullo, J.F., Grussenmeyer, P. and Fares, S. (2009) 'Photogrammetry and dense stereo matching approach applied to the documentation of the cultural heritage site of Kilwa (Saudi Arabia)', *22nd CIPA Symposium*. Kyoto, Japan.
- Intrieri, E., Gigli, G., Mugnai, F., Fanti, R. and Casagli, N. (2012) 'Design and implementation of a landslide early warning system', *Engineering Geology*, 147, pp. 124-136.
- James, M.R. and Robson, S. (2012) 'Straightforward reconstruction of 3D surfaces and topography with a camera: Accuracy and geoscience application', *Journal of Geophysical Research: Earth Surface*, 117(F3).
- Janeras, M., Jara, J.-A., Royán, M.J., Vilaplana, J.-M., Aguasca, A., Fàbregas, X., Gili, J.A. and Buxó, P. (2017) 'Multi-technique approach to rockfall monitoring in the Montserrat massif (Catalonia, NE Spain)', *Engineering Geology*, 219, pp. 4-20.
- Javernick, L., Brasington, J. and Caruso, B. (2014) 'Modeling the topography of shallow braided rivers using Structure-from-Motion photogrammetry', *Geomorphology*, 213, pp. 166-182.
- Kääb, A. (2002) 'Monitoring high-mountain terrain deformation from repeated air-and spaceborne optical data: examples using digital aerial imagery and ASTER data', *ISPRS Journal of Photogrammetry and remote sensing*, 57(1-2), pp. 39-52.
- Kaiser, A., Neugirg, F., Rock, G., Müller, C., Haas, F., Ries, J. and Schmidt, J. (2014) 'Small-scale surface reconstruction and volume calculation of soil erosion in

complex Moroccan gully morphology using structure from motion', *Remote Sensing*, 6(8), pp. 7050-7080.

Kapeller, G., Rocha, R.P.O., de Lacerda, L.A. and Aufleger, M. (2013) 'Evaluation of Temperature Effects on Strain Measurements with DTSS', in *Landslide Science and Practice*. Springer, pp. 479-485.

Karimi, H.A. and Roongpiboonsopit, D. (2012) 'Are Clouds Ready for Geoprocessing?', in *Cloud Computing and Services Science*. Springer, pp. 295-312.

Kehl, C., Buckley, S.J., Gawthorpe, R., Viola, I. and Howell, J.A. (2016) 'Direct image-to-geometry registration using mobile sensor data', *International Annals of the Photogrammetry, Remote Sensing & Spatial Information Sciences*, III-2.

Koizumi, K., Hirata, K., Oda, K., Fujita, Y. and Kamide, S. (2013) 'Slope Disaster Monitoring System Using Battery-Operated Wireless Sensor Network', in Margottini, C., Canuti, P. and Sassa, K. (eds.) *Landslide Science and Practice*. Springer Berlin Heidelberg, pp. 109-116.

Kristensen, L. and Blikra, L.H. (2013) 'Monitoring displacement on the Mannen rockslide in Western Norway', in *Landslide Science and Practice*. Springer, pp. 251-256.

Kuhn, D. and Prüfer, S. (2014) 'Coastal cliff monitoring and analysis of mass wasting processes with the application of terrestrial laser scanning: A case study of Rügen, Germany', *Geomorphology*, 213, pp. 153-165.

Lague, D., Brodu, N. and Leroux, J. (2013) 'Accurate 3D comparison of complex topography with terrestrial laser scanner: Application to the Rangitikei canyon (N-Z)', *ISPRS Journal of Photogrammetry and Remote Sensing*, 82(Supplement C), pp. 10-26.

Lee, E.M. and Jones, D.K.C. (2004) *Landslide risk assessment*. Thomas Telford.

Lee, K. and Kang, S. (2013) 'Mobile cloud service of geo-based image processing functions: a test iPad implementation', *Remote Sensing Letters*, 4(9), pp. 910-919.

Liao, W.-H., Chen, P.-W. and Kuai, S.-C. (2017) 'A Resource Provision Strategy for Software-as-a-Service in Cloud Computing', *Procedia Computer Science*, 110, pp. 94-101.

Lillesand, T.M., Kiefer, R.W. and Chipman, J.W. (2008) *Remote sensing and image interpretation*. 6th ed.. edn. Hoboken, N.J.: Hoboken, N.J. : John Wiley & Sons.

Lim, M., Petley, D.N., Rosser, N.J., Allison, R.J., Long, A.J. and Pybus, D. (2005) 'Combined digital photogrammetry and time-of-flight laser scanning for monitoring cliff evolution', *The Photogrammetric Record*, 20(110), pp. 109-129.

Lowe, D. (2004) 'Distinctive Image Features from Scale-Invariant Keypoints', *International Journal of Computer Vision*, 60(2), pp. 91-110.

- Lucieer, A., Jong, S.M.d. and Turner, D. (2014) 'Mapping landslide displacements using Structure from Motion (SfM) and image correlation of multi-temporal UAV photography', *Progress in Physical Geography*, 38(1), pp. 97-116.
- Luhmann, T., Fraser, C. and Maas, H.-G. (2016) 'Sensor modelling and camera calibration for close-range photogrammetry', *ISPRS Journal of Photogrammetry and Remote Sensing*, 115, pp. 37-46.
- Luhmann, T., Robson, S., Kyle, S. and Harley, I. (2006) *Close range photogrammetry: Principles, methods and applications*. Whittles.
- Malet, J.-P., Ulrich, P., Déprez, A., Masson, F., Lissak, C. and Maquaire, O. (2013) 'Continuous monitoring and near-real time processing of GPS observations for landslide analysis: a methodological framework', in *Landslide Science and Practice*. Springer, pp. 201-209.
- Martha, T.R., Kerle, N., van Westen, C.J., Jetten, V. and Kumar, K.V. (2012) 'Object-oriented analysis of multi-temporal panchromatic images for creation of historical landslide inventories', *ISPRS journal of photogrammetry and remote sensing*, 67, pp. 105-119.
- Mazzanti, P., Brunetti, A. and Bretschneider, A. (2015) 'A new approach based on terrestrial remote-sensing techniques for rock fall hazard assessment', in *Modern Technologies for Landslide Monitoring and Prediction*. Springer, pp. 69-87.
- Merritt, A.J., Chambers, J.E., Murphy, W., Wilkinson, P.B., West, L.J., Gunn, D.A., Meldrum, P.I., Kirkham, M. and Dixon, N. (2014) '3D ground model development for an active landslide in Lias mudrocks using geophysical, remote sensing and geotechnical methods', *Landslides*, 11(4), pp. 537-550.
- Meyer, G.E. and Neto, J.C. (2008) 'Verification of color vegetation indices for automated crop imaging applications', *Computers and Electronics in Agriculture*, 63(2), pp. 282-293.
- Micheletti, N., Chandler, J.H. and Lane, S.N. (2015a) 'Investigating the geomorphological potential of freely available and accessible structure-from-motion photogrammetry using a smartphone', *Earth Surface Processes and Landforms*, 40(4), pp. 473-486.
- Micheletti, N., Lane, S.N. and Chandler, J.H. (2015b) 'Application of archival aerial photogrammetry to quantify climate forcing of alpine landscapes', *The Photogrammetric Record*, 30(150), pp. 143-165.
- Milenkovic, S., Jelisavac, B., Vujanic, V. and Jotic, M. (2013) 'Monitoring of the "Razanji" Landslide in Serbia', in *Landslide Science and Practice*. Springer, pp. 25-31.
- Miller, P., Mills, J., Edwards, S., Bryan, P., Marsh, S., Mitchell, H. and Hobbs, P. (2008) 'A robust surface matching technique for coastal geohazard assessment and

management', *ISPRS Journal of Photogrammetry and Remote Sensing*, 63(5), pp. 529-542.

Miller, P.E., Mills, J.P., Barr, S.L., Birkinshaw, S.J., Hardy, A.J., Parkin, G. and Hall, S.J. (2012) 'A remote sensing approach for landslide hazard assessment on engineered slopes', *IEEE Transactions on Geoscience and Remote Sensing*, 50(4), pp. 1048-1056.

Monserrat, O., Crosetto, M. and Luzi, G. (2014) 'A review of ground-based SAR interferometry for deformation measurement', *ISPRS Journal of Photogrammetry and Remote Sensing*, 93, pp. 40-48.

Motta, M., Gabrieli, F., Corsini, A., Manzi, V., Ronchetti, F. and Cola, S. (2013) 'Landslide displacement monitoring from multi-temporal terrestrial digital images: Case of the Valoria Landslide site', in *Landslide science and practice*. Springer, pp. 73-78.

Niethammer, U., James, M.R., Rothmund, S., Travelletti, J. and Joswig, M. (2012) 'UAV-based remote sensing of the Super-Sauze landslide: Evaluation and results', *Engineering Geology*, 128(0), pp. 2-11.

Nocerino, E., Lago, F., Morabito, D., Remondino, F., Porzi, L., Poiesi, F., Bulo, S.R., Chippendale, P., Locher, A. and Havlena, M. (2017) 'A smartphone-based 3D pipeline for the creative industry—The Replicate EU project', *The International Archives of Photogrammetry, Remote Sensing and Spatial Information Sciences*, 42, p. 535.

Ohmori, S., Yamao, Y. and Nakajima, N. (2001) 'The future generations of mobile communications based on broadband access methods', *Wireless Personal Communications*, 17(2), pp. 175-190.

Ondrúška, P., Kohli, P. and Izadi, S. (2015) 'Mobilefusion: Real-time volumetric surface reconstruction and dense tracking on mobile phones', *IEEE transactions on visualization and computer graphics*, 21(11), pp. 1251-1258.

Oughton, E.J. and Frias, Z. (2017) 'The cost, coverage and rollout implications of 5G infrastructure in Britain', *Telecommunications Policy*.

Palenzuela, J.A., Irigaray, C., Jiménez-Perálvarez, J.D. and Chacón, J. (2013) 'Application of terrestrial laser scanner to the assessment of the evolution of diachronic landslides', in *Landslide science and practice*. Springer, pp. 517-523.

PCL (2017) *The Point Cloud Library*.

Peppas, M.V., Mills, J.P., Moore, P., Miller, P.E. and Chambers, J.E. (2016) 'Accuracy assessment of a UAV-based landslide monitoring system', *The International Archives of Photogrammetry, Remote Sensing and Spatial Information Sciences*, 41, p. 895.

- Perrone, A., Lapenna, V. and Piscitelli, S. (2014) 'Electrical resistivity tomography technique for landslide investigation: A review', *Earth-Science Reviews*, 135, pp. 65-82.
- Petley, D.N., Mantovani, F., Bulmer, M.H. and Zannoni, A. (2005) 'The use of surface monitoring data for the interpretation of landslide movement patterns', *Geomorphology*, 66(1), pp. 133-147.
- Piermattei, L., Carturan, L. and Guarnieri, A. (2015) 'Use of terrestrial photogrammetry based on structure-from-motion for mass balance estimation of a small glacier in the Italian alps', *Earth Surface Processes and Landforms*, 40(13), pp. 1791-1802.
- Reci, H., Muceku, Y. and Jata, I. (2013) 'The use of ERT for investigation of berzhita landslide, tirana area, Albania', in *Landslide Science and Practice*. Springer, pp. 117-123.
- Regmi, N.R., Giardino, J.R., McDonald, E.V. and Vitek, J.D. (2015) 'Chapter 11 - A Review of Mass Movement Processes and Risk in the Critical Zone of Earth', in John, R.G. and Chris, H. (eds.) *Developments in Earth Surface Processes*. Elsevier, pp. 319-362.
- Rosser, N., Petley, D., Lim, M., Dunning, S. and Allison, R. (2005) 'Terrestrial laser scanning for monitoring the process of hard rock coastal cliff erosion', *Quarterly Journal of Engineering Geology and Hydrogeology*, 38(4), pp. 363-375.
- Sarkar, S., Ghosh, A., Kanungo, D.P. and Ahmad, Z. (2013) 'Slope stability assessment and monitoring of a vulnerable site on Rishikesh-Uttarkashi highway, India', in *Landslide science and practice*. Springer, pp. 67-71.
- Sassa, K., Fukuoka, H., Wang, F. and Wang, G. (2007) *Progress in landslide science*. Springer Science & Business Media.
- Sawyer, S.M., Ni, K. and Bliss, N.T. (2012) *High Performance Extreme Computing (HPEC), 2012 IEEE Conference on*. IEEE.
- Scaioni, M. (2015) *Modern Technologies for Landslide Monitoring and Prediction*. Springer.
- Schütz, M. (2015) *Potree 1.3*.
- Segalini, A. and Carini, C. (2013) 'Underground landslide displacement monitoring: a new MMES based device', in *Landslide science and practice*. Springer, pp. 87-93.
- Stefani, M., Mantovani, M., Mair, V., Marcato, G., Pasuto, A. and Nössing, L. (2013) 'The Ganderberg Landslide (South Tyrol, Italy): Mitigation of Residual Risk by Real-Time Monitoring', in *Landslide Science and Practice*. Springer, pp. 531-535.

- Stumpf, A., Malet, J.P., Allemand, P., Pierrot-Deseilligny, M. and Skupinski, G. (2015) 'Ground-based multi-view photogrammetry for the monitoring of landslide deformation and erosion', *Geomorphology*, 231, pp. 130-145.
- Teza, G., Galgaro, A., Zaltron, N. and Genevois, R. (2007) 'Terrestrial laser scanner to detect landslide displacement fields: a new approach', *International Journal of Remote Sensing*, 28(16), pp. 3425-3446.
- Theiler, P.W., Wegner, J.D. and Schindler, K. (2013) 'Markerless point cloud registration with keypoint-based 4-points congruent sets', *ISPRS Annals of Photogrammetry, Remote Sensing and Spatial Information Sciences*, 1(2), pp. 283-288.
- Travelletti, J., Delacourt, C., Allemand, P., Malet, J.P., Schmittbuhl, J., Toussaint, R. and Bastard, M. (2012) 'Correlation of multi-temporal ground-based optical images for landslide monitoring: Application, potential and limitations', *ISPRS Journal of Photogrammetry and Remote Sensing*, 70(0), pp. 39-55.
- Tuan, N.A., Marianne, S., José, D., Marc, O., Gerardo, H.G., Carlos, G.L.-D.J., Celestino, G.N., Inmaculada, Á.F., Bernard, M. and Joaquim, M.D.P. (2013) 'Spatio-temporal evolution of Ground displacement of the Tena landslide (Spain)', in *Landslide Science and Practice*. Springer, pp. 133-140.
- Uchimura, T., Towhata, I., Wang, L. and Qiao, J. (2013) 'Validation and interpretation of monitored behavior of slopes vulnerable to failure', in *Landslide Science and Practice*. Springer, pp. 589-595.
- Uhlemann, S., Smith, A., Chambers, J., Dixon, N., Dijkstra, T., Haslam, E., Meldrum, P., Merritt, A., Gunn, D. and Mackay, J. (2016) 'Assessment of ground-based monitoring techniques applied to landslide investigations', *Geomorphology*, 253, pp. 438-451.
- Uren, J. and Price, W.F. (2010) *Surveying for engineers*. 5th ed. edn. Basingstoke: Basingstoke : Palgrave Macmillan.
- van Westen, C.J., Ghosh, S., Jaiswal, P., Martha, T.R. and Kuriakose, S.L. (2013) 'From landslide inventories to landslide risk assessment; an attempt to support methodological development in India', in *Landslide science and practice*. Springer, pp. 3-20.
- Waldhäusl, P. and Ogleby, C.L. (1994) '3 x 3 rules for simple photogrammetric documentation of architecture', *The International Archives of Photogrammetry and Remote Sensing*, XXX(Part 5), pp. 426-429.
- Wang, C.-H. (2013) *A cost-effective, mobile platform-based, photogrammetric approach for continuous structural deformation monitoring*. PhD thesis. Newcastle University.
- Wang, Y.M., Li, Y. and Zheng, J.B. (2010) *Information Sciences and Interaction Sciences (ICIS), 2010 3rd International Conference on*. IEEE.

- Wasowski, J., Lamanna, C., Gigante, G., Casarano, D. and Limoni, P.P. (2013) 'HR Satellite Imaging and Borehole Monitoring of Landslides in Daunia, Italy', in *Landslide Science and Practice*. Springer, pp. 185-191.
- Westoby, M.J., Brasington, J., Glasser, N.F., Hambrey, M.J. and Reynolds, J.M. (2012) 'Structure-from-Motion' photogrammetry: A low-cost, effective tool for geoscience applications', *Geomorphology*, 179(0), pp. 300-314.
- Wilkinson, P.B., Chambers, J.E., Meldrum, P.I., Gunn, D.A., Ogilvy, R.D. and Kuras, O. (2010) 'Predicting the movements of permanently installed electrodes on an active landslide using time-lapse geoelectrical resistivity data only', *Geophysical Journal International*, 183(2), pp. 543-556.
- Yoon, D., Kee, C., Seo, J. and Park, B. (2016) 'Position Accuracy Improvement by Implementing the DGNSS-CP Algorithm in Smartphones', *Sensors*, 16(6), p. 910.
- Yun, M., Kim, J., Seo, D., Lee, J. and Choi, C. (2012) 'Application possibility of smartphone as payload for photogrammetric UAV system', *The International Archives of the Photogrammetry, Remote Sensing and Spatial Information Sciences*, XXXIX(Part B4), pp. 349-352.
- Zhan, Z. and Lai, B. (2015) 'A novel DSM filtering algorithm for landslide monitoring based on multiconstraints', *IEEE Journal of Selected Topics in Applied Earth Observations and Remote Sensing*, 8(1), pp. 324-331.
- Zhang, C.-C., Zhu, H.-H., Liu, S.-P., Shi, B. and Zhang, D. (2018) 'A kinematic method for calculating shear displacements of landslides using distributed fiber optic strain measurements', *Engineering Geology*, 234, pp. 83-96.
- Zhang, L., Liao, M., Balz, T., Shi, X. and Jiang, Y. (2015) 'Monitoring landslide activities in the three gorges area with multi-frequency satellite SAR data sets', in *Modern Technologies for Landslide Monitoring and Prediction*. Springer, pp. 181-208.
- Zhang, W., Jiang, T. and Han, M. (2010) *Image and Signal Processing (CISP), 2010 3rd International Congress on*. IEEE.